



THE HONG KONG
POLYTECHNIC UNIVERSITY

香港理工大學

Pao Yue-kong Library

包玉剛圖書館

Copyright Undertaking

This thesis is protected by copyright, with all rights reserved.

By reading and using the thesis, the reader understands and agrees to the following terms:

1. The reader will abide by the rules and legal ordinances governing copyright regarding the use of the thesis.
2. The reader will use the thesis for the purpose of research or private study only and not for distribution or further reproduction or any other purpose.
3. The reader agrees to indemnify and hold the University harmless from and against any loss, damage, cost, liability or expenses arising from copyright infringement or unauthorized usage.

If you have reasons to believe that any materials in this thesis are deemed not suitable to be distributed in this form, or a copyright owner having difficulty with the material being included in our database, please contact lbsys@polyu.edu.hk providing details. The Library will look into your claim and consider taking remedial action upon receipt of the written requests.

THE HONG KONG POLYTECHNIC UNIVERSITY
DEPARTMENT OF CIVIL AND STRUCTURAL
ENGINEERING

THE CONTROL OF BENDING RESONANCE OF VIBRATION
ISOLATION SYSTEM

HUI CHUN KAM

A thesis submitted in partial fulfillment of the requirements for

Degree of Master of Philosophy

April 2007

 Pao Yue-kong Library
PolyU • Hong Kong

DECLARATION

I hereby declare that this thesis entitled “The Control of Bending Resonance of Vibration Isolation System” is my own work and that, to the best of my knowledge the belief, it reproduces no material previously published or written, nor material which has been accepted for the award of any other degree or diploma, except where due acknowledgment has been made in the text.

Signed by

Hui Chun Kam

Abstract of thesis entitled

**The Control of Bending Resonance of Vibration
Isolation System**

Submitted by HUI Chun-kam

For the Master of Philosophy

AT The Hong Kong Polytechnic University

April 2007

ABSTRACT

Structure-borne noise radiation from concrete box infrastructures, such as railway viaduct, buildings and ductwork, cause considerable nuisance to neighbours. Floating system is generally used on these box structures to reduce the vibration transmission into the receiver. Some studies have found that the bending resonances on floating slab can affect the vibration isolation performance. However, there is still a lack of comprehensive experimental and theoretical results to confirm this situation and no published guideline for the design of the floating slab. This study was an attempt to establish the responses of the global/local modes for any rectangular box structures and identify their interaction with dynamic response of floating slab/floor and, in addition, to control the effects of bending mode of floating slab/floor on the isolation efficiency.

The extensive results in this study confirmed that the bending vibration modes of isolation system can degrade the vibration isolation performance. The effects becomes more significant when the bending resonance frequencies of floating slab match the supporting structure resonant frequency, passage support frequency or vertical isolator natural frequency.

Two types of interaction modes between rectangular concrete box and floating slab have been established. The first one is between the local distortion mode of box structure and the rotation mode of isolated slab. The second one is between the local combined mode of box structure and the first bending mode of isolated slab.

The results suggest that decreasing the length of floating slab/floor can increase the bending resonance frequency, which can improve the vibration isolation performance. To reduce the effect of bending resonance of floating system, isolators should be placed at the nodal points of the lowest symmetric bending mode of isolated panel.

The research establishes the additional rules for the design of floating system; (1) the overlap of floating slab resonant mode with those of supporting structure and passage support

frequency of the track should be avoided; 2) the installation of smaller floating slab/floor and nodal point support can reduce the bending modes effects on vibration isolation.

ACKNOWLEDGEMENT

I would like to express my sincerest gratitude to my supervisor; Dr. C. F. Ng for always supporting and encouraging me. He had been patient to provide me useful guidelines for overcoming any difficulties that I have encountered during the study time.

I would also like to express my sincere gratitude to Dr. Y. Y. Lee for giving valuable advice in my study direction and precious information about the project. Further, thanks are given to Ms. K.C. Fung for her assistance in the arrangement of important instrument, and Mr. Y. K. Lai for his technical assistance. I also offer thanks to Dr. W. Y. Poon and Miss. M. T. Leong for their suggestion and help in the overseas site measurement.

Last but not least, special acknowledgements are given to my father and mother for their love and support to encourage me to pursue an academic career.

CONTENTS

ABSTRACT	IV
ACKNOWLEDGEMENTS	VI
CONTENTS	VII
LIST OF FIGURES	XIV
LIST OF TABLES	XXI
CHAPTER 1 INTRODUCTION	1-1
1.1 BACKGROUND	1-1
1.2 LITERATURE REVIEW OF SOURCE CONTROL	1-3
1.3 LITERATURE REVIEW OF RECEIVER CONTROL	1-5
1.4 OBJECTIVE AND SCOPE	1-6
1.5 ORGANIZATION OF THIS DISSERTATION	1-7
REFERENCES	1-9
CHAPTER 2 ANALYSIS ON THE VIBRATION ISOLATION STUDY	2-1
2.1 INTRODUCTION	2-1
2.2 MODAL ANALYSIS	2-2
2.3 TRANSMISSIBILITY OF ISOLATION SYSTEM	2-3
2.3.1 EVALUATION OF TRANSMISSIBILITY	2-5
2.3.2 EXPERIMENTAL VERIFICATION OF TRANSMISSIBILITY	2-6
2.4 VIBRATION RESONANCES OF ISOLATED BEAM AND PLATE	2-7

2.5	SUMMARY	2-9
	REFERENCES	2-11
CHAPTER 3	RAILWAY TRACK DYNAMICS	3-1
3.1	INTRODUCTION	3-1
3.2	SOME VIBRAITON GENERATION MECHANISMS	3-2
3.2.1	LONG WAVELENGTH IRREGULARITIES	3-3
3.3	DYNAMIC PROPERTIES OF RAIL TRAIN AND TRACK	3-4
3.4	SOME PRINCIPLES OF VIBRAITON REDUTION	3-5
3.5	FLOATIGN SLAB TRACKS	3-7
3.5.1	SHORT-LENGTH FLOATIGN SLAB	3-7
3.5.2	MEDIUM-LENGTH FLOATIGN SLAB	3-8
3.6	SUMMARY	3-8
	REFERENCES	3-10
CHAPTER 4	BENDING RESONANCES OF FLOATING SLAB AND SUPPORTING CONCRETE BOX STRUCTURE	4-1
4.1	INTRODUCTION	4-1
4.2	THEORETICAL VIBRATION ANALYSIS OF TWO DIFFERENT LENGTHS OF BOX STRUCTURES	4-3
4.2.1	DEFINITION OF LOCAL MODE AND GOBAL MODE OF HOLLOW BOX STRUCTURE	4-3
4.2.2	THEORETICAL ANALYSIS	4-4
4.2.3	THE SIMILARITIES OF SHORT AND LONG BOXES	4-5

4.2.4	THE DIFFERENCES BETWEEN SHORT AND LONG BOXES	4-5
4.2.5	ANALYSIS OF THE MAJOR LOCAL MODES	4-6
4.3	EXPERIMENTAL VIBRATION ANALYSIS OF SHORT CONCRETE BOX	4-7
4.3.1	EXPERIMENTAL SETUP	4-7
4.3.2	EXPERIMENTAL VIBRATION RESULTS OF SHORT CONCRETE BOX	4-8
4.4	EXPERIMENTAL VIBRATION ANALYSIS OF FLOATING SLABS WITH SUPPORTING BOX STRUCTURE	4-8
4.4.1	FLOATING SLAB AND ISOLATOR DESIGNS	4-9
4.4.2	MODE SHAPES AND RESOANCE FREQUENCIES OF FLOATING SLABS	4-10
4.4.3	FLOATING SLAB WITH ISOLATOR A	4-11
4.4.4	FLOATING SLAB WITH ISOLATOR B	4-11
4.5	EXPERIMENTAL STRUCTURE-BORNE NOISE ANALYSIS OF FLOATING SLABS WITH SUPPORTING BOX STRUCTURE	4-12
4.5.1	FLOATING SLAB WITH ISOLATOR A	4-13
4.5.2	FLOATING SLAB WITH ISOLATOR B	4-13
4.5.3	THE OPTIMUM FLOATING SLAB	4-14
4.6	SUMMARY	4-14
	REFERENCES	4-16
CHAPTER 5	BENDING-RESONANCE EFFECTS ON VIBRATION REDUCTION OF IN-SERVICE RAIL VIADUCT	5-1
5.1	INTRODUCTION	5-1
5.2	THE EFFECTS OF BENDING RESONANCES OF FLOATING SLABS ON	5-3

VIBRATION REDUCTION		
5.3	CONSIDERATION IN THEORETICAL MODEL	5-4
5.4	PROCEDURES OF SITE TEST	5-5
5.5	SITE TEST ON MEDIUM FLOATING SLAB IN THE KOREA HIGH SPEED RAILWAY	5-5
RAILWAY		
5.5.1	PARAMETERS FOR FINITE ELEMENT MODEL	5-6
5.5.2	ANALYSIS OF RESULTS	5-6
5.6	SITE TEST ON FLOATING LADDER TRACK IN JAPAN (TOKYO)	5-8
5.6.1	PARAMETERS FOR FINITE ELEMENT MODEL	5-8
5.6.2	ANALYSIS OF RESULTS	5-8
5.7	SITE TEST ON SHORT-LENGTH FLOATING SLAB TRACK IN CHINA (HONG KONG)	5-10
5.7.1	PARAMETERS FOR FINITE ELEMENT MODEL	5-10
5.7.2	ANALYSIS OF RESULTS	5-11
5.8	SUMMARY	5-12
	REFERENCES	5-13
 CHAPTER 6 BENDING-RESONANCE EFFECTS ON VIBRATION REDUCTION OF ISOLATED FLOOR AND BOX		 6-1
6.1	INTRODUCTION	6-1
6.2	VIBRATION ANALYSIS OF ISOLATED FLOORS	6-2
6.2.1	EXPERIMENTAL SETUP	6-2
6.2.2	ANALYSIS OF RESULTS	6-3
6.3	NOISE AND VIBRATION ANALYSIS ON ISOLATED BOX	6-4
6.3.1	EXPERIMENTAL SETUP	6-4

6.3.2	THEORETICAL ANALYSIS	6-5
6.3.3	ANALYSIS OF RESULTS	6-6
6.4	FIELD TEST OF ISOLATED BOX (HOTEL) IN TOKYO JAPAN	6-6
6.5	SUMMARY	6-8
	REFERENCES	6-9
CHAPTER 7	OPTIMUM ISOLATOR POSITION TO CONTROL BENDING RESONANCE	7-1
7.1	INTRODUCTION	7-1
7.2	MODE SHAPE MEASUREMENT AND NODAL LINE IDENTIFICATION	7-3
7.2.1	EXPERIMENTAL SETUP	7-3
7.2.2	EXPERIMENTAL RESULTS	7-4
7.2.3	COMPARISON WITH THEORETICAL ANALYSIS	7-5
7.3	THEORETICAL ANALYSIS OF THE EFFECT OF ISOLATOR POSITION ON TRANSMISSIBILITY	7-5
7.4	THEORETICAL ANALYSIS OF THE EFFECT OF ISOLATOR POSITION ON TRANSMISSIBILITY	7-6
7.4.1	EXPERIMENTAL SETUP	7-6
7.4.2	EXPERIMENTAL RESULTS	7-7
7.5	TEST TO VERIFY THE EFFECT OF AIR-BORNE ENERGY TRANSMISSION PATH ON CEMENT BASE STRUCTURE	7-8
7.5.1	EXPERIMENTAL SETUP	7-8
7.5.2	EXPERIMENTAL RESULTS	7-9
7.6	TEST TO VERIFY THE EFFECT OF ISOLATOR POSITION WITH A CEMENT BASE STRUCTURE AND ACOUSTIC INSULATION	7-10

7.6.1	EXPERIMENTAL SETUP	7-10
7.6.2	EXPERIMENTAL RESULTS	7-11
7.7	COMPARISON WITH CONVENTIONAL FLOATING FLOOR DESIGNS	7-12
7.8	POTENTIAL APPLICATION OF THE NEW FLOATING FLOOR DESIGN	7-12
7.9	SUMMARY	7-13
	REFERENCES	7-15
CHAPTER 8	DISCUSSION	8-1
8.1	THE SIGNIFICANCE OF BENDING VIBRATION MODE ON THE ISOLATION SYSTEM DESIGN	8-1
8.2	THE SIGNIFICANCE OF ISOLATOR POSITION	8-3
8.3	THE LIMITATIONS	8-4
8.4	THE EXPERIMENTAL TECHNIQUES	8-5
	REFERENCES	8-7
CHAPTER 9	CONCLUSIONS AND RECOMMENDATIONS	9-1
9.1	CONCLUSIONS	9-1
9.2	RECOMMENDATIONS	9-2
APPENDIX A	THEORETICAL ANALYSIS ON THE STRUCTURE RADIATED NOISE	A-1
A.1	STRUCTURE ACOUSTICS IN PLATE ELEMENT	A-1
	REFERENCES	A-3

APPENDIX B	NODALIZATION TEST ON SHAKER	B-1
B.1	EXPERIMENTAL SETUP	B-1
B.2	EXPERIMENTAL RESULTS	B-2
B.3	SUMMARY	B-3
APPENDIX C	LIST OF INSTRUMENTS	C-1

LIST OF FIGURES

Figure 2.1	Schematic of vibration transmissibility	2-12
Figure 2.2	The requirements of experimental setup in noise reduction measurement of a pure isolated panel	2-12
Figure 2.3	Comparisons between experimental and theoretical transmissibility results	2-13
Figure 2.4	Three basic bending mode shapes of free-free beam (assume total length of beam is 1)	2-13
Figure 2.5	The first eleven mode shapes of rectangular floating panel (1.8m x 1m x 0.15m) estimated by FEM	2-14
Figure 2.6	The first nine mode shapes of square floating panel (0.5m x 0.5m x 0.015m) estimated by FEM	2-16
Figure 3.1	Description of the excitation source of parametric excitation at passage support frequency 13	3-13
Figure 3.2	The sketch of the estimation on the force of rail-pad support passage frequency. $\Delta 2$ is the static deflection due to dead load. Fluctuation in static deflection = $\Delta 1 - \Delta 2$	3-13
Figure 3.3	Description of the excitation source due to roughness of rail and wheel	3-13
Figure 3.4	Basic structure isolation function of floating slab track	3-14
Figure 3.5	Basic structure isolation function of ballast track	3-14
Figure 3.6	Schematic of generic track form layouts (Source from ISO 14837-1:2005)	3-15
Figure 3.7	Loading distribution description of short size and medium size of floating slabs	3-16
Figure 3.8	Dome isolator used in short size floating slab	3-16
Figure 3.9	Resilient base plate installed between the rail and floating slab	3-17
Figure 4.1	The applications of concrete box structure (not to scale)	4-18
Figure 4.2a	Global translation mode shape of box structure	4-18
Figure 4.2b	Global rotation mode shape of box structure	4-19
Figure 4.2c	Global torsion mode shape of box structure	4-19
Figure 4.2d	Global bending mode shape of box structure	4-20
Figure 4.2e	Local distortion (edge) mode shape of box structure	4-20
Figure 4.2f	Local center mode shape of box structure	4-21

Figure 4.2g	Local combined (edge and center) mode shape of box structure	4-21
Figure 4.3	Dimensions and physical properties of short and long concrete box models (not to scale)	4-22
Figure 4.4	Average mobility results of 30m (x-direction) concrete box model	4-23
Figure 4.5	Average mobility results of 1.5m (x direction) concrete box model	4-23
Figure 4.6a	Local distortion (edge) mode of short concrete box at 42Hz marked with (6a) in Figure 4.5	4-24
Figure 4.6b	Local bending (combined edge and center) mode shape of short concrete box at 153Hz marked with (6b) in Figure 4.5	4-24
Figure 4.6c	Local distortion (edge) mode together with minor 1 st global torsion mode shape of long concrete box at 44Hz marked with (6c) in Figure 4.4	4-25
Figure 4.6d	Local bending (combined edge and center) mode together with minor 1 st global bending mode shape of long concrete box at 154Hz marked with (6d) in Figure 4.4	4-25
Figure 4.7a	Local distortion (edge) mode together with minor 2 nd global torsion mode shape of long concrete box at 50Hz marked with (7a) in Figure 4.4	4-26
Figure 4.7b	Local distortion (edge) mode together with minor 3 rd global torsion mode shape of long concrete box at 61Hz marked with (7b) in Figure 4.4	4-26
Figure 4.7c	Local distortion (edge) mode together with minor 4 th global torsion mode shape of long concrete box at 79Hz marked with (7c) in Figure 4.4	4-27
Figure 4.8	Local combined (edge and center) mode together with minor 2 nd global bending mode shape of long concrete box at 155Hz marked with (8) in Figure.4.4	4-27
Figure 4.9a	1 st global torsion mode shape of long concrete box at 41Hz marked with (9a) in Figure 4.4	4-28
Figure 4.9b	2 nd global torsion mode shape of long concrete box at 46Hz marked with (9b) in Figure 4.4	4-28
Figure 4.9c	3 rd global torsion mode shape of long concrete box at 81Hz marked with (9c) in Figure 4.4	4-29
Figure 4.10a	4 th global bending mode together with minor local bending combined mode shape of long concrete box at 40.6Hz marked with (10a) in Figure 4.4	4-29
Figure 4.10b	5 th global bending mode together with minor local bending combined mode shape of long concrete box at 66Hz marked	4-30

	with (10b) in Figure 4.4	
Figure 4.10c	6 th global bending mode together with minor local bending combined mode shape of long concrete box at 92Hz marked with (10c) in Figure 4.4	4-30
Figure 4.11a	Mode shape of short concrete box at 58Hz marked with (11) in Figure 4.5	4-31
Figure 4.11b	The details of the mode shape of short concrete box at 58Hz showed in Figure 4.11a	4-31
Figure 4.12	Experimental setup for the test on concrete box	4-32
Figure 4.13a	Average mobility results of short concrete box in experimental	4-32
Figure 4.13b	Mode shapes results of short concrete box in experimental	4-33
Figure 4.14	Vibration response measurement location on box structure (not to scale)	4-33
Figure 4.15a	Vibration responses of the concrete box with and without floating slab T1A	4-34
Figure 4.15b	Vibration responses of the concrete box with and without floating slab T2A	4-34
Figure 4.15c	Vibration responses of the concrete box with and without floating slab T3A	4-35
Figure 4.15d	Vibration responses of the concrete box with and without floating slab T1B	4-35
Figure 4.15e	Vibration responses of the concrete box with and without floating slab T2B	4-36
Figure 4.15f	Vibration responses of the concrete box with and without floating slab T3B	4-36
Figure 4.15g	Coupling mode shapes of floating slab and box structure	4-37
Figure 4.16	Structure-borne noise measurement method on concrete box (not to scale)	4-37
Figure 4.17a	Sound pressure responses of the concrete box with and without floating slab T1A	4-38
Figure 4.17b	Sound pressure responses of the concrete box with and without floating slab T2A	4-38
Figure 4.17c	Sound pressure responses of the concrete box with and without floating slab T3A	4-39
Figure 4.17d	Sound pressure responses of the concrete box with and without floating slab T1B	4-39
Figure 4.17e	Sound pressure responses of the concrete box with and without floating slab T2B	4-40
Figure 4.17f	Sound pressure responses of the concrete box with and without	4-40

	floating slab T3B	
Figure 5.1	The transmissibility measurement of floating slab model	5-15
Figure 5.2a	Comparison of vibration reduction performance of floating slab model	5-15
Figure 5.2b	Theoretical vibration reduction performance of different size (in transverse direction) of floating slabs	5-16
Figure 5.3	The first eleven resonant modes of floating slab model estimated by Finite Element Method	5-17
Figure 5.4	Photograph of Korean KTX station with medium floating slab installation	5-18
Figure 5.5	Sketch of in-situ vibration measurement in Korean KTX station	5-19
Figure 5.6a	Vibration velocity levels measured at KTX station in Seoul (Korea)	5-19
Figure 5.6b	Experimental and theoretical vibration velocity level at station with medium size floating slab for Korean KTX	5-20
Figure 5.7	Experimental and theoretical vibration reduction levels for without floating slab minus with floating slab. (KTX station in Korea)	5-20
Figure 5.8	Sketch of in-situ vibration measurement at station with floating ladder in Japan (Tokyo)	5-21
Figure 5.9a	Vibration velocity levels measured at station in Japan (Tokyo)	5-22
Figure 5.9b	Experimental and theoretical vibration velocity level at station with floating ladder track in Japan (Tokyo)	5-22
Figure 5.10	Vibration reduction levels at station with floating ladder in Japan (Tokyo)	5-23
Figure 5.11	Resilient base plate installed between the rail and floating slab	5-24
Figure 5.12	Sketch of in-situ vibration measurement station with short size floating slab in China (Hong Kong)	5-25
Figure 5.13a	Vibration velocity levels measured at station with short size floating slab in China (Hong Kong)	5-25
Figure 5.13b	Experimental and theoretical vibration velocity levels at station with short size floating slab (Hong Kong)	5-26
Figure 5.14	Experimental and theoretical vibration reduction levels for ballast track minus floating slab track. (West Rail station in Hong Kong)	5-26
Figure 6.1	The transmissibility measurement of floating floor	6-10
Figure 6.2	Motion transmissibility at the center point of isolated floors	6-10
Figure 6.3	Measurement setup , dimension and material properties of isolated box	6-11
Figure 6.4	Motion transmissibility levels at the center point of isolated box	6-12

Figure 6.5	Sound Pressure levels measured inside and outside isolated area in isolated box	6-12
Figure 6.6	Photograph of a train pass over the isolated box (hotel) in Japan (Tokyo)	6-13
Figure 6.7	Sketch of vibration isolation systems and vibration measurement room in the isolated box (hotel)	6-13
Figure 6.8a	Vibration velocity levels measured inside and outside isolated area of the isolated box (hotel)	6-14
Figure 6.8b	Calculated Vibration reduction level of the isolated box (hotel)	6-14
Figure 6.9	Sound Pressure level measured inside and outside isolated area in isolated box (hotel)	6-15
Figure 7.1	Experimental setup of the mode shapes and resonance frequencies measurement	7-17
Figure 7.2	Motion transmissibility (magnitude) and damping ratio of paper honeycomb panel and cement panel	7-18
Figure 7.3	The mode shapes and identified common nodal points for the lowest two symmetric bending modes of paper honeycomb panel	7-19
Figure 7.4	Theoretical results of motion transmissibility of honeycomb panel when isolators placed at the edge and nodal points	7-20
Figure 7.5	Energy transmission paths of typical floating floor structure from the base structure to the floating floor via the intermediate layer. The paths marked with S are structure-borne energy transmission path via isolator; the paths marked A are air-borne energy transmission path via air gaps; the paths marked A' are air-borne energy transmission path with energy attenuation device of absorption material	7-20
Figure 7.6	Experimental setup for the motion transmissibility measurement with structure-borne energy transmission path only. (a) isolators placed at the edge (b) isolators placed at the identified common nodal points of the lowest two symmetric bending modes	7-21
Figure 7.7	Motion transmissibility results with structure-borne energy transmission path only. 7a) Magnitude 7b) Phase 7c) Coherence —— Sw+Awo+Ie+Amn (see Figure 7.6a) ----- Sw+Awo+In+Amn (see Figure 7.6b)	7-22
Figure 7.8	Experimental setup for the motion transmissibility measurement for air-borne energy transmission path investigation.(a) air-borne energy transmission path only (b) isolators placed at the identified common nodal points of the lowest two symmetric bending modes with both air-borne and structure-borne energy transmission paths	7-23
Figure 7.9	Motion transmissibility results for the air-borne energy	7-24

	transmission path investigation. a) Magnitude b) Phase c) Coherence ----- Swo+ Aw+Ino+Amn (see Figure 7.8a) ——Sw+Aw+In+Amn(see Figure 7.8b)	
Figure 7.10	Figure 7.10 Acoustic induced response results for the air-borne energy transmission path. a) Magnitude b) Phase c) Coherence ——Swo+ Aw+Ino+Amn (see Figure 7.8a)	7-26
Figure 7.11	Experimental setup for the motion transmissibility measurement for the conventional and new floating floor design investigation. (a) isolators were placed at identified nodal points and with sound insulation (b) Isolators placed at the edge and with sound insulation	7-26
Figure 7.12a	Comparison of vibration isolation performance with the conventional and new floating floor design. ----- Sw+Aw+In+Am (see Figure 7.11a) —— Sw+Aw+Ie+Am (see Figure 7.11b)	7-27
Figure 7.12b	Autospectrum of vibration on cement base and honeycomb floor panel when the isolator placed at the edge of the honeycomb panel (see Figure 7.11b)	7-28
Figure 7.12c	Autospectrum of vibration on cement base and honeycomb floor panel when the isolator placed at the nodal points of the honeycomb floor panel (see Figure 7.11a)	7-28
Figure 7.13	Comparison of the vibration isolation performance with typical floating floor design	7-29
Figure 7.14	A special method to reduce the anti-symmetric bending resonances and overturn problem with the new proposed floating floor design	7-29
Figure 7.15	A general method to reduce the anti-symmetric bending resonances and overturn problem with new proposed floating floor design	7-30
Figure 7.16	Vibration reduction devices a) isolators placed with in-line arrangement b) isolator placed with alternate arrangement. (From Du et. al ,2005)	7-30
Figure 8.1	Recommendation design of medium size floating slab for high speed rail	8-6
Figure A.1	Design curve for the approximation of radiation efficiency σ in general condition	A-4
Figure B.1	Experimental setup for the motion transmissibility measurement for the conventional and new floating floor design investigation. (a) isolators were placed at identified nodal points and with sound	B-4

insulation (b) Isolators placed at the edge and with sound insulation

Figure B.2a	Motion transmissibility of honeycomb panel with nodal point and edge support on shaker test	B-4
Figure B.2b	Phase of the corresponding transmissibility measurement on honeycomb panel with nodal point and edge support on shaker test	B-5
Figure B.2c	Coherence of the corresponding transmissibility measurement on honeycomb panel with nodal point and edge support on shaker test	B-5

LIST OF TABLES

Table 1.1	Comparisons between high-speed rail and highway road traffic	1-14
Table 2.1	Effects of resonances on vibration isolation of floating systems	2-18
Table 2.2	Dimensions and material properties of the testing material	2-18
Table 2.3	Typical boundary conditions and mode shape equation for beam structure	2-19
Table 2.4	Convergence of 1 st bending resonance frequency by Sap 2000	2-19
Table 3.1	Parameters defined for rail track resonance frequencies	3-18
Table 4.1	Design of three types of floating slabs and two types of isolators	4-41
Table 4.2.	Measured resonance frequencies and corresponding mode shapes of six types of floating slabs	4-41
Table 4.3	The summary of the vibration and noise reduction performance of six combinations of floating slabs	4-42
Table 5.1	Parameters used in track models for medium-length floating slab and control ballast track located in Korea (Seoul)	5-27
Table 5.2	Calculated rail track resonance frequencies	5-29
Table 5.3	Moving load at support passage frequency (parametric excitation)	5-29
Table 5.4	Natural frequency results for medium size floating slab located in Korean KTX station	5-30
Table 5.5	Parameters used in track models for floating ladder track and control ballast track located in Japan (Tokyo)	5-31
Table 5.6	Natural frequency results for floating ladder track located in Japan (Tokyo)	5-33
Table 5.7	Parameters used in track models for short size floating slab track and control ballast track located in China (Hong Kong)	5-34
Table 5.8	Natural frequency results for short size floating slab located in China (Hong Kong)	5-35
Table 6.1	Dimensions and material properties of the testing material	6-15
Table 6.2	Resonance frequencies and corresponding mode shapes for the thick concrete floating floor	6-16
Table 6.3	Resonance frequencies and corresponding mode shapes for the thin cement floating floor	6-17
Table 6.4	Theoretical and measured symmetric bending mode shapes and resonance frequencies of two isolated box structures	6-18

Table 7.1	Dimensions and material properties of the testing material	7-31
Table 7.2a	The lowest two theoretical and experimental resonance frequencies of symmetric bending mode shapes for square honeycomb panel and cement panel	7-31
Table 7.2b	Prediction of the lowest four resonance frequencies of anti-symmetric bending mode shapes for square honeycomb panel and cement panel	7-32
Table 7.3	Summary of experiments	7-33

CHAPTER 1

INTRODUCTION

This Chapter is the introduction of the research dissertation entitled “The Control of Bending Resonance of Vibration Isolation System” undertaken during the period from September 2005 to June 2007 at The Hong Kong Polytechnic University in Hong Kong.

1.1 BACKGROUND

Safety and speed have already been major concerns for railway development in the world for past decades. The other major concerns, nowadays, are the attenuation of noise pollution for noise sensitive receivers nearby tracks. According to the data given in Table 1.1 (Lee and Wong, 2005), there is less energy consumption, less air pollution and higher capacity but more noise from the rail traffic. Thus, the construction of rail traffic is one of the environmental friendly transportation systems when the noise problem can be eliminated.

The noise of rail traffic can be divided into two parts: (1) air-borne noise, (2) structure-borne noise (20-200Hz). Previous mitigation measures on air-borne noise have been quite successfully implemented; while structure-borne noise is still a growing concern. It is noted that the low frequency rumble noise can travel to adjacent building because of the long wavelength. Furthermore, the most significant structure-borne noise radiated from rail is passing through the viaduct (or bridge) because of the viaduct-structure vibration. Various previous literatures (Walker and Chan, 1996; Ngai and Ng, 2002 & Moritoh et al., 1996) have

confirmed that the structure-borne noise from rail traffic (tunnel and viaduct) in the frequency range of 20-200Hz with the tonal peak at around 50Hz.

According to ISO 2631-2:2003, the effect of vibration below 80Hz can induce adverse effects on human health, comfort and perception. Mirowska (2000) also verifies that the increase in depression, anxiety, fatigue, insomnia, and heat ailment can be caused by the low-frequency structure-borne noise.

The rapid railway system is one of the main systems of public transportation in Hong Kong. Extension work has been planned to satisfy the growing demand for local and inter-city services. Public institutes and residential buildings are often close to existing metro lines for convenient access. As a result, more people may suffer from the rumbling noise and vibration problems from old and new rail networks. There are many structure-borne noise complaints from rail traffic near viaducts such as Tsing Yi, Tai Wai and Kwai Fong in Hong Kong.

Based on the traditional isolation design for machine vibration control, floating systems has been developed to reduce the low frequency vibration transmission from trains. The isolation design is simply to install concrete slab on isolators and control the natural frequency in order to reduce vibration transmission to the receiver.

Discontinuous floating slabs have been applied in viaduct and some tunnel sections of West Rail in Hong Kong (Southward and Cooper, 2002 & Crockett and Pyke, 1999). The excellent vibration isolation design contributes to the achievement of a very quiet railway (Ho, 2007). However, the maximum speed for West Rail is 130km/h due to the maximum allowable static rail deflection of the floating slab. Further study of floating system should be conducted to improve the isolation efficiency and satisfy the requirement of higher speed.

In this dissertation, the focus is the evaluation and control of the vibration generated from rail traffic on concrete viaduct with various floating systems. To protect noise sensitive

receiver, including residents and sensitive facilities, vibration isolation systems can be applied at the source and at the receiver.

1.2 LITERATURE REVIEW OF SOURCE CONTROL

Isolation design was originally used in machine vibration control, but is now widely applied to control vibration from trains. In the floating slab track design, the slab rests on a resilient mat, and the natural frequency is selected to reduce vibration transmission (Dings, 1997). The isolation design is usually based on the basic one-degree-of-freedom theory to control the natural frequency, which depends on the static deflection of the isolator. The vibration transmission can be attenuated when the ratio of excitation frequency is more than $\sqrt{2}$ times the natural frequency. Heckl et al. (1996) suggest that the best vibration isolation for floating slab track can be obtained when the stiffness of isolator is made as soft as possible within the static deflection requirement, and when the mass between rail and the isolator is designed as large as the space can allow.

In practice, however, Saurenman et al. (1982) point out that other than the natural frequency of the mass-spring system, vibration isolation also depends on the wave motion of slab supporting structure and bending resonances of floating slabs. Kawaharazuka et al. (1996), Cox et al. (2006), Lombaert et al. (2006) and Zach (2000) have analysed floating slab for rail vibration. Their results demonstrate that the vibration isolation efficiency of floating slab can be degraded by the bending resonant vibration at low frequency range around 50Hz. In the previous studies, most of them analysed the floating slab only and very few made the investigation on both floating slab on viaduct box structure.

The length of the floating slab is an important design parameter currently and varies from one to several hundreds meters. The short and long floating slabs are also called

discontinuous and continuous floating slab separately. They have been widely applied in the rail track over the world. For example, continuous floating slab have been used in: (1) tunnel section of San Francisco Airport with vertical resonance frequency of 10Hz. (Saurenman and Phillips, 2006); (2) Washington Metropolitan Area Transit system with natural frequency of 16Hz (Nelson, 1996). Discontinuous floating slab have been applied to: (1) at-grade track in Concord, San Francisco with the slab-length of 1.8m and the fundamental resonance frequency is 8Hz (Saurenman and Phillips, 2006); (2) Viaduct of West Rail in Hong Kong with the slab-length of 1.2m and the natural frequency is 14Hz.

Hussein and Hunt (2006) showed that the bending mode of floating slab can be estimated with free-free-beam equation, and derived mathematical methods to analyse bending mode of discontinuous floating slab with different length of 3m, 6m and 12m. The results indicate that the shorter the floating slabs the higher the bending resonance frequency for the same, thickness and material properties of the slabs.

On the basis of the prediction by Southward and Cooper (2002), rumble noise radiation is mainly from the vibration of the cross-section bending modes (local modes) of the concrete viaduct. Many studies (Lees et al., 1975; Křístek, 1979; Hinton et al., 1995; Ngai and Ng, 2002; Lu et al., 2002; Lee et al., 2004; Hamed and Frostig, 2005; Lee and Wooh, 2004 & Ngai et al., 2006) provided detailed studies on vibration made shapes of box structures. Some of them use a section of viaduct box model to define the cross-section bending modes of rail viaduct structure. However, the comparison of short and long viaduct box section have not been analysed in the published studies and this will be conducted in this dissertation.

The concrete viaduct box design in West Rail in Hong Kong was modified several times so that the webs at the edge had high impedance for the first local bending mode (Southward and Cooper, 2002 & Crockett and Pyke, 2000).

High resonant vibration may be excited resulting from the bending mode of the viaduct box and the bending mode of the floating slab. The bending modes of viaduct box are an efficient sound radiator because the resonant frequency may be close to coincident frequency. (Wallace, 1972). Thus, the analysis of mode shapes of floating slab and supporting structure is critical for vibration isolation performance. It is noted that experimental studies on coupling resonance of slab and supporting box structure have not been found in any published literature to date. This should be due to the difficulties of the construction of massive viaduct box and floating slab for experimental analysis, and the requirement for powerful excitation device used on heavy concrete.

1.3 LITERATURE REVIEW OF RECEIVER CONTROL

When a noise sensitive receiver is built after the rail track is established, the vibration isolation devices may be constructed at the receiver. Floating floor is a conventional vibration isolation design. The sound reduction requirement from ISO 140-11:2005 started from 100Hz, thus most design in floating floor have low vibration attenuation below 100Hz band.

The critical design parameters of floating floors include stiffness, dimension, mass of the floating floor (Jutulstand, 1985; Baron, 2004 & Jeon and Yoo, 2006), and the position of isolators (Mead, 1998 & Yan and Xie, 1999). The selection of material, size of floating floor and position of isolators should be more flexible than floating slab on rail track, since there is no maximum allowable static deflection track and less restriction on the size of floating floor. The vibration isolation of isolated floor may couple with supporting structure (Wilson, 2004).

In the previous analysis the position of isolator are generally at the edge of the isolated floor, there is no optimization of isolator position to reduce the critical bending mode of the isolated floor. The important design feature of isolator position is rarely mentioned in

previous study. It should be noted that the bending mode of floating floor may be reduced by the optimum isolator position, which will be discussed in this dissertation.

In recent years, a further development has been to isolate a box inside building to alleviate vibration transmission from train. For example, the two-storey hotel of isolated box design is constructed underneath a rail viaduct of ballast track in Tokyo, Japan (Osako et al., 2004). The site noise and vibration data of the isolated box and building near rail traffic is difficult to be recorded because of the change of measurement results by factors like the train speeds, soil conditions or distances between source and receiver.

1.4 OBJECTIVE AND SCOPE

The objectives of this research are

(1) to establish the responses of the global/local modes for any rectangular box structures like viaduct, buildings and ductworks and identify their interaction with dynamic response of floating slab.

(2) to evaluate and control the effects of bending mode of floating slab/ floor on the isolation efficiency.

The bending vibration modes of floating slab/floor may produce adverse effects on the vibration isolation, and the coupling modes with viaduct box structure may lead to vibration amplification.

Regarding experimental measurement, the concrete box structure and floating slabs were constructed for studying the dynamic and acoustic characteristics of the bending mode and the probable coupling modes of the structures. Furthermore, the concrete, cement and honeycomb floor panels were also constructed for studying the effects of bending resonance on vibration isolation, and the optimum isolator position of isolated floor. Regrading site

measurement, the vibration of existing railway viaduct with various floating slab design was conducted to investigate the vibration reduction performance of them. The degradation of isolation efficiency of floating systems is interpreted according to excitation resonance from moving load, resonances of rail track and bending modes of floating slab. The vibration reduction of an existing isolated box (hotel) was measured to examine the vibration isolation performance. The measured signals in field test were recorded and selected for post-analysis.

A Finite Element Method (FEM) is applied to analyze the mode shapes, resonance frequency and vibration transmissibility (Motion transmissibility and Force transmissibility). The results of mathematic model can be used to interpret and validate the experimental findings, and also further study for large or complex structures which can not be constructed in laboratory for experimental measures.

Concrete structure is a famous material to construct civil structure, including rail viaduct, floating slab and buildings. Increasing the thickness of the concrete may not decrease the noise as the resonance frequency and may become closer to the coincidence frequency. This dissertation investigates the floating slab and viaduct structure constructed with concrete material but not steel bridge. Also, the development of computer program prediction and detailed investigation of sound radiation efficiency will not be carried out in this dissertation.

1.5 ORGANIZATION OF THIS DISSERTATION

This dissertation consists of nine chapters and three appendixes. Chapter 1 is the introduction that presents the background information, relevant past research works and the objectives of this dissertation. The analytical equations, including modal analysis, vibration transmissibility equation and bending modes estimation, used in the dissertation to predict the detrimental effects on vibration isolation efficiency due to bending modes are described in

Chapter 2. Chapter 3 interprets the vibration characteristics of train source from moving train excitation and resonant frequencies of the components from car-body to the rail structures; also the pros and cons of different length of floating slab used on viaduct. Chapters 4 and 5 are related to the vibration isolation at the source. In Chapter 4, the experimental vibration responses and radiated noise on the models of concrete box and floating slabs are examined; and coupling resonances of concrete box and floating slab also are established. The parameter studies in this chapter can be useful for the initial design of floating slab system or other vibration control devices to avoid coupling resonances with supporting structures. Chapter 5 describes and interprets the characteristics and vibration isolation performances of rail viaduct systems with various floating slab designs in terms of the existing railway vibration data in local and overseas railway systems. Chapters 6 and 7 are related to the vibration isolation at the receiver. The motion transmissibility of typical size of isolated floors, and isolated box structures are investigated in Chapter 6. Chapter 7 introduces the new design of isolated floor with the concept of optimum isolator position to attenuate the effect of bending mode on vibration isolation. In Chapter 8, the discussions of the two significant findings in this dissertation are described in detail. Finally, Chapter 9 gives the conclusions of the dissertation and proposes the strategy for further investigation on this subject.

REFERENCES

- Baron, N. (2004). Some Acoustical Properties of Floating Floors Used in Trains. KTH Aeronautical and Vehicle Engineering, Thesis.
- Cox, S.J., Wang, A., Morison, C., Carels, P., Kelly, R. and Bewes, O.G. (2006). A test rig to investigate slab track structures for controlling ground vibration. *Journal of Sound and Vibration*, 293(3–5), 901–909.
- Crockett, A.R. and Pyke, J.R. (2000). Viaduct design for minimization of direct and structure-radiated train noise. *Journal of Sound and Vibration*, 231(3), 883-897.
- Dings, P. (1997). Measures for noise reduction on steel railway bridges. *Proceedings of Inter-noise*, 143-145.
- Hamed, E. and Frostig, Y. (2005). Free vibrations of multi-girder and multi-cell box bridges with transverse deformations effects. *Journal of Sound and Vibration*, 279 (3-5), 699-722.
- Heckl, M., Hayck, G. and Wettschureck, R. (1996). Structure-borne sound and vibration from rail traffic. *Journal of Sound and Vibration*, 193(1), 175–184.
- Hinton, E. Özakça, M., Rao, N.V.R. (1995). Free vibration analysis and shape optimization of variable thickness plates, prismatic folded plates and curved shells: Part 1: finite strip formulation. *Journal of Sound and Vibration*, 181(4), 553-566.

Ho, S.K. (2007). Hong Kong West Rail – One of the quietest rail tracks in the world. Chinese Article, Tsinghua Tongfang Optical Disc Co. Ltd.

Hussein, M.F.M. and Hunt, H.E.M. (2006). Modelling of floating-slab track with discontinuous slab, part 1: response to oscillating moving loads. *Journal of Low Frequency Noise, Vibration and Active Control*, 25(1), 23-39.

International Standard, ISO 140-11 (2005). Acoustics— Measurement of sound insulation in buildings and of building elements —Part 11: Laboratory measurements of the reduction of transmitted impact sound by floor coverings on lightweight reference floors.

International Standard, ISO 2631-2 (2003). Mechanical vibration and shock —Evaluation of human exposure to whole body vibration —Part 2: vibration in buildings (1 Hz to 80 Hz).

Jeon, J.Y. and Yoo, S.Y. (2006). Effects of the structural stiffness of concrete slabs on floor impact sounds. *Proceedings of Inter-noise 2006*.

Jutulstad, H. (1985). Flytende gulv på fjaerer – lydreduserende konstruksjon for fartoy. Universitet I Trondheim. Norges Tekniske Hogskole, Institutet for Husbyggnadteknik, Norway.

Kawaharazuka, T., Hiramatsu, T., Ohkawa, H. and Koyasu, M. (1996). Experimental study on vibration reduction by isolated railway. *Internoise*, 1549–1552.

Křístek, Vladimír. (1979). *Theory of box girders*. John Wiley & Sons, Chichester.

Lee, S.Y. and Wooh, S.C. (2004). Finite element vibration analysis of composite box structures using the high order plate theory. *Journal of Sound and Vibration*, 277(4-5), 801-814.

Lee, Y.Y., Ngai, K.W. and Ng, C.F. (2004). The local vibration modes due to impact on the edge of a viaduct. *Journal of Applied Acoustic*, 65, 1077-1093.

Lees, A.W., Thomas, D.L. and Wilson, R.R. (1975). Analysis of the vibration of box beams. *Journal of Sound and Vibration*, 45(4), 559–568.

Lee, H.G. and Wong, M.S. (2005). *Technology in high speed railway*. Beijing: Zhongguo tie dao chu ban she.

Lombaert, G., Degrande, G., Vanhauwere, B., Vandeborghht, B. and François, S. (2006). The control of ground-borne vibrations from railway traffic by means of continuous floating slabs. *Journal of Sound and Vibration*, 297(3–5), 946–961.

Lu ,Y., Hao, H., Ma, G. (2002). Experimental investigation of structural response to generalized ground shock excitation. *Experimental Mechanics*, 42(3), 261–71.

Mead, D. J. (1998). *Passive vibration control*. Chichester; New York: Wiley.

Mirowska, M. (2000). Effect of low-frequency noise at low levels on human health in light of questionnaire investigation. *Internoise 2000 Special*, 41-45.

Moritoh, Y., Zenda, Y. and Nagakura, K. (1996). Noise Control of High Speed Shinkansen. *Journal of Sound and Vibration*, 193(1):319-334.

Nelson, J.T. (1996). Recent developments in ground-borne noise and vibration control. *Journal of Sound and Vibration*, 193(1), 367–376.

Ngai, K.W. and Ng, C.F. (2002). Structure-borne noise and vibration of concrete box structure and rail viaduct. *Journal of Sound and Vibration*, 255(2) 281-297.

Ngai, K.W., Ng, C.F. and Lee, Y.Y. (2006). The control of structure-borne noise from a viaduct using floating honeycomb panel. *JSME international Journal, Serious C*, 49 (2), 494-504.

Osako, K., Hayashiand, A. and Yamada M. (Summer 2004). Development of the sound-and-vibration-proofing method (suspended seismic isolation method) for buildings under elevated railway tracks. *JR East Technical review*. No.4, 34-40.

Saurenman, H.J., Nelson, J.T. Wilson, G.P. (1982). *Handbook of Urban Rail Noise and Vibration control*. Prepared under contract to US DOT/Transportation Systems Center, Report UMTA-MA-06-0099-82-2.

Saurenman, H. and Phillips, J. (2006). In-service tests of the effectiveness of vibration control measures on the BART rail transit system. *Journal of Sound and Vibration*, 293(3–5), 888–900.

Southward, N.J. and Cooper, J.H. (January 2002). The alternative design of the West Rail Viaducts . Hong Kong Engineer On Line, Cover Story.

Walker, J.G. and Chan, M.F.L. (1996). Human response to structurally radiated noise due to underground railway operations. *Journal of Sound and Vibration*, 193 (1), 49-63.

Wallace, C. E. (1972). Radiation Resistance of a rectangular panel. *Journal of the Acoustical Society of America*, 51 (3), 946-952.

Wilson, G.P. (2004). Isolation of the Jazz @ Lincoln Center Performance and Education Concert Theater, Rose Theate. *Proceedings of Inter-noise*.

Yan, X. L. and Xie, Y. (1999). The effect of arrangement of isolators in coupled vibration. *Chinese Journal of Electronics Machinery Engineering*, 82(6).

Zach, A. (2000). Vibration insulation research results in Switzerland. *Journal of Sound and Vibration*, 231(3), 877–882.

Table 1.1. Comparisons between high-speed rail and highway road traffic

Traffic ways	High speed rail	Highway road traffic
Average speed (km/h)	200-250	~100
Accident (per hundred million people *km)	Dead :0.29 Wounded:0.72	Dead :10.5 Wounded:24.88
Energy source	electric power	petroleum
CO ₂ emission ratio	1 (including electric production)	3
Energy consumption ratio	1	5.3
Noise pollution (overall level at 50m)	Lmax~80dB(A)	Lmax~70dB(A)
Transportation capacity ratio	1	0.2
Flexibility	(lower) city to city	(higher) point to point

CHAPTER 2

ANALYSIS ON THE VIBRATION ISOLATION STUDY

This Chapter describes the plate vibration formulae application in this dissertation. The fundamental theory for the identification of resonance phenomena by modal analysis is described. It can be applied to derive the simple transmissibility equation of floating system. The predictions of vibration resonance frequency of beam and plate structure are also presented.

2.1 INTRODUCTION

In this dissertation, the dynamic behaviour of floating systems and supporting concrete box structures will be examined. The analytical formulae of structure behaviour, finite plate and box structures are assumed to be linear. Vibration isolation performance of floating system on box-like structure can be calculated with multi degree of freedom equation based on modal analysis. The simple beam and plate equations are used to estimate resonant modes (frequency and mode shape) of plate structure, and the FEM can be used to analyse the free or forced vibration of a more complex box-like model with floating panel. The related analytical equations are presented in the following sections.

2.2 MODAL ANALYSIS

Resonance phenomena are critical for most practical noise and vibration problems. Modal analysis is an efficient tool for modelling structural behaviour. Excitation on a structure leads to one or more modes of vibration which depends on the excitation frequency range. The simplest situation is the single degree of freedom (SDOF) model which can be extended to multiple degree of freedom (MDOF) equations to analyse complete dynamic mechanical vibration component. Analytical mathematic analysis is based on the discrete parameter model with idealized elements including the mass, spring, damper and excitation. The excitation force on mass are stored in the mass as kinetic energy and in the spring as potential energy and dissipated through damping (Ewins, 1995)

For a general MDOF system, with N degrees of freedom, the governing equation of motions in matrix form is shown in Equation 2.1.

$$[M]\{\ddot{x}\} + [C]\{\dot{x}\} + [K]\{x\} = \{f(t)\} \quad (2.1)$$

Where $[M]$ is a mass matrix; $[K]$ is a stiffness matrix; and $[C]$ is a viscous damping matrix; $\{x\}$ is displacement vector; $\{f(t)\}$ is force vector various with time.

To solve Equation 2.1, the r^{th} eigenvalue $[\omega_r^2]$ and the corresponding mode shape vector $\{\Psi_r\}$ should be obtained first by eigenvalue analysis on the free vibration situation: $\{f(t)\} = \{0\}$, and set the determinate to be equalled to zero.

Mode shape matrix and then preceding the normalization process to simplify the mass, damping to stiffness matrix to be diagonal matrix, and $\{x\} = [\Psi]\{q\}$, $\{q\}$ is modal displacement. Thus, $[\Psi]^T [M] [\Psi]\{\ddot{q}\} + [\Psi]^T [C] [\Psi]\{\dot{q}\} + [\Psi]^T [K] [\Psi]\{q\} = [\Psi]^T \{f\}$ can be established.

A simpler matrix $[m_r]\{\ddot{q}\} + [c_r]\{\dot{q}\} + [k_r]\{q\} = [\Psi]^T \{f\}$ can be obtained where from which the r^{th} individual equation is: $m_r \ddot{q}_r + c_r \dot{q}_r + k_r q_r = f_k \psi_{kr}$

$$q_r = \frac{f_k \psi_{kr}}{(k_r - \omega^2 m_r) + j(\omega c_r)} \text{ and } \psi_{ir} q_r = x_i$$

Then $\omega_r^2 = \frac{k_r}{m_r}$ and $\zeta_r = \frac{c_r}{2\sqrt{k_r m_r}}$ can be obtained, ζ_r is the r^{th} damping ratio. In this

dissertation, structural damping η is modelled as equivalent viscous damping using the approximation of $\zeta_r = 2\eta$.

The individual general receptance frequency response function (FRF) in terms of mass, damping and stiffness elements can be established as shown in Equation 2.2:

$$\alpha_{ik}(\omega) = \sum_{r=1}^N \frac{(\psi_{ir})(\psi_{kr})}{(k_r - \omega^2 m_r) + j(\omega c_r)} \quad (2.2)$$

where $\alpha_{ik} = \left(\frac{x_i}{f_k} \right) = \alpha_{ki} = \left(\frac{x_k}{f_i} \right)$, ψ_{ir} is the i^{th} element of the r^{th} eigenvector $\{\psi\}_r$, and

ψ_{kr} is the k^{th} element of the r^{th} eigenvector.

Simplification of the Equation 2.2 is given in Equation 2.3 in Section 2.3, which is used for simple structure of beam and plate, also FEM for complex structures.

2.3 TRANSMISSIBILITY OF ISOLATION SYSTEM

The isolation designs have been used in ships, trains, airplanes, and buildings to enhance human comfort and decrease damage to equipment. A general isolation system were initially derived as a rigid-body motion, the matrix approach was then developed on the basis of the theory of modal analysis. The system was simplified as the problem of a rigid body supported with isolators which consist of spring and damping elements.

Muster and Plunkett (1988) developed MDOF Equation 2.3 according to modal analysis theory (see Figure 2.1) to identify the ratio of vibration velocity on the foundation with the isolator to that without. The Equation 2.3 is useful for the verification of the vibration transmissibility measurement results in the following chapters.

$$\text{Vibration transmissibility (Tr)} = \frac{V}{V_o} = \frac{|M_m|}{|M_i + M_m|} \quad (2.3)$$

$$\text{Where, } M_i = \frac{1}{\frac{k_o}{j\omega} + c_o}, \quad M_m = \frac{1}{m_o j\omega} + \sum_{r=1}^N \frac{R_r}{\frac{k_r}{j\omega} + m_r j\omega + c_r}$$

V = the velocity of the floating slab,

V_o = the velocity of the base structure,

M_m = the mobility of the floating slab,

M_i = the mobility of the isolator,

k_o = the stiffness of isolator,

m_o = the mass of slab,

m_r = the modal mass of r^{th} bending resonance, (from Equation 2.9)

c_o = the damping of isolator,

c_r = the modal damping of r^{th} bending resonance, and

R_r = the mode shape factor of r^{th} bending resonance (estimated from Table 2.3).

On the basis of Equation 2.3, the magnitudes of transmissibility at the resonance of isolator and at the resonance of first bending of the slab are shown in Equations 2.4 and 2.5.

$$\text{At the resonance of isolator:} \quad \text{Tr}(\omega_o) = \frac{1}{2\zeta_o} \quad (2.4)$$

Where, ζ_o is the damping of isolator

$$\text{At the first symmetric bending resonance of of slab: } \text{Tr}(\omega_1) = B \frac{R_1}{\zeta_o \gamma_1^2} \quad (2.5)$$

Where, $\gamma_1 = \frac{\omega_1}{\omega_o}$ and B is a factor dependent on the modal mass.

In summary, the effect of bending resonances depends on the mode shape factor and the resonance frequency as given by Equation 2.5. The effects of resonances on vibration isolation are considered and listed in Table 2.1.

2.3.1 EVALUATION OF TRANSMISSIBILITY

By definition, there are two kinds of transmissibility which are distinguished by the location of excitation source. The first one is force transmissibility at the source and defined as the proportion of excitation force transmitted from the floating slab to the supporting structure (e.g. viaduct box or ground). The other one is the motion transmissibility at the receiver and defined as the proportion of vibration amplitude transmitted from the base structure to the floating floor.

In experiment, force transmissibility is usually found by the ratio of vibration amplitudes of the supporting structure resulting from the constant excitation force with and without floating slab; whereas motion transmissibility is measured with the base excitation method from frequency response functions (FRFs; the acceleration on the isolated panel/ acceleration on base structure). However, the mathematical equations of two kinds of transmissibility are the same. The vibration reduction is defined as one minus vibration transmissibility.

In the investigation of the vibration isolation performance, the “vibration reduction” and “noise reduction” should be interchangeable. However, in fact, this is hard to be proved by experimental method since the different paths of noise sources can confuse the measurement results. For example, the noise reduction for a pure isolated panel (noise radiation with and

without floating panel) should be measured at the same volume of box with same absorption area (same room constant), and the vibration resonant modes of covered box, or the impact source may radiate higher noise level than the floating panel. (See Figure 2.2). In this dissertation, various methods have considered to control the measured sound transmission path of in different measurement conditions.

2.3.2 EXPERIMENTAL VERIFICATION OF TRANSMISSIBILITY

To verify the Equation 2.3, a cement board was employed to conduct motion transmissibility measurement with base excitation by a shaker. Soft rubber was placed between the center of the panels and the vibrating shaker head. The boundary conditions were assumed to be free along the circumference of the plate. A white noise signal was used to drive the shaker to generate a wide band frequency (0-1.6 kHz) force, and an accelerometer was mounted on the shaker head to register the input acceleration to the panels. A lightweight accelerometer was mounted at centre point on the panels to measure their acceleration response. The two acceleration signals were fed into the analyzer and a computer for data processing. The analyzer worked in real time at the frequency resolution of 6,400 lines in the range of 0-1.6 kHz. The frequency response functions (FRFs; the accelerations on the panel/shaker head), were compared with SDOF and MDOF mathematical modals from Equation 2.3. The damping ratios of different modes were calculated with half power method with a small sample. Mode shape factors were estimated with mode shape equation in Table 2.3; modal mass was estimated with Equation 2.9. The dimensions, material properties of the test panel are given in Table 2.2.

Comparisons of the experimental and theoretical transmissibility results are shown in Figure 2.3. The experimental transmissibility levels ($10\log(\text{Tr}^2)$) are higher than those of

SDOF results due to the effects of slab bending resonance at 146Hz and 338Hz. It is obvious that the MDOF Equation 2.3 can model the transmissibility of the isolated structure with the deviation less than 5dB; the discrepancy should be mainly because of the error in the prediction of damping. From Table 2.1, it is noted that the resonance frequency as well as mode shape are important for the effects of bending resonance. The equations to calculate bending resonance frequency of simple structures are given in the following part.

2.4 VIBRATION RESONANCES OF ISOLATED BEAM AND PLATE

Regarding the calculation of free vibration resonances of discontinuity slab, the simple beam equation can be applied as shown in Equation 2.6 which is capable of predicting the transverse and longitudinal vibration resonance separately.

$$f = \frac{\lambda^2}{2\pi l^2} \left(\frac{EI}{m} \right)^{\frac{1}{2}} \quad (2.6)$$

where,

- f = the resonance frequency (Hz),
- l = the length of the panel (m),
- m = the mass per unit length (kgm^{-1}),
- E = the Young's modulus (Nm^{-2}),
- I = the moment of inertia (m^4), and
- λ = the frequency parameter.

λ is the coefficient depending on the boundary conditions, the typical boundary conditions with different frequency parameters and the corresponding three basic mode shapes are listed in Table 2.3 and the corresponding mode shapes of free-free beam are plotted in Figure 2.4. Equation 2.6 is assumed that all the imparted KE transferred to PE in

two directions bending separately. However, when the panel has similar length in both directions, the imparted KE can be transferred to PE in both directions at the same time, thus the plate equation should be employed to estimate the free vibration resonance with plate equations which are presented by Blevins (1979) and Leissa (1960). Different boundary conditions with different width to length ratios and the frequency parameters λ of different modes, and estimate the resonance frequencies by

$$\omega = \sqrt{\frac{D}{\rho}} \left(\frac{\lambda}{a^2}\right), \quad (2.7)$$

where,

ω = the angular resonance frequency (rad/s),

a = the length of the panel (m),

ρ = the mass density per unit area of the panel (kg/m²),

D = the flexural rigidity, and

λ = the frequency parameter.

$$D = \frac{Eh^3}{12(1-\nu^2)}, \quad (2.8)$$

where,

E = Young's modulus (N/m²),

h = the panel thickness (m), and

ν = Poisson's ratio.

Based on Equations 2.6-2.8 and the frequency parameters λ that are provided by Blevins (1979), can gain an initial idea for the designed floating systems. In practice, however, a more precise method should use FEM to predict the dynamic behaviour of complex mechanical

structures. In this dissertation, both simple equations and FEM are applied to estimate the vibration mode.

Various researchers (Saurenman et al., 1982; Lee et al., 2004 & Hussein and Hunt, 2006) have supported that the boundary condition of floating slab is free. The free vibration of the first eleven mode shape of a rectangular and the first nine mode shapes of a square panel were modelled by FEM with Sap 2000 v.8, which is a finite element software package. The mode shapes and the shape description were presented in Figures 2.5-2.6. Thin shell elements were used for the computer modelling. There are four nodes for each element and six degree of freedom at each node. Ten times eighteen elements were applied for the rectangular floating slab study (Figure 2.5). It is found that the increasing in no of element give no significant change (less than 5%) in 1st bending resonance frequency (Table 2.4). The first two symmetric bending modes should be important for vibration isolation performance. They are useful for the study in the following chapters.

The simple equations for modal mass, stiffness and damping for simple beam or plate are presented in Equations 2.9-2.11. They are useful for the transmissibility calculation in Equation 2.3.

$$m_r = m \int_0^1 [\psi_r]^2 dx \quad (2.9)$$

$$k_r = \omega_r^2 m_r \quad (2.10)$$

$$c_r = 2m_r \omega_r \zeta_r \quad (2.11)$$

The structure radiated noise is a complex topic because of the large variation of the surroundings and this will not be investigated in detail in this dissertation. Some simple equations for structure radiated noise are discussed in Appendix A in order to introduce the general idea about the parameters that affect the structure-radiated noise from plate structure.

2.5 SUMMARY

Modal analysis is the fundamental method to understand the dynamic properties of the structure including resonant mode (frequency and mode shape). On the basis of the theory of modal analysis equations, MDOF transmissibility equation can be derived. This can help to understand the ratio of the energy input from a source to the output at the receiver, and the degradation of vibration isolation performance by the bending mode of the slab. The simple beam and plate equations can be used for the initial design for the bending resonance frequency of isolated panel.

REFERENCES

Blevins, R. D. (1979). *Formulas for natural frequency and mode shape*. New York: John Wiley and Sons.

Ewins, D.J. (1995). *Modal Testing- Theory and Practice*. Taunton, England: Research Studies Press.

Hussein, M.F.M. and Hunt, H.E.M. (2006). Modelling of floating-slab track with discontinuous slab, part 1: response to oscillating moving loads. *Journal of Low Frequency Noise, Vibration and Active Control*, 25(1), 23-39.

Leissa, A.W. (1960). *Vibration of plates*. NASA SP-160 , NASA Washington, DC.

Muster, D. and Plunkett, R. (1988). Isolation of Vibrations. In L.L. Beranek (Ed.), *Noise and Vibration Control* (pp. 406-475). Washington D.C: Institute of Noise Control Engineering.

Saurenman, H.J., Nelson, J.T. Wilson, G.P. (1982). *Handbook of Urban Rail Noise and Vibration control*. Prepared under contract to US DOT/Transportation Systems Center, Report UMTA-MA-06-0099-82-2.

Lee, Y.Y., Ngai, K.W. and Ng, C.F. (2004). The local vibration modes due to impact on the edge of a viaduct. *Journal of Applied Acoustic*, 65, 1077-1093.

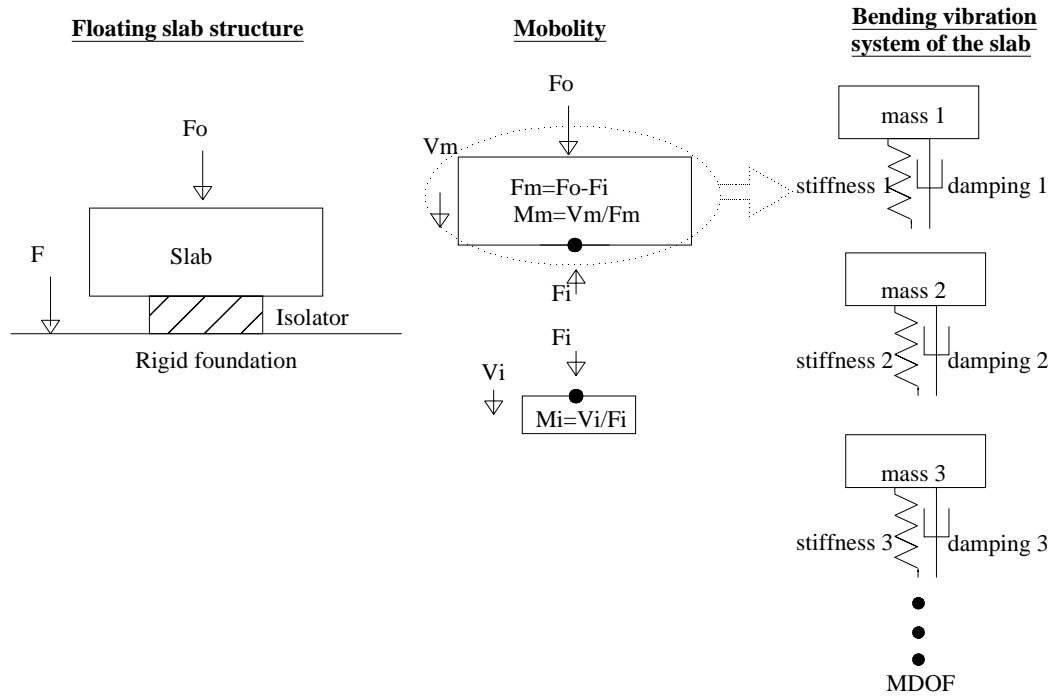


Figure 2.1 Schematic of vibration transmissibility

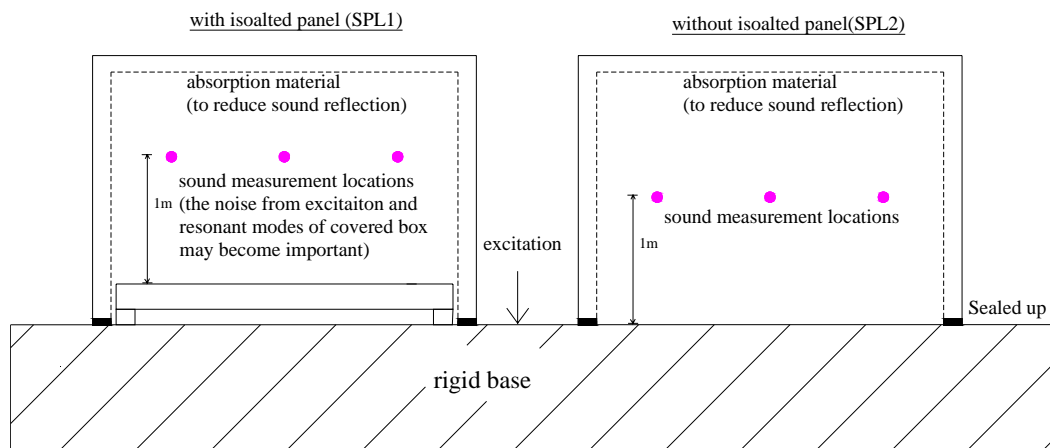


Figure 2.2 The requirements of experimental setup in noise reduction measurement of a pure isolated panel (not to scale)

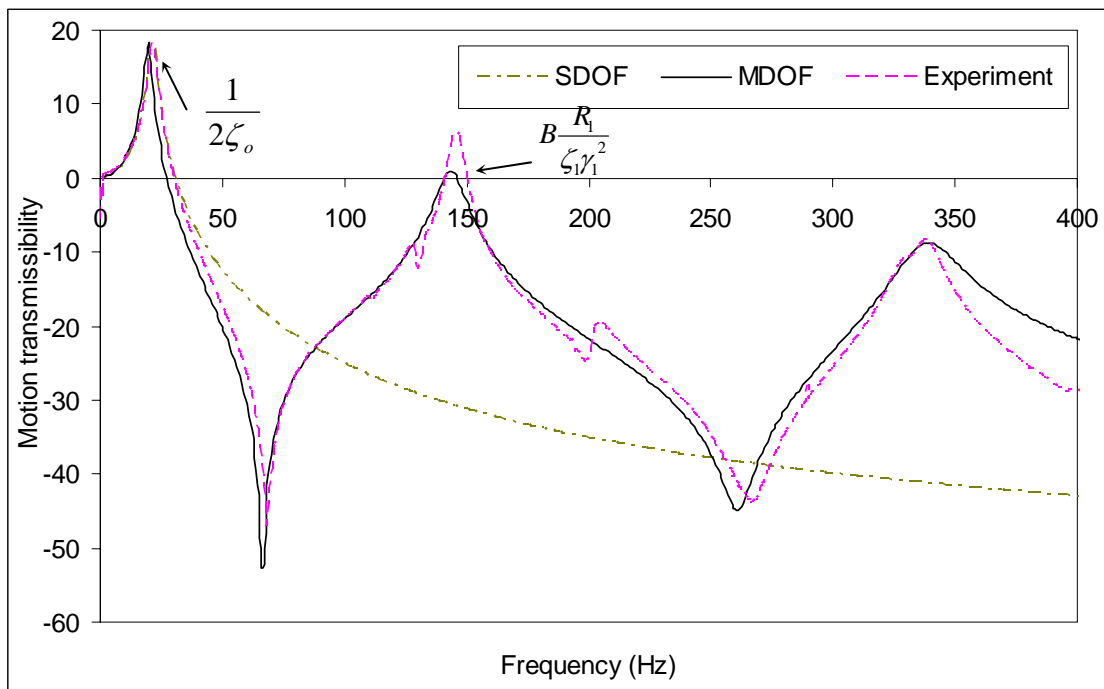


Figure 2.3 Comparisons between experimental and theoretical transmissibility results

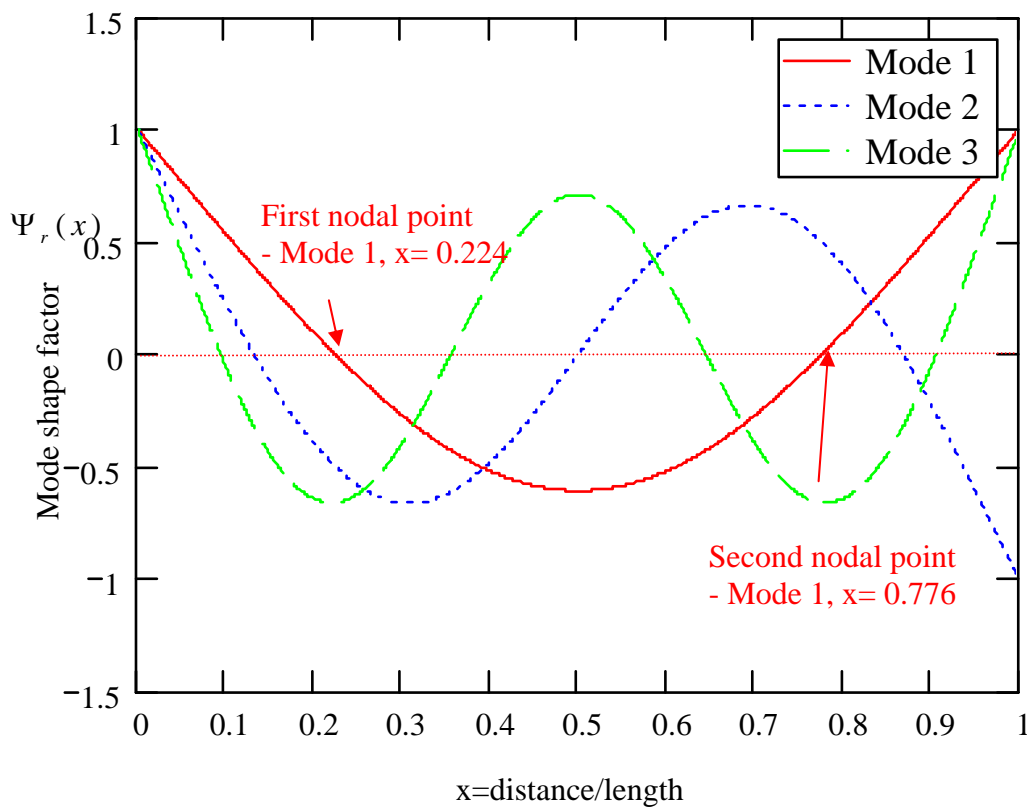
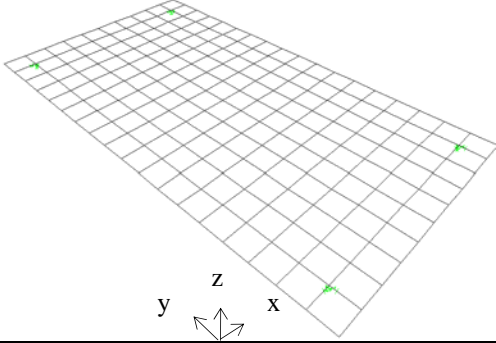
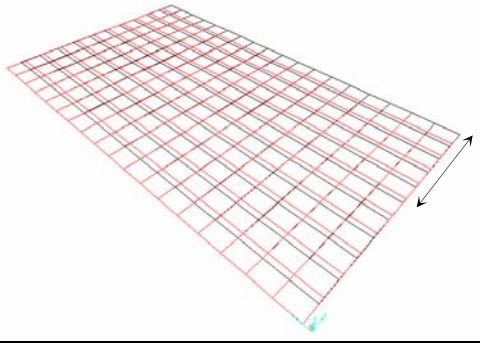
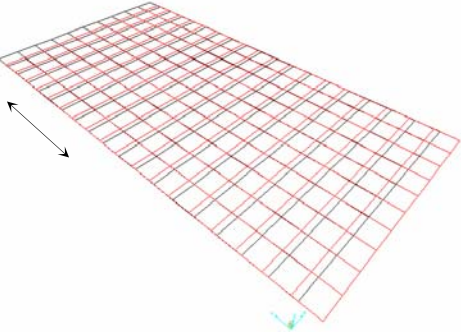
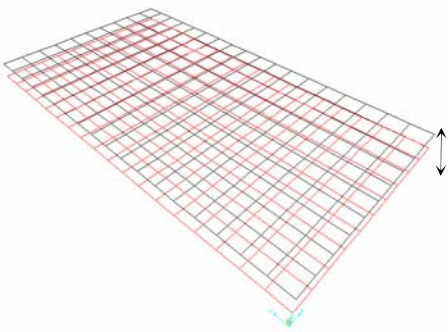
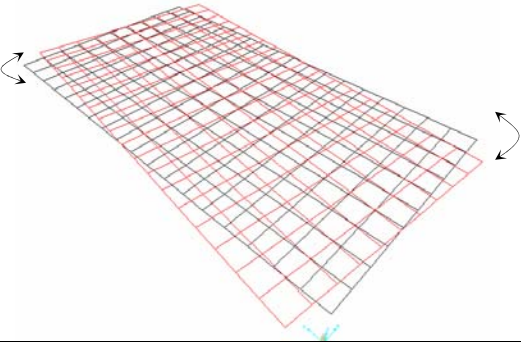
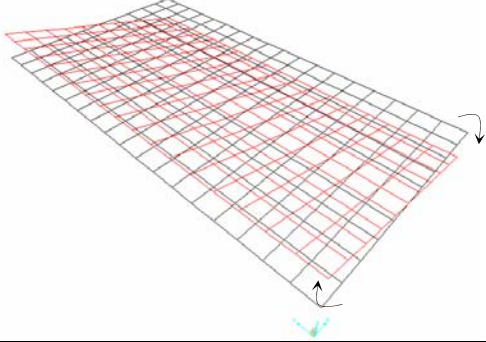
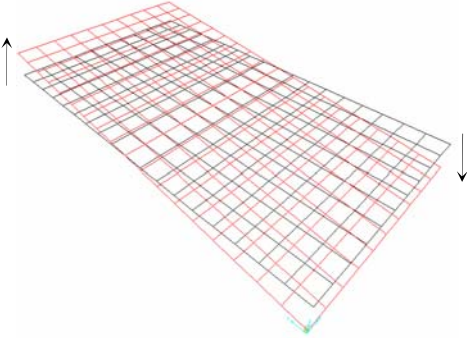
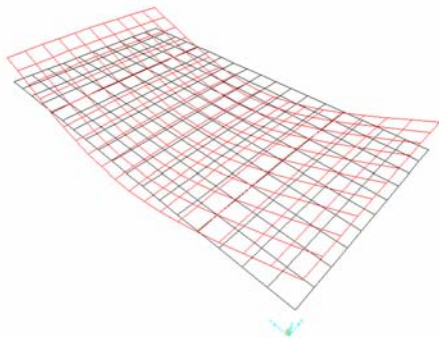


Figure 2.4 Three basic bending mode shapes of free-free beam (assume total length of beam is 1)

 <p>Original shape</p>	 <p>1. Rigid body mode – In x direction</p>
 <p>2. Rigid body mode – In y direction</p>	 <p>3. Rigid body mode –In z direction (vertical)</p>
 <p>4. Rigid body mode – Pitch</p>	 <p>5. Rigid Body mode –Yaw</p>
 <p>6. Rigid Body mode –roll</p>	 <p>7. 1st symmetric bending mode in y direction</p>

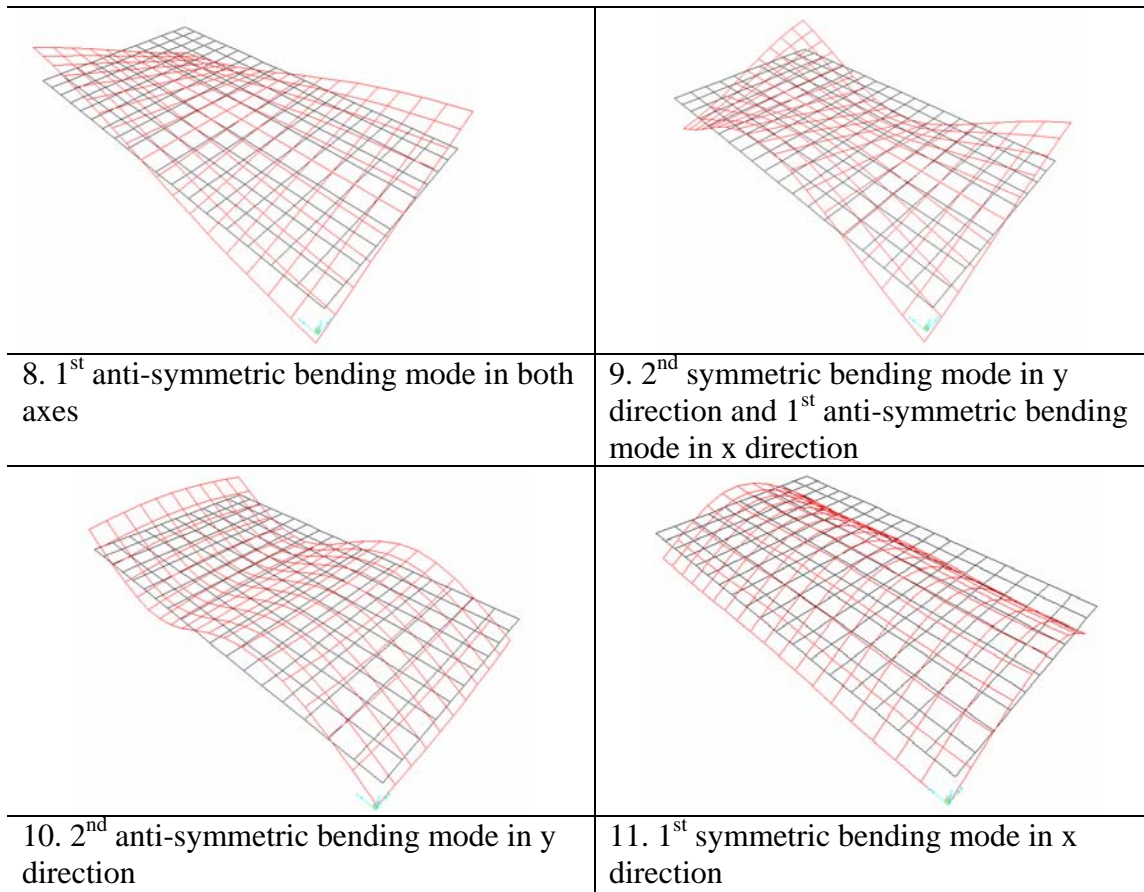
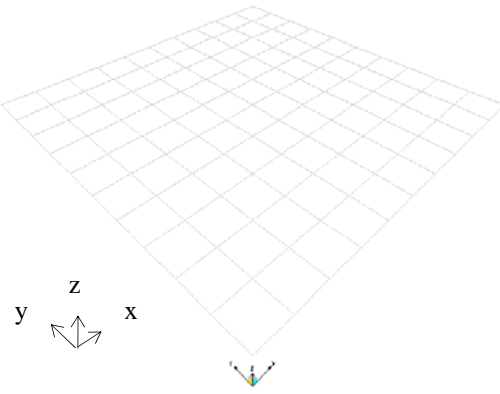
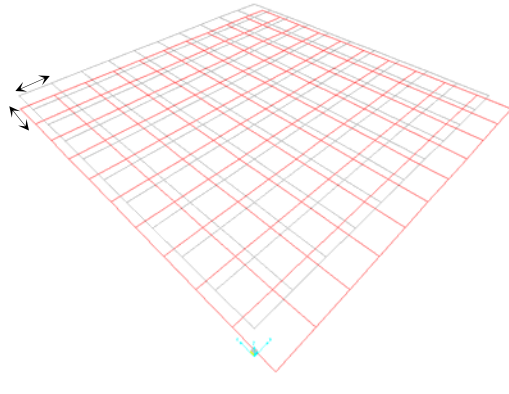
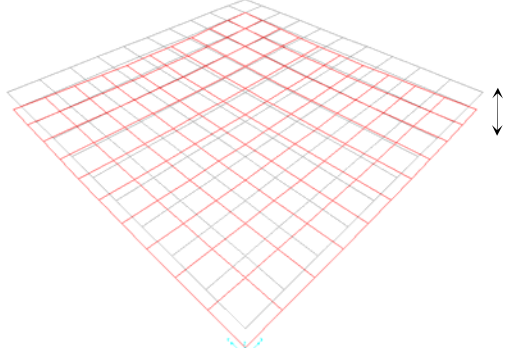
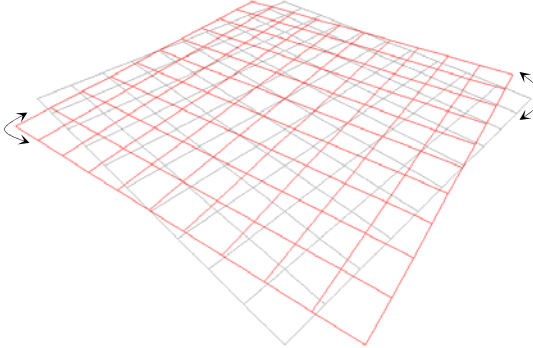
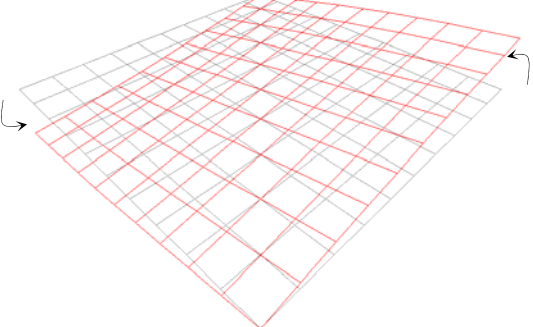
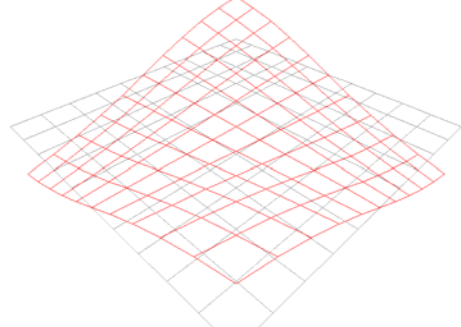
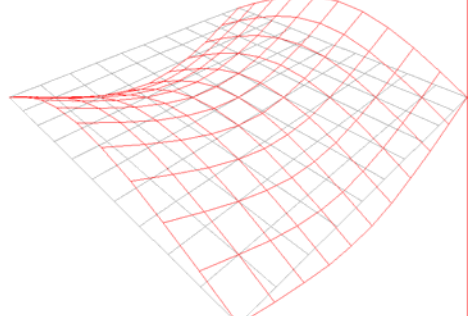
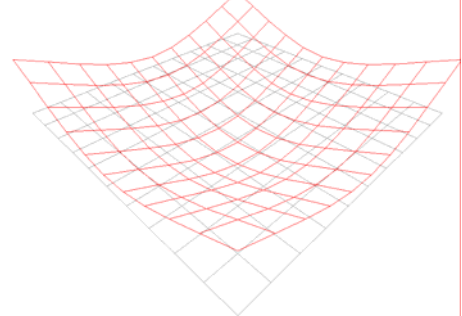


Figure 2.5 The first eleven mode shapes of rectangular floating panel (1.8m x 1m x 0.15m) estimated by FEM

	
<p>Original shape</p>	<p>1. Rigid body mode – In x and y direction</p>
	
<p>2. Rigid body mode – In z direction (vertical)</p>	<p>3. Rigid body mode – Pitch</p>
	
<p>4. Rigid Body mode – Yaw and Roll</p>	<p>5. 1st anti-symmetric bending mode</p>
	
<p>6. 2nd anti-symmetric bending mode</p>	<p>7. 1st sym`metric bending mode</p>

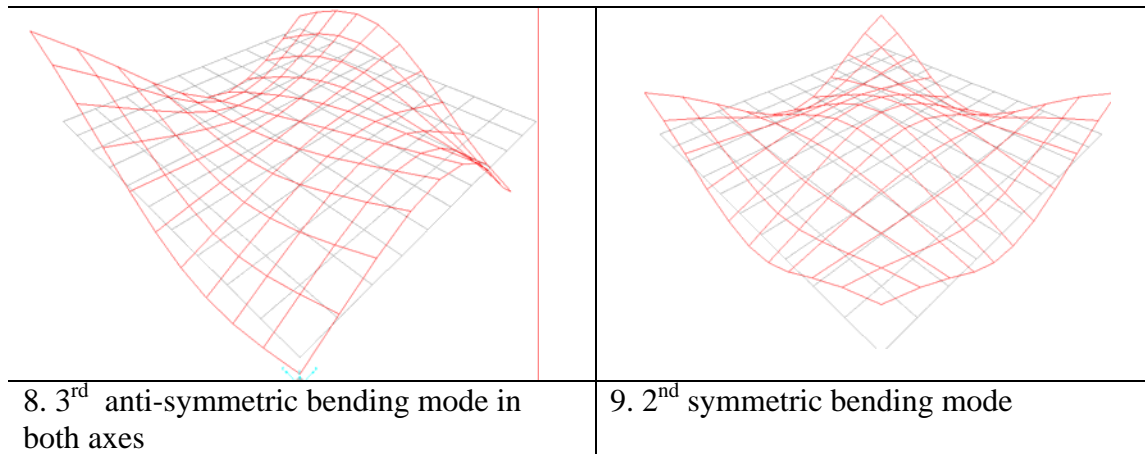


Figure 2.6 The first nine mode shapes of square floating panel (0.52m x 0.52m x 0.015m) estimated by FEM

Table 2.1 Effects of resonances on vibration isolation of floating systems

	Resonance of isolator ω_o	Resonance of slab bending ω_1
Factors	Increase with stiffness of isolator	Increase with bending stiffness of slab
Effect on vibration isolation	Amplification	Degradation
Frequency range	~3-15Hz	~30-200Hz
Notification in current design	Coupling with global mode of supporting structure (i.e. viaduct, building)	Coupling with resonance of isolator
Transmissibility at resonance	$\text{Tr}(\omega_o) = \frac{1}{2\zeta_o}$	$\text{Tr}(\omega_1) = B \frac{R_1}{\zeta_1 \gamma_1^2}$ <p>Where, $\gamma_1 = \frac{\omega_1}{\omega_o}$,</p> <p>B depends on modal mass</p>

Table 2.2 Dimensions and material properties of the testing material

Material	Description	Panel Size(mm) (Length x width x height)	Young's Modulus (x10 ⁹ N/m ²)	Density (kg/m ²)
Cement	Wood fibre chemically treated and mixed with Portland cement, compressed and cured under temperature controlled conditions	520x520x15	6.8	21.4

Table 2.3 Typical boundary conditions and mode shape equations for beam structure

Boundary conditions of beam	λ_r , $r=1, 2, 3\dots$	Mode shape equation $\Psi_r(x) =$	σ_r , $r=1, 2, 3\dots$
Simply-supported	$r\pi$	$\sin\left(\frac{r\pi x}{L}\right)$	
Free-Free	4.7300474 7.85320462 10.9956078	$\cosh\frac{\lambda_r x}{L} + \cos\frac{\lambda_r x}{L} - \sigma_r \left(\sinh\frac{\lambda_r x}{L} + \sin\frac{\lambda_r x}{L}\right)$	0.982502215 1.000777312 0.999966450
Clamped-free	1.87510407 4.69409113 7.85475744	$\cosh\frac{\lambda_r x}{L} - \cos\frac{\lambda_r x}{L} - \sigma_r \left(\sinh\frac{\lambda_r x}{L} - \sin\frac{\lambda_r x}{L}\right)$	0.734095514 1.018467319 0.999224497

Table 2.4 Convergence of 1st bending resonance frequency by Sap 2000

Number of elements	Resonance frequency of 1 st bending mode (Hz)	Percentage of change (%)
5 x 3	118.5	
5 x 9	149.9	20.9
10 x 18	154.1	2.7
20 x 36	155.3	0.8

CHAPTER 3

RAILWAY TRACK DYNAMICS

This Chapter focuses on the source of dynamic force from moving train. The excitation sources due to train-track interaction and the dynamic properties of different components of train and track will be discussed in the first two parts. These properties are important for the understanding of spectral characteristics come from rail traffic and the selection of vibration reduction devices. Finally, the pros and cons of the various types of floating slabs used in rail viaduct are presented.

3.1 INTRODUCTION

When a train runs on railway track, dynamic excitation force is generated because of the irregularities of the wheels/rails or track. The irregularities include wheel/rail roughness, defects and discontinuities of the track etc. The dynamic force may be amplified when the excitation frequency coincides with any of the rail track resonance frequency. The prediction of the excitation sources and the vibration properties of train and track are thus required for the design of suitable vibration isolation devices.

There are numerous researches on the vibration and noise radiation frequency characteristics from rail transit or railroad tunnels. Heckl et al. (1996) suggest that the structure-borne noise transmission from rail traffic is in the frequency range of 40-200Hz and for underground trains the vibration peak is typically in the 40-80Hz range. Morii (1975)

found that the vibration peak of a viaduct structure without ballast mat ranges from 40-60Hz. Thus, the problem of structure-radiated noise is important at the low frequency range up to 200Hz.

In this chapter, the mechanisms of vibration excitation by trains moving on track and the dynamic properties of track which cause low frequency structure-borne noise are introduced. These parameters are useful for the explanation of site vibration measurements in the latter chapters. The propagation of structure-borne sound in ground is not analysed in this dissertation due to a large amount of parameters and empirical data required for reliable predictions.

3.2 SOME VIBRATION GENERATION MECHANISMS

Three types of train-track excitation sources are categorized in this dissertation according to Dahlberg (2003): 1) long wavelength irregularities-300mm or longer wavelength; 2) short wavelength irregularities - around 30-300mm wavelength, and 3) impact load. There are different classifications of long and short wavelength by various authors (e.g. Alias, 1986 & Levy, 1989).

The short wavelength irregularities are usually caused by railhead corrugation which is studied by Sato et al. (2002), and defects on wheel treads when block-braked are used (Nielsen and Johansson, 2000). The full explanation for the reasons of rail corrugation is not yet available. This excitation source may lead to damages on railpads, fastenings and sleepers (Clark et al. 1982).

The impact load can come from the discontinuity of the track, for example, rail joint, switch crossing passage, dipped rail, etc. The dynamic impact force become serious when the

length of joint is in the vicinity of the spacing between bogies of the vehicle (ISO 14837-1:2005).

The rail corrugation usual induces high frequency oscillation (Valdivia, 1988), and the impact load is not deal with in this dissertation, thus there is only some remarks on those. The long wavelength excitation sources are explained in more detail below.

3.2.1 LONG WAVELENGTH IRREGULARITIES

The long wavelength irregularity results in low-frequency excitation on train and track. Two types of typical long wavelength irregularities (300mm or longer) are described in this part (1) geometric irregularities on wheel or track; (2) non-uniform support stiffness of track.

Irregularities in rail may be induced during the manufacturing process; the typical machine roller spacing is around 1.8m (Sharif, 1998). Furthermore, one or several frequencies may be excited on train and track resulting from various wavelength of the out-of-round wheel, which have been studied by Nielsen and Johansson (2000).

The non-uniform support stiffness are attributable to the spacing of rail support of railpads or sleepers and the spacing of wheels as shown in Figure 3.1. A track is stiffer at railpad and softer between two railpads. When the wheel is between two railpads the maximum deflection can be induced in the middle of the track (Figure 3.2). Hussein and Hunt's finding (2006) show that static deflection fluctuates due to wheel moving on the rail with non-uniform stiffness, and thus can induce dynamic forces at the wheel-rail interface, even in the absence of rail roughness. According to ISO 14837-1:2005, the parametric excitation (support passage frequency) f_n is the given by

$$f_n = (v/3.6l_n) \text{ [Hz]} \quad (3.1)$$

Where, v is the train speed in km/h and l_n is the spacing between the support materials. The systematic method to estimate the force at rail-pad support passage frequency is shown in Figure 3.2. Sharif (1998) states that the main source of perceptible vibration from rail trains are the support passage frequency which is usually less than 50Hz.

On the basis of ISO 14837-1:2005, for the low speed train (~80km/h), the primary excitation by train running on the rail should be attributed to the roughness of the wheel/rail (Figure 3.3). The term of roughness here is defined as the defects on wheels or rails and can produce wideband excitation frequency (0-200Hz). Force at the rail pad support passage frequency should be the secondary excitation. For the high speed train (~250km/h), the force at rail-pad and intra-bogie support passage frequency becomes more important factor.

The vibrations may become significant if the dynamic force at support passage frequency coincides with any of the rail track resonance frequency, the natural frequency of a floating slab railway system or the supporting structure. It is well known that the higher the speed of train the larger the dynamic force. Consequently, to maintain the low vibration excitation amplitudes from wheel-rail interaction, dynamic properties of train, track and supporting structure must be analysed.

3.3 DYNAMIC PROPERTIES OF RAIL TRAIN AND TRACK

There is very low natural frequency (~1-5Hz) for the first and second suspension systems, and the resonance of bogie can be filter from the primary suspension. Yau et al. (1999) observed that the rail roughness, stiffer suspension and very high or low stiffness of ballast layer can dramatically deteriorated the riding quality.

The parameters of some important natural frequency are listed in Table 3.1. Regarding floating slab track as showed in Figure 3.4, the wheel-rail pad resonance (mass depends on

unsprung mass and stiffness depends on vertical stiffness of rail pad/resilient plate) is around 30-60Hz. The natural frequency of floating slab (mass depends on slab and stiffness depends on isolator) is 6-20Hz. For the ballast track as shown in Figure 3.5, the wheel-ballast resonance (mass depends on the unsprung mass and stiffness depends on the vertical stiffness of ballast system) is around 50-60Hz. Heckl et al. (1996) analysed the vibration measurement results for rail traffic and found out that the characteristic peak near 50Hz resulted from the resonance of wheel mass and stiffness of track. Thus, the wheel-rail resonance at 50Hz may be close to the sleeper passage frequency (Sharif, 1998).

3.4 SOME PRINCIPLES OF VIBRATION REDUCTION

Intensive vibration isolation devices have been installed in current rail tracks. Ballast and slab tracks are the common methods in rail traffic. The principles of the vibration isolation devices of two types of tracks are similar. Resilient elements installed in the vibration transmission path to reduce vibration transmission, the stiffness of resilient material should be as low as possible to satisfy the maximum rail deflection requirement, and the mass on the soft material should be as heavy as space and cost considerations allow.

The different component of traditional ballast track and the floating slab track in Hong Kong West Rail are shown in Figures 3.4-3.5. For the typical ballast track, the basic vibration isolation mechanism in rail track are that the vibration first is blocked by fastening spring, and then attenuated by the rail pad. The loading is distributed through the sleeper to ballast bed which absorbed vibration by stone friction. The fastening spring and rail pad in ballast track usual have higher stiffness, and thus comparatively the main isolation device is the ballast friction. In some of the ballast tracks, ballast mat are placed at the base of the ballast to absorb the vibration energy. Regarding floating slab track, the vibration is blocked by resilient base

plate (Cologne egg) underneath the rail, and the transmitted vibration attenuated by isolator of floating slab.

Various rail track designs are created in the world to satisfy the safety, low noise and high speed requirements. In the common classification, there are five types of ballast track systems and seven types of slab track systems as shown in Figure 3.6 (ISO 14837-1:2005). Sometimes, the combination of track designs are applied, such as, the floating slab track in the viaduct section of Hong Kong West Rail, combined the design of resilient baseplate and floating track slab (Figure 3.6).

Noise radiated from rail passing through the viaduct (bridge) should be higher since there will be a higher vibration responses of the viaduct itself. Floating slab track design is often chosen in viaduct structure instead of the traditional ballast tracked design because of its lower loading burden. This can lead to lower construction cost of viaduct, and also favourite in rail tunnel resulting in the lower maintenance (Esveld, 2001). There is still a lack of comprehensive site vibration measurement data on rail viaduct section with different floating slab design. This will be conducted in this dissertation, and the analysis of the adverse effects on isolation efficiency of floating systems are based on the excitation resonance from moving loading, resonances of rail track and bending modes of floating slabs. Furthermore, the vibration isolation may be degraded when coupling frequency appears in floating slab and the supporting viaduct structure which will be analysed with experimental tests in Chapter 4. The vibration isolation devices of different length of floating slabs on viaduct section is discussed in detail below.

3.5 FLOATING SLAB TRACKS

In the design of slab track, various lengths of slabs rest on isolators are applied in the world. It is still a crucial design issue.

Floating slab systems are simply classified into three categories in this paper: (1) long slab – the slab length more than 20m ; (2) medium slab – the slab length between 5m to 20m ; and (3) short slab – the slab length around 1m to 5m.

Long floating slab is usually used in tunnels and seldom used on viaduct structures since the track on viaducts will be exposed to weather changes, thermal expansion and contraction. The pros and cons of medium- and short-length floating slabs used in rail viaducts are discussed below.

3.5.1 SHORT-LENGTH FLOATING SLAB

The short-length slab has joints at short intervals. It sits on four rubber isolators with two side rubber isolators to provide more horizontal restraint and safeguard of derailment because of the lower inertia mass of short-length floating slab track compared with medium-length floating slab track.

The isolators cannot be too soft because the short-length floating slabs need to withstand larger static loadings compared with medium-length floating slab. When a train passes on a track, the deflection of rail under each wheel extends only to two slabs (See Figure 3.7). Thus, to avoid excessive static deflection, stiffer isolators should be used, and thus have higher natural frequency of around 14Hz.

The problem of different loadings on a chain of slabs can be dealt with by using rubber isolators with a domed surface, whereby the surface area increases with the loading increase (see Figure 3.8). To increase the isolation performance, resilient base plates (rail pads) can

also be installed between the rail and the slab (see Figure 3.9) to form a two-stage isolation system. Short floating slabs, however, have a lower speed limit compared with the long floating slab due to the larger static deflection. The benefit of mini floating slabs is that it has a higher bending resonance frequency and can also be easily manufactured using the precast method.

3.5.2 MEDIUM-LENGTH FLOATING SLAB

The medium-length slab is a floating slab with joints widely spaced. It can be found in the Chonan station viaduct section on the Korea High Speed Railway line through Seoul and Pusan. This kind of floating slab is relatively heavy, so that no side pad is needed on the slab. The loading can be equally distributed on the floating slab and transmitted to the isolators as shown in Figure 3.7. Hence, softer isolators can be installed and a lower natural frequency of around 6Hz can be achieved. Furthermore, the medium-size floating slab tracks can allow higher speeds (more than 130km/h).

The bending resonance frequency of the slab, however, may lead to degradation of vibration isolation performance. The bending resonance frequency for medium-size floating slabs may be within the dominated structure-borne vibration frequency generated from rail viaduct structures.

3.6 SUMMARY

The dynamic force from train is usually resulting from the irregularities on wheels and rails. The dynamic force at support passage frequencies are also generated from the changing stiffness of track during the wheel moving on track. The vibration may become serious when

the dynamic force at support passage frequency coincides with any of the rail track resonance frequency.

The vibration isolation device of floating slabs on viaduct section can be of short and medium lengths, and they have limitation of noise reduction ability and speed requirement. The bending resonance frequency on floating slab may deteriorate the noise and vibration isolation. The vibration resonances interaction between the viaduct box and floating slab are established in the next Chapter.

REFERENCES

- Alias, J. (1986). Characteristics of wave formation in rails, *Rail International*, Vol 17(11), 17-23.
- Clark, R.A., Dean, P. A., Elkins, J. A. and Newton, S.G. (1982). An investigation into the dynamic effects of railway vehicles running on corrugated rails, *Journal Mechanical Engineering Science*, Vol 24(2), 65-76.
- Dahlberg, T. (2003). *Railway track dynamics - a survey*. Solid Mechanics/IKP, Linköping University SE-581 83 Linköping, Sweden.
- Hamed, E., and Frostigm, Y. (2005). Free vibrations of multi-girder and multi-cell box bridges with transverse deformations effects. *Journal of Sound and Vibration*, 279 (3-5), 699-722.
- Heckl, M., Hayck, G. and Wettschureck, R. (1996). Structure-borne sound and vibration from rail traffic. *Journal of Sound and Vibration*, 193(1), 175–184.
- Esveld, Coenraad. (2001). *Modern Railway Track* (2nd edn), Zaltbommel: MRT-Productions.
- Hinton, E., Özakça, M., Rao., N.V.R. (1995). Free vibration analysis and shape optimization of variable thickness plates, prismatic folded plates and curved shells: Part 1: finite strip formulation. *Journal of Sound and Vibration*, 181(4): 553-566.

Hussein, M.F.M. and Hunt, H.E.M. (2006). Modelling of floating-slab track with discontinuous slab, part 2: response to moving trains. *Journal of Low Frequency Noise, Vibration and Active Control*, 25(2): 111-118.

International Standard, ISO 14837-1:2005(E). Mechanical vibration – Ground-borne noise and vibration arising from rail systems – Part 1: Guidance.

Lévy, D. (1989). Conception d'un système de mesure et d'analyse de l'usure ondulatoire des rails, *Revue Général des Chemins de Fer*, Vol 108, 51-57.

Morii, Takashi. (1975). Development of Shinkansen Vibration-isolation Techniques Structure Laboratory, Railway, Technical Research Institutes J.N.R.

Nielsen, J. C. O. and Johansson, A. (2000). Out-of round railway wheels a literature survey. *Proceedings of the Institution of Mechanical Engineers, Part F, Journal of Rail and Rapid Transit*, Vol 214(F2), 79-91.

Sato, Y., Matsumoto, A. and Knothe, K. (2002). Review on rail corrugation studies. *Wear*, Vol 253(1-2), 130-139.

Shaif, A.K. (1998). Dynamic Performance Investigation of Base Isolated Structures. PhD thesis, University of Pretoria, South Africa.

Valdivia, A.R. (1988). A linear dynamic wear model to explain the initiating mechanism of corrugation, In M. Apetaur, (Editor), Proceedings 10th IAVSD-Symposium The Dynamics of Vehicles on Roads and on Tracks, held in Prague August 24-28, 1987. Swets & Zeitlinger B V, Lisse, 493-496.

Yau, J.D., Yang, Y.B., Kuo, S.R. (1999). "Impact response of high speed rail bridge and riding comfort of rail cars", Journal of Engineering Structures, 21, 836-844.

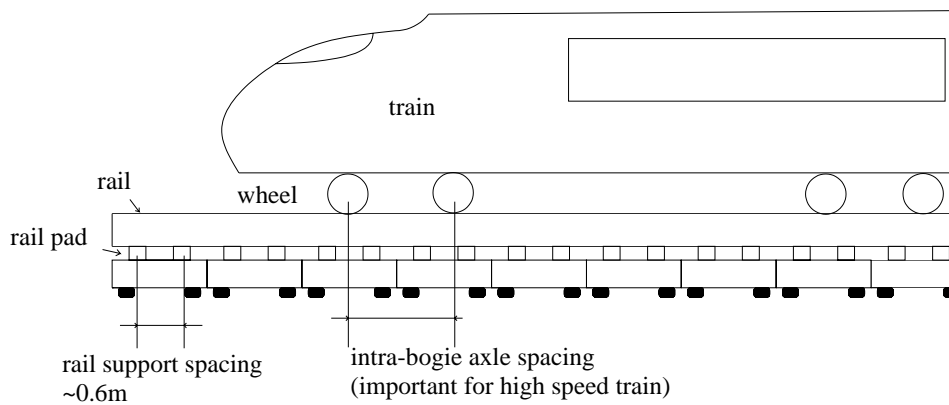


Figure 3.1 Description of the excitation source of parametric excitation at passage support frequency

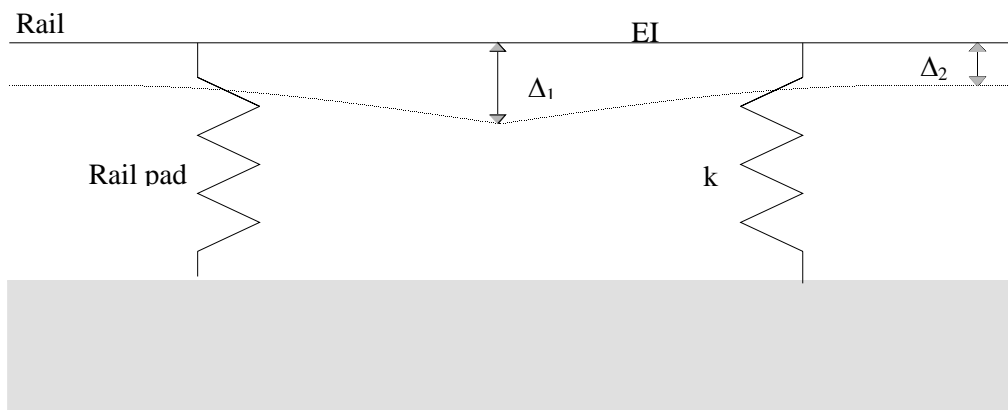


Figure 3.2 The sketch of the estimation on the force of rail-pad support passage frequency. Δ_2 is the static deflection due to dead load. Fluctuation in static deflection = $\Delta_1 - \Delta_2$

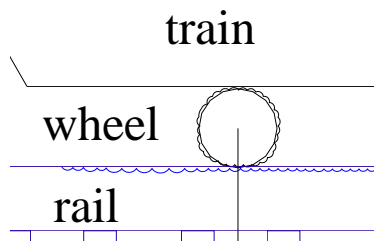


Figure 3.3 Description of the excitation source due to roughness of rail and wheel

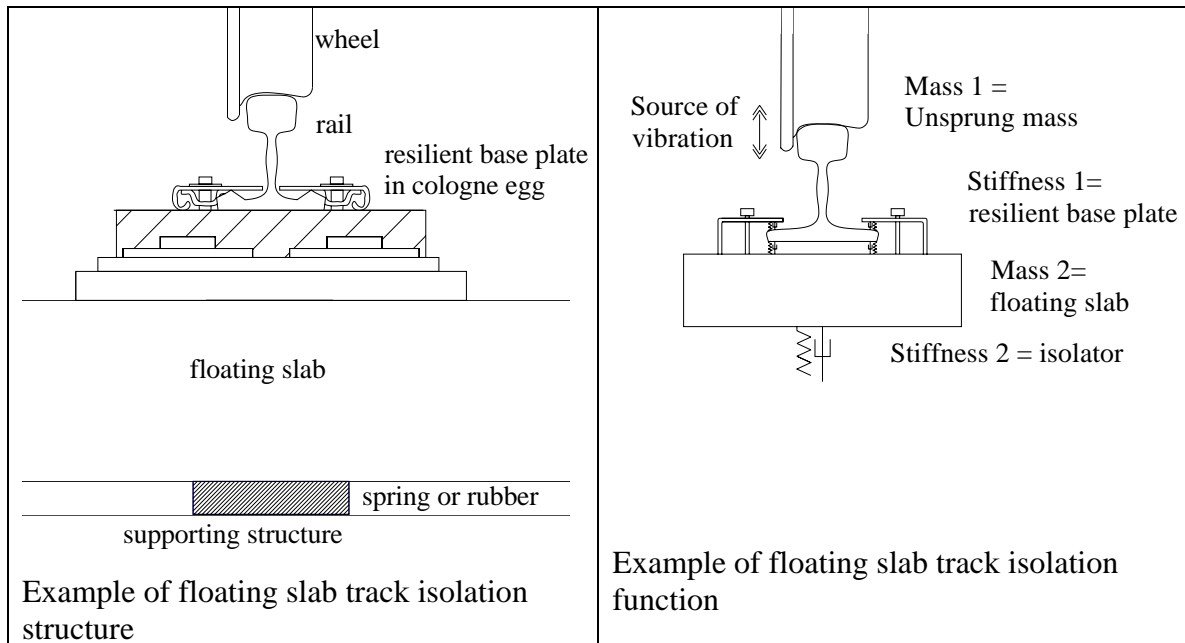


Figure 3.4 Basic structure isolation function of floating slab track

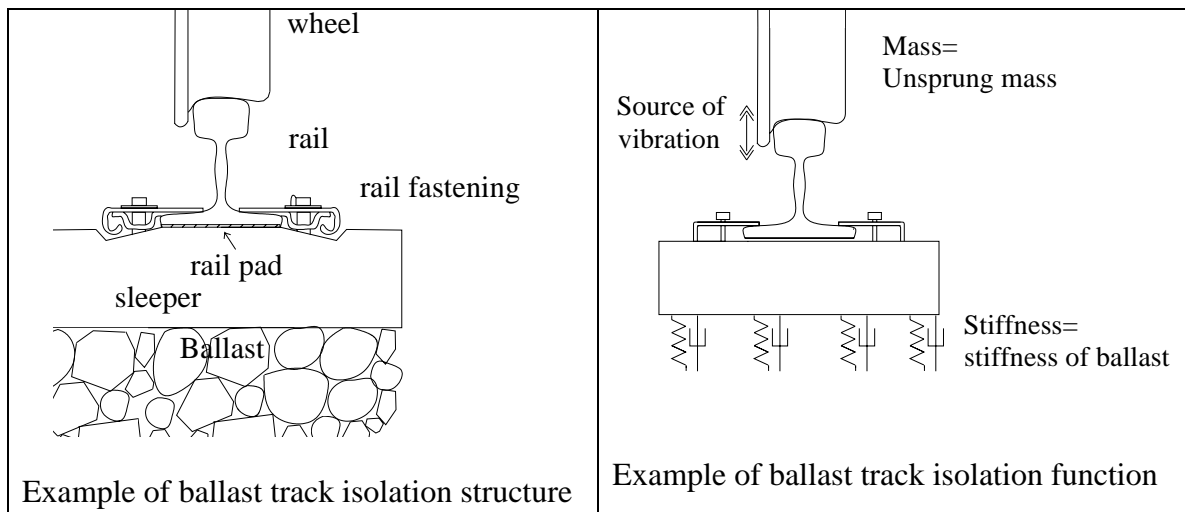
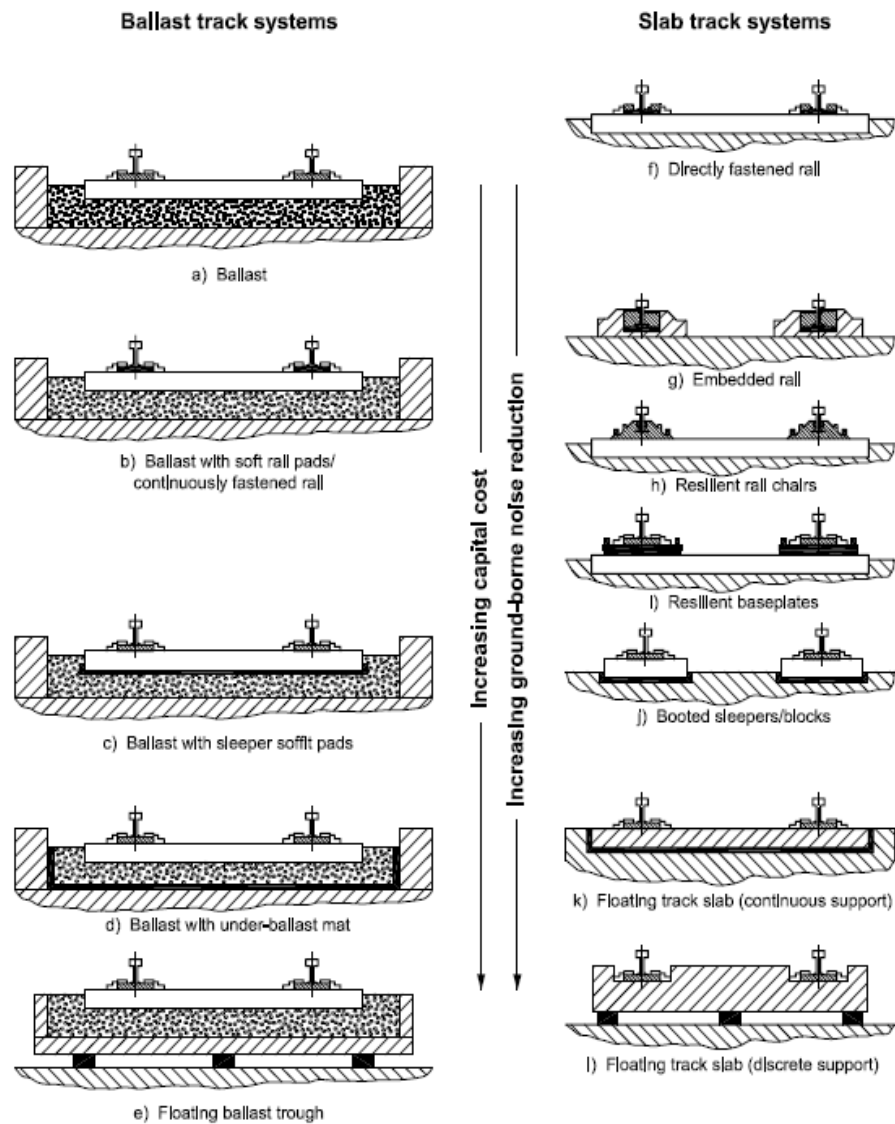


Figure 3.5 Basic structure isolation function of ballast track



NOTE 1 Main resilient elements are shown in black.

NOTE 2 The slab track systems g), h), i), j) could be designed to be as effective as each other in terms of ground-borne noise with little cost difference.

Figure 3.6 Schematic of generic track form layouts (Source from ISO 14837-1:2005)

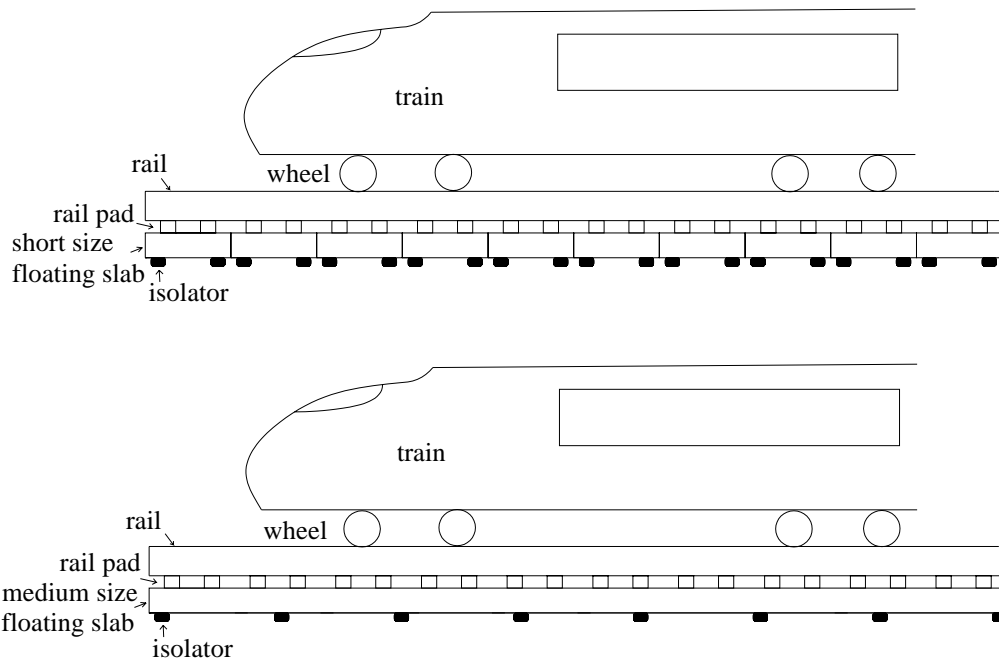


Figure 3.7 Loading distribution description of short size and medium size of floating slabs

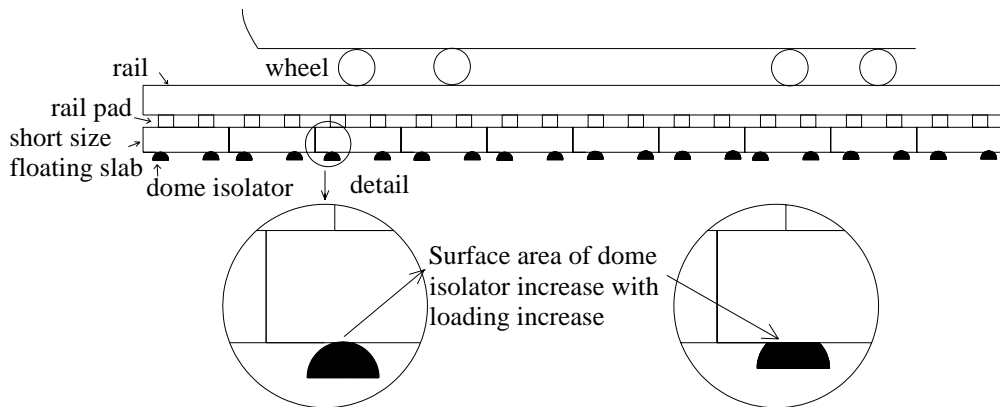


Figure 3.8 Dome isolator used in short size floating slab

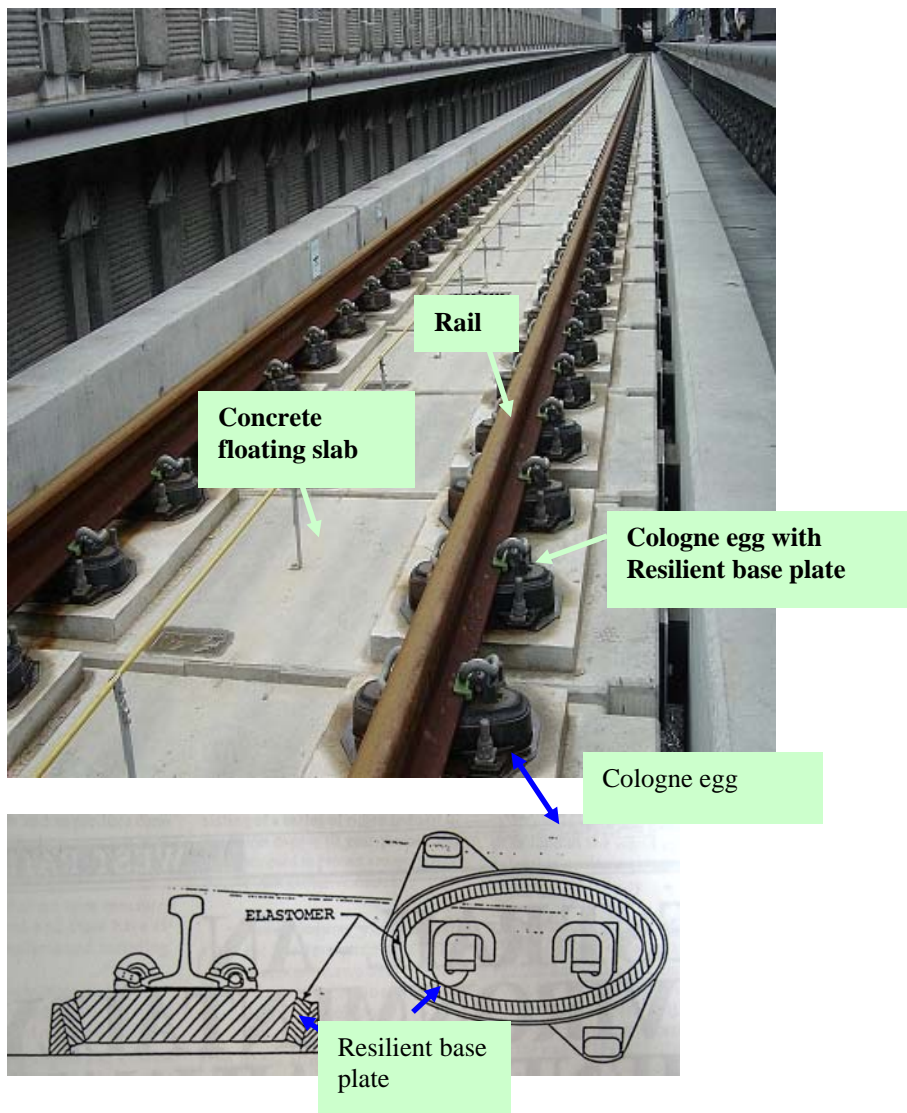


Figure 3.9 Resilient base plate installed between the rail and floating slab

Table 3.1 Parameters defined for rail track resonance frequencies

Resonance name		Stiffness	Mass
Floating slab rigid body resonance		Stiffness of isolator	Mass of slab
Bending resonance of slab		Bending stiffness of slab	Bending modal mass
Wheel-track resonance frequency	Wheel-rail pad resonance	Vertical stiffness of rail pad	Unsprung mass (mass of supported wheel and rail)
	Wheel-ballast resonance	Vertical stiffness of ballast	Unsprung mass (mass of supported wheel and rail)

Chapter 4

BENDING RESONANCES OF FLOATING SLAB AND SUPPORTING CONCRETE BOX STRUCTURE

This Chapter mainly investigates the effects of bending resonances of floating slab and supporting concrete box on vibration isolation performance. The similarities and differences in vibration behaviors between long (30m) and short (1.5m) lengths of concrete box structures with the same cross-section are analyzed with FEM.

A short concrete hollow box is constructed to verify the theoretical vibration results, and six combinations of floating slabs are installed on the box to identify the vibration and structure-borne sound control by experimental method. The coupling modes of floating slab and supporting box structure will also be established.

4.1 INTRODUCTION

Concrete hollow box structures provide a broad range of structural applications. These structures are popular in civil structure on account of their high stiffness to weight ratio and the high efficiency of supporting combinations of static and/or dynamic loads. Dynamic structure response investigation requires comprehensive modal characteristics analysis with experimental or mathematical methods. Box structure can be applied to support a variety of heavy objects, such as, machinery on a concrete table, a rail support in the form of a concrete box girder viaduct, as well as humans and machinery in apartment buildings (Figure 4.1).

As mentioned in Chapter 1, structure-radiated noise should be contributed to the local modes of viaduct structure (Southward and Cooper, 2002), and thus vibration modes of box structure should therefore be investigated for a better railway viaduct design.

Hinton et al. (1995) and Hamed and Frostig (2005) developed accurate mathematical methods to identify the free vibration behavior of box structures, and the bending and distortion local modes of a long (about 30m) cell box were also identified. Lee and Wooh (2004) used finite element method to analyze mode shapes of 20m and 10m cantilever beam structures; it was shown that the local modes are dominant for the shorter beam.

In practice, various lengths of box structure can be constructed for building an apartment, supporting table and viaduct box. Two different lengths of concrete box structures are studied with theoretical method to analyze the similarities and differences in mode shapes and resonance frequencies, and to examine the critical vibration modes. This will be presented in Section 4.2 in this Chapter.

When vibration appears in a concrete box structure, floating slab is one of the conventional systems to attenuate the vibration transmission to the surroundings. The noise and vibration control performance depends not only on the design of the concrete box itself, but also on the floating slabs and isolators. For example, Wilson (2004) states that one of the design requirements for an isolated theater located at the fifth level in an existing relatively lightweight steel frame structure is that the bending resonance frequency of the theater floor slab should be higher than 15Hz to avoid coupling bending modes of the theater floor slab and the supporting structures.

There have been various studies to analyze the vibration isolation behavior of floating slabs in laboratory experiments. Regarding machine operation, Mead (1998) suggests varying methods for minimizing the vibration input from a vibrating machine by controlling the bending resonance of the supporting structure. For train operation, Kawaharazuka et al.

(1996) constructed a full-scale concrete slab model to study the vibration response of a railway with floating slabs. They noted that the vibration isolation efficiency was degraded by the bending resonant frequencies at 63Hz. Furthermore, Cox et al. (2006) constructed a floating slab model to conduct rail receptance measurement; an interesting feature found was that peaks in the response at 40–50Hz represent the response at the bending resonances of the floating slab.

The experimental investigation of vibration and noise radiation of three different sizes of floating slabs and isolators at two different parameters of stiffness on the short box structure will be presented. It is noted that studies on coupling resonance of slab and supporting box structure have not been found in any published literature to date.

4.2 THEORETICAL VIBRATION ANALYSIS OF TWO DIFFERENT LENGTHS OF BOX STRUCTURES

4.2.1 DEFINITION OF LOCAL MODE AND GLOBAL MODE OF HOLLOW BOX STRUCTURE

In this dissertation, pure local modes means that there is deformation present on the cross-section of the box structure, whereas pure global modes means that there is no deformation present on the cross-section of the box. There is a specific name for each simple vibration shape (Figures 4.2a-4.2g). The cross-section shape of the global rotation mode (Figure 4.2b) and global torsion mode (Figure 4.2c) are similar. However, the torsion mode possesses a different angle of rotation along the x-axis, whereas the rotation mode possesses the same angle of rotation along the x-axis. The local distortion (edge) mode (Figure 4.2e), local center mode (Figure 4.2f) and local combined mode (Figure 4.2g) are defined with the movement

situation of the top panel of the box structure. Edge mode means that the center of the top panel is fixed but the edge (supported by web) can move. Center mode means the center of the top panel can move but the edge (supported by web) is fixed. Combined mode means that both the center and edge of the top panel can move. In many cases, there are complex vibration shapes that combine different simple mode shapes including global mode and local mode. The resonance frequencies of local modes are usually higher than those of the global modes which structural engineers generally pay more attention to.

4.2.2 THEORETICAL ANALYSIS

Two concrete boxes (1.5m and 30m lengths) were developed by FEM using Sap 2000 v.8. The similarities and differences of point mobility, resonance frequencies and mode shapes were analysed.

The theoretical model dimensions and physical properties of the concrete boxes are shown in Figure 4.3. Their cross-section is the same but the only difference is the length in the x-direction. The models were developed with shell elements; the 1.8m width of the section in the y-direction was divided into four elements and the 2.3m height in the z-direction was divided into five elements. The models took into consideration the bending in the x-y-z dimensions. Both free vibration mode shapes and force vibration of point mobility were identified. An input force in the frequency range of 30-200Hz was used to examine the major local modes. The force was applied along the top edge of the boxes (Figure 4.3). The averaged point mobility of long and short boxes are presented in Figures 4.4 and 4.5 respectively.

4.2.3 THE SIMILARITIES OF SHORT AND LONG BOXES

The higher the point mobility peaks the lower the energy dissipation from damping, thus the larger the vibration magnitude that results. For the short concrete box structure, the point mobility peaks are present at 42Hz, 58Hz and 153Hz. The similar point mobility peaks and mode shapes can also be observed at 44Hz and 154Hz for long box structures. The cross-section mode shapes for short box at 42Hz and long box at 44Hz both had local distortion (edge) mode (Figures 4.6a and 4.6c). Short box at 153Hz and long box at 154Hz were also the same with local combined mode (Figures 4.6b and 4.6d).

4.2.4 THE DIFFERENCES BETWEEN SHORT AND LONG BOXES

For the short box model, the bending mode resonant frequencies in a short span in the x-direction should be made higher meaning that the local modes can be dominated, while vibration modes of the long box should be controlled by both local and global modes. There are many varieties of mobility peaks appearing with the long box, thus their mode shapes should be more complex.

The higher order modes of local distortion together with minor global torsion mode are marked with (7a), (7b) and (7c) in Figure 4.4 and are shown in Figures 4.7a-4.7c; the higher order modes of local combined bending (edge and center) mode together with minor 1st global bending mode shapes marked with (8) are shown in Figure 4.8. Furthermore, the higher order modes of global torsion mode shapes marked with (9a), (9b) and (9c) in Figure 4.4 are shown in Figures 4.9a-4.9c, and finally the higher order modes of global bending mode together with minor local bending combined (edge and center) mode are marked with (10a), (10b) and (10c) in Figure 4.4 and are shown in Figures 4.10 a-4.10c. The mode shapes and the corresponding

resonance frequencies presented in Figures 4.7-4.10 cannot be identified in the short box structure.

The vibration at 58Hz (Figure. 4.11a) of the short concrete box is a very special mode of vibration. From the top view, the top panel and bottom panel are rotating in the opposite direction, there are minor deformations. From the side view, the front panel and back panel are also rotating in the opposite direction, there are minor deformations. From the cross-section view, the front and back section is deforming in the opposite direction (detail in Figure 4.11b). There is no similar vibration mode at around 58Hz for the long concrete box.

4.2.5 ANALYSIS OF THE MAJOR LOCAL MODES

Critical structure-borne noise radiation should be emitted at frequencies higher than the coincidence frequency of the concrete box. The coincidence frequency of the box model is calculated to be 100Hz according to the Equation A.7 of Appendix A. Thus, it is important that the long concrete box has a local combined bending (edge and center) mode together with minor global bending mode shapes at 154Hz which can also be identified with the short box structure that has a local combined bending (edge and center) mode at 153Hz. Hence, the local modes at around 153Hz, which higher than coincidence frequency are significant structure-borne noise radiators.

In the frequency range of 30-100Hz, both of the large peaks at 42Hz for short box and 44Hz for long box can be observed in Figures 4.4 and 4.5, and they possess the same local distortion (edge) mode. The other lower mobility peaks found with the long box are the pure global modes as well as the local and higher order global modes along x-direction. Hence, the local modes which contribute significantly to the vibration response of short and long box structures are the distortion and combined bending modes at around 42Hz and 153Hz. The

extra peak at 58Hz for the short concrete box is a special vibration mode that cannot be found in the long box.

4.3 EXPERIMENTAL VIBRATION ANALYSIS OF SHORT CONCRETE BOX

A 1.5m short box was constructed to identify the important local modes and the effect of vibration and noise reduction of different floating slabs and isolators. The point mobility and the mode shapes of the short box were measured to verify the theoretical results in Section 4.2, thus the effectiveness of the vibration reduction of the floating slabs can be further studied in the following sections.

4.3.1 EXPERIMENTAL SETUP

Figure 4.12 shows the experimental setup of the short concrete box. The concrete box dimensions and material properties were constructed according to the short concrete box design in Figure 4.3. Soft rubber pads were placed near four edges under the concrete box model.

Impact force was created by dropping a 3kg steel ball, from a height of 0.57m with five impacts per measurement. Resilient pad was placed under the impact point of the ball to control the duration of impact in order to generate flat-force spectrum-covered interested low frequency. The impact force was measured via an HBM force transducer with bridge amplifier, studded on the structure. The vibration responses were measured via a PCB ICP accelerometer which was mounted with a magnet on the model. The input force and output acceleration signals were processed by the B&K PULSE analyzer. The acceleration signal

was under pre-processing integration to velocity before the frequency response function (FRF) analysis. The analyzer worked in real-time mode from 30-200Hz with 1Hz resolution. Lu et al. (2002) confirms that the local mode of a concrete frame structure is usually at a higher frequency of around 60-70Hz.

For the point mobility measurement, the excitation edge point on the top of the model was recorded. The FRFs (Velocity/ Force) were identified.

For the mode shape measurement, edge excitation forces with velocity response along the box model surfaces were measured. The value of the real part of the FRFs (Velocity/Force) at resonance is proportional to the modal displacement and therefore the mode shapes can be established (Ewins, 1995).

4.3.2 EXPERIMENTAL VIBRATION RESULTS OF SHORT CONCRETE BOX

The point mobility of the short box is shown in Figure 4.13a. The peaks are at 42Hz, 59Hz and 153Hz and the resonance frequencies agree well with the theoretical point mobility in Figure 4.5. The corresponding mode shapes in Figure 4.13b are the same as the theoretical finding. Thus, the concrete box was applied to investigate the vibration isolation effect on the installation of different floating slabs.

4.4 EXPERIMENTAL VIBRATION ANALYSIS OF FLOATING SLABS WITH SUPPORTING BOX STRUCTURE

The mode shapes and the mobility measurement are the important parameters for the first view of the supporting box structure design. Based on the above results, there are two

significant local modes with short concrete box structure at 42Hz and 153Hz. According to the relative magnitude of point mobility of the concrete box, the lower peak at 153Hz indicates heavier damping to dissipate the input energy and leads to lower vibration amplitude than the higher point mobility peak at 42Hz. In spite of the lower vibration magnitude at 153Hz, the radiated structure-borne noise may be higher resulting from the effect of coincidence frequency of the concrete box at 100Hz.

Three different sizes of floating slabs and two different parameters of stiffness of isolators were designed to examine the effects of resonances on the floating slab and concrete box on vibration and structure-borne noise reduction performance.

4.4.1 FLOATING SLAB AND ISOLATOR DESIGNS

The Equation 2.6 in Chapter 2 of beam natural bending frequencies was applied to estimate the bending resonance frequency in y and x directions in the initial design stage of the floating slab. The floating slab can be estimated as a free-free supported beam, and thus λ is equal to 4.73 for the first bending resonance frequency.

There were six combinations of floating slab systems in this experimental analysis; three pieces of floating slabs of the same weight (621kg) with different sizes and two types of isolators with different parameters of stiffness. One type of isolator named A had a tuned natural frequency of 14Hz. The other harder isolator B had a 23Hz vertical resonance frequency. Isolator B may have been harder because of the heavy weight of the supporting machine or the hardening effect after aging (Cui and Chew, 2000).

The different sizes of the floating slabs were designed to have different first bending mode resonances in order to investigate bending vibration effects of floating slabs on concrete box vibrations. As shown in Table 4.1, there were three types of floating slabs marked T1, T2 and

T3. The designed bending mode for the T1 floating slab was at 157Hz which was close to that of the box structure. T2 had no coupling modes with the concrete box and the final type T3 had a bending mode at 105Hz in the y-direction and a bending mode at 151Hz in the x-direction near the local distortion mode of the short box structure at 153Hz.

The natural frequency, weight and the designed bending resonances in both directions of the six floating slabs are listed in Table 4.1, with different combinations of floating slabs marked as T1A, T2A, T3A and T1B, T2B, T3B. A and B denote the two types of isolators.

4.4.2 MODE SHAPES AND RESONANCE FREQUENCIES OF FLOATING SLABS

The mode shapes and corresponding resonance frequencies of the six combinations of floating slabs were found experimentally with the same technique as short box vibration analysis. The measured resonance modes and the corresponding resonance frequencies are listed in Table 4.2. The measured vertical resonance frequency was around 13-14Hz for type A, and the bending resonance frequencies in the x- and y-directions for different sizes of floating slab were similar to the design results listed in Table 4.1 using Equation 2.6. The three dimensional mode shapes for rectangular floating panel can refer to Figure 2.5 in Chapter 2.

The 3kg steel ball was excited with 0.57m height for 5 impacts per measure on the top edge of the box or the top edge of the floating slabs. The vibration response measurement location is marked in Figure 4.14. This point can identify the direct vibration transmission (force transmissibility) through vibration isolation to the box structure.

4.4.3 FLOATING SLAB WITH ISOLATOR A

The vibration responses of concrete box with and without floating slabs T1A, T2A and T3A are shown in Figures 4.15a-4.15c. Those isolation systems have tuned resonance frequency at around 14Hz. However, the vibration attenuation was low at around 43Hz due to the distortion (edge) mode of the concrete box structure.

For the local combined mode at 153Hz in the concrete box, the effect on floating slab vibration isolation was lower (see Figure 4.15b). The vibration isolation performance of T2A was the best in the three cases because of the uncoupled bending resonance of the floating slab at 310Hz and the concrete box structure at 153Hz. For slabs T1A and T3A there were similar vibration modes at round 153Hz with the concrete box structure. The detrimental effects on vibration reduction can be observed in Figures 4.15a and 4.15c.

For the floating slab T3A design, there was bending resonance at around 102Hz which did not exist in the concrete box. However, the vibration response in Figure 4.15c shows that the vibration isolation performance of the floating slab had a significant degrade at around 102Hz.

4.4.4 FLOATING SLAB WITH ISOLATOR B

The rigid body vibration of yaw and roll modes were around 40Hz (see Table 4.2) and the mode shape was similar to the distortion mode of the concrete box. The coupled distortion mode of the concrete box and roll or yaw modes of the floating slab (Figure 2.5 in Chapter 2) could be observed at around 40Hz; the vibration response frequencies of the concrete box changed to 37Hz and 45Hz and the vibration was amplified (Figures 4.15d-4.15f). The bending modes of the floating slab mainly depend on the material properties of the concrete slab. Thus the bending modes of T1A, T2A and T3A were similar to the bending modes of T1B, T2B and T3B. The bending vibration effects of floating slab on the concrete box were

similar to the A set floating slabs, but the vibration isolation performance was further degraded because of the higher natural frequency of the isolator B.

In summary, the coupling resonance can appear when the local distortion (edge) mode frequency is closed to the rigid body rotation modes of floating slabs, and there is vibration amplification to the concrete box at this coupling mode. Furthermore, the bending modes at either the concrete box or floating slab can deteriorate the vibration isolation performance of the floating slab. The coupling vibration at around 43Hz and 153Hz are significant due to the similarity of the movement positions in the mode shapes (Figure 4.15g.)

4.5 EXPERIMENTAL STRUCTURE-BORNE NOISE ANALYSIS OF FLOATING SLABS WITH SUPPORTING BOX STRUCTURE

The structure-borne noise was measured for the six types of floating slabs. The structure-borne noise transmission mainly came from the bottom of the concrete box. A B&K microphone was employed to measure this from 0.5m below the bottom surface of the box structure (Figure 4.16). Since the microphone was in close proximity to this surface, the structure-radiated sound acted as a plane wave, furthermore, the two web panels can be a barrier to minimize the sound come from impact source and slab vibration.

For the structure-borne sound measurement for the concrete box only, the highest noise was at around 160Hz in one third octave band which was above the coincidence frequency of the concrete box at 100Hz (Figures 4.17a-4.17f).

4.5.1 FLOATING SLAB WITH ISOLATOR A

The measured levels were averaged at 3 points on each measurement and the sound pressure responses of the concrete box with and without floating slab T1A; T2A and T3A are shown in Figures 4.17a-4.17c. The structure-borne sound attenuation performance at around 43Hz is low; this should be due to the distortion (edge) mode of the concrete box at 40Hz band. The best structure-borne sound attenuation performance came from the T2A floating slab; there was no coupling of bending mode frequency at 308Hz with the concrete box. There was low noise level at 160Hz band, and therefore the noise at 40Hz band became important since the low frequency vibration attenuation for the floating system was more difficult.

Slabs T1A and T3A have a bending mode at around 153Hz which was near the local combined mode of the concrete box and this led to unfavorable effects on the structure-borne noise reduction of the floating slab (Figures 4.17a and 4.17c). For slab T3A, there was a bending mode at around 100Hz. The structure-borne sound reduction was also degraded at 100Hz in one third octave band.

4.5.2 FLOATING SLAB WITH ISOLATOR B

For the floating slab with isolator B, the sound pressure responses are shown in Figures 4.17d-4.17f. It was obvious that the structure-borne sound increased at around the 40Hz band resulting from the coupled distortion (edge) mode of the concrete box and rigid body rotation modes of the floating slab. This agrees well with the vibration measurement results and showed that the vibration was amplified at around 40Hz. The structure-borne noise due to the bending modes of the B set floating slabs on the concrete box is similar to the A set floating

slabs, but the structure-borne sound attenuation performance was further deteriorated and even amplified due to the higher natural frequency at around 23Hz.

4.5.3 THE OPTIMUM FLOATING SLAB

The summary of the sound and vibration reduction of six combinations of floating systems is listed in Table 4.3. It should be noted that a larger size and higher stiffness of support by the isolator is required for the safe operation of machines or vehicles on the box structure, whereas the best noise and vibration attenuation is achieved by the T2A floating system with lower stiffness and shorter size.

4.6 SUMMARY

From the modal analysis of the two concrete box structures, the two major local modes are identified as the distortion mode and combined bending mode.

Based on the experimental analysis of the floating slabs and box structure, the resonance modes resulting from either the concrete box or floating slab should produce adverse effects on the vibration reduction of the floating systems. The coupling modes at 43Hz and 153Hz of the floating slab and supporting box structure are critical because of the similarity of movement locations of the mode shapes (Figure 4.15g).

The local distortion mode at around 43Hz is not a significant sound radiator because of the mode shape and the low frequency, whereas the local combined mode at around 153Hz is an efficient sound radiator. However, the noise at around 153Hz is comparatively easier to attenuate, and the noise at around 43Hz may become critical for the concrete box with the floating slab. Furthermore, the harder isolator can further degrade the vibration and sound attenuation performance of the floating system. The resonance of rotation mode (rolls or yaw

mode) of the floating system and distortion (edge) mode of the box structure at around 43Hz may be dynamically coupled. In this case, the vibration peak can be split into two peak resonances and vibration magnitude may be amplified. Therefore, the optimum noise and vibration reduction can be achieved by a floating slab with low isolator resonance of 14Hz and high bending resonance of 310Hz.

REFERENCES

- Cox, S.J., Wang, A., Morison, C., Carels, P., Kelly, R. and Bewes, O.G. (2006). A test rig to investigate slab track structures for controlling ground vibration. *Journal of Sound and Vibration*, 293(3–5), 901–909.
- Cui, F., and Chew, C.H. (2000). The effectiveness of floating slab track system, Part I. Receptance method. *Applied Acoustics*, 61:441-453.
- Ewins, D.J. (1995). *Modal Testing- Theory and Practice*. Taunton, England: Research Studies Press.
- Kawaharazuka, T., Hiramatsu, T., Ohkawa, H. and Koyasu, M. (1996). Experimental study on vibration reduction by isolated railway. *Internoise*, 1549–1552.
- Hamed, E. and Frostig, Y. (2005). Free vibrations of multi-girder and multi-cell box bridges with transverse deformations effects. *Journal of Sound and Vibration*, 279 (3-5), 699-722.
- Hinton, E., Özakça, M. and Rao, N.V.R. (1995). Free vibration analysis and shape optimization of variable thickness plates, prismatic folded plates and curved shells: Part 1: finite strip formulation. *Journal of Sound and Vibration*, 181(4): 553-566.
- Lee, S.Y. and Wooh, S.C. (2004). Finite element vibration analysis of composite box structures using the high order plate theory. *Journal of Sound and Vibration*, 277(4-5), 801-814.
- Lu, Y., Hao, H. and Ma, G. (2002). Experimental investigation of structural response to

generalized ground shock excitation. *Experimental Mechanics*, 42(3): 261-271. Hong Kong Engineer.

Mead, D. J. (1998). *Passive vibration control*. Chichester; New York: Wiley.

Southward, N.J. and Cooper, J.H. (January 2002). The alternative design of the West Rail Viaducts . Hong Kong Engineer On Line, Cover Story.

Wilson, G.P. (2004). Isolation of the Jazz @ Lincoln Center Performance and Education Concert Theater, Rose Theater, Proceedings of Inter-noise.

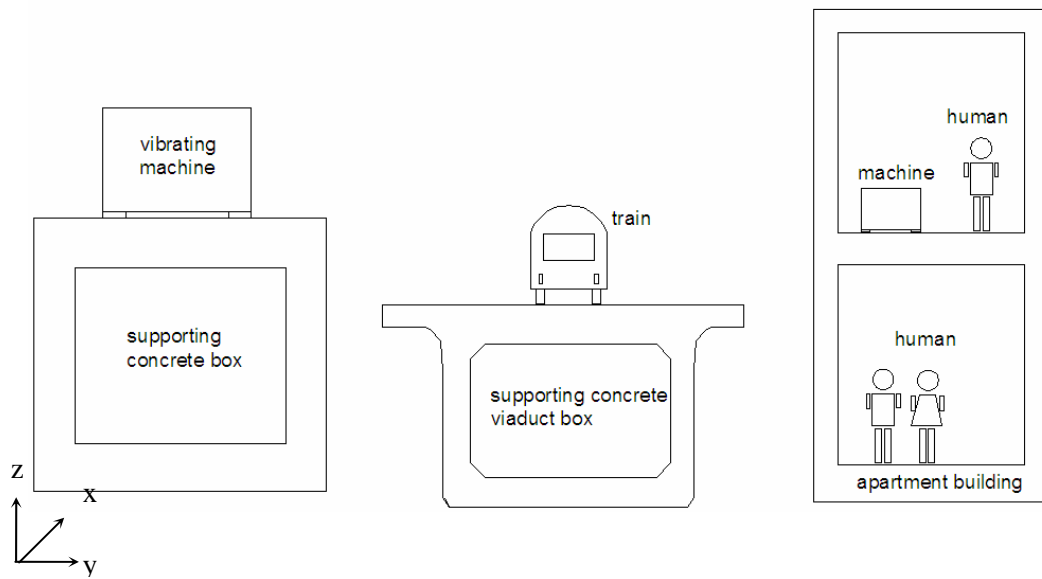


Figure 4.1 The applications of concrete box structure (not to scale)

Global translation mode	
Front view (cross-section) from left	Top view
Front view (cross-section) from right	Side view

Figure 4.2a Global translation mode shape of box structure

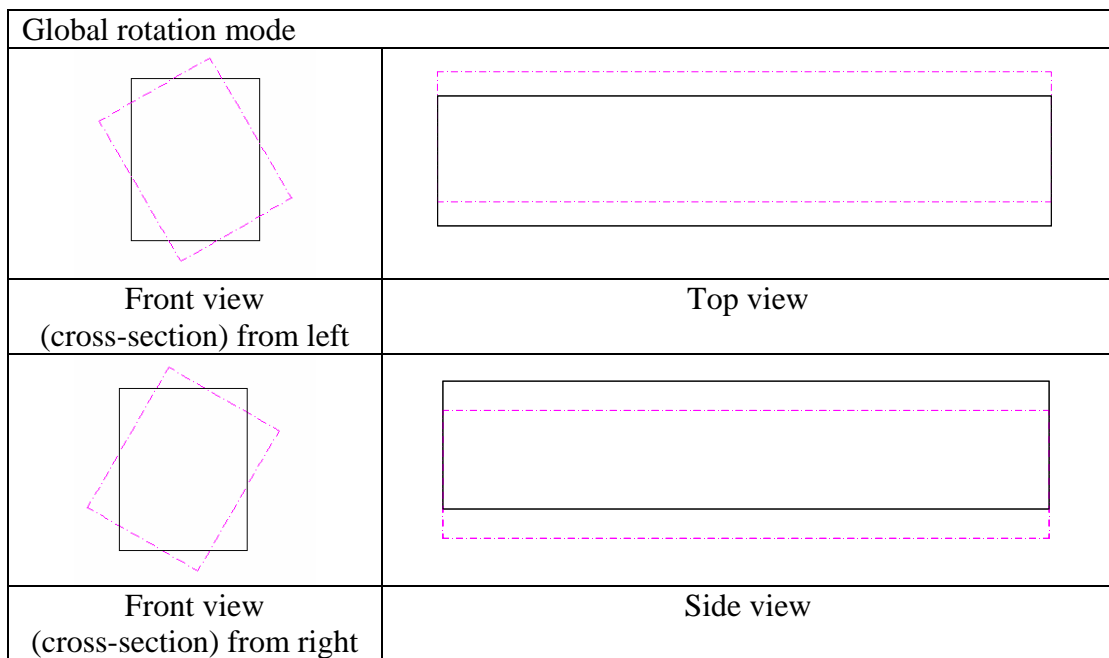


Figure 4.2b Global rotation mode shape of box structure

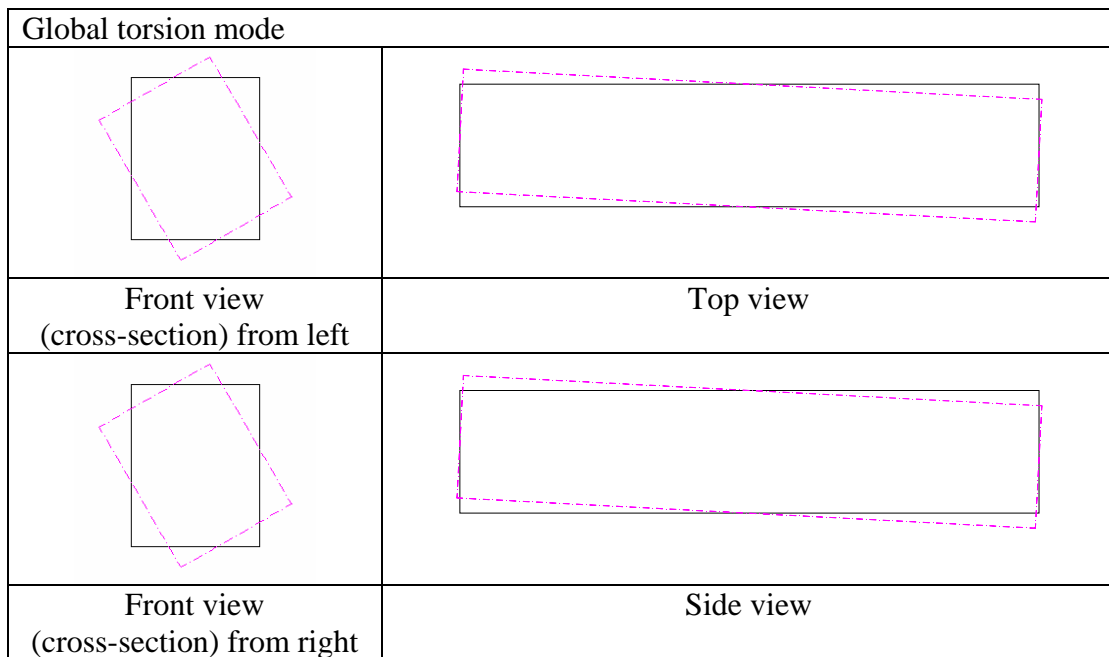


Figure 4.2c Global torsion mode shape of box structure

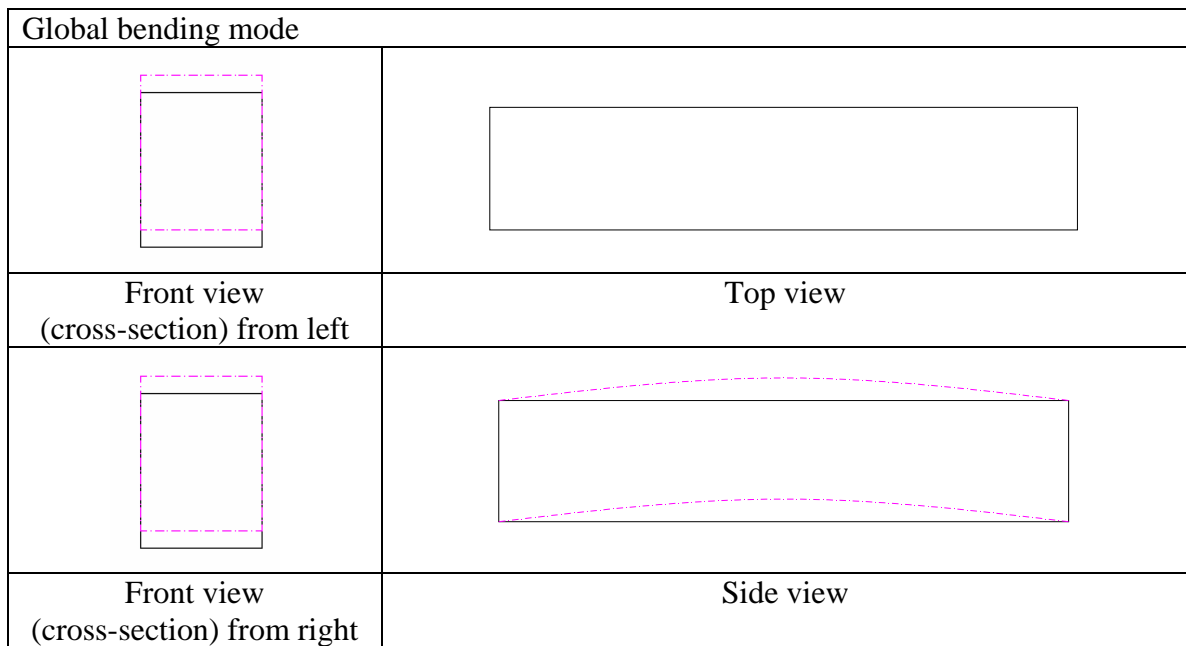


Figure 4.2d Global bending mode shape of box structure

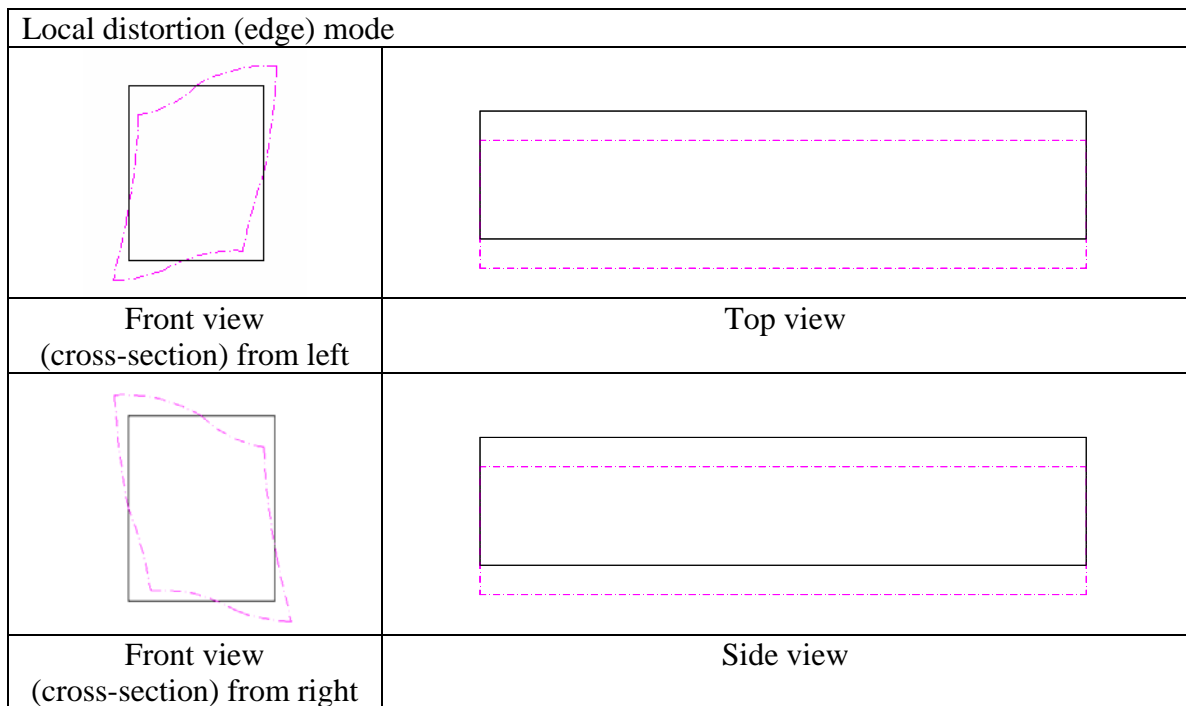


Figure 4.2e Local distortion (edge) mode shape of box structure

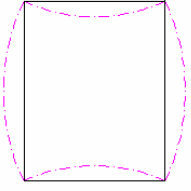
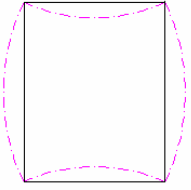
Local center bending mode	
	
Front view (cross-section) from left	Top view
	
Front view (cross-section) from right	Side view

Figure 4.2f Local center mode shape of box structure

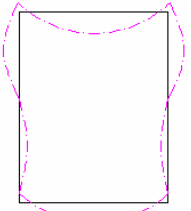
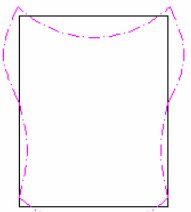
Local combined (edge and center) bending mode	
	
Front view (cross-section) from left	Top view
	
Front view (cross-section) from right	Side view

Figure 4.2g Local combined (edge and center) mode shape of box structure

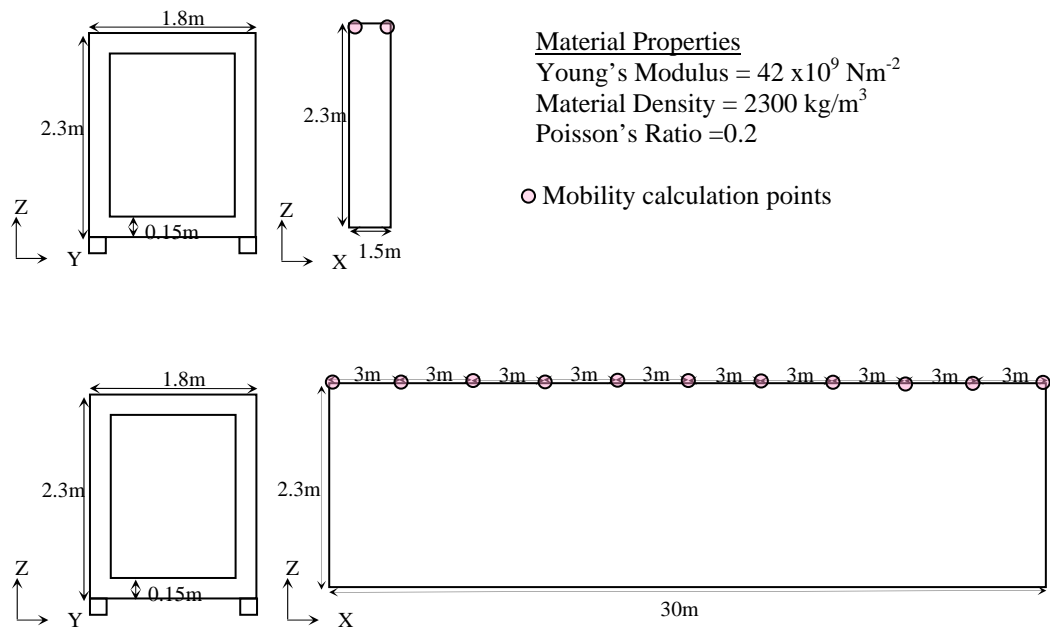


Figure 4.3 Dimensions and physical properties of short and long concrete box models (not to scale)

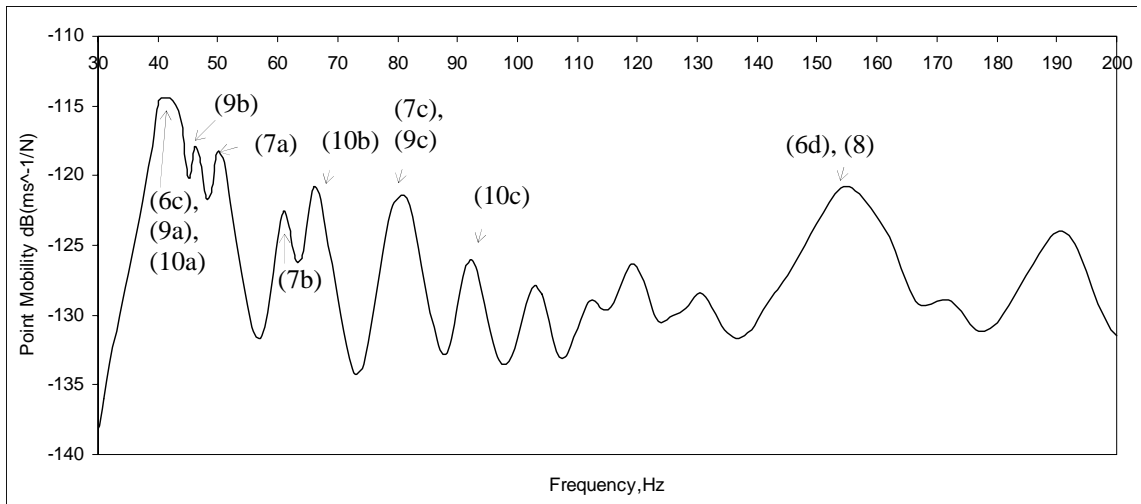


Figure 4.4 Average mobility results of 30m (x-direction) concrete box model

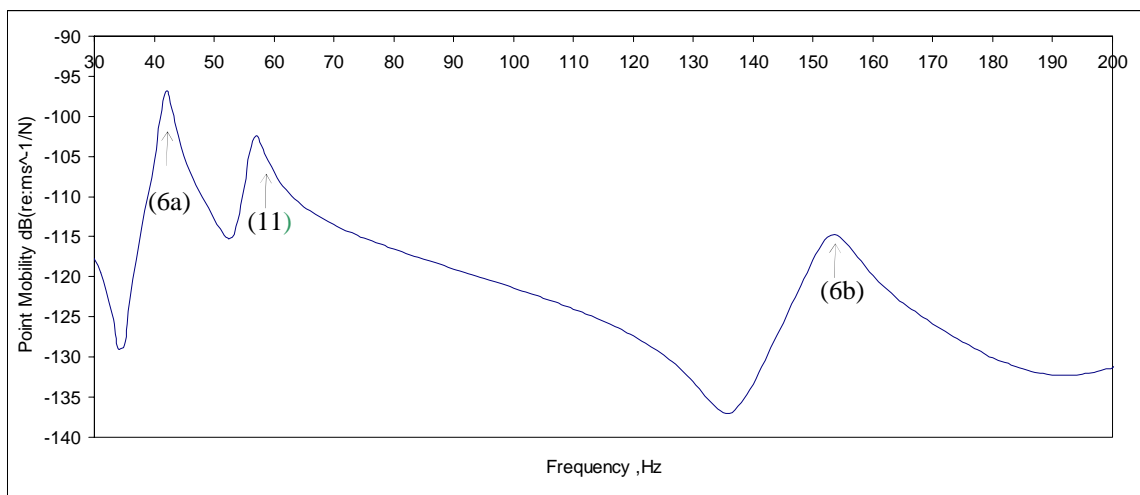


Figure 4.5 Average mobility results of 1.5m (x direction) concrete box model

Different views:

Mode shape in y-z plane Front view(cross-section) from left	Mode shape in x-y plane (top view)
Mode shape in y-z plane Front view (cross-section) from right	Mode shape in x-z plane (side view)

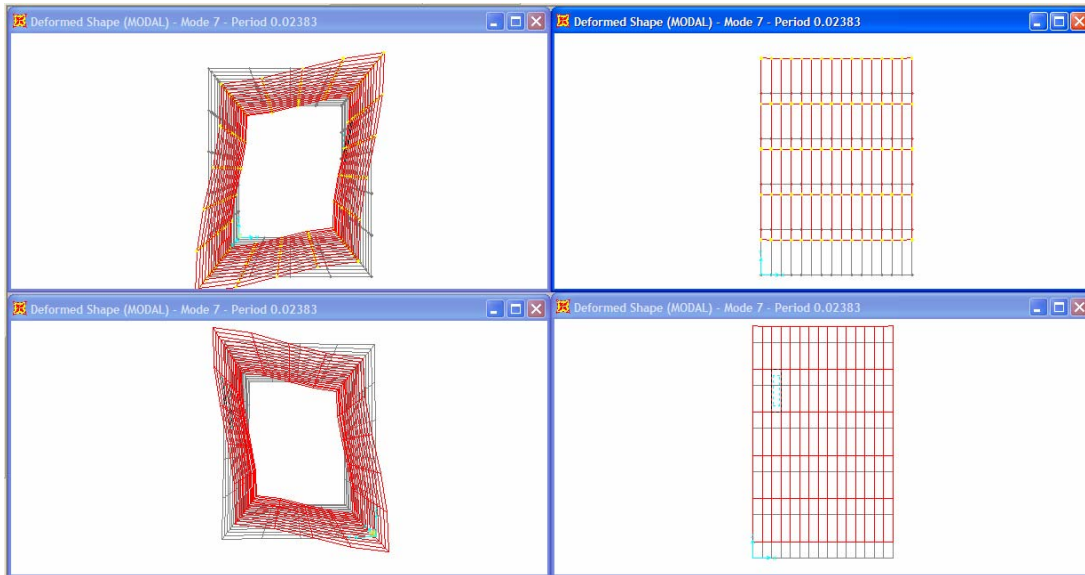


Figure 4.6a Local distortion (edge) mode of short concrete box at 42Hz marked with (6a) in Figure 4.5

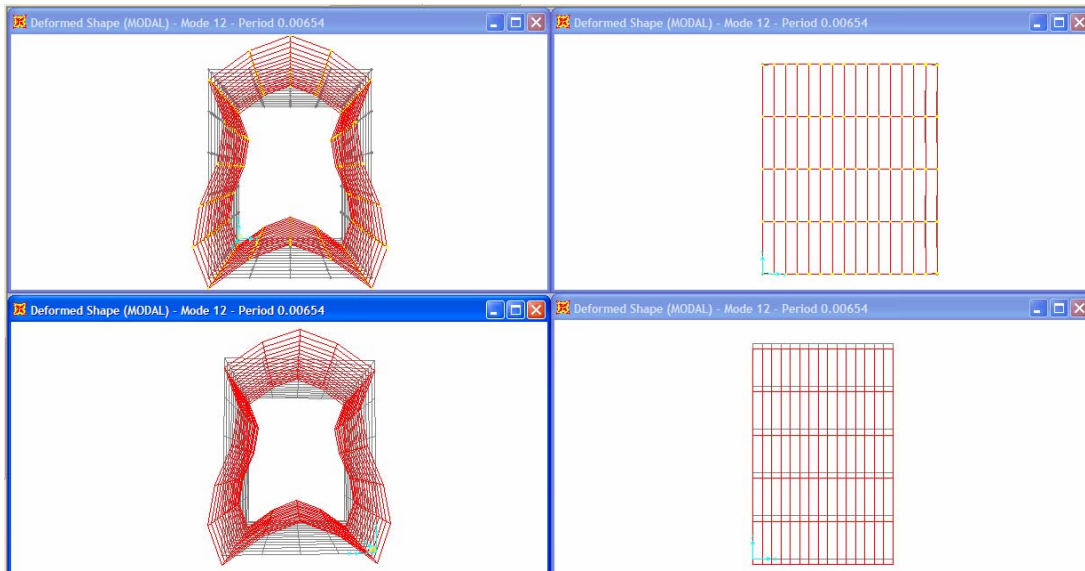


Figure 4.6b Local bending (combined edge and center) mode shape of short concrete box at 153Hz marked with (6b) in Figure 4.5

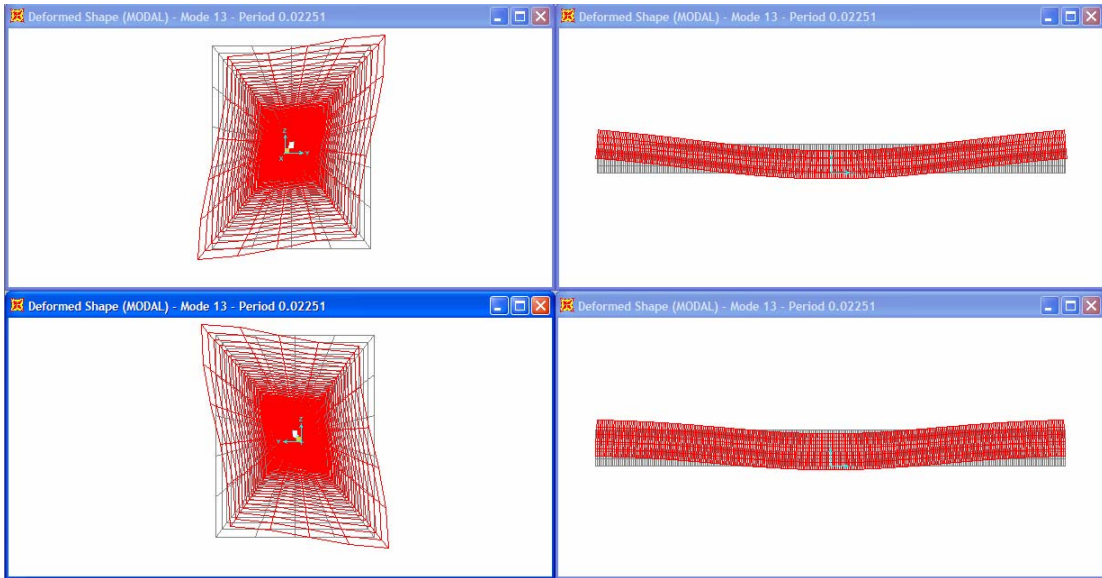


Figure 4.6c Local distortion (edge) mode together with minor 1st global torsion mode shape of long concrete box at 44Hz marked with (6c) in Figure 4.4

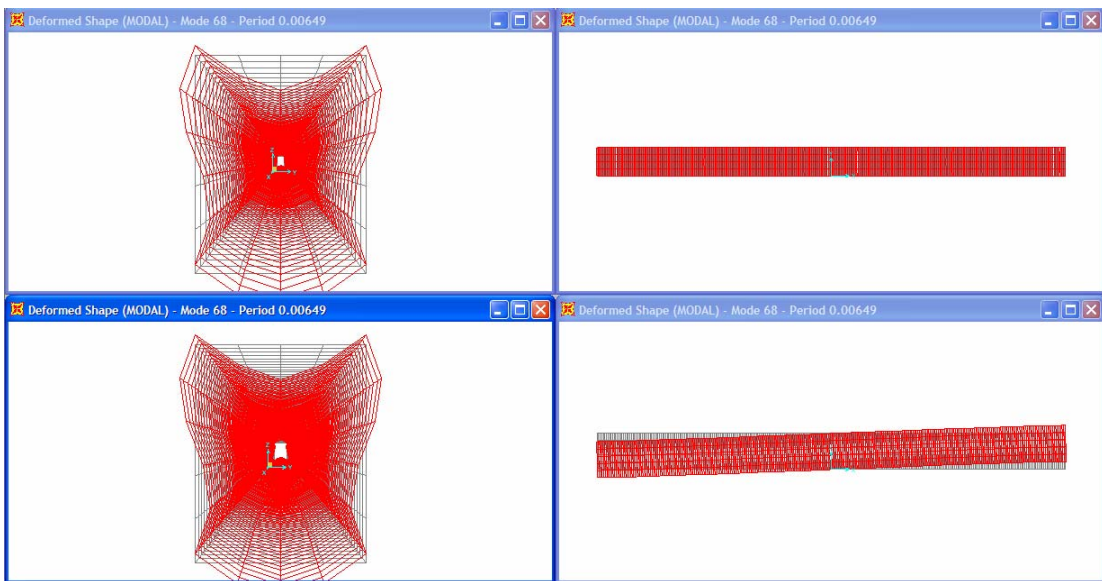


Figure 4.6d Local bending (combined edge and center) mode together with minor 1st global bending mode shape of long concrete box at 154Hz marked with (6d) in Figure 4.4

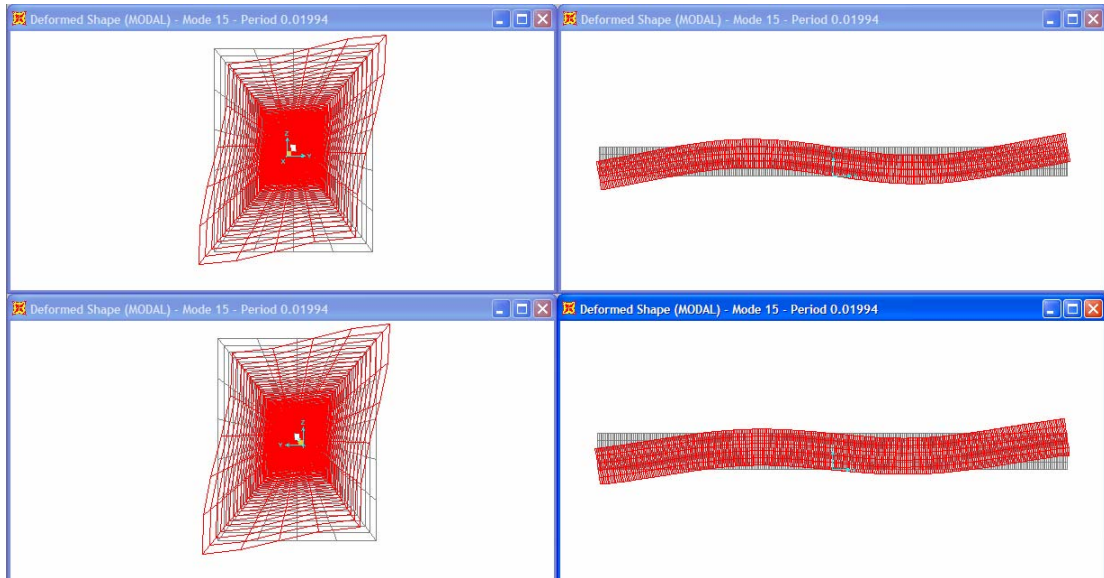


Figure 4.7a Local distortion (edge) mode together with minor 2nd global torsion mode shape of long concrete box at 50Hz marked with (7a) in Figure 4.4

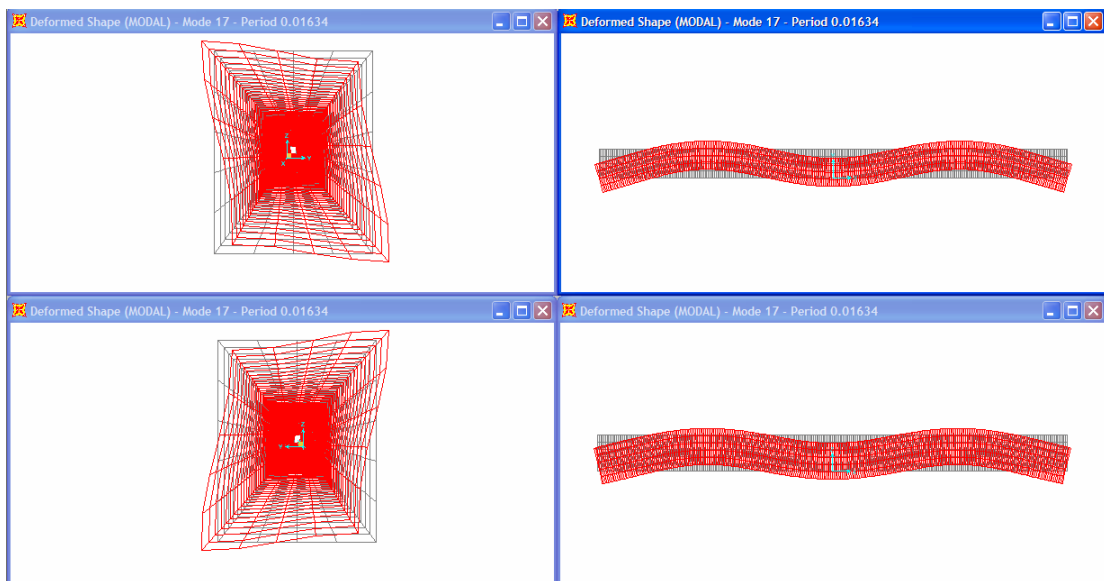


Figure 4.7b Local distortion (edge) mode together with minor 3rd global torsion mode shape of long concrete box at 61Hz marked with (7b) in Figure 4.4

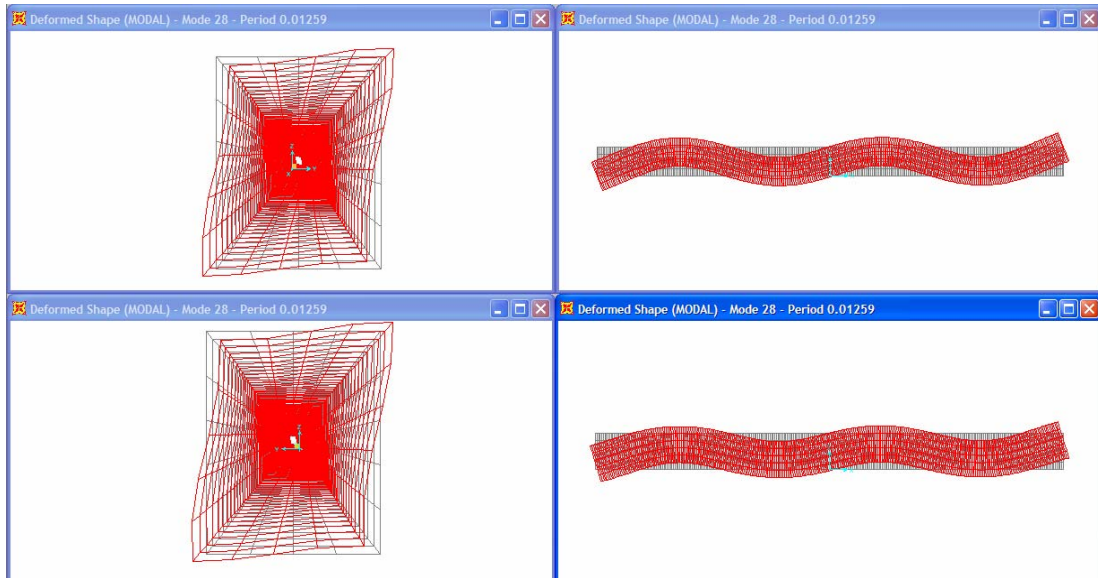


Figure 4.7c Local distortion (edge) mode together with minor 4th global torsion mode shape of long concrete box at 79Hz marked with (7c) in Figure 4.4

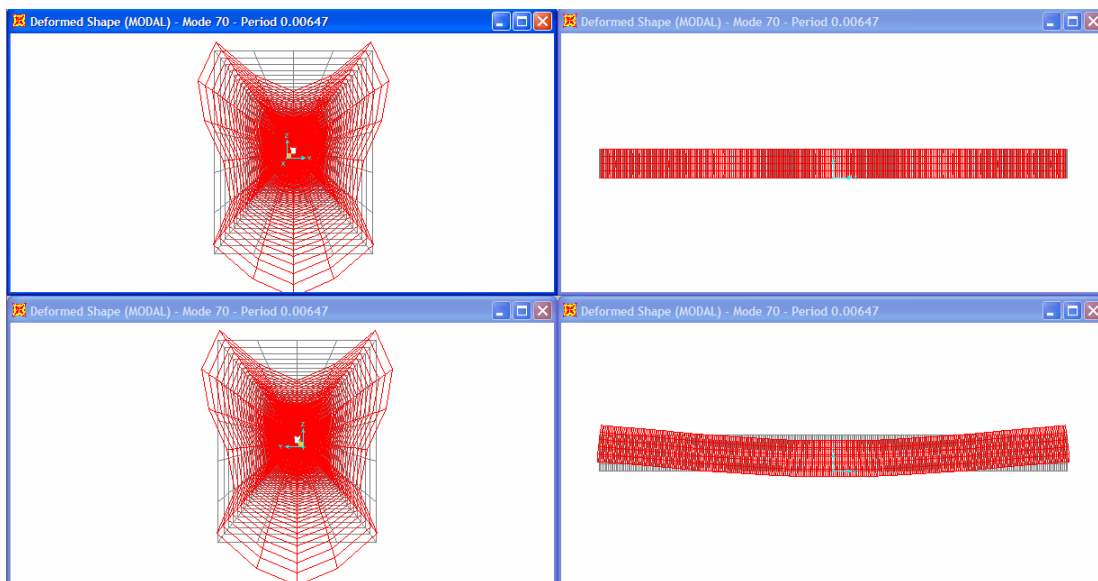


Figure 4.8 Local combined (edge and center) mode together with minor 2nd global bending mode shape of long concrete box at 155Hz marked with (8) in Figure.4.4

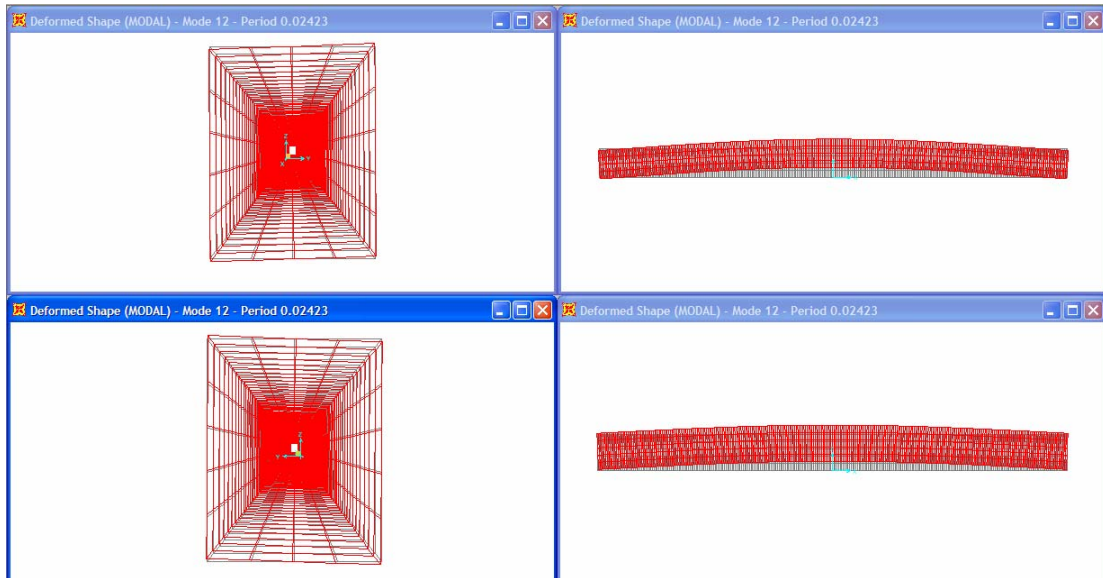


Figure 4.9a 1st global torsion mode shape of long concrete box at 41Hz marked with (9a) in Figure 4.4

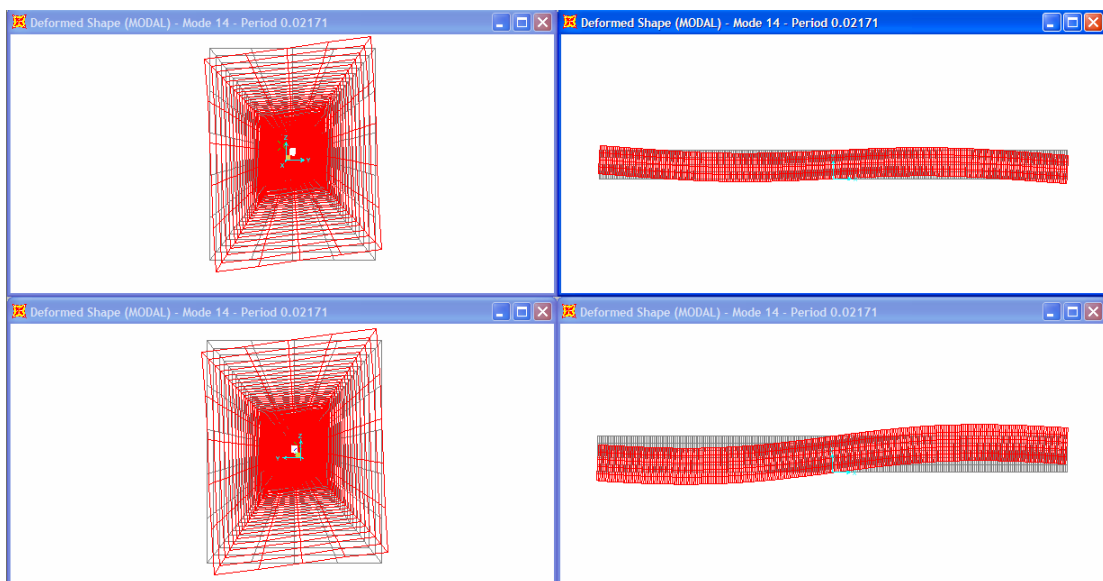


Figure 4.9b 2nd global torsion mode shape of long concrete box at 46Hz marked with (9b) in Figure 4.4

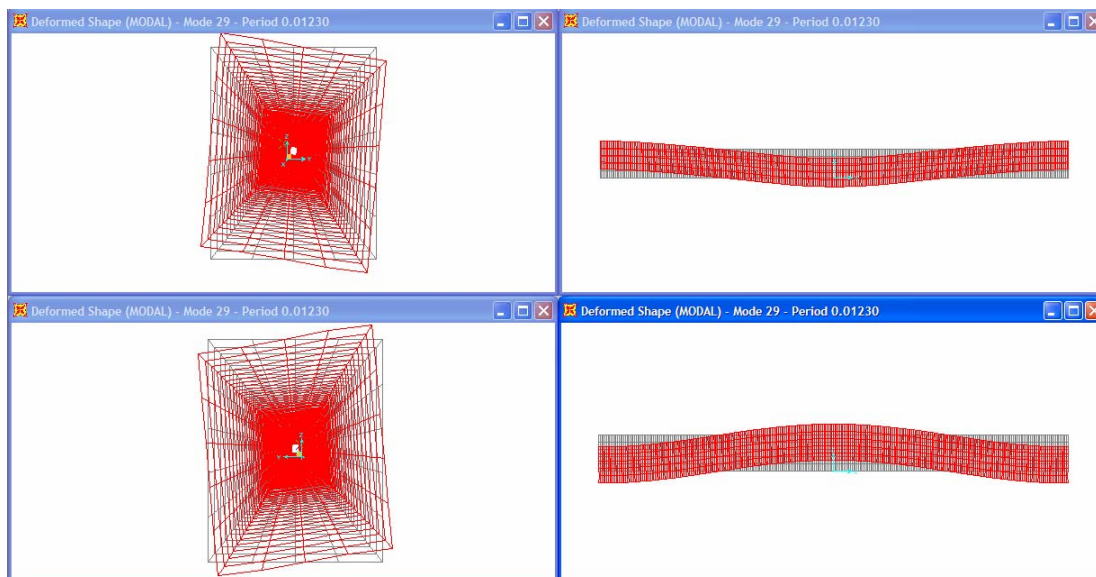


Figure 4.9c 3rd global torsion mode shape of long concrete box at 81Hz marked with (9c) in Figure 4.4

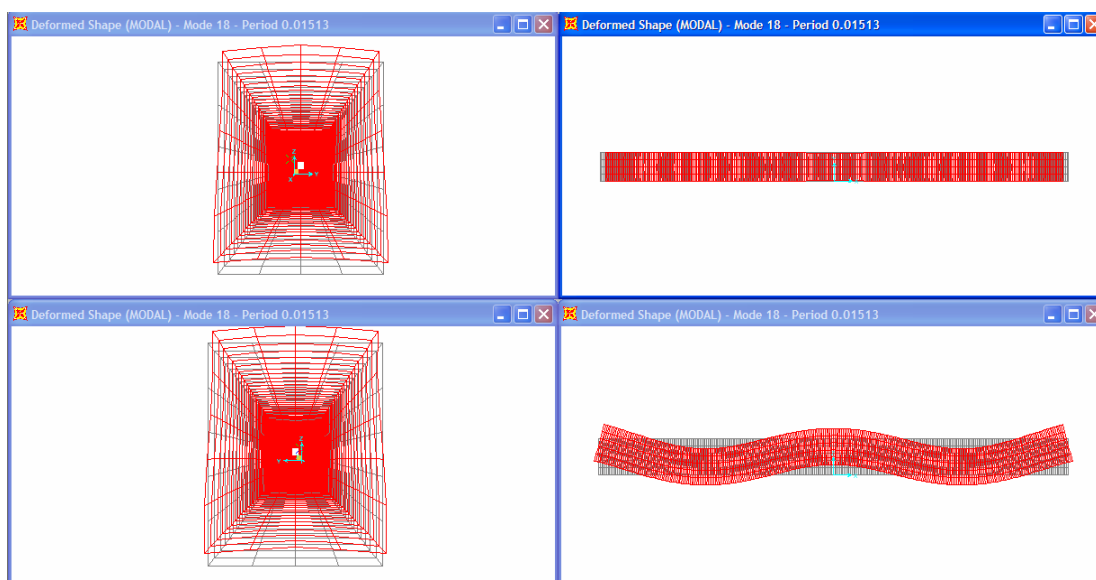


Figure 4.10a 4th global bending mode together with minor local bending combined mode shape of long concrete box at 40.6Hz marked with (10a) in Figure 4.4

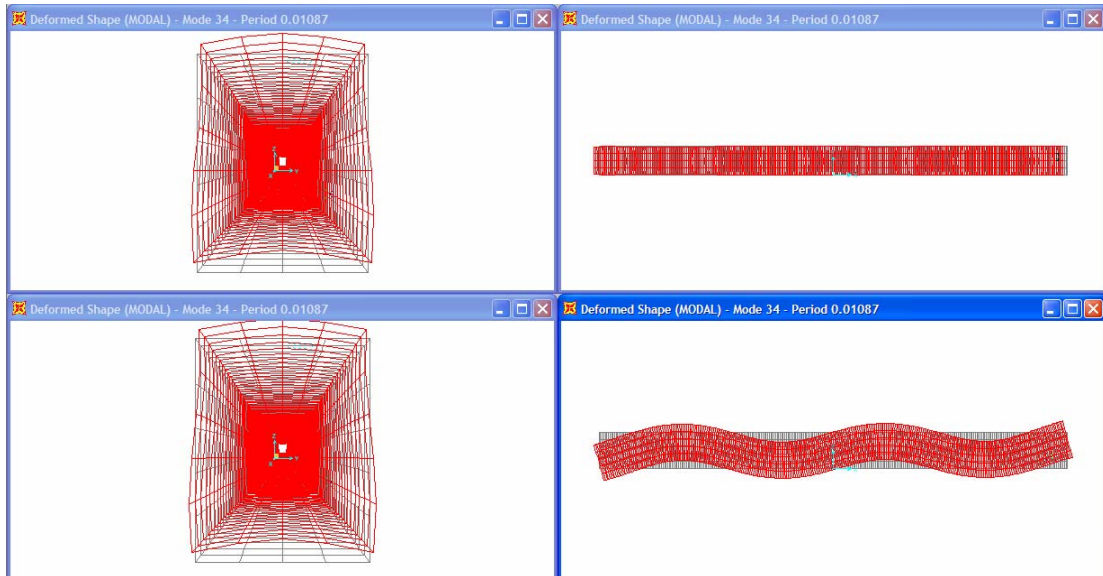


Figure 4.10b 5th global bending mode together with minor local bending combined mode shape of long concrete box at 66Hz marked with (10b) in Figure 4.4

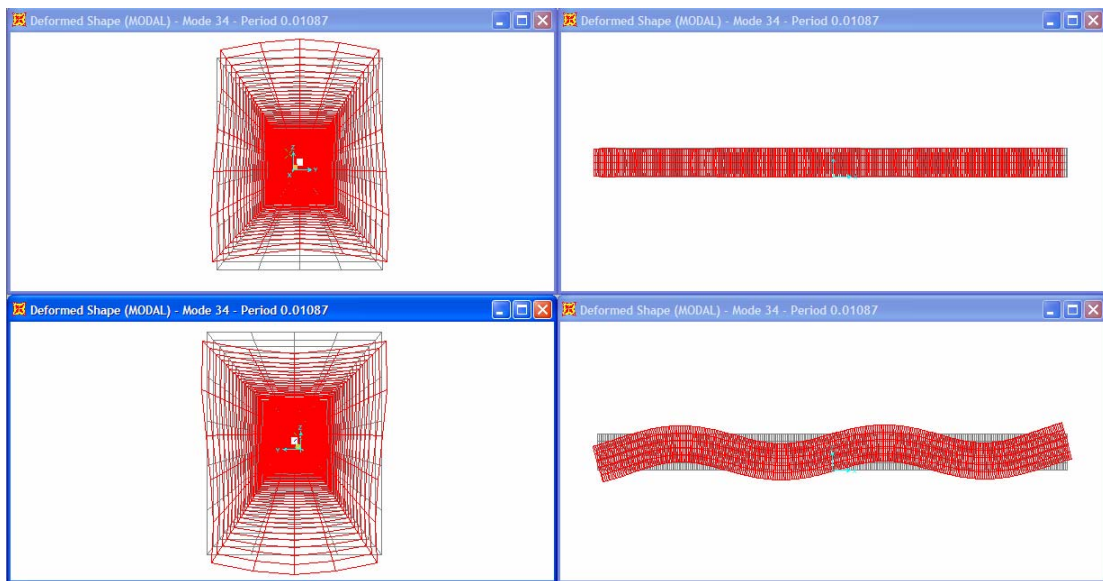


Figure 4.10c 6th global bending mode together with minor local bending combined mode shape of long concrete box at 92Hz marked with (10c) in Figure 4.4

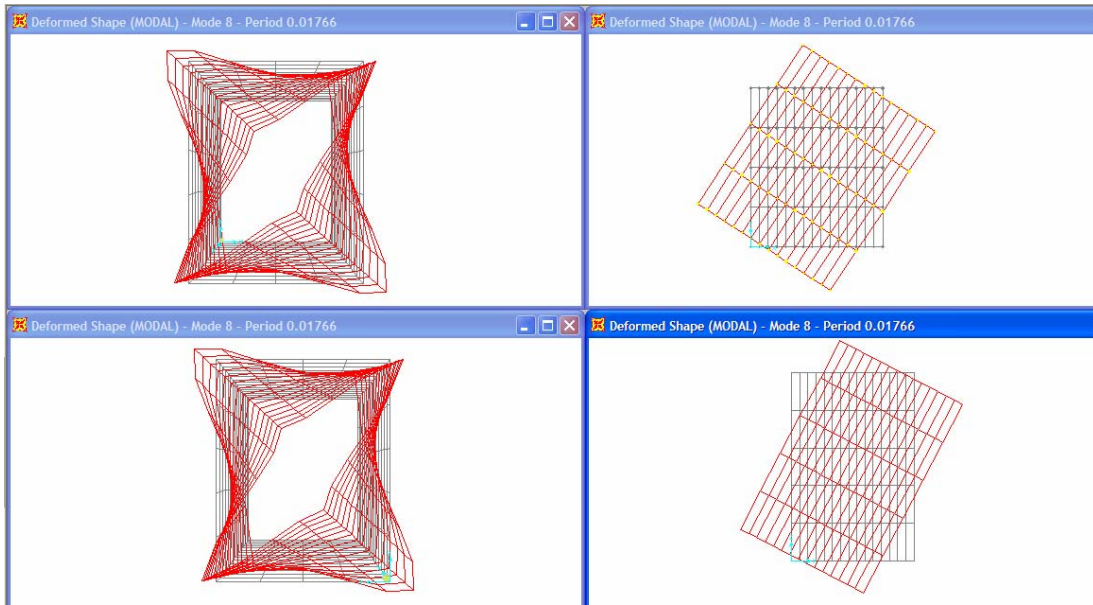


Figure 4.11a Mode shape of short concrete box at 58Hz marked with (11) in Figure 4.5

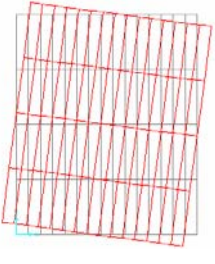
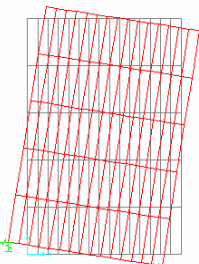
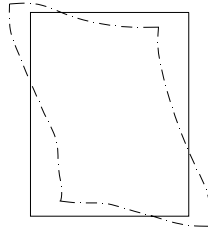
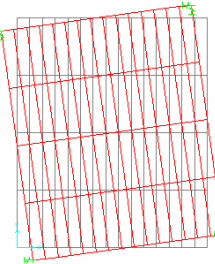
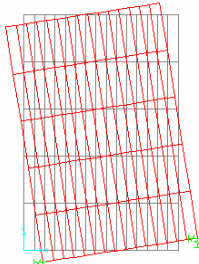
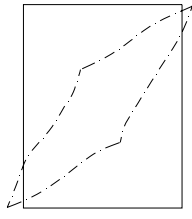
		
Top view	Side view (from left)	Cross-sectional view (from back)
		
Bottom view	Side view (from right)	Cross-sectional view (from front)

Figure 4.11b The details of the mode shape of short concrete box at 58Hz showed in Figure 4.11a

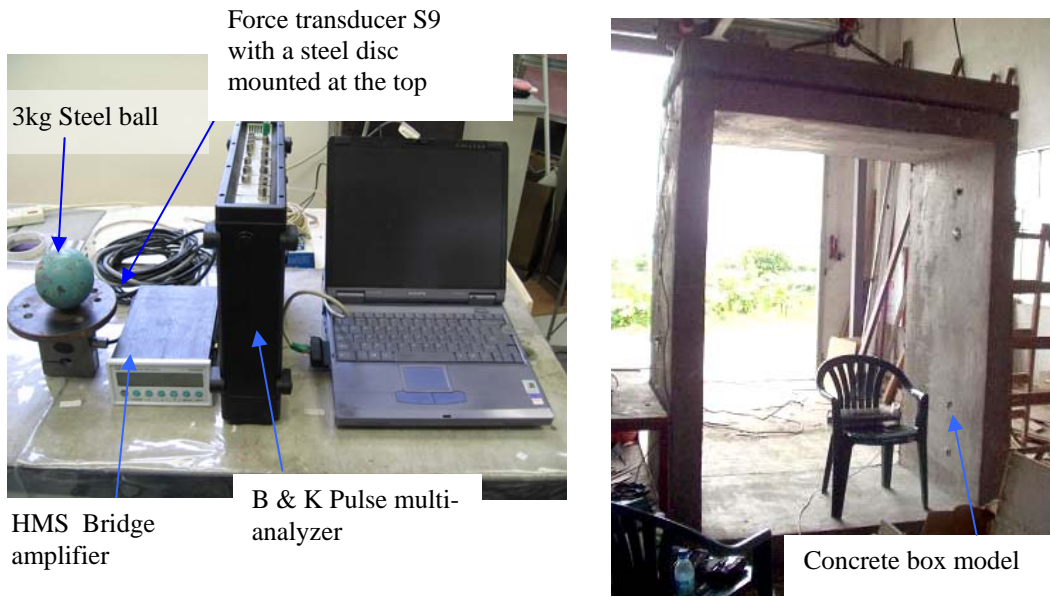


Figure 4.12 Experimental setup for the test on concrete box

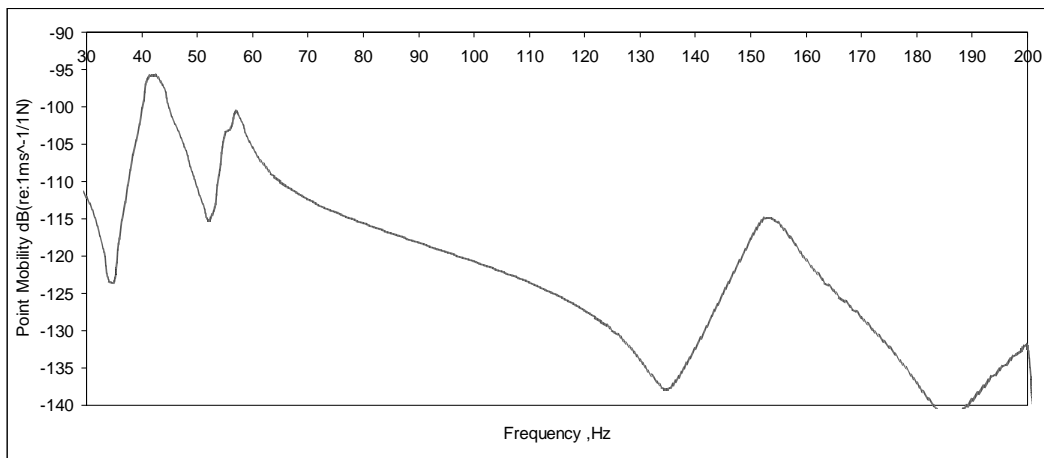


Figure 4.13a Average mobility results of short concrete box in experimental

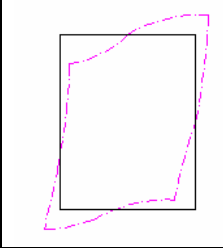
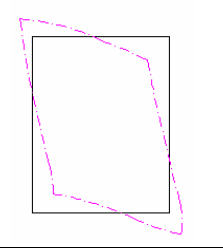
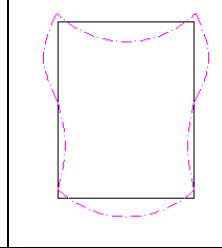
Mode shapes			
Resonance frequency	42Hz	59Hz	153Hz

Figure 4.13b Mode shapes results of short concrete box in experimental

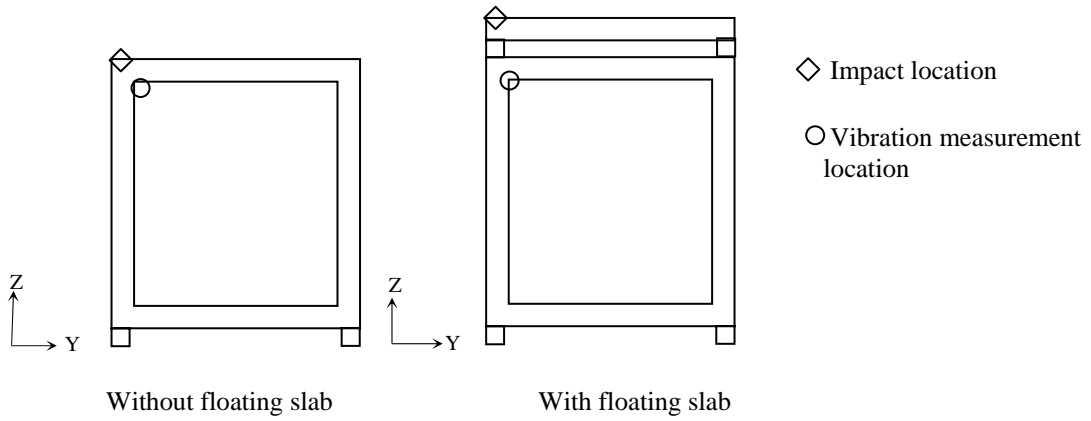


Figure 4.14 Vibration response measurement location on box structure (not to scale)

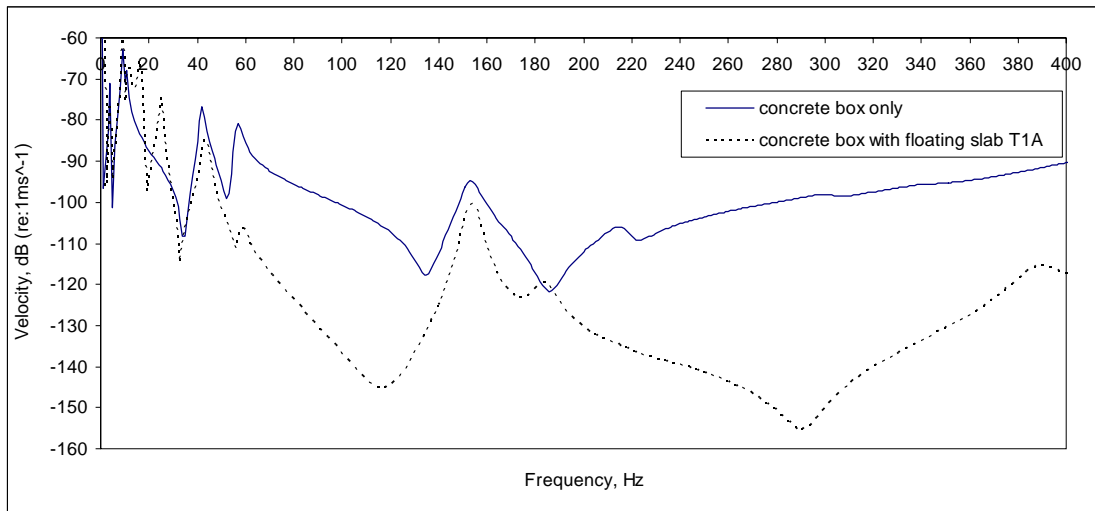


Figure 4.15a Vibration responses of the concrete box with and without floating slab T1A

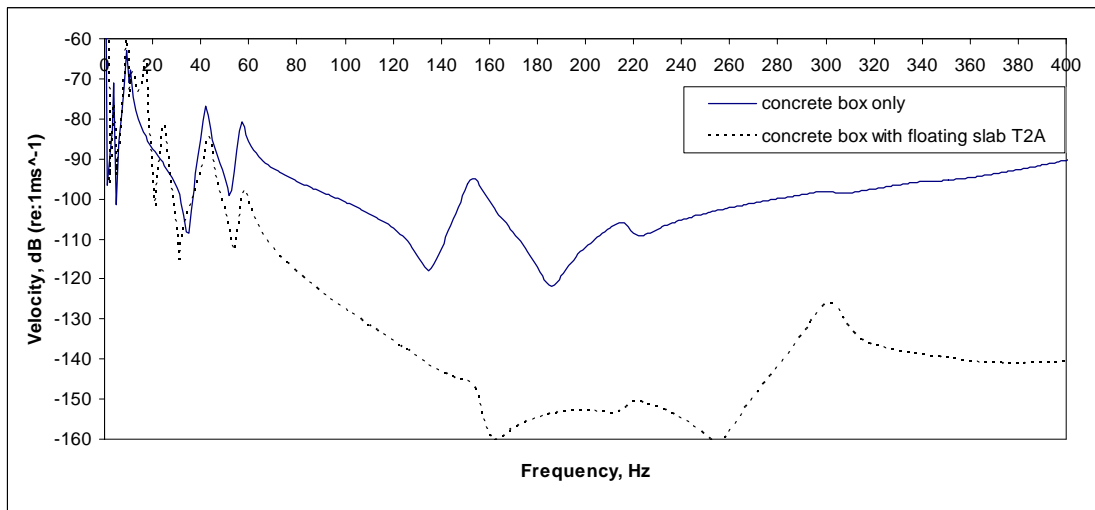


Figure 4.15b Vibration responses of the concrete box with and without floating slab T2A

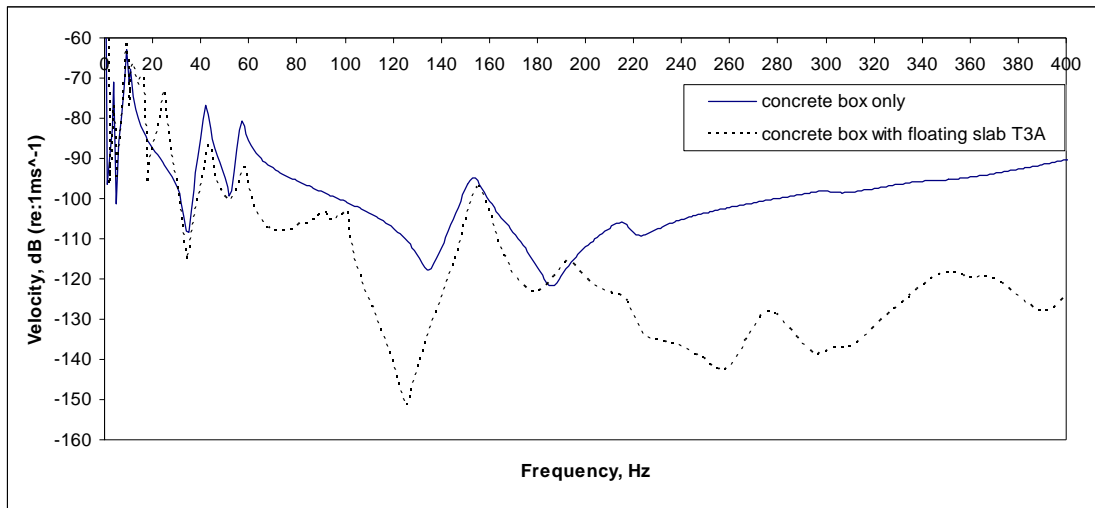


Figure 4.15c Vibration responses of the concrete box with and without floating slab T3A

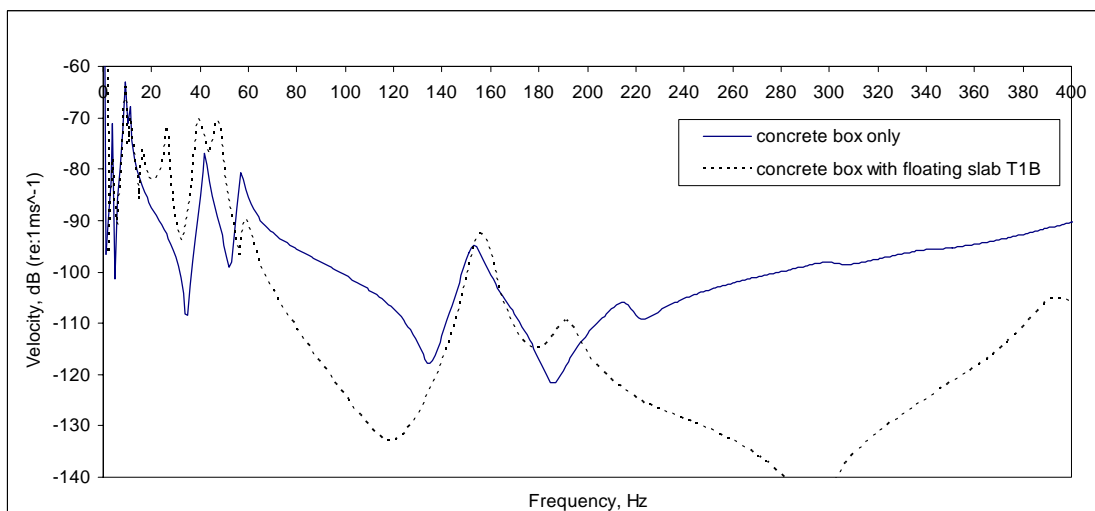


Figure 4.15d Vibration responses of the concrete box with and without floating slab T1B

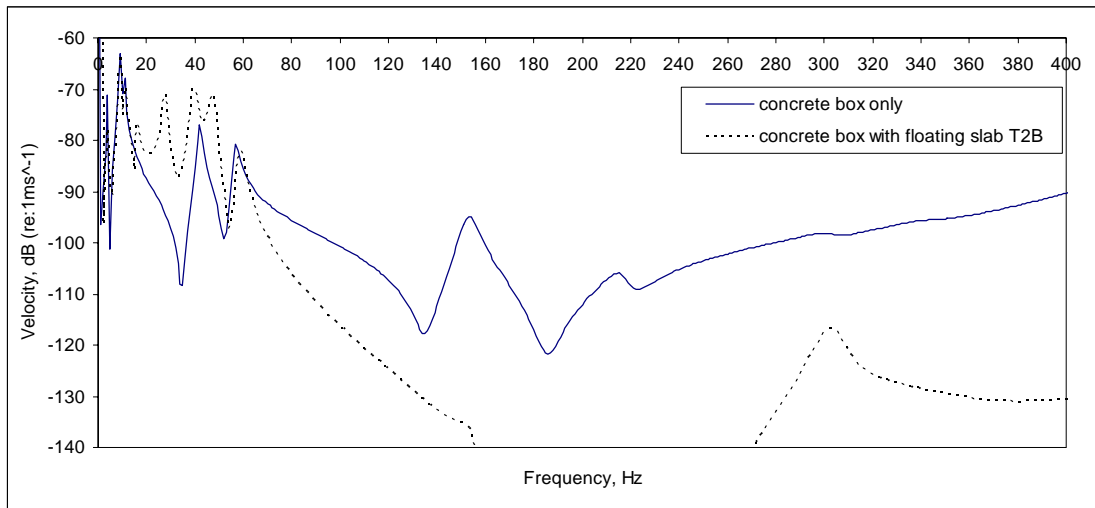


Figure 4.15e Vibration responses of the concrete box with and without floating slab T2B

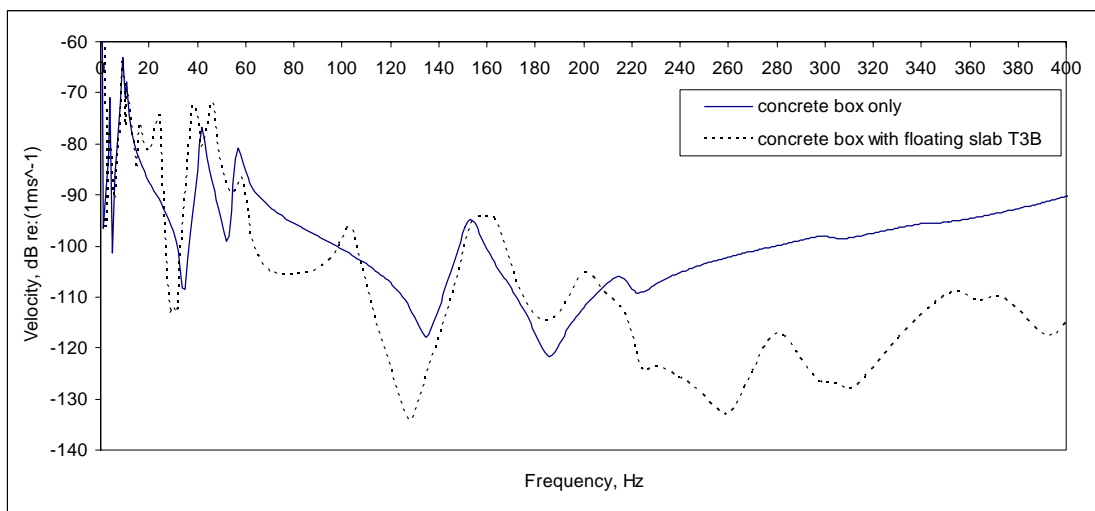


Figure 4.15f Vibration responses of the concrete box with and without floating slab T3B

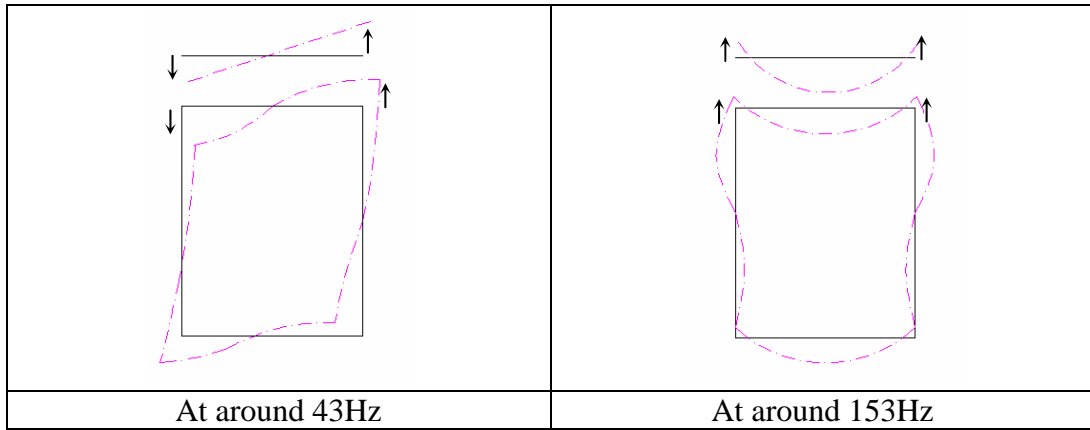


Figure 4.15g Coupling mode shapes of floating slab and box structure

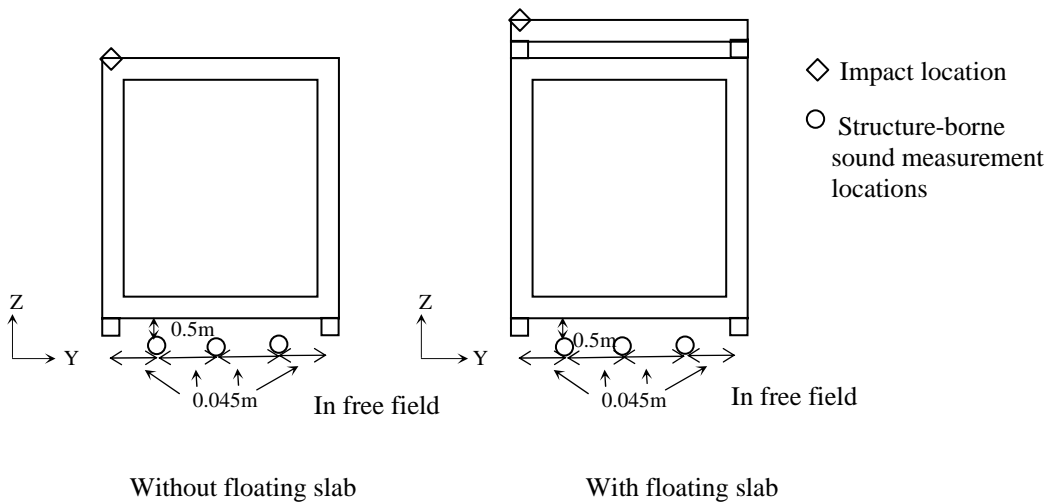


Figure 4.16 Structure-borne noise measurement method on concrete box (not to scale)

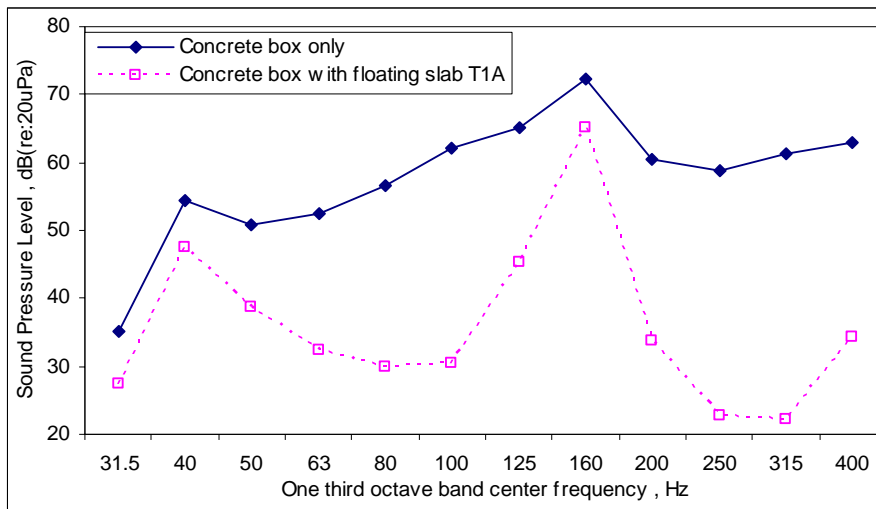


Figure 4.17a Sound pressure responses of the concrete box with and without floating slab T1A

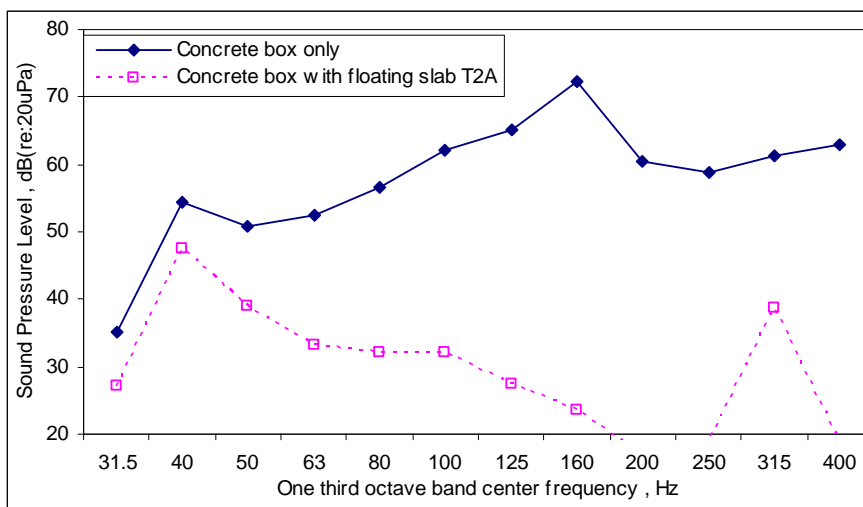


Figure 4.17b Sound pressure responses of the concrete box with and without floating slab T2A

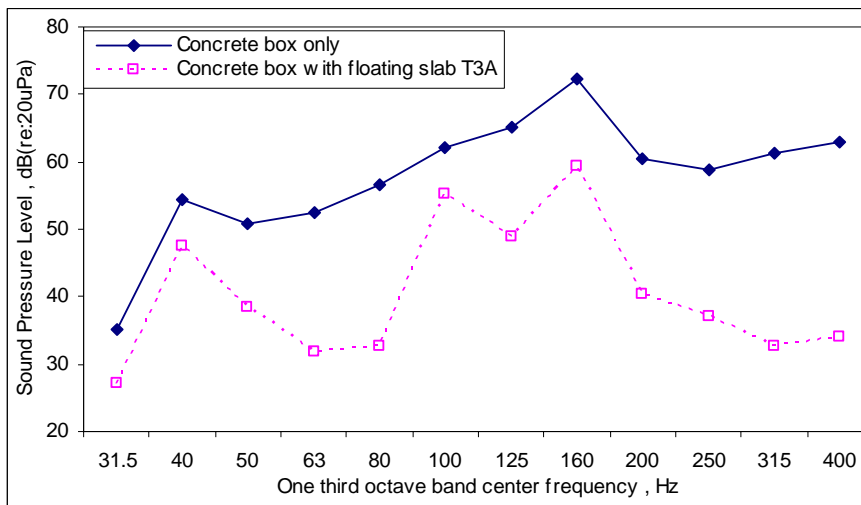


Figure 4.17c Sound pressure responses of the concrete box with and without floating slab T3A

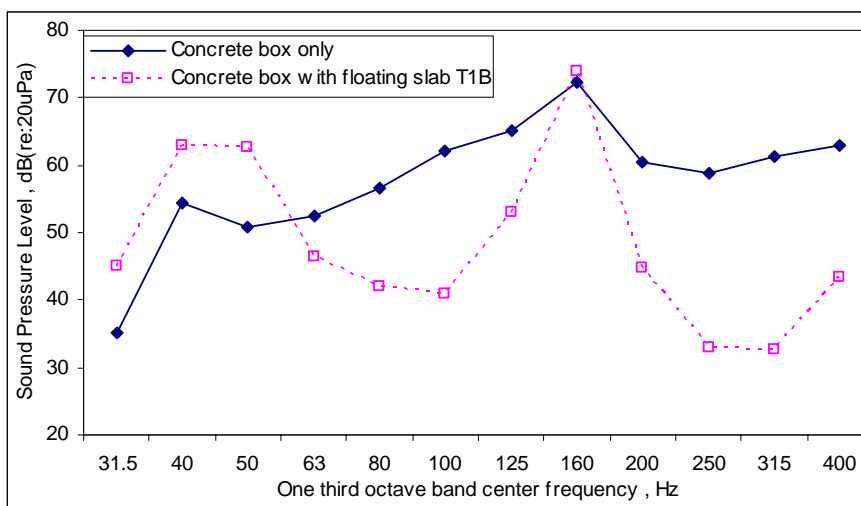


Figure 4.17d Sound pressure responses of the concrete box with and without floating slab T1B

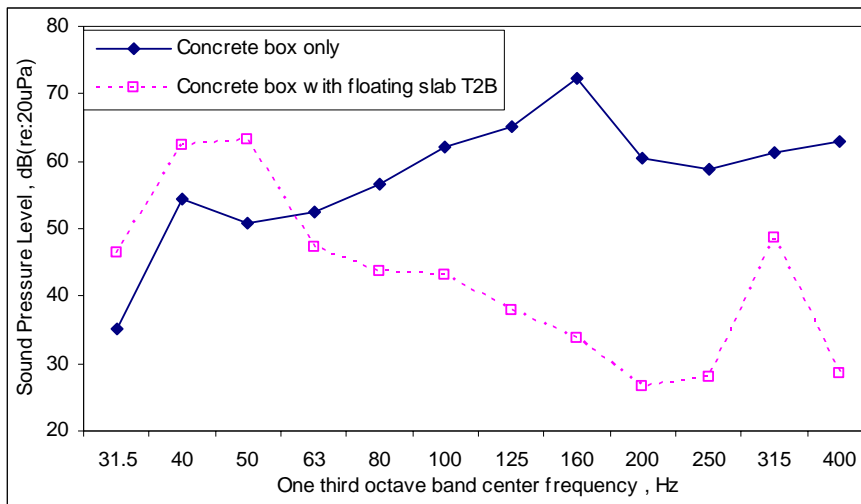


Figure 4.17e Sound pressure responses of the concrete box with and without floating slab T2B

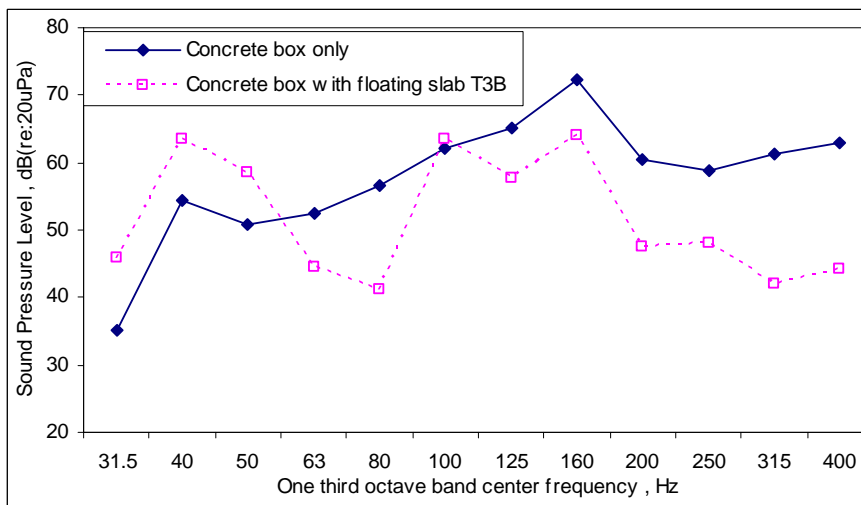


Figure 4.17f Sound pressure responses of the concrete box with and without floating slab T3B

Table 4.1. Design of three types of floating slabs and two types of isolators

Type	Length in x-direction (m)	Design first bending resonance in x-direction (Hz)	Length in y-direction (m)	Design first bending resonance in y-direction (Hz)	Thickness (m)	Stiffness of each isolator (total with 4) (kN/m)	Design tuned natural frequency (Hz)
T2A	0.5	4067	1.8	314	0.3	1201	14
T2B	0.5	4067	1.8	314	0.3	2966	23
T1A	1	508	1.8	157	0.15	1201	14
T1B	1	508	1.8	157	0.15	2966	23
T3A	1.5	151	1.8	105	0.1	1201	14
T3B	1.5	151	1.8	105	0.1	2966	23

Table 4.2. Measured resonance frequencies and corresponding mode shapes of six types of floating slabs.

Mode shape in y-direction					
Mode shape in x-direction					
Name of mode shape	Rigid body mode - Vertical	Rigid Body mode -Yaw	Rigid Body mode -Roll	1 st symmetric bending mode in y direction	1 st symmetric bending mode in x direction
T2A	14Hz	23Hz	24Hz	310Hz	Nil
T2B	23Hz	41Hz	42Hz	308Hz	Nil
T1A	14Hz	23Hz	24Hz	153Hz	501Hz
T1B	23Hz	41Hz	41.5Hz	156Hz	503Hz
T3A	13.5Hz	23Hz	24Hz	102Hz	155Hz
T3B	23Hz	40Hz	41Hz	102Hz	160Hz

Table 4.3. The summary of the vibration and noise reduction performance of six combinations of floating slabs

Name of mode shape	Length in x-direction (m)	Static Stiffness of each isolator (total with 4) (kN/m)	Vibration reduction at 43Hz	Noise reduction at 153Hz
T2A	0.5	1201	+6dB	+48dB
T2B	0.5	2966	37Hz(-6dB) 45Hz(-5Hz)	+33dB
T1A	1	1201	+6.5dB	+7dB
T1B	1	2966	37Hz(-7dB) 45Hz(-7Hz)	-2dB
T3A	1.5	1201	+5dB	+12dB
T3B	1.5	2966	37Hz(-5dB) 45Hz(-5Hz)	+7dB

Notice: “+” is defined as reduction in response;
“-” is defined as amplification in response

CHAPTER 5

BENDING-RESONANCE EFFECTS ON VIBRATION REDUCTION OF IN-SERVICE RAIL VIADUCT

The experimental results of Chapter 4 show that the bending modes in the box structure and the floating slab can degrade the vibration isolation performance. The coupling modes may appear in the floating system and the supporting box structure because of the similar resonance mode shapes and the resonance frequencies.

In this Chapter, site tests are performed on several isolation designs to control vibration transmissions from concrete rail viaducts. The analysed isolation systems include medium- and short-length floating slabs, and floating ladders. The vibrations are measured in Japan, Korea and Hong Kong, where extensive rail infrastructure is located near residential areas. The effects of bending modes of floating slab and moving load at support passage frequency on vibration isolation performance are analysed in the measurement results.

5.1 INTRODUCTION

Various studies have analysed the bending behaviour of floating slabs in both mathematical models and site experiments vibration due to moving train.

Lombaert et al. (2006) developed a continuous floating slab numerical model to study the effectiveness of the vibration interaction of train, track and soil. Hussein and Hunt (2006a) created a new mathematical model with rail, rail pad, continuous slab and slab-bearings to

analyse cut-on frequency and critical velocity of the track. Both of these models considered the important bending wave transmission of floating slab tracks. In another two papers, displacement of a discontinuous floating slab track under oscillating moving loads due to the wheel/rail roughness (Hussein and Hunt, 2006b) and moving static load resulting from the parametric excitation (Hussein and Hunt, 2006c) are modelled with new mathematical methods. It is found that the effect on the force at the wheel rail interface should be increased by 1% only for speed train less than 100km/h.

Moritoh et al. (1996) conducted an in-situ noise measurement under a concrete bridge structure for a train passing at 240km/h and the measured peak at around 50Hz. Zach (2000) conducted site rail vibration measurement on different traditional and new rail track types in Switzerland. Saurenman and Phillips (2006) measured rail vibration with various floating slabs in the San Francisco Bay Area Rapid Transit, and they point out that there is noticeable degradation on floating slab vibration isolation when the natural frequency is close to the wheel rotation resonance. Both of them analyse the floating slab used at grade or in a tunnel, but not on a viaduct structure. The maximum vibration reductions of these results were about 20dB.

This Chapter reports on in-situ rail viaduct vibration measured at the base of viaducts with various isolation systems and analyse the effects of bending vibration resonance on vibration isolation performance. The floating slab systems analysed included:

- 1) Medium-size floating slab track on the Korean High Speed Railway (KTX): Ballast bed mat rests on the track bed isolated from the station structure by spring boxes. The floating slab is large – 20.5m x 21.6m. The designed vertical resonance frequency is 6Hz. It is classified as a floating ballast trough as shown in Fig. B.1(e) of ISO 14837-1-2005(E) (ref. to Figure 3.6 in Chapter 3).

2) Floating ladder track in Japan (Tokyo): The floating ladder track consists of two longitudinal concrete beams 6.2m long resting on rubber pads. Transverse steel pipes are embedded into the longitudinal concrete beams. The designed vertical resonance frequency is estimated to be 25Hz. It is similar to booted blocks as shown in Fig. B.1(j) of ISO 14837-1-2005(E) (ref. to Figure 3.6 in Chapter 3), but the concrete block is heavier.

3) Short-size floating slab track in China (Hong Kong): A mini-type floating slab (2.65m x 1.17m) that rests on four rubber pads designed vertical resonance frequency at 14Hz. It is classified as the combination of resilient baseplates and floating track slabs with discrete support as shown in Fig. B.1(i & l) of ISO 14837-1-2005(E) (ref. to Figure 3.6 in Chapter 3).

5.2 THE EFFECTS OF BENDING RESONANCES OF FLOATING SLABS ON VIBRATION REDUCTION

To understand and evaluate the effects of bending resonance of floating slabs on the vibration isolation efficiency of a railway, vibration reduction is measured with a floating slab made of reinforced concrete where the Young's modulus is $25 \times 10^9 \text{ Nm}^{-2}$ and density is 2300 kgm^{-3} , and the total stiffness of isolators is $11.5 \times 10^6 \text{ Nm}^{-1}$. The dimensions of slab are 1.8m (L) \times 1 m (W) \times 0.16 m (H) (Figure 5.1). The excitation force was generated by the free fall of a 3kg steel ball from a 0.2m height with five impacts for each measurement. The vibration reduction value (defined as one minus force transmissibility) is calculated from the difference between the acceleration levels measured via PCB ICP accelerometer on base gained without and with the isolation system. The measured results can be verified by the calculation with Equation 2.3 (1-Tr).

The experimental and theoretical vibration reductions of the concrete floating slab are shown in Figure 5.2a. It is obvious that there is an adverse effect on the vibration isolation at

the first bending resonance frequency at 170Hz. The discrepancy of the measured vibration reduction and the theoretical level was attributable mainly to the acoustic pressure trapped between the rigid base and the floating slab model. Furthermore, the deviation of the measured level of the dip at around 170Hz should come from the error in modal damping.

The theoretical vibration reduction performances for floating slabs with different size are shown in Figure 5.2b. This shows that the longer the floating slab, the lower the first bending resonance can be observed and the worse the vibration reduction performance.

The mode shapes of rectangular floating panel are given in Figure 2.5. The natural frequency of those mode shapes of the test panel in this Chapter is shown in Figure 5.3. The longitudinal (y direction) bending for floating slab using in train refers to bending waves in the direction of the train's movement. The first six modes are rigid body modes, with a frequency between 14Hz and 32Hz. The last five modes are bending modes. The seventh one is the first symmetric bending mode in transverse direction at 168.9Hz, which is also near the experimental result of the second resonance at 170Hz (see Figure 5.2a).

The bending mode in the transverse direction (1.8m length) calculated from Equation 2.6 is 167Hz which agrees well with the FEM calculation at 168.9Hz and the experimental result at 170Hz.

5.3 CONSIDERATION IN THEORETICAL MODEL

The measured velocity responses at the viaduct base when a train pass-by on the tracks in the following sections were compared with the theoretical model constructed with Sap 2000 FEM programme. Two types of excitation forces are considered in the models. The first one is the vibration results from moving train on various hardness of track leads to fluctuating force at rail-pad or sleeper support passage frequency are calculated with Equation 3.1. The

intra-bogie axle support passage frequency mentioned in Chapter 3 is not considered since the train speeds are lower than 250km/h for the measurement trains. The FEM for the estimation on the force at support passage frequency are sketched in Figure 3.2. The other excitation force is generated by the wheel/rail surface roughness (ref. to Figure 3.3), this is approximated with oscillating moving loads of wideband frequencies up to 200Hz.

5.4 PROCEDURES OF SITE TEST

The purpose of the experimental on-site measurement is mainly to determine the practical vibration reduction of different rail viaduct vibration-mitigation measures of isolation systems.

At least five-time measurements were conducted using B&K PULSE data recorder at all measurement locations and the repeatable data are used for analysis. In addition, to eliminate the effects of localised geology on vibration measurement, vibration velocity with and without floating slab are measured at the same or nearby locations with the same types of trains.

In the following pages site measurements were conducted on the current vibration isolation systems for rail viaduct structures. The resonance frequency will be analysed in detail with FEM. Owing to the variation of workmanship in different parts of the structures, there may be up to a 20% deviation in the bending resonance frequency calculation.

5.5 SITE TEST ON MEDIUM FLOATING SLAB IN THE KOREA HIGH SPEED RAILWAY

The Chonan station is built on a three-storey concrete frame. It has operated since 2004 and the area under the track will be used as a conference centre. (see Figure 5.4). The

vibration-mitigation measure systems include medium-size floating slabs resting on spring boxes combined with viscous dampers sitting on a ballast bed mat. The designed vertical resonance frequency is 6Hz. The track section outside the station is traditional ballast track.

The vibration velocity was recorded under the station (Figure 5.5) continuously when a train was passing at 230km/h through the ballast track outside the station (without floating system) and the train on the station (with floating ballast trough). The start and end time for train passing through the ballast track, and the floating ballast trough portions were noted. The different time history signals recorded from the train were replayed and selected separately for frequency analysis.

5.5.1 PARAMETERS FOR FINITE ELEMENT MODEL

The parameters used in FEM are detailed in Table 5.1. The important parameters used for the analysis are: mass per unit length of the rail 60.3kg/m, moment of inertia $39.6 \times 10^{-6} \text{ m}^4$. For rail pad, dynamic stiffness is 90MN/m. For the ballast bed, the stiffness of the ballast with 0.35m thickness is 70MN/m approximately. The dimensions of the medium size floating slab in longitudinal direction are 20.5m (length) x 1.7m (thickness); and in transverse side are 21.6m (length) x 1.04m (thickness), and the total stiffness of isolators for each slab is $1586 \times 10^6 \text{ Nm}^{-1}$. The dimensions of the supporting viaduct structure are shown in Table 5.1. For both concrete slab and supporting structures, Young's modulus is $25 \times 10^9 \text{ Nm}^{-2}$, density is 2300 kgm^{-3} .

5.5.2 ANALYSIS OF RESULTS

The 1/3 octave band vibration spectra when the train passed over the section with and without floating slabs are shown in Figure 5.6a. The peak at 40Hz band should correspond to

the response at resonance frequency of wheel-ballast (Table 5.2). The peak at 100Hz band for with and without floating slab should represent the response at the moving load of sleeper support passage frequency at 106Hz (Table 5.3).

The peak at 12.5Hz band with floating slab (Figure 5.6a) results in lower vibration reduction as shown in Figure 5.7. This should be due to the bending resonance of the side beams of floating slab in longitudinal direction at 12.4Hz, which is confirmed by both FEM modelling as well as the simple Equation 2.6 (Table 5.4). Whereas, there is no prominent peak can be observed at 8Hz band due to the first transverse symmetric bending. The bending mode may be reduced by the damping of the viscous damper in the spring isolator.

The experimental and theoretical vibration velocity spectra of floating slab track are shown in Figure 5.6b. In general, the deviation is less than 10dB, and should be mainly because of the error in the prediction of the damping.

Comparisons of the experimental and theoretical vibration reduction are shown in Figure 5.7. For the 1-dof theory, the vibration reduction increases by 12dB per octave band. The experimental reduction levels are less than those of 1-dof results representing the effects of floating slab bending resonances. The negative vibration reduction in the 5Hz and 6.3Hz bands should correspond to the spring isolator resonance at 6Hz (see Figure 5.7). The unfavourable effects on vibration reduction compared with the ideal 1-dof prediction can also be observed and resulted from bending resonances at 12.5Hz band.

In general, the floating slab design achieved an effective vibration reduction of 10- 45dB in the frequency range of 12.5-200Hz. The vibration reduction decreased because of the lower train vibration source level above 100Hz. The vibration is not greatly affected by bending resonances which are attenuated by the heavy damping of the viscous damper in the spring isolators. The dominant excitation force generated at the passage support frequency of 106Hz (Table 5.3) is effectively reduced.

5.6 SITE TEST ON FLOATING LADDER TRACK IN JAPAN (TOKYO)

Measurement was conducted in a station with floating ladder track which is currently under reconstruction in 2006. There are two types of track forms in the station including traditional ballast track and floating ladder track with a concrete bed. The whole station is an elevated structure. The floating ladder track consists of two longitudinal concrete beams joined with transverse steel pipes. The vibration velocities were recorded when the trains were passing the ballast track and the floating ladder track separately. (see Figure 5.8). The measured vibrations for the same trains at 80km/h were compared.

5.6.1 PARAMETERS FOR FINITE ELEMENT MODEL

The parameters used in FEM are detailed in Table 5.5. The important parameters used for the analysis of the measured tracks are: mass per unit length of the rail 60 kg/m, moment of inertia $30.9 \times 10^{-6} \text{ m}^4$. For rail pad, dynamic stiffness is 490MN/m. For the ballast bed, the stiffness of the ballast is 70MN/m approximately. The dimensions of the floating ladder in longitudinal direction are 6.2m (length) x0.2m (thickness); and in transverse are 0.5m (length) x0.2m (thickness), and the total stiffness of isolators for each ladder is $28.1 \times 10^6 \text{ Nm}^{-1}$. The dimensions of the supporting viaduct structure are shown in Table 5.5. For both concrete slab and supporting structures, Young's modulus is $25 \times 10^9 \text{ Nm}^{-2}$, density is 2300 kgm^{-3} .

5.6.2 ANALYSIS OF RESULTS

The vibration spectra when the train passed on the ballast track and the floating ladder track are shown in Figure 5.9a. The peak at 31.5Hz band should represent the response at the moving load of sleeper passage frequency at 36Hz as shown in Table 5.3. The peak observed

when train pass-on ballast track at 63Hz band should correspond to the wheel-ballast resonance (Table 5.2).

The peaks at 31.5Hz, 50Hz and 100Hz bands for vibration data with the floating ladder can be observed in Figure 5.9a. The peak at 31.5Hz should be due to the first bending resonance of the floating ladder. This can be verified by the FEM that the first longitudinal symmetric bending is found to be 28.7Hz. The calculated frequency with Equation 2.6, however, is predicted to be at 18Hz. (see Table 5.6). This is because the designed vertical resonance frequency at 25Hz is coupled with the bending resonance calculated from Equation 2.6. The peaks at the 50Hz and 100Hz bands should correspond to the second and third longitudinal bending resonances at 53Hz and 97.3Hz. (Table 5.6). The experimental and theoretical vibration velocity spectra of floating slab track agree quite well (Figure 5.9b).

Comparisons of the experimental and theoretical vibration reduction are shown in Figure 5.10. The negative vibration reduction at 25Hz band results from the floating slab system resonance at around 25Hz. The adverse effect on vibration reduction compared with ideal 1-dof prediction should represent the response of bending resonances at 31.5Hz, 50Hz and 100Hz bands and parametric excitation frequency at 31.5Hz band can be observed in Figure 5.10. The dynamic force should be magnified since the moving load of rail-pad support passage frequency at 36Hz coincides with the first bending resonance of the floating ladder at around 30Hz.

In general, the vibration can be attenuated in the measured frequency range except the 20-31.5Hz bands. Thus, the overlapping of moving load excitation frequency and bending resonance should be avoided in the future design.

5.7 SITE TEST ON SHORT-LENGTH FLOATING SLAB TRACK IN CHINA (HONG KONG)

The West Rail viaduct track was about 13km long and started operation in 2003. The noise and vibration reduction is designed to be 25dB because there are low rise villages at a distance of only 10m from the viaduct. Short-length floating slabs with a designed vertical resonance frequency of 14Hz were applied on the whole length of viaduct track. Figure 5.11 is a photograph of the floating slab combined with resilient base-plate to form a 2-stage isolation system which is used in the measurement location.

The vibration level at location 1 in Figure 5.12 was down to the background level and therefore measurements were made at location 2 underneath the viaduct. The vibration velocity results are compared with those underneath ballast viaduct track in the same rail line, because there is no directly fixed slab track on viaduct can be selected for the comparison. The measured velocities for the same train at 80km/h are compared.

5.7.1 PARAMETERS FOR FINITE ELEMENT MODEL

The parameters used in FEM are detailed in Table 5.7. The important parameters used for the analysis of the measured tracks are: mass per unit length of the rail 60.3kg/m, moment of inertia $39.6 \times 10^{-6} \text{ m}^4$. For rail pad, dynamic stiffness is 21MN/m. For the ballast bed, the stiffness is 70MN/m approximately. The dimensions of the floating slab in longitudinal direction are 2.65m (length) x0.39m (thickness); and in transverse are 1.17m (length) x0.39 m (thickness), and the total stiffness of isolators for each slab is $21.7 \times 10^6 \text{ Nm}^{-1}$. The dimensions of the supporting viaduct structure are shown in Table 5.7. For both concrete slab and supporting structures, Young's modulus is $25 \times 10^9 \text{ Nm}^{-2}$, density is 2300 kgm^{-3} .

5.7.2 ANALYSIS OF RESULTS

The three spectra curves of floating slab track, ballast track and the background levels measured underneath the viaduct are shown in Figure 5.13a. The peak at 40Hz band should be contributed from the parametric excitation of rail-pad support passage frequency as shown in Table 5.3. The peak observed at 63Hz band should represent the response at the wheel-ballast resonance (Table 5.2).

The minor peak at 200Hz in the 1/3 octave band with floating slab (Figure 5.13a) should be due to the bending resonance of the floating slab in transverse direction. The first transverse symmetric bending is found to be 192Hz by FEM (see Table 5.8). However, the short-length slab (1.17m) in longitudinal direction has the bending resonance frequency much higher than the frequency of interest for structure-borne vibration of rail traffic. In general, the theoretical resonance frequencies agree well with the experimental result (Figure 5.13b).

Comparisons of the experimental and theoretical vibration reduction are shown in Figure 5.14. The negative vibration reduction in the 16Hz and 20Hz bands should correspond to the isolation system resonance at 14Hz (see Figure 5.14). The degradation of vibration efficiency compared with ideal 1-dof prediction at the 200Hz band should be due to the bending resonance of the floating slab in a transverse direction. This is not a serious problem since the reduction is still above 25dB.

In general, the floating slab design achieved an effective vibration reduction of 10- 45dB in the frequency range of 25-250 Hz bands. The detrimental effect of floating slab bending resonance is slight because the bending mode is at 192Hz which is far away from the passage support frequency at 36Hz. The vibration reduction performance can be better than 1-dof ideal prediction since the isolation consist of 2-stage. The maximum train speed for West Rail, however, is limited to be lower than 130km/h since the static deflection of the slab is about 9mm, which is not acceptable for the safe operation of higher speed train.

It is also observed that bending resonances on supporting structure, as mentioned in Chapter 4, have no significant effects on the vibration isolation performance of all above viaduct tracks in measurement locations; this should be mainly because of the high impedance of the supporting structures.

5.8 SUMMARY

On the basis of the laboratory test and site measurement results on rail viaduct vibration with various isolation systems, the following conclusions can be drawn:

The bending resonance of a floating slab has a negative influence on the vibration isolation performance. The bending resonance of the floating slab can be easily estimated with a simple free-free beam formula which can be applied in the initial design of the slab.

The effects on vibration reduction becomes more significant when the bending resonance frequencies of floating slab is close to the passage support frequency or vertical natural frequency.

There is a benefit for vibration isolation using mini-size floating slabs which gives the high bending resonance frequencies. It, however, may not be suitable for higher speed trains (>130km/h) due to the high static deflection.

The medium-length floating slab with spring isolator and viscous damper can achieve effective vibration isolation for high-speed railways.

The use of floating ladder track should be an economic way of attenuating vibration transmission from rail viaduct structures, but the vibration isolation performance is limited by the bending resonances of the ladder.

REFERENCES

Hussein, M.F.M. and Hunt, H.E.M. (2006a). Modelling of floating-slab tracks with continuous slabs under oscillating moving loads. *Journal of Sound and Vibration*, 297(1–2): 37–54.

Hussein, M.F.M. and Hunt, H.E.M. (2006b). Modelling of floating-slab track with discontinuous slab, part 1: response to oscillating moving loads. *Journal of Low Frequency Noise, Vibration and Active Control*, 25(1): 23-39.

Hussein, M.F.M. and Hunt, H.E.M. (2006c). Modelling of floating-slab track with discontinuous slab, part 2: response to moving trains. *Journal of Low Frequency Noise, Vibration and Active Control*, 25(2): 111-118.

Lombaert, G., Degrande, G., Vanhauwere, B., Vandeborghht, B. and François, S. (2006). The control of ground-borne vibrations from railway traffic by means of continuous floating slabs. *Journal of Sound and Vibration*, 297(3–5), 946–961.

Moritoh, Y., Zenda, Y. and Nagakura, K. (1996). Noise Control of High Speed Shinkansen. *Journal of Sound and Vibration*, 193(1):319-334.

Saurenman, H. and Phillips, J. (2006). In-service tests of the effectiveness of vibration control measures on the BART rail transit system. *Journal of Sound and Vibration*, 293(3–5), 888–900.

Zach, A. (2000). Vibration insulation research results in Switzerland. *Journal of Sound and Vibration*, 231(3), 877–882.

International Standard, ISO 14837-1:2005(E). Mechanical vibration – Ground-borne noise and vibration arising from rail systems – Part 1: Guidance.

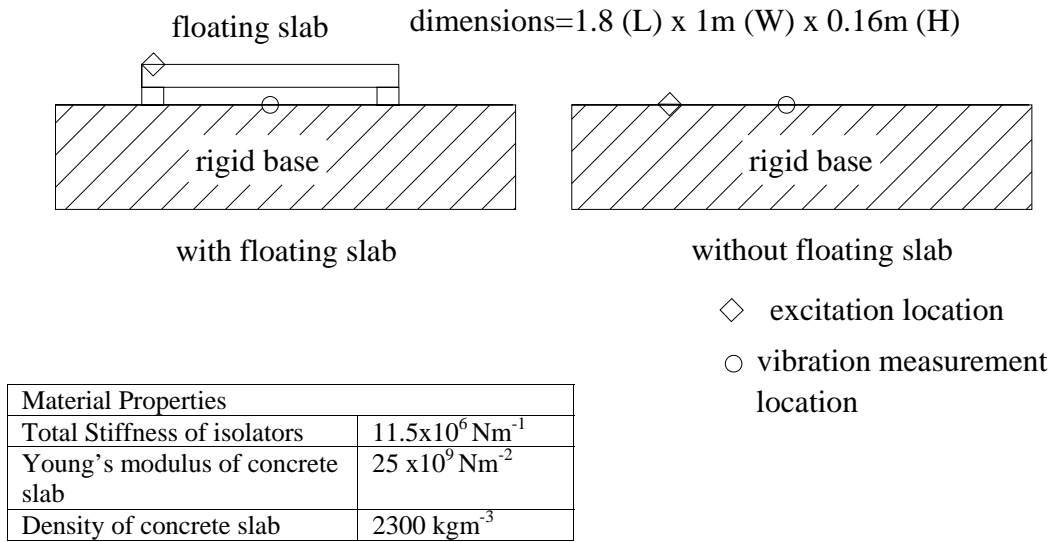


Figure 5.1 The transmissibility measurement of floating slab model

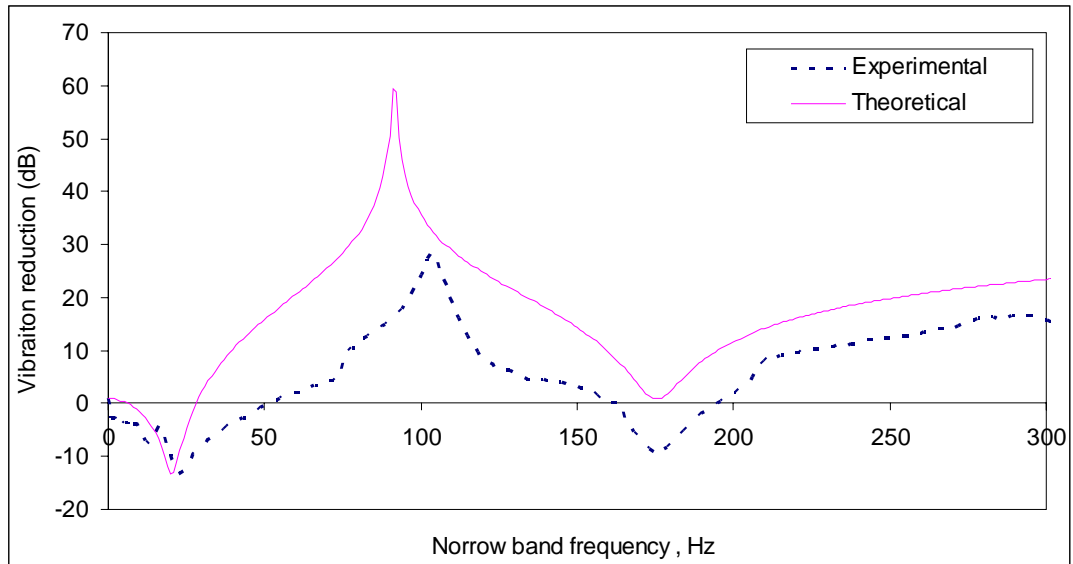


Figure 5.2a Comparison of vibration reduction performance of floating slab model

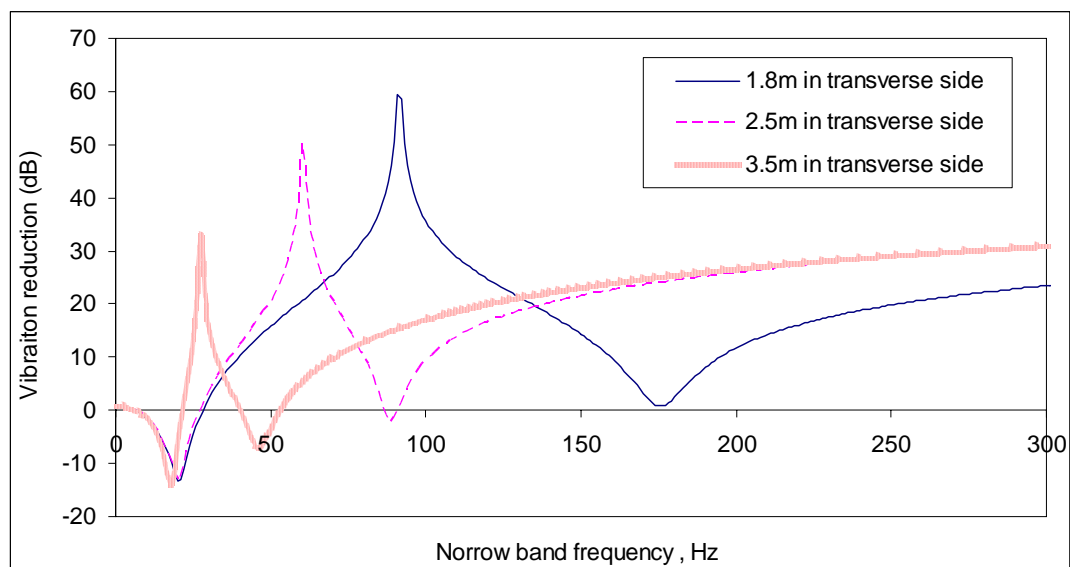
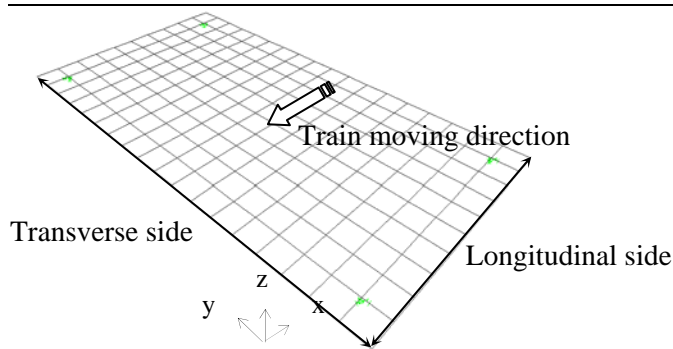


Figure 5.2b Theoretical vibration reduction performance of different size (in transverse direction) of floating slabs



Original shape

Resonance frequency (Hz)			Mode shape description (Ref. Figure 2.5)
No.	FEM	Simple equation	
1	14.8		Rigid body mode – longitudinal
2	14.9		Rigid body mode - Transverse
3	20.6	21 (design)	Rigid body mode -Vertical
4	22.2		Rigid body mode – Pitch
5	28.7		Rigid Body mode –Yaw
6	32.2		Rigid Body mode –roll
7	168.9	167 (Equation 2.6)	Bending mode – 1st transverse symmetric
8	197.3		Bending mode – 1 st anti-symmetric in both axes
9	426.1		Bending mode – 2 nd transverse symmetric and 1 st longitudinal anti-symmetric
10	456.4		Bending mode – 2 nd transverse anti-symmetric
11	534.5	542 (Equation 2.6)	Bending mode- 1st longitudinal symmetric

Figure 5.3 The first eleven resonant modes of floating slab model estimated by Finite Element Method

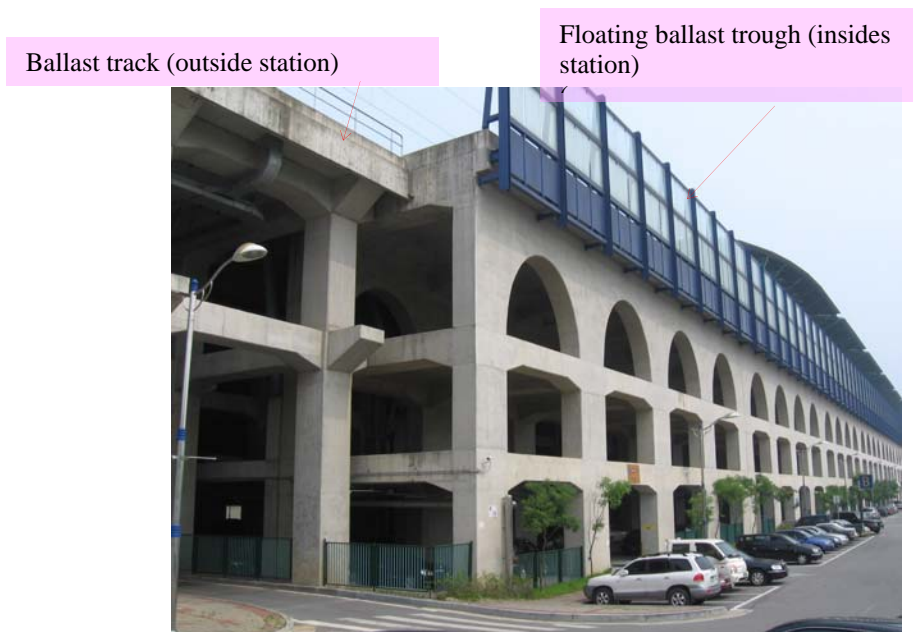


Figure 5.4 Photograph of Korean KTX station with medium floating slab installation

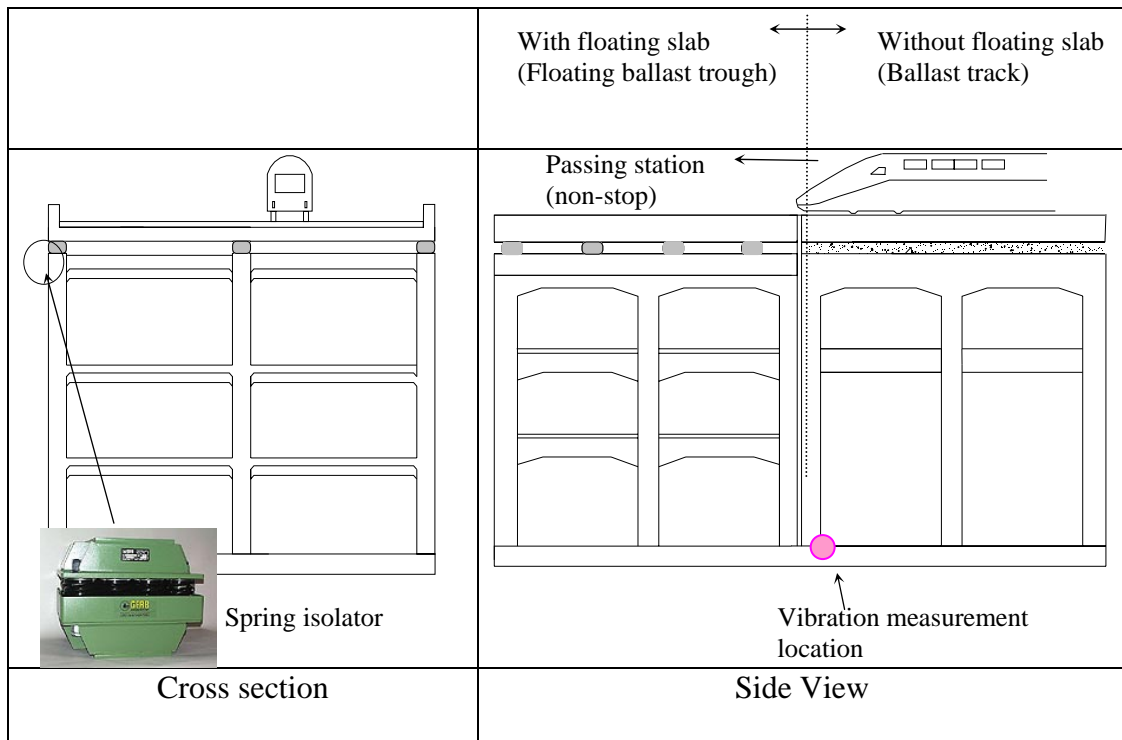


Figure 5.5 Sketch of in-situ vibration measurement in Korean KTX station

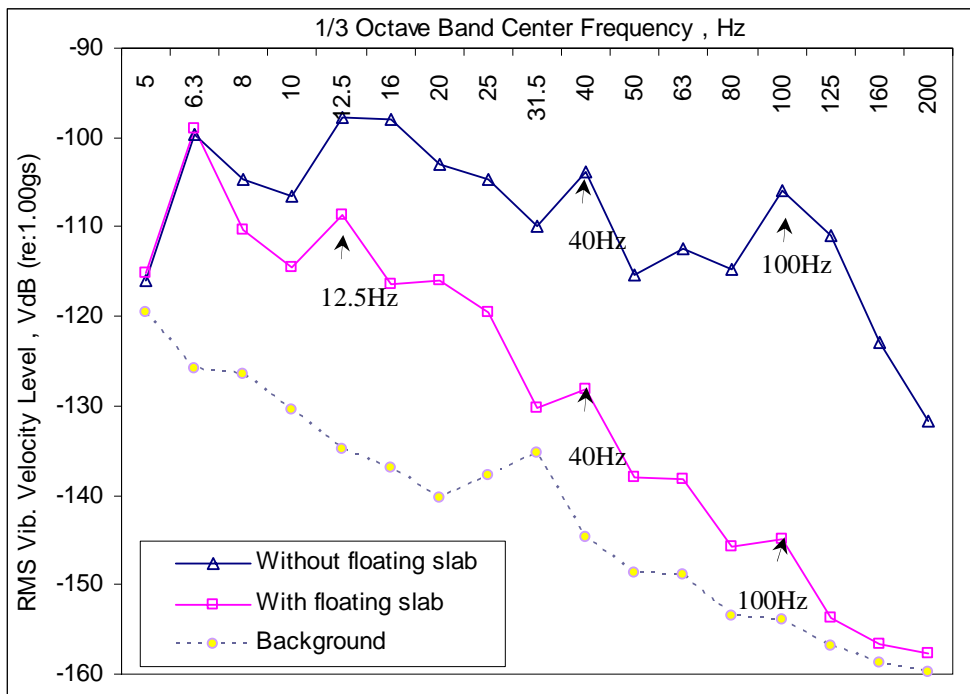


Figure 5.6a Vibration velocity levels measured at KTX station in Seoul (Korea)

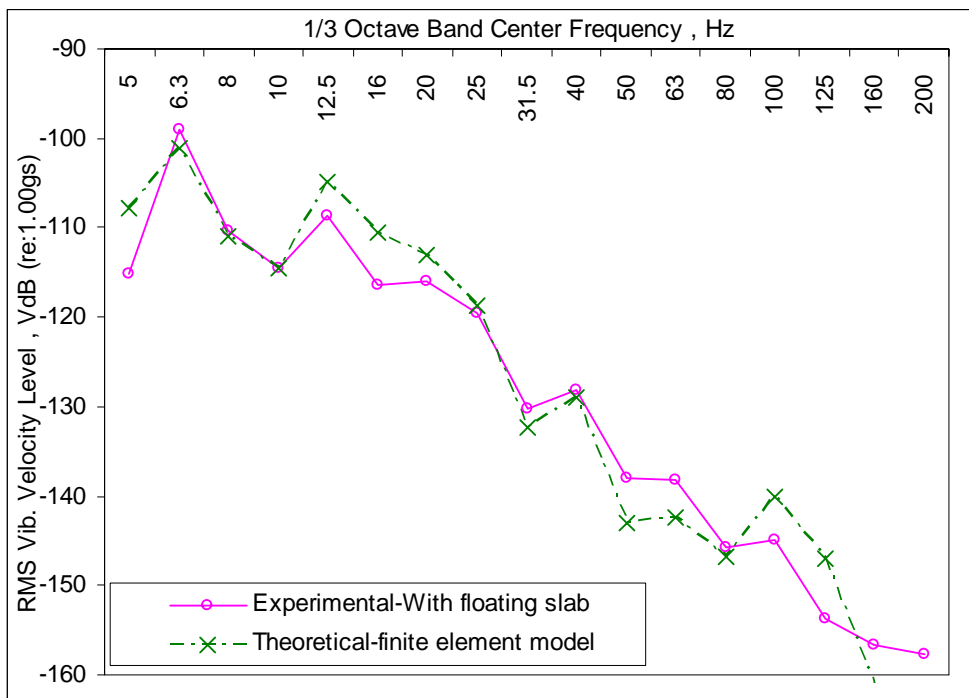


Figure 5.6b Experimental and theoretical vibration velocity level at station with medium size floating slab for Korean KTX

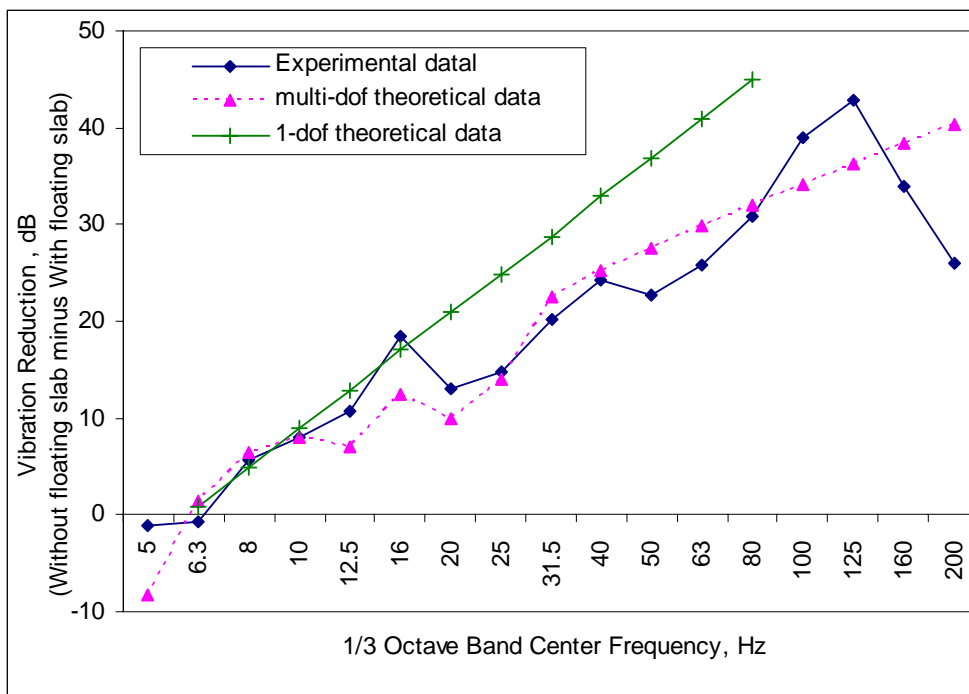


Figure 5.7 Experimental and theoretical vibration reduction levels for without floating slab minus with floating slab. (KTX station in Korea)

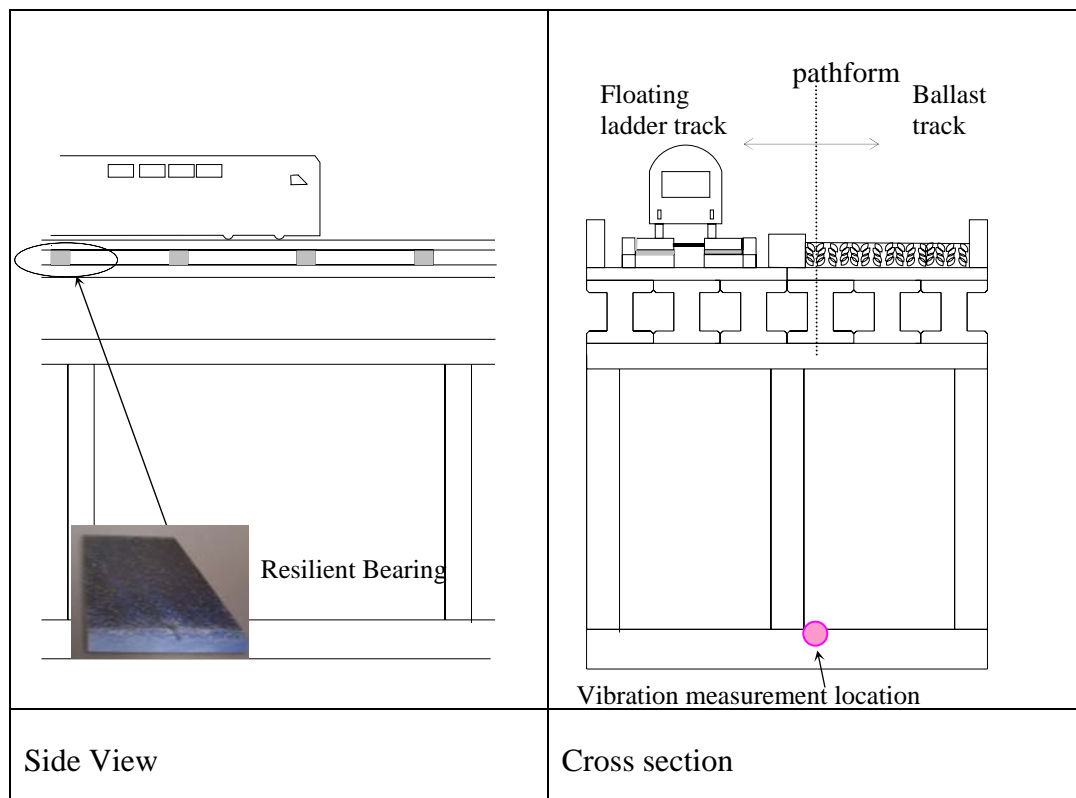


Figure 5.8 Sketch of in-situ vibration measurement at station with floating ladder in Japan (Tokyo)

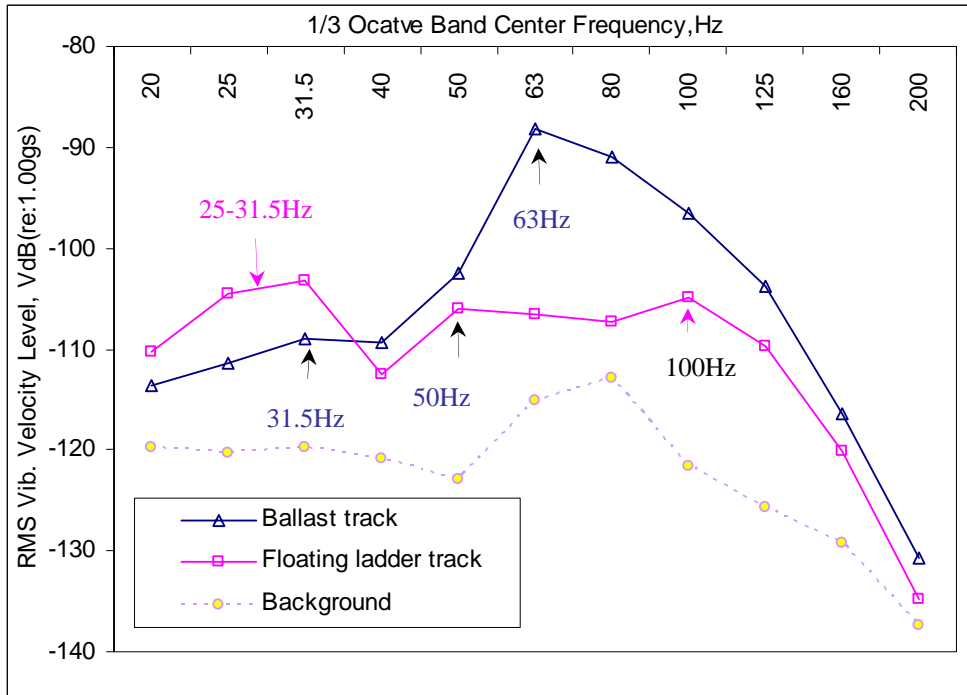


Figure 5.9a Vibration velocity levels measured at station in Japan (Tokyo)

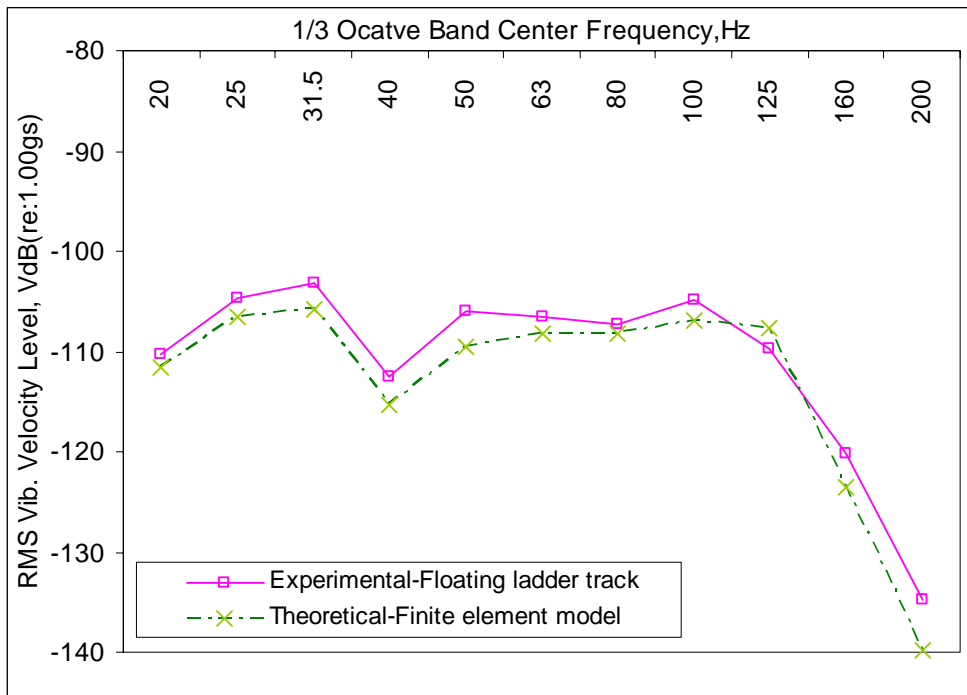


Figure 5.9b Experimental and theoretical vibration velocity level at station with floating ladder track in Japan (Tokyo)

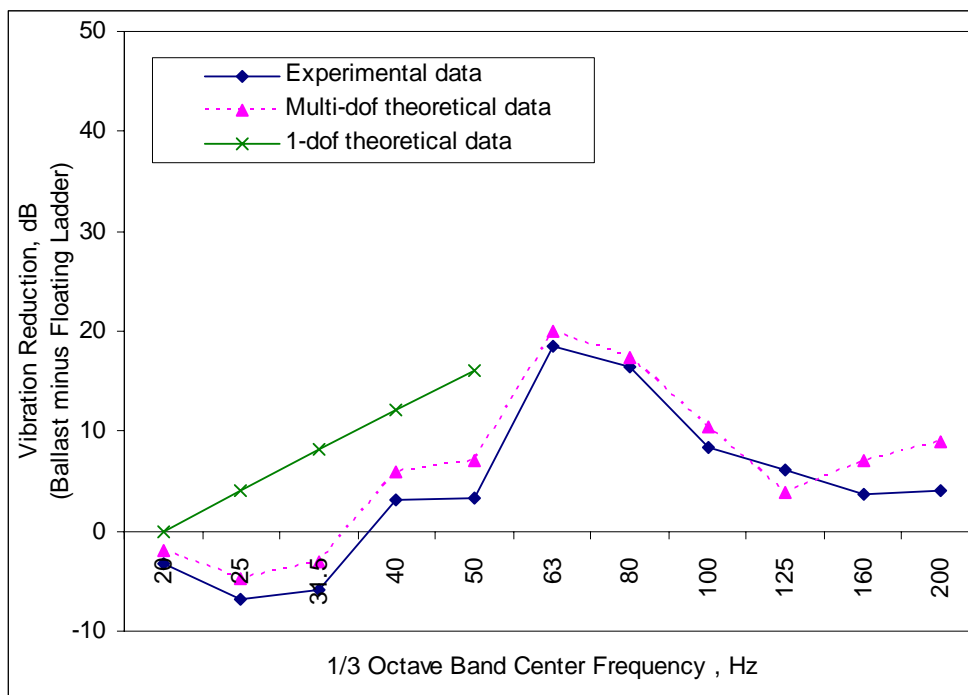


Figure 5.10 Vibration reduction levels at station with floating ladder in Japan (Tokyo)

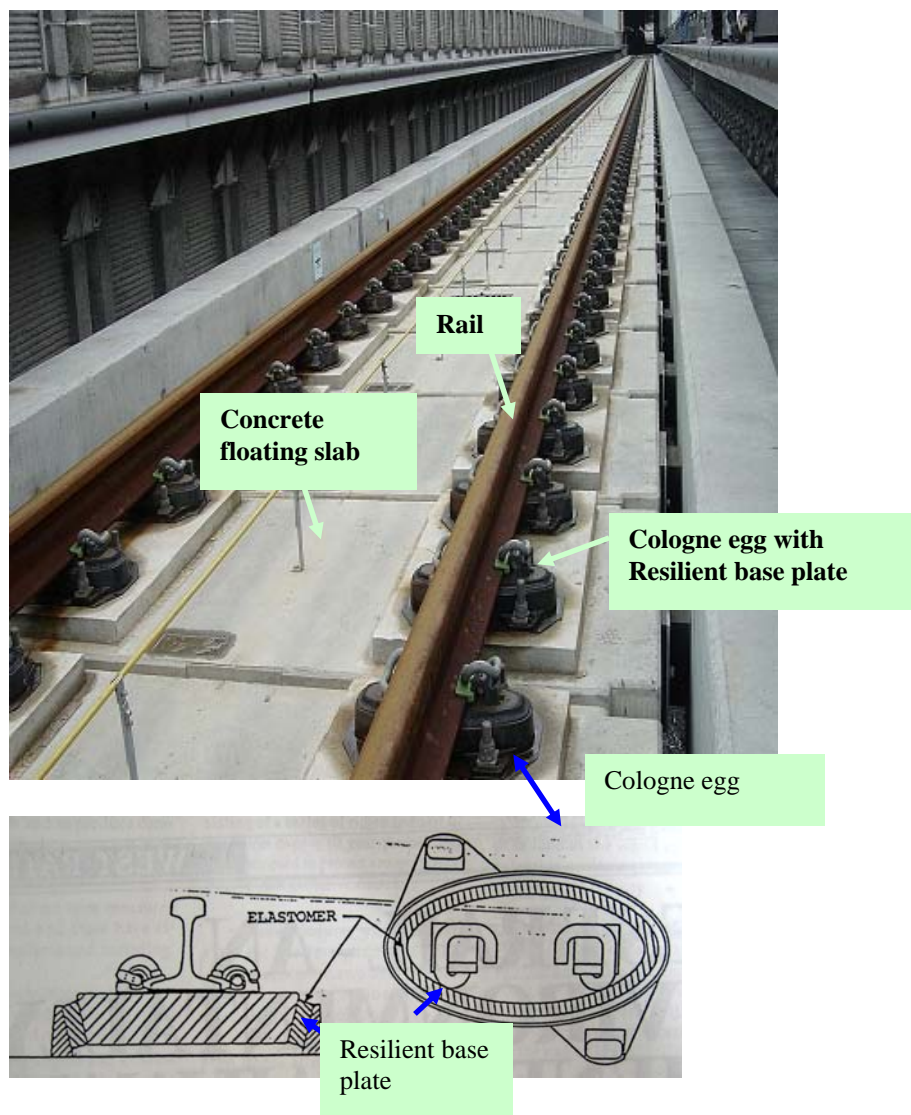


Figure 5.11 Resilient base plate installed between the rail and floating slab

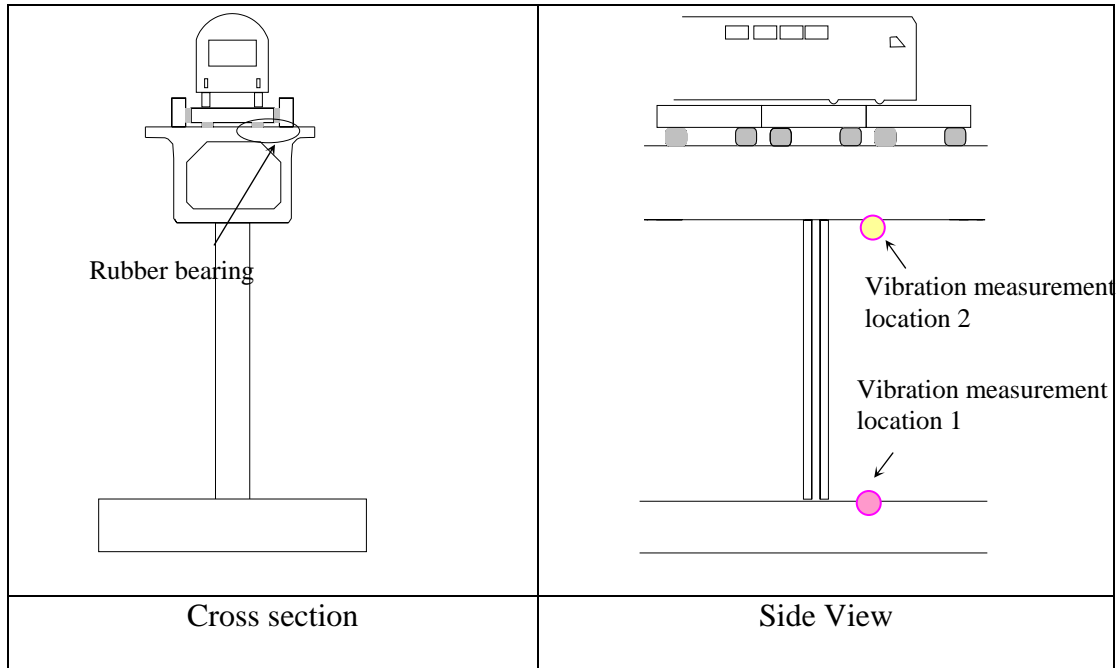


Figure 5.12 Sketch of in-situ vibration measurement station with short size floating slab in China (Hong Kong)

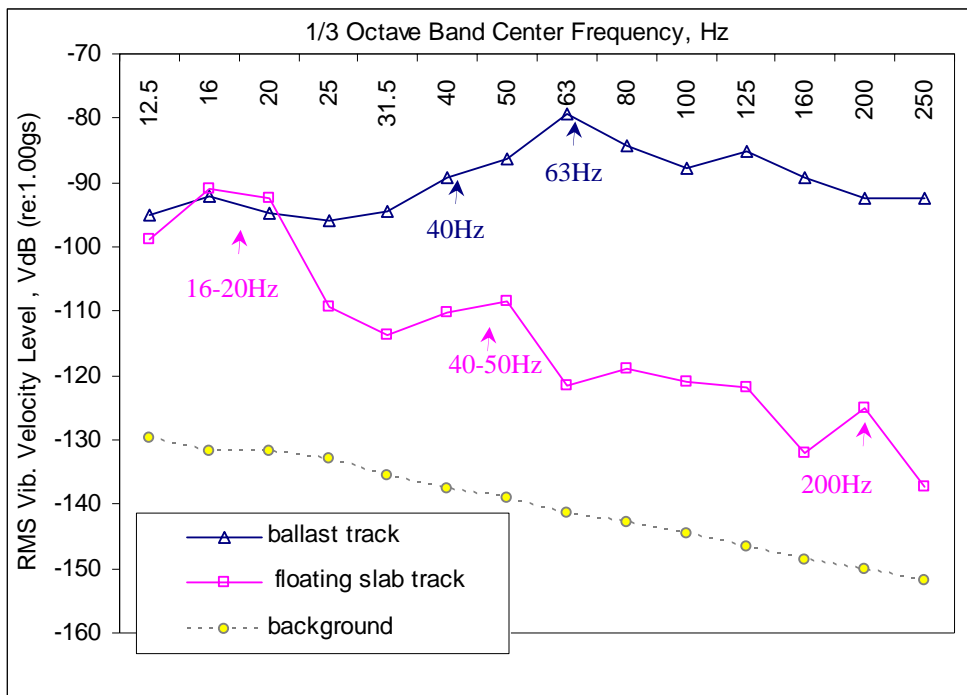


Figure 5.13a Vibration velocity levels measured at station with short size floating slab in China (Hong Kong)

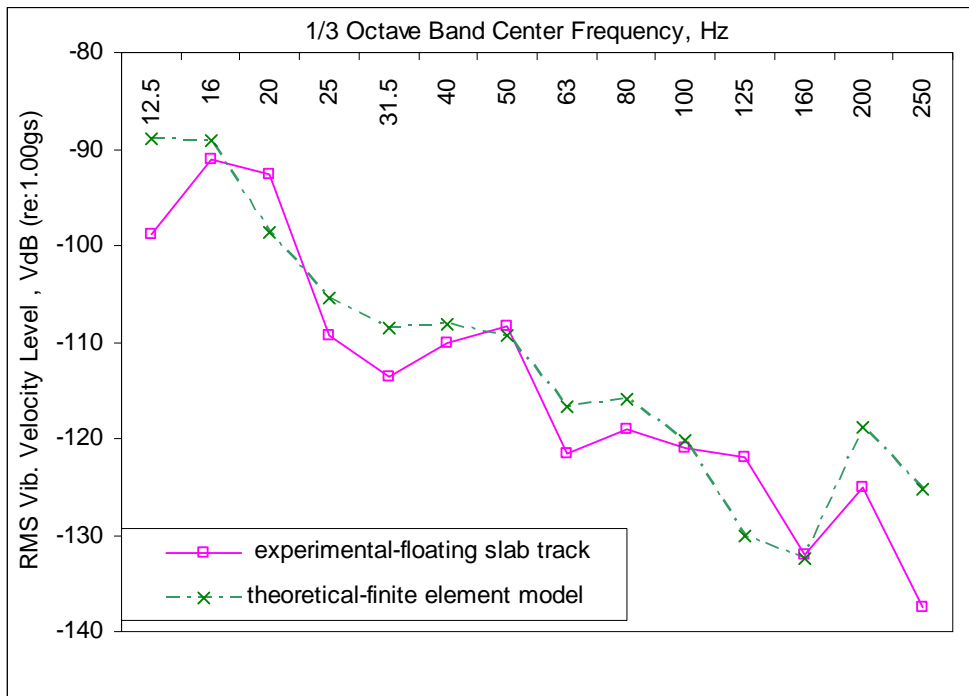


Figure 5.13b Experimental and theoretical vibration velocity levels at station with short size floating slab (Hong Kong)

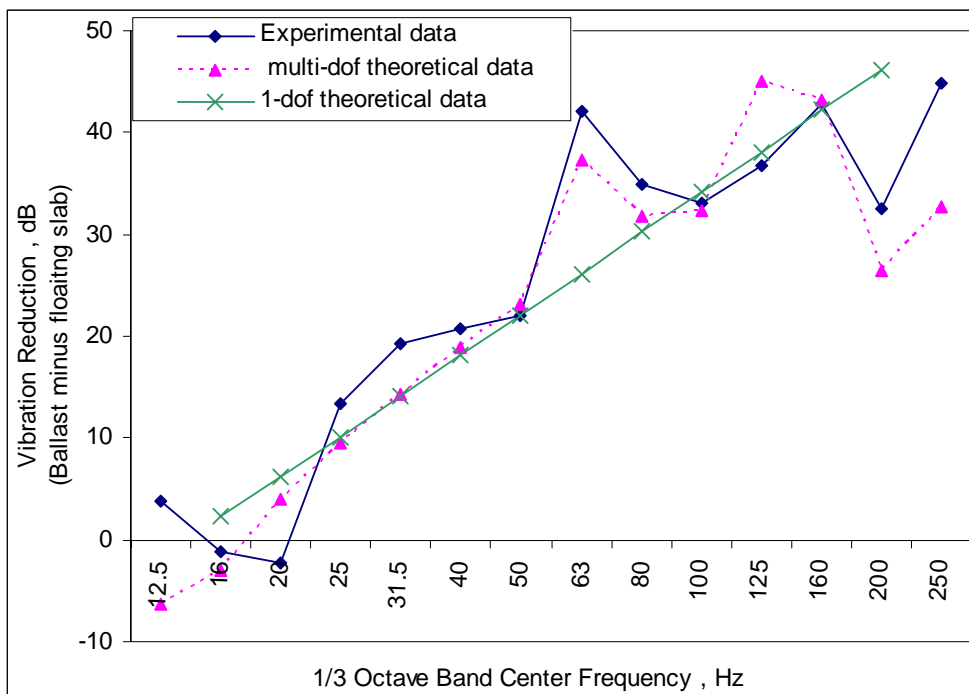
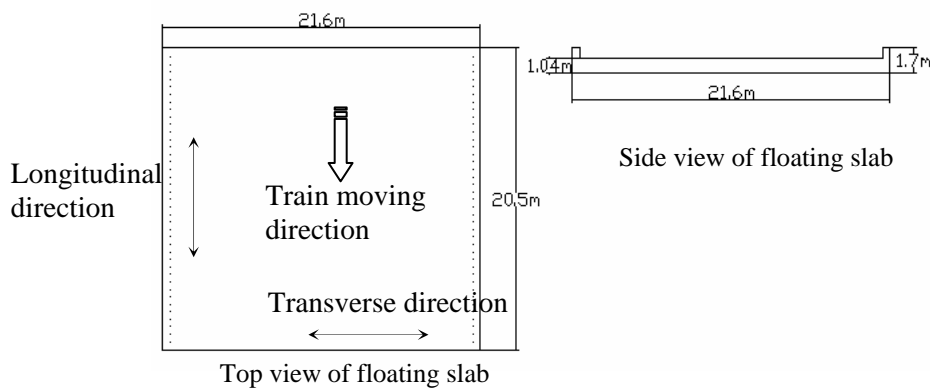


Figure 5.14 Experimental and theoretical vibration reduction levels for ballast track minus floating slab track. (West Rail station in Hong Kong)

Table 5.1 Parameters used in track models for medium-length floating slab and control ballast track located in Korea (Seoul)

Train	Mass of car body	26000 kg
	Train speed	230 km/h
	Unsprung mass per wheel	1000 kg
	Primary suspension resonance	3.2 Hz
Rail	Young's modulus	$210 \times 10^9 \text{ N/m}^2$
	Mass	60.3 kg/m
	Moment of inertia	$39.6 \times 10^{-6} \text{ m}^4$
	Section area	0.015 m^2
	Poisson ratio	0.3
Rail pad	Dynamic stiffness	90 MN/m
	Static stiffness	45 MN/m
	Damping	~0.1
	Rail pad spacing	0.6 m
Ballast	Stiffness	~70 MN/m
	Damping	~0.1
	Sleeper spacing	0.6 m
Concrete floating slab	Young's modulus	$25 \times 10^9 \text{ Nm}^{-2}$
	Slab density	2300 kgm^{-3}
	Total stiffness of isolators per slab	$1586 \times 10^6 \text{ Nm}^{-1}$
	Poisson ratio	0.2
	Damping	0.025

Sketch of floating slab and dimensions (not to scale)

Supporting concrete structure	Young's modulus	$\sim 25 \times 10^9 \text{ Nm}^{-2}$
	Concrete density	2300 kgm^{-3}
	Poisson ratio	0.2
	Damping	0.02
<u>Sketch of supporting structure and dimensions (not to scale)</u>		
Cross section		Side view

Table 5.2 Calculated rail track resonance frequencies

	Medium-size floating slab track on the Korean High Speed Railway (KTX) (Hz)	Floating ladder track in Japan (Tokyo) (Hz)	Short-size floating slab track in China (Hong Kong) (Hz)
Floating slab rigid body resonance	6	~25	14
Bending resonances of floating slab	8 (1 st transverse) 12 (1 st longitudinal)	29(1 st longitudinal) 53(2 nd longitudinal) 97(3 rd longitudinal)	192(1 st transverse) 910(1 st longitudinal)
Wheel-rail pad resonance (cut-on frequency)	48	152	32 (resilient baseplate)
Wheel-ballast resonance (relative control experiment on ballast track)	42	57	58

Table 5.3 Moving load at support passage frequency (parametric excitation)

	Medium-size floating slab track on the Korean High Speed Railway (KTX)	Floating ladder track in Japan (Tokyo)	Short-size floating slab track in China (Hong Kong)
Rail-pad or sleeper support passage frequency	106Hz	36Hz	37Hz

Table 5.4 Natural frequency results for medium size floating slab located in Korean KTX station

Resonance frequency (Hz)		Description
FEM	Simple equation	
4.13		Rigid body mode – Transverse
4.14		Rigid body mode – Longitudinal
4.32		Rigid body mode – Pitch
5.68		Rigid body mode – Roll
5.75	6 (design)	Rigid body mode – Vertical
6.56		Rigid body mode – Yaw
8.3		Bending mode – 1 st anti-symmetric in both axes
8.5	8 (Equation 2.6)	Bending mode – 1st transverse symmetric
12.4	13 (Equation 2.6)	Bending mode- 1st longitudinal symmetric

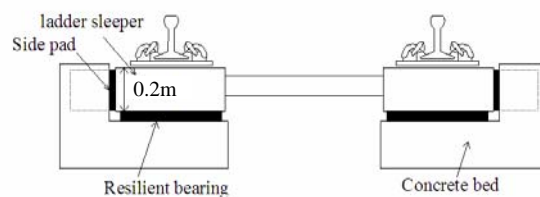
Remarks:

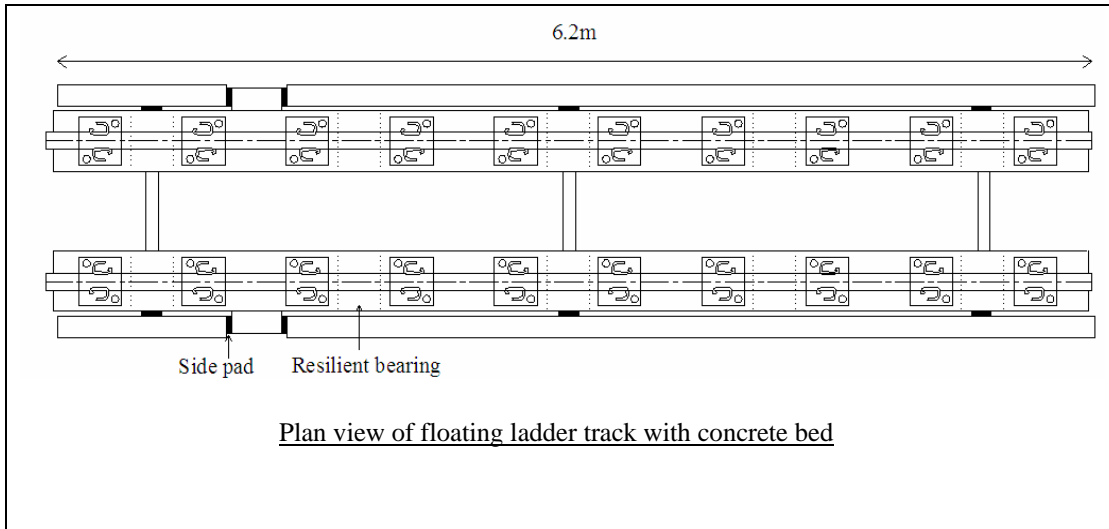
Size of floating slab in transverse direction = 21.6m (length) x 1.04m (thickness)

Size of floating slab in longitudinal direction = 20.5m (length) x 1.7m (thickness)

Table 5.5 Parameters used in track models for floating ladder track and control ballast track located in Japan (Tokyo)

Train	Mass of car body	44000 kg
	Train speed	80 km/h
	Unsprung mass per wheel	~500 kg
	Primary suspension resonance	~5 Hz
Rail	Young's modulus	$210 \times 10^9 \text{ N/m}^2$
	Mass	60 kg/m
	Moment of inertia	$30.9 \times 10^{-6} \text{ m}^4$
	Section area	0.01 m^2
	Poisson ratio	0.3
Rail pad	Dynamic stiffness (rail pad)	~490 MN/m
	Static stiffness (rail pad)	~245 MN/m
	Damping (rail pad)	~0.1
	Rail pad spacing	0.6 m
Ballast	Stiffness	~70 MN/m
	Damping	~0.1
	Sleeper spacing	0.6 m
Concrete floating ladder	Young's modulus	$25 \times 10^9 \text{ Nm}^{-2}$
	Slab density	2300 kgm^{-3}
	Total stiffness of isolators per slab	$28.1 \times 10^6 \text{ Nm}^{-1}$
	Poisson ratio	0.2
	damping	0.025

Sketch of floating ladder and dimensions (not to scale)Side view of floating ladder



Supporting concrete structure	Young's modulus	$\sim 25 \times 10^9 \text{ Nm}^{-2}$
	Concrete density	2300 kgm^{-3}
	Poisson ratio	0.2
	Damping	0.02

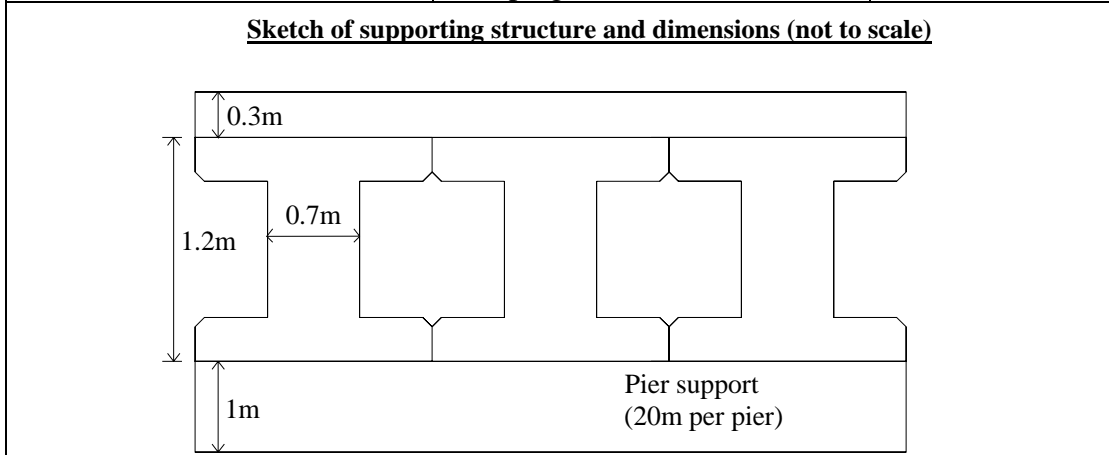


Table 5.6 Natural frequency results for floating ladder track located in Japan (Tokyo)

Resonance frequency (Hz)		Description
FEM	Simple equation	
0.0001		Rigid body mode – Roll
16.7		Rigid body mode – Pitch
17.6		Rigid body mode – Transverse
17.7		Rigid body mode – Longitudinal
23.2		Rigid body mode – Yaw
24.6	25 (design)	Rigid body mode – Vertical
28.7	18 (Equation 2.6)	Bending mode- 1st longitudinal symmetric
53	49 (Equation 2.6) ($\lambda = 7.85$)	Bending mode- 2nd longitudinal symmetric
97.3	95 (Equation 2.6) ($\lambda = 7.85$)	Bending mode- 3rd longitudinal symmetric

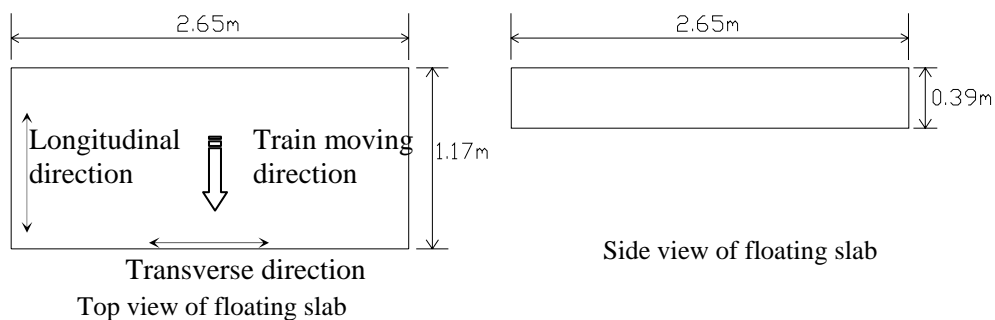
Remarks:

Size of floating ladder in transverse direction = 0.5m (length) x 0.2m (thickness)

Size of floating ladder in longitudinal direction = 6.2m (length) x 0.2m (thickness)

Table 5.7 Parameters used in track models for short size floating slab track and control ballast track located in China (Hong Kong)

Train	Mass of car body	68000kg
	Train speed	80km/h
	Unsprung mass per wheel	~500kg
	Primary suspension resonance	6.5Hz
Rail		
	Young's modulus	$210 \times 10^9 \text{ N/m}^2$
	Mass	60.3kg/m
	Moment of inertia	$39.6 \times 10^{-6} \text{ m}^4$
	Section area	0.015 m^2
	Poisson ratio	0.3
Rail pad		
	Dynamic stiffness	21MN/m
	Static stiffness	10.5MN/m
	Damping	~0.1
	Rail pad spacing	0.6 m
Ballast		
	Stiffness	~70MN/m
	Damping	~0.1
	Sleeper spacing	0.6 m
Concrete floating slab		
	Young's modulus	$25 \times 10^9 \text{ Nm}^{-2}$
	Slab density	2300 kgm^{-3}
	Total stiffness of isolators per slab	$21.7 \times 10^6 \text{ Nm}^{-1}$
	Poisson ratio	0.2
	Damping	0.025

Sketch of floating slab and dimensions (not to scale)

Supporting concrete structure	Young's modulus	$\sim 25 \times 10^9 \text{ Nm}^{-2}$
	Concrete density	2300 kgm^{-3}
	Poisson ratio	0.2
	Damping	0.02
<u>Sketch of supporting structure and dimensions (not to scale)</u>		
<p style="text-align: center;">Pier support (30m per pier)</p>		

Table 5.8 Natural frequency results for short size floating slab located in China (Hong Kong)

Resonance frequency (Hz)		Description
FEM	Simple equation	
9.77		Rigid body mode – Longitudinal
9.78		Rigid body mode – Transverse
13.8	14 (design)	Rigid body mode – Vertical
15.8		Rigid body mode – Yaw
20.2		Rigid body mode – Roll
192	195 (Equation 2.6)	Bending mode – 1st transverse symmetric
271.7		Bending mode – 1 st anti-symmetric in both axes
537.6		Bending mode – 2 nd transverse symmetric and 1 st longitudinal anti-symmetric
584.8		Bending mode – 2 nd transverse anti-symmetric
909.1	917 (Equation 2.6)	Bending mode- 1st longitudinal symmetric

Remarks:

Size of floating slab in transverse direction = 2.65 (length) x 0.39m (thickness)

Size of floating slab in longitudinal direction = 1.17m (length) x 0.39m (thickness)

CHAPTER 6

BENDING-RESONANCE EFFECTS ON VIBRATION REDUCTION OF ISOLATED FLOOR AND BOX

Both experimental and site measurement results in the previous two chapters show that bending resonances of floating slab using at the source can degrade the vibration isolation performance. The effects of bending resonance of a typical heavy weight isolated concrete floor, and a lighter cement floor, as well as an advance design of box-within-box structures on vibration isolation performance at the receiver are examined in this Chapter.

6.1 INTRODUCTION

Vibration reductions of different sizes of floating slabs were examined in experimental and/or theoretical aspects in Chapters 4 and 5. For the constant of isolator natural frequency, material and thickness of the floating slab, the longer of the slab, the lower the bending resonance frequency and the worse the vibration isolation performance.

When a noise sensitive receiver is built after the rail track is established, the buildings may need to be isolated: floating floor and box-within-box structure are the popular vibration isolation designs to reduce the energy transmission from the base to the isolated floor.

The choices of the size and material for floating floor, however, should be more flexible as mentioned in Chapter 1. The sizes of traditional floating floor panels are usually rather large (about 1m x 2m) for production and installation convenience. Experimental investigations on

these large floor panels have been conducted by various authors (Clark and Harry, 1996; Nilsson, 1977 & Wollström, 2000).

Floating floor panels are usually made of concrete, wood, or steel. Concrete slabs have generally lower acoustic transmission levels than lightweight floor panels at high frequencies (Harris, 1994), but are not commonly used because of their heavy weight, thus thinner cement panel around 15 to 40 mm thick was selected to instead.

In this study, the resonant modes, motion transmissibility of two floating floors, and an existing isolated box structure were performed in experimental method, to understand the effects of bending modes on the vibration isolation performance. The experimental vibration results were verified with theoretical prediction. Finally, a field noise and vibration test were conducted and analyzed at an existing isolated box (hotel); the two-storey hotel of isolated box design is constructed underneath a rail viaduct of ballast track in Japan (Tokyo). The special isolation design gives a natural frequency of 3Hz, which is lower than the traditional isolated box structure (Osako et al. 2004).

6.2 VIBRATION ANALYSIS OF ISOLATED FLOORS

Two isolated panels were employed to conduct the experimental test. The first one is the traditional heavy concrete panel, the other one is the thinner and lighter cement panel. Those isolation systems have similar resonance frequency at around 20 Hz with different isolators in order to study the effects of bending modes on vibration isolation performance.

6.2.1 EXPERIMENTAL SETUP

The dimensions and material properties of the test panels are listed in Table 6.1. The dimensions of the concrete floor are 2m (L) x 1m (W) x 0.15m (H) ; the thinner cement floor

are 0.52m (L) x 0.52m (W) x 0.015m (H). Floor panel supported with four soft rubber isolators placed near the four edges.

Figure 6.1 shows the experimental measurement for motion transmissibility identification. Impact force was created with the same technique used in Section 5.2 of chapter 5; however, the difference was the excitation position of the steel ball should be on the rigid base.

The impact vibration spectrum was measured via an ENDEVCO accelerometer which was mounted on the rigid floor as the reference, and the corresponding vibration responses were registered via B&K accelerometer along the short and long sides (center lines) of the isolated floors. The input and output acceleration signals were processed by the B&K PULSE analyzer worked in real-time modes at a frequency resolution of 1Hz from 0-200Hz. The motion transmissibility results of impact excitation source and response spectrums under the frequency response function analysis (FRFs) (Response (Acceleration) / Excitation (Acceleration)) were established.

The center point vibration is the highest for symmetric bending modes and the vertical rigid body mode. Thus, the motion transmissibility at center point of the floors was presented in narrow band (1Hz resolution).

The value of the imaginary part of the FRFs at resonance was proportional to the modal displacement and therefore the mode shapes can be established. As in previous chapters, the vibration mode shapes and corresponding resonances frequency were verified with FEM and simple beam and plate equations (Equations 2.6 to 2.8).

6.2.2 ANALYSIS OF RESULTS

The transmissibility appeared amplification at a rigid body resonance frequency for both panels at around 20Hz as presented in Figure 6.2. Table 6.2 describes the concrete panel

vibration mode shapes of corresponding resonance peaks in Figure 6.2. The second transmissibility peak at 130Hz should represent the response at the first bending mode in long span (y-direction); the third peak at 492Hz should represent the response at the first bending mode in short span (x-direction). For cement panel, the second and third transmissibility peaks at 145Hz and 367Hz (Figure 6.2) should be due to the first and second symmetric bending modes (Table 6.3).

It is noted that both first and second symmetric bending modes can produce detrimental effects on vibration reduction of two panels. The resonance at first symmetric bending mode can even amplify the vibration. Comparatively, the transmissibility values at the first symmetric bending resonance frequency are similar for two panels. The vibration isolation performance of cement panel, however, is worse in the frequency range from 150-450Hz because of the lower second bending resonance frequency at 367Hz. Thus, the improvement of vibration isolation performance of thin cement panel should be considered.

6.3 NOISE AND VIBRATION ANALYSIS ON ISOLATED BOX

The resonance modes and motion transmissibility and structure-radiated sound in a box-within-box laboratory room were measured to identify the effects of local modes of isolated box on vibration isolation. The mode shapes and corresponding resonance frequencies were verified with Finite Element Model (FEM).

6.3.1 EXPERIMENTAL SETUP

An existing isolated box structure has a special design to achieve 6Hz natural frequency with spring isolators. The experimental set up, dimensions and material properties of the

isolated box are described in Figure 6.3. The dimensions of the isolated laboratory box were 6.57m (L) x 3.84m (W) x 3.24m (H).

The source signal was generated with the similar method as the previous isolated floor analysis; however, the height to drop the steel ball was increased to around 0.6m because of the larger structure to be excited. The motion transmissibility, cross-sectional mode shapes and corresponding resonance frequencies were obtained with the same technique as the isolated floor analysis. The center point vibration is the highest for symmetric bending modes and the vertical rigid body mode. Thus, the motion transmissibility at center point of the floors was presented in narrow band (1Hz resolution).

The sound pressure levels were measured at 1m above the ground in two rooms with and without isolated box. The two rooms have the similar volume of room and absorption area as shown in Figure 6.3. The sound pressure levels at 5 points were averaged separately for two rooms and presented in one-third octave band.

6.3.2 THEORETICAL ANALYSIS

The vibration modes of the isolated room were predicted by a finite element software package Sap 2000 v.8. The isolated room was modelled with shell elements. For the room, the 6.57m length in the x-direction was divided into 20 elements, the 3.84m width in the y-direction was divided into 12 elements, and the 3.24m height in the z-direction was divided into 12 elements. The models took into consideration the bending in the x-y-z dimensions. The elasticity of isolator was selected to give the natural frequency of 6Hz.

6.3.3 ANALYSIS OF RESULTS

The measured center motion transmissibility level is shown in Figure 6.4. The theoretical and the sketched experimental mode shapes for corresponding resonance frequencies of the isolated box are shown in Table 6.4. They confirm that the measured motion transmissibility peaks at 5Hz can represent the resonance at the natural frequency of the isolation system, and at the peaks at 22Hz and 70Hz should be due to the first and second symmetric bending modes of the floor. It is noted that the first symmetric bending modes have vibration amplification.

The measured sound pressure levels are presented in Figure 6.5, the measured sound pressure level peaks at 20Hz and 63Hz bands in the isolated box should correspond to the vibration resonance peaks at around 22Hz and 70Hz. The vibration and noise can be attenuated by around 20dB in the measured frequency of 100-200Hz using the isolated box. The isolated box, however, has lower vibration isolation performance compare with isolated floor below 100Hz because of the effects of local modes at low frequency range.

6.4 FIELD TEST OF ISOLATED BOX (HOTEL) IN TOKYO JAPAN

The two-storey hotel with isolated box design was constructed underneath a rail viaduct station in order to utilize the unused space under the viaduct rail line, and to satisfy the increasing demand of tourists to the new Tokyo Disney Sea opened in 2001 (Osako et al. 2004). The outside view of the hotel under the rail viaduct is shown in Figure 6.6. The building was designed to attenuate the vibration generated from trains and earthquakes. The two-story structure was built with isolated reinforced concrete box. The hotel is a suspended building with suspension rods connected with rubber cushions on the top to the primary viaduct column structure. Dampers were also installed under the floor as described in Figure

6.7. This special design has a vertical resonance frequency of 3Hz. The viaduct rail is a conventional ballast track.

The sound and vibration time-history data were recorded inside a guest room with isolation, and near the reception outside the suspended building and were reordered when trains passed through with a speed of 100km/h. The signals at isolated place and non-isolated place were recorded separately on account of the assessment problem. To reduce the inconsistency of measured data, measurements were conducted at least five times and select the repeatable data for each place.

The spectrums of measured vibration velocity, vibration reduction level and the corresponding sound pressure levels are shown in Figures 6.8a-6.8b and 6.9 separately. Different from Chapter 5 the site vibration measurement levels in this chapter are presented in narrow band (resolution 1Hz), since a more precise identification for mode shape of the isolated box.

For the vibration velocity recorded at the non-isolated floor, the vibration peaks around 50Hz can represent the response at support rail-pad passage frequency. Also the peaks of around 70Hz are attributed to the wheel-ballast resonance. Regarding resonances of rail track has been investigated and studied in Chapters 3 and 5.

The vibration was amplified at 13Hz which should correspond to the response at the first bending resonance in the long span of the measured floor in the isolated guest room, and the other peak at 44Hz should be contributed by the second symmetric bending resonance of the floor. The dips appeared at 24Hz, 62Hz and 84Hz of the floor without isolation and thus the peaks resulted in the vibration reduction spectrum as shown in Figure 6.8b. Therefore, those peaks should not appear if the correlation of vibration signals presented at with or without isolation positions.

The sound reduction performance is degraded at 50Hz band resulting from the bending mode of the floor at 44Hz. The bending mode shapes of the measured isolated room were verified with site measured with free fall a mass of 3kg from height of 0.6m, the same as the laboratory test on the previous isolated box. Two accelerometers registered the vibration motion along the cross-section of the isolated room, one was used as the reference and the other being moved along the room. The sketched experimental mode shapes and corresponding resonance frequencies are shown in Table 6.4. The first and second symmetric bending mode shapes are similar to the isolated box found in previous section, and the resonance frequencies at 12Hz and 45Hz from FEM agree well with the peaks at 13Hz and 44Hz in vibration reduction as show in Figure 6.8b.

In general, the sound and vibration reduction performance above 100Hz is around 25dB. This is an innovative design ensuring that the space under the rail viaduct can be fully used. The local bending modes, however, can induce an adverse effect on the vibration reduction of the isolated hotel below 50Hz.

6.5 SUMMARY

The experimental measurement of isolated floors and isolated boxes confirmed that the bending vibration of them resulting in the degradation of vibration isolation efficiency.

The bending resonances of isolated boxes are even in the low frequency range and the vibration has amplification. Thus, the further investigation in the vibration isolation device at the receiver should be conducted to improve the isolation performance.

REFERENCES

Clark, M. D. and Harry, H. L. (1996). A systematic approach used to design floor panel isolation for a commercial aircraft, *Internoise*, 455-460.

Harris, C. M. (1994). *Noise control in buildings: a guide for architects and engineers*. New York: McGraw-Hill.

Nilsson, A. (1977). Some acoustical properties of floating-floor constructions, *JASA. Journal of the acoustical society of America*, 61(6) 1533-1539.

Osako, K., Hayashiand, A. and Yamada, M. (2004). Development of the sound-and-vibration-proofing method (suspended seismic isolation method) for buildings under elevated railway tracks. *JR East Technical review*. No.4, 34-40.

Wollström, M. (2000). *Floating floors models and simulations of vibration characteristics*, Stockholm.

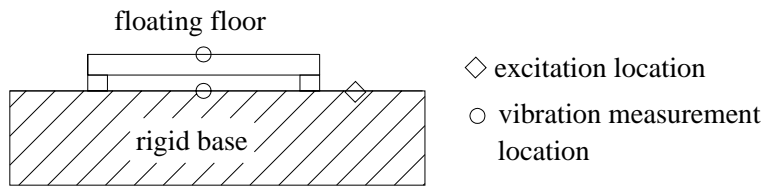


Figure 6.1 The transmissibility measurement of floating floor

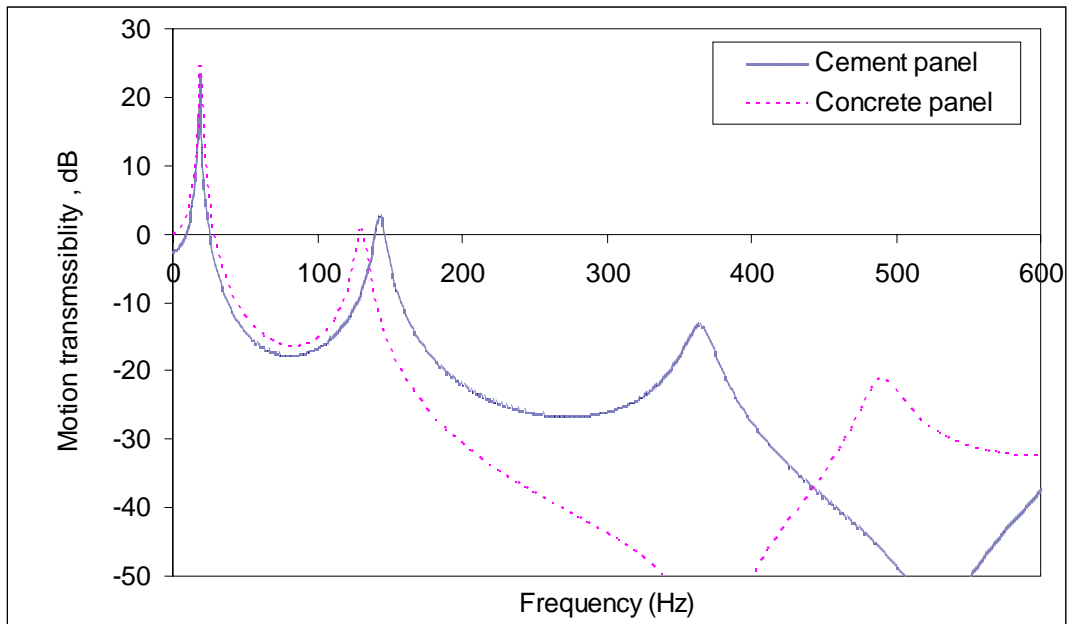


Figure 6.2 Motion transmissibility at the center point of isolated floors

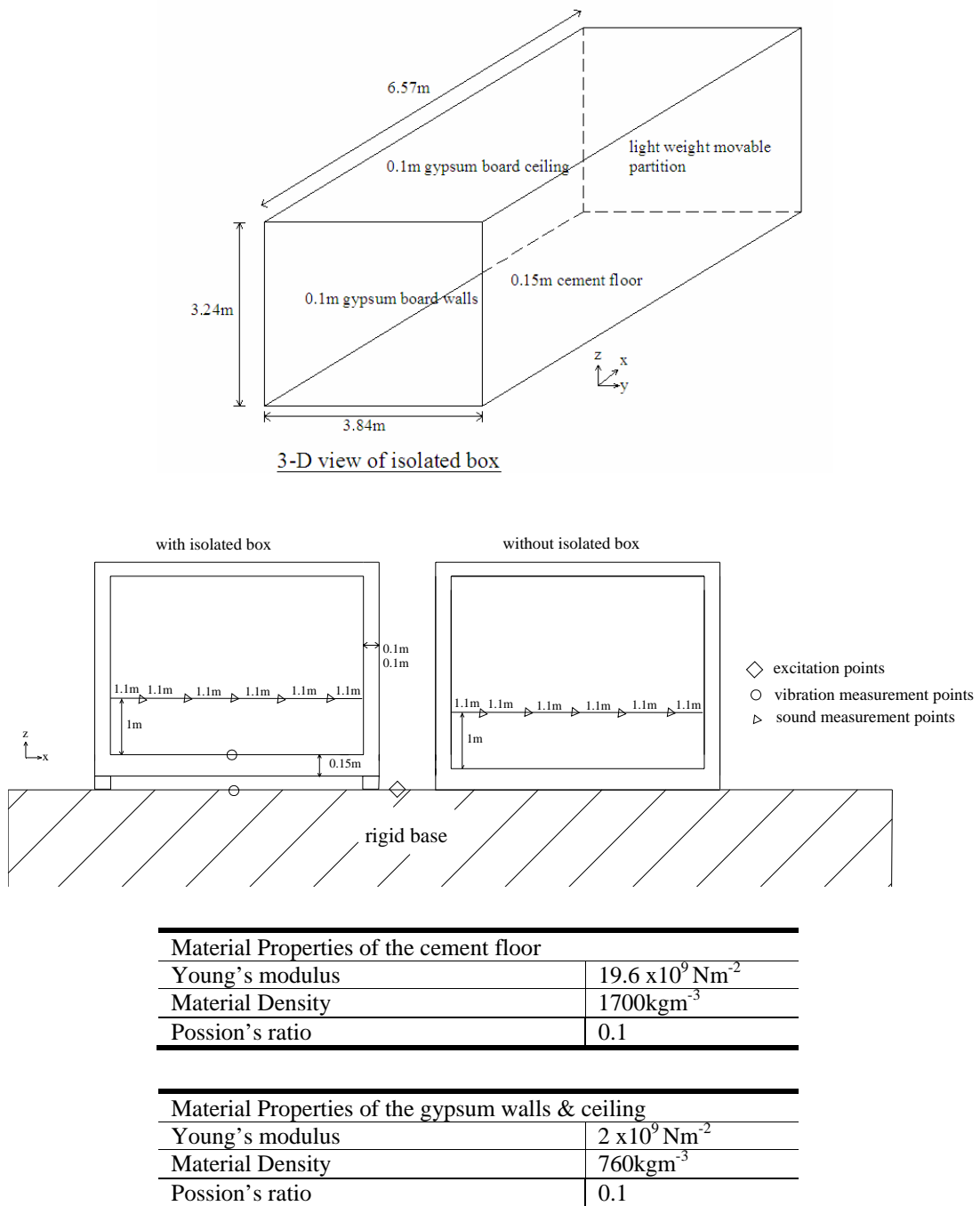


Figure 6.3 Measurement setup , dimension and material properties of isolated box

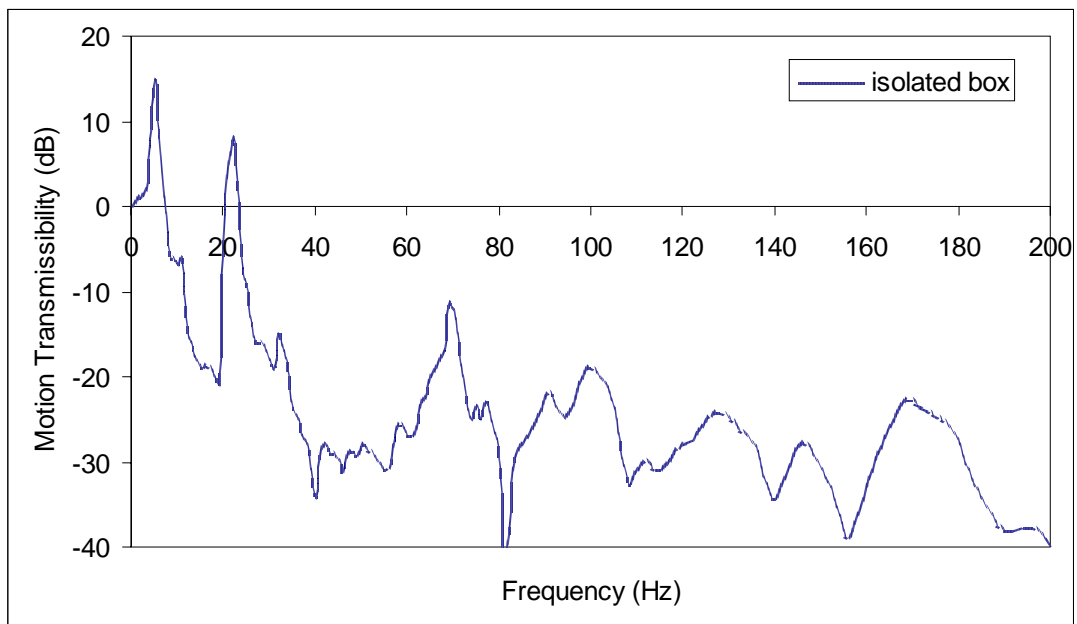


Figure 6.4 Motion transmissibility levels at the center point of isolated box

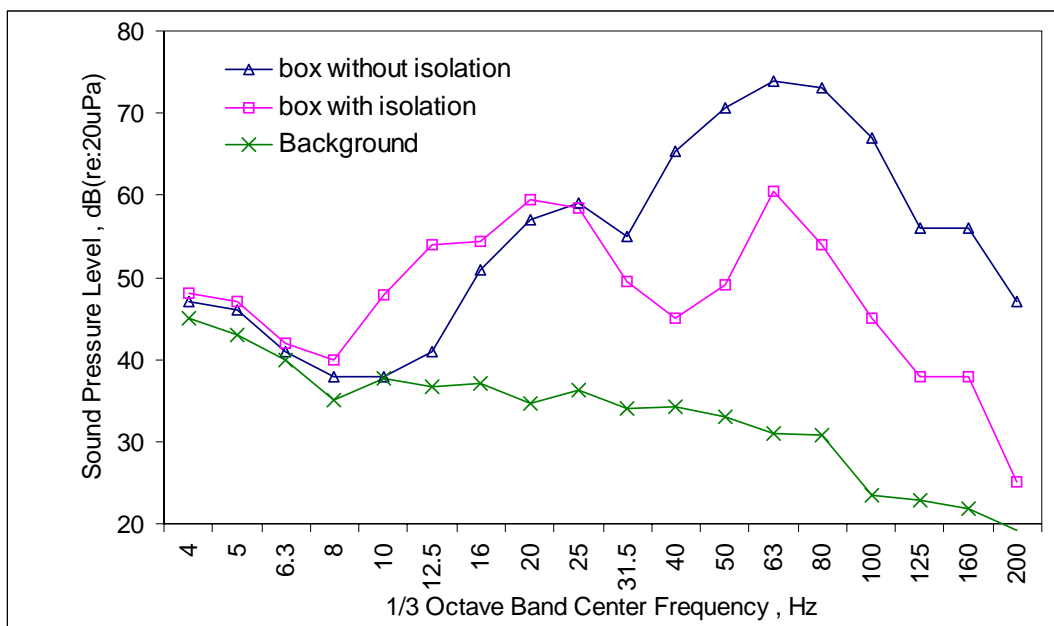
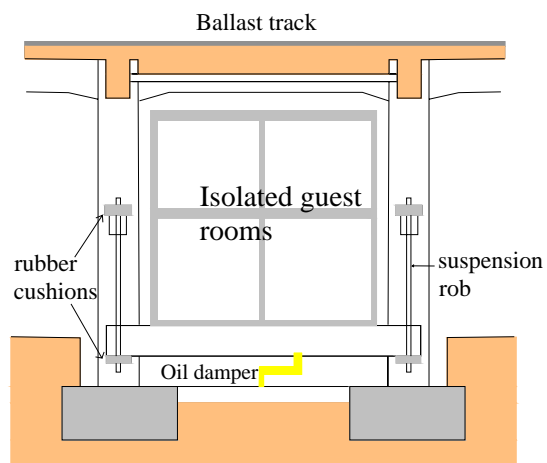


Figure 6.5. Sound Pressure levels measured inside and outside isolated area in isolated box



Figure 6.6. Photograph of a train pass over the isolated box (hotel) in Japan (Tokyo)



Vibration measurement location in guest room 138 of 1/F

Figure 6.7. Sketch of vibration isolation systems and vibration measurement room in the isolated box (hotel)

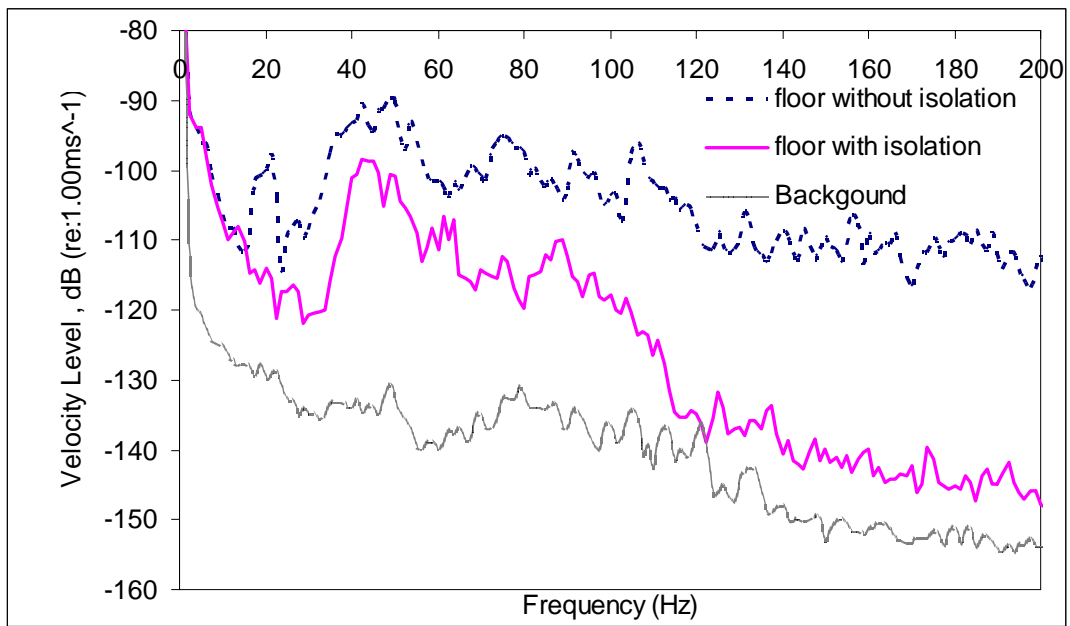


Figure 6.8a. Vibration velocity levels measured inside and outside isolated area of the isolated box (hotel)

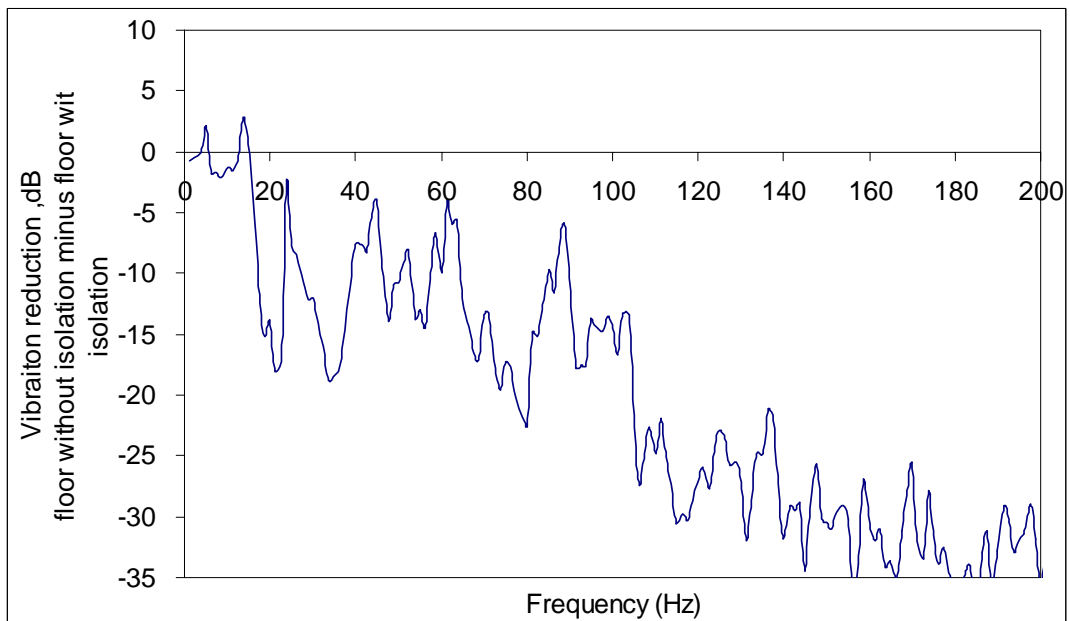


Figure 6.8b. Calculated Vibration reduction level of the isolated box (hotel)

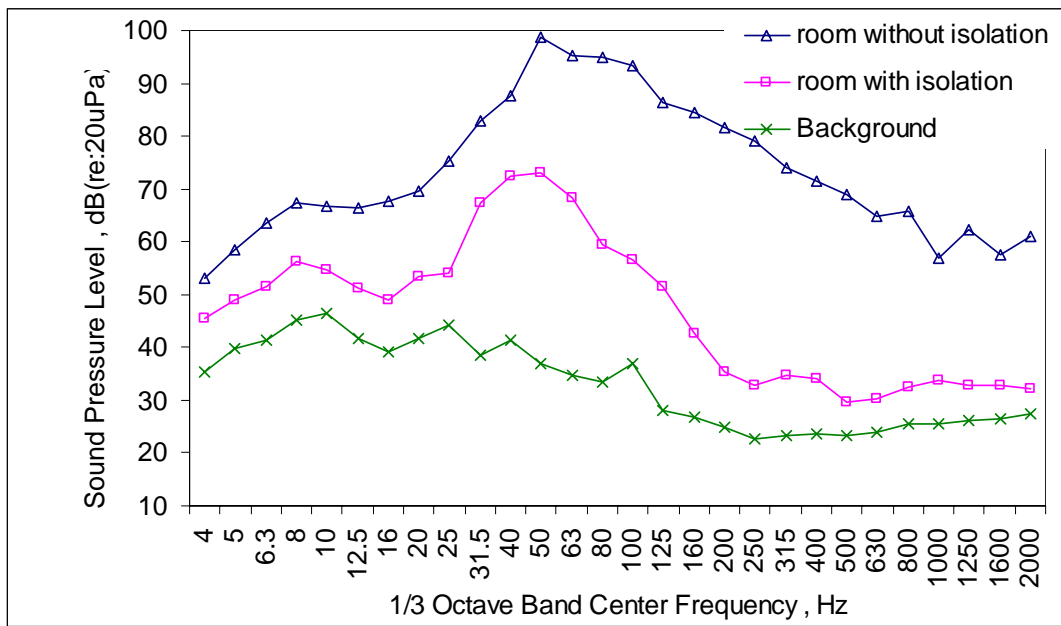


Figure 6.9. Sound Pressure level measured inside and outside isolated area in isolated box (hotel)

Table 6.1 Dimensions and material properties of the testing material

Material	Description	Panel Size(m) (Length x width x height)	Young's Modulus (E) ($\times 10^9$ N/m ²)	Density(ρ) (kg/m ²)
Concrete	Reinforced concrete	2 x 1 x 0.15	25	360
Cement	Ref. to Table 2.2			

Table 6.2 Resonance frequencies and corresponding mode shapes for the thick concrete floating floor

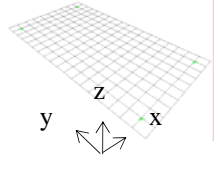
	Sketch of measured cross-section bending mode shapes		Resonance frequencies		
	Mode shape in y-direction	Mode shape in x-direction	FEM	Simple equation	Measured
Mode shape description (Theoretical mode shape Ref. Figure 2.5)					
Rigid body mode –In z direction (vertical)			19	20	19
1st symmetric bending mode in y direction			131	127 (Equation 2.6)	130
1st symmetric bending mode in x direction			495	508 (Equation 2.6)	492

Table 6.3 Resonance frequencies and corresponding mode shapes for the thin cement floating floor

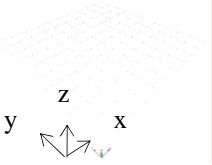
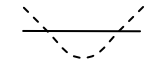
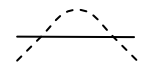
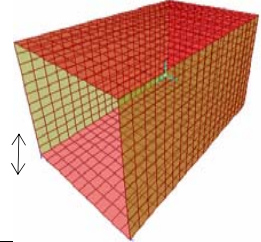
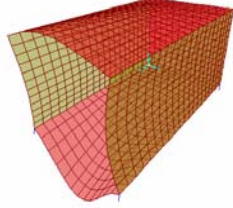
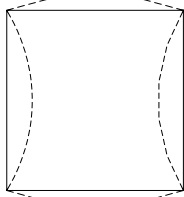
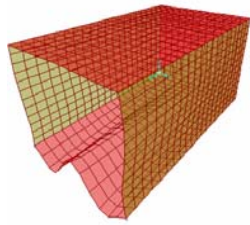
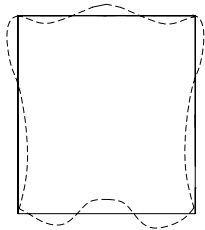
 Mode shape description (Theoretical mode shape Ref. Figure 2.6)	Sketch of measured cross-section bending mode shapes		Resonance frequencies		
	Mode shape in y- direction	Mode shape in x- direction	FEM	Simple equation	Measured
Rigid body mode –In z direction (vertical)			19	20 (design)	19
1 st symmetric bending mode			144	141.9 (Equations 2.7 and 2.8)	145
2 nd symmetric bending mode			368	357.5 (Equations 2.7 and 2.8)	367

Table 6.4. Theoretical and measured symmetric bending mode shapes and resonance frequencies of two isolated box structures

	Mode shapes of isolated boxes		Isolated box-laboratory		Isolated box-hotel	
	FEM Mode shape	Sketch of measured cross-section bending mode shape	FEM resonance frequency	Measured resonance frequency	FEM resonance frequency	Measured resonance frequency
Vertical rigid body mode			6 Hz	5 Hz	3Hz	4Hz
1 st symmetric bending mode			25 Hz	22 Hz	12 Hz	14 Hz
2 nd symmetric bending mode			76 Hz	70 Hz	45 Hz	44 Hz

CHAPTER 7

OPTIMUM ISOLATOR POSITION

TO CONTROL BENDING RESONANCE

The study in Chapter 6 shows that bending resonances of floating floor for building-isolation at the receiver can deteriorate the noise and vibration isolation performance.

In this aspect, optimum isolator position for the floating floor is studied to reduce bending resonance effects of the floating panel with the typical cement base panel.

7.1 INTRODUCTION

Thinner cement panels with thickness of 15 to 40 mm are often used instead of concrete slab to reduce loading, but their vibration isolation performance is still unsatisfactory as stated in Chapter 6. To enhance the vibration isolation performance of typical lightweight cement floor panels, small honeycomb panels with a high stiffness to damping ratio should be employed. Honeycomb floor panels have a greater stiffness to mass ratio, and are used extensively in aircraft for vibration reduction and sound insulation (Huang and Ng, 1998 & Cunningham et al., 2000).

Most research in this area has focused on the identification of the best combination of material parameters in floating floor systems to enhance the vibration isolation performance at the receiver. Jutulstad (1985) created a model to identify the best combination of the bending stiffness of plates and the distance between isolators. Baron (2004) investigated the

effects of different parameters of floating floors, including stiffness, dimension, and mass, on their isolation efficiency. Mead (1998) suggests the method of nodalization to reduce the vibration input from a source by placing the source at the nodal points of a beam. Yan and Xie (1999) analyzed the effect of positioning isolators at the base of electronic equipment to achieve rigid body vibration attenuation. However, no theoretical model or experimental study has developed the concept of arranging the isolators at the nodal points of a plate to attenuate the bending mode vibration.

From previous test results, it can be established that very few floating floor types can provide a vibration isolation of 30 dB in the frequency range of 120-600 Hz. Some typical levels of vibration reduction for various material are 10 dB at 250 Hz and 15 dB at 500 Hz for honeycomb floor panel systems that are designed for aircraft (Clark and Harry, 1996) 15 dB at 250 Hz and 20 dB at 500 Hz for metal floor panels that are used in ships (Nilsson, 1977), and 15 dB at 250 Hz and 25dB at 500 Hz for cement floor panels that are used in dwellings (Beranek, 1988) .The main reasons for the poor vibration isolation performance of typical floating floor designs are the large size of the floor panels and the placement of the isolators at the edge of the panel.

In this chapter, experimental modal analysis is conducted to examine the method of increasing the vibration isolation performance of typical lightweight cement panels by the addition of a honeycomb floor panel with a high stiffness to mass ratio. An isolator position design is proposed to reduce the bending mode resonance of floor panels, which is the main cause of poor vibration isolation performance.

Sections 7.2 evaluates the dynamic properties of square honeycomb and cement panels with free boundary conditions through center excitation using a shaker, and identifies the common nodal point of the lowest symmetric bending modes of the two panels. Section 7.3 introduces the theory of the effect of isolator position on transmissibility. In Sections 7.4 to

7.6, the air-borne and structure-borne energy transmissions from the base structure to the floor panel receiver are analysed separately with different measurement techniques. In section 7.7, the vibration isolation performance of the proposed technique is compared to some conventional floating floor designs. In the final section, the application of the proposed design is discussed.

7.2 MODE SHAPE MEASUREMENT AND NODAL LINE IDENTIFICATION

7.2.1 EXPERIMENTAL SETUP

The experimental setup that is shown in Figure 7.1 aims to find the resonance response and mode shape of cement and honeycomb panels and to identify the nodal points precisely on shaker test. The dimensions and material properties of the honeycomb panel (including the core design) and the cement panel that are studied are given in Table 7.1. The experimental methods are similar to the section 2.3.1 in Chapter 2 to measure the motion transmissibility on cement panel. The different is the lightweight accelerometer was mounted at various points (not only at the center point) on the panels to measure their acceleration response. Thus, the center excitation acceleration with response acceleration along the surfaces of the panels was measured. The value of the imaginary part of the FRFs for a given resonance was assumed to be proportional to the modal displacement, and thus the mode shapes were established.

7.2.2 EXPERIMENTAL RESULTS

The motion transmissibility at the center point of the cement panel and the honeycomb panel is shown in Figure 7.2. The damping ratio of each mode, which was identified using the half-power point method, is also given in Figure 7.2. The resonance frequencies are 37.25 Hz, 300.5 Hz, and 556 Hz for the honeycomb panel, and 21.5 Hz, 145.5 Hz, and 337.5 Hz for the cement panel, which are similar to the resonance frequency found using impact method in Section 6.2 in Chapter 6. The lowest resonance frequency is the rigid body mode, and the others are the bending modes. The negative value of the motion transmissibility implies that there was some vibration reduction from the vibration source to the receiver on the panel. The first bending resonance frequency of the honeycomb panel is much higher than that of the cement panel because of the higher stiffness to mass ratio. It can also be observed in Figure 7.2 that there is a weak point of vibration isolation on the conventional cement panel at the first bending resonance frequency of 145.5 Hz. Fortunately, the honeycomb panel has an anti-resonance dip, and thus reduces the first bending mode of the cement panel at 145.5 Hz if it is added to the cement panel as a type of floating floor. However, the cement panel still has an additional resonance at 337.5 Hz that is close to that of 300.5 Hz of the honeycomb panel. This problem must be tackled by the suitable positioning of the isolators to isolate the vibration resonance near 300 Hz.

The identified mode shapes of the honeycomb panel at 300.5 Hz and 556 Hz are shown in Figure 7.3. They are similar to the square panel modelled with FEM and show in Figure 2.6. In the contour plot graphs, the solid lines and the dashed lines represent the positive and negative displacement, respectively. The transition regions between the solid lines and dashed lines are the nodal lines without displacement. The common nodal point of the two lowest symmetric bending modes is located and marked with circles in Figure 7.3.

7.2.3 COMPARISON WITH THEORETICAL ANALYSIS

Based on Equations 2.5 and 2.6 and the frequency parameters λ (where the boundary condition is free along the circumference of the plate) that are provided by Blevins (1979), the lowest two symmetric and the lowest four anti-symmetric bending resonance frequencies and corresponding mode shapes are given in Tables 7.2a and 7.2b separately. The measured mode shapes of the honeycomb panel agree well with the predicted results. The resonance frequency of the honeycomb panel and cement panel of the lowest symmetric mode resonance agrees with the predicted results with errors less than 10% (Table 7.2a) Furthermore, it should be noted that the center point is the common nodal point of the anti-symmetric modes (Table 7.2b).

7.3 THEORETICAL ANALYSIS OF THE EFFECT OF ISOLATOR POSITION ON TRANSMISSIBILITY

The degradation of transmissibility that is attributed to the bending resonance has been predicted in (Kawaharazuka et al., 1996 & Hui and Ng, 2006) predicted values of transmissibility can be obtained from Equation 2.3.

Figure 7.4 shows the transmissibility (center response/base excitation) when the isolators are placed at the edge and the nodal points of the first bending mode when the vibration transmission path is structure borne only. When the isolators are placed at the four edges, the bending resonance peak occurs at around 300 Hz for the honeycomb panel. As the mobility depends on the bending vibration of the panel, it should be minimized when the isolators are placed at the nodal points. Thus, the peak is attenuated significantly when the isolators are placed at the nodal points of the first bending mode.

The concept of nodalization (Mead, 1998) may be theoretically easy to implement, but in practice several additional features must be considered. First, only a few modes of the floating floor should be controlled, which requires a small, stiff, and lightweight panel design. Second, the acoustic transmission path should be blocked effectively in the air cavity. Third, the receiver point should be at the center to avoid the effects of the anti-symmetric modes.

The following experimental tests were carried out to verify the importance of these design features.

7.4 TEST TO VERIFY THE EFFECT OF ISOLATOR POSITION IN THE ABSENCE OF ACOUSTIC PATH

7.4.1 EXPERIMENTAL SETUP

The energy communication paths from the base to the floating floor along the structure-borne and air-borne paths are depicted in Figure 7.5. It is necessary to employ experimental techniques to reduce the air-borne path to investigate the two paths separately. The experimental setup that is shown in Figures 7.6a and 7.6b aims to verify the effect of isolator position on the vibration transmissibility of floating floors without an air-borne energy transmission path, which is an idealized situation. To eliminate the air-borne energy transmission path to the floor panel, four small bricks of 100 mm x 100 mm x 60 mm were arranged under the isolators to form the base structure. Impact excitation was applied to the bricks. The air-borne energy that was transmitted from the small bricks included the rigid body and bending vibration modes. The sound energy that was generated by the rigid body vibration depended on the brick surface area, which was so small that the magnitude of the sound that came from the rigid body vibration could be neglected. The sound energy that was generated by the bending modes of the brick could also be neglected in this measurement, as

the length of each brick was only 100mm, which meant that the first bending mode frequency was above 1 kHz. (The energy transmission from the base structure to the floor panel along the air-borne energy transmission path can be neglected). Rubber isolators were placed on the bricks (each of which was 30 mm x 30 mm x 30 mm with a stiffness of 6,847 N/m) to support the honeycomb floor panel. A steel hammer was employed to excite the structure base to generate vibration in the frequency range of 120-600 Hz. The generated acceleration on the base structure and the response acceleration on the center point of the floor panel were then measured using two accelerometers. The FRFs (acceleration on the floor panel/acceleration on the base structure), which are known as the motion transmissibility, were identified.

7.4.2 EXPERIMENTAL RESULTS

The motion transmissibility when the isolators were located near the corners (Figure 7.6a) and when they were placed at four common nodal points (Figure 7.6b) was obtained. Figures 7.7a-7.7c show the effect of the position of the isolators on the motion transmissibility at the receiver when the transmission path was structure borne. The high coherence from 120-600 Hz shows that the measurement of the magnitude of the motion transmission was accurate in the test frequency range. The sudden dips below 120 Hz were probably because of a low vibration signal at the source or receiver. The phase angle of 90 degrees at the two lowest symmetric bending mode resonance frequencies confirms the effects of the resonances on the motion transmissibility. When the isolators were placed at the nodal points, the vibration reduction was 10-30 dB higher in the frequency range of 120-600 Hz. These experimental results also confirm the effect of isolator position that is detailed in Figure 7.3. However, in this experimental analysis, the peak at around 300 Hz was not totally eliminated, because the areas of the rubber isolators were larger than the nodal points.

7.5 TEST TO VERIFY THE EFFECT OF AIR-BORNE ENERGY TRANSMISSION PATH ON CEMENT BASE STRUCTURE

7.5.1 EXPERIMENTAL SETUP

In the following experiments, the cement panel used in the shaker test was selected as the structure base. The panel was a lightweight floor structure of the type that is commonly used in buildings with steel or wood frames. The honeycomb panel used in shaker test was applied as the floating floor. To prevent the overlap of the nodal points of the cement and honeycomb panels, the cement base panel was designed to be larger than the honeycomb panel.

The experimental setup that is shown in Figures 7.8a and 7.8b aims to verify the effect of an air-borne energy transmission path on the vibration transmissibility of the floating floor. To eliminate the structure-borne energy transmission path, the honeycomb panel was robustly suspended above the cement panel at a height of 100 mm, as shown in Figure 7.8a. A steel hammer was used to excite the cement panel to generate an air-borne sound that was then transmitted to the honeycomb panel. A microphone was placed between the two panels to detect the energy transmission from the base structure to the honeycomb panel through the air cavity. The vibration response of the honeycomb panel to the acoustic pressure was then measured.

The experimental setup in Figure 7.8b includes both air-borne and structure-borne energy transmission paths. Four wooden blocks (each of which was 70 mm x 70 mm x 70 mm) were employed to support the rubber isolators to maintain a typical cavity depth of 100 mm between the floor and base panels. The wooden blocks were designed to support the rubber isolators at both the edge and nodal positions. This can ensure the vibration energy transmission from the cement panel via the wooden blocks to the honeycomb floor panel was constant for different isolator positions.

Two strips of soft rubber were used to support the cement base panel to avoid any change in the resonance frequencies of the base panel. The boundary condition of both the honeycomb floor and the cement base panel were free at the circumference.

The shaker test in Section 7.2 could not be applied in the experimental test for two reasons. First, the cement base panel would have had to be tightly fixed to the vibrating head of the shaker to avoid static instability when the floor panel was placed on the cement panel, which would have affected the bending vibration resonances of the cement panel. Second, to avoid fixing the cement panel on the shaker, a large rigid panel would have had to be placed on the vibrating head of the shaker to support the test panels, which would have made the static weight of the large rigid panel too heavy for the shaker. Thus, an impact test was used instead of a shaker test.

7.5.2 EXPERIMENTAL RESULTS

The motion transmissibility of the cases in which no isolator was used and the honeycomb panel was suspended above the cement base structure (Figure 7.8a) and when the isolators were placed at four nodal points between the honeycomb and cement panels (Figure 7.8b) was studied.

The coherence values of the vibration (on the base panel) induced response (on the floor panel) are shown in Figure 7.9c, and those of the acoustic (between the two panels) induced response (on the floor panel) are shown in Figure 7.10c. In general, the coherence values are high (above 0.7) in the frequency range of 120-600 Hz. The sudden dips at certain frequencies imply that the motion transmissibility results are less accurate at these frequencies. Furthermore, a phase angle of 90 degrees can be observed in the resonance frequencies (Figures 7.9b and 7.10b), which proves that the vibration resonances were due to the acoustic pressure. The magnitude of motion transmissibility in the two cases is similar at the first and

second bending modes, as shown in Figure 7.9a. Hence, the test confirms that to enhance the vibration isolation performance at the receiver, both the structure-borne and air-borne energy transmission paths should be effectively isolated. This finding agrees well with the suggestion that the air that is trapped between the structure base and the floating floor plays an important role in the vibration isolation performance of floating floors (Harris , 1994).

In theory, the larger the air cavity the lower the air stiffness under the panel and the better the vibration isolation performance. (Lee et al., 2002). However, in practice, the air gap should not be too large because of the standing wave resonance and limited space. As the typical air cavity between the structure base and floor panel is around 100 mm, acoustic insulation material could be installed in the cavity to absorb the energy transmission.

7.6 TEST TO VERIFY THE EFFECT OF ISOLATOR POSITION WITH A CEMENT BASE STRUCTURE AND ACOUSTIC INSULATION

7.6.1 EXPERIMENTAL SETUP

The foregoing experimental results demonstrate that it is practical to use a honeycomb panel as a floating floor to improve the vibration isolation performance of lightweight cement base panels. The experimental setup in Figures 7.11a and 7.11b aims to verify the effectiveness of the improvement in vibration isolation that is achieved by the installation of a honeycomb floor panel with a nodal point isolator design.

The experimental setup in this section is similar to the setup in Figure 7.8b, except that insulation materials of air-borne paths have been added. The acoustic path was insulated using a vinyl sheet to cover the porous foam material, as shown in Figures 7.11a and 7.11b. Vinyl sheeting is a flexible and highly damped material that is widely used in acoustic isolation in lightweight floor panels.

7.6.2 EXPERIMENTAL RESULTS

The motion transmissibility when the isolators were placed at the identified nodal points (Figure 7.11a) and when they were placed at the edge (Figure 7.11b) was studied. A sound insulation device was installed in both cases. As shown in Figure 7.12a, there was a 20-30 dB vibration reduction in the frequency range of 120-600 Hz. This was due to the reduction in both the structure-borne and air-borne energy communication paths through the placement of the isolators at the nodal points and installation of acoustic insulation material. The importance of the position of the isolators can also be observed in Figure 7.12a, which shows a significant vibration reduction of 30 dB in the range of 120-550 Hz when the isolators were placed at the nodal points.

The vibration spectrum of the cement and honeycomb panels is shown in Figures 7.12b and 7.12c, respectively, for the edge and nodal point isolator positions. It is noted that there is a significant peak at 145.5 Hz for the cement panel that is reduced in the honeycomb panel in both cases. Figure 7.12b confirms that the bending resonance of the honeycomb panel at 300 Hz degraded the vibration isolation performance of the base panel when the isolators were placed at the edge. However, when the isolators were placed at the nodal points of the honeycomb floor panel, the vibration magnitude of the bending resonance at 300 Hz was considerably reduced (see Figure 7.12c).

These findings are consistent with the theoretical analysis in Section 7.3, which reports that the peak vibration of a floor panel can be reduced by placing the isolators at the nodal points of the bending resonance. The summary of the experimental targets, findings and reasons from Sections 7.2 to 7.6 are listed in Table 7.3.

7.7 COMPARISON WITH CONVENTIONAL FLOATING FLOOR DESIGNS

In Figure 7.13, the motion transmissibility of the proposed new floating floor installation design that is shown in Figure 7.12a (dashed line) is compared with that of the conventional designs of a lightweight aluminum sandwich floating floor (Baron, 2004) and a cement floating floor (Beranek, 1988) at a range of 100-800 Hz in a one-third octave band. The honeycomb floor panel of the proposed design achieves a much better vibration reduction. The poorer vibration isolation performance of the aluminum panel and concrete floor is likely to be due to the isolator positions and lower bending resonances, as the floor panels in these conventional designs are larger. Furthermore, the concrete floating floor is difficult to use in practice due to its heavy static loading at the base.

7.8 POTENTIAL APPLICATION OF THE NEW FLOATING FLOOR DESIGN

In the experimental analysis in this paper, the acceleration at the center point, which is the location of the common nodal point in the anti-symmetric bending modes (see Table 7.2b), is considered. This means that the vibration reduction performance may be even lower at other points, as the anti-symmetric bending modes of the panel may be excited. To reduce the effect of these anti-symmetric modes, the receiver should be placed at the common nodal point (center point) in these modes. Another problem is that the placement of the isolators at the identified nodal points may cause overturning when a load is added to the edge of the panel. There are two methods to tackle this problem to maintain the improved vibration isolation performance. The first is to use a table with legs that are placed at the center points of the proposed floating panel new design, as shown in Figure 7.14. The device that is to be

protected from vibration can then be placed on the table. The second method is to add an additional panel to the original floating floor panel, with additional isolators that are placed at the center point of the lower panel (see Figure 7.15). This would reduce both the symmetric and anti-symmetric vibration resonances. This is a two-stage isolation system and is similar to the floating raft technique that is used to reduce vibration and reduce damage to equipment on ships. The arrangement of alternate isolators in the floating raft system has been theoretically found (Du et al., 2005) (see Figure 7.16) to achieve a higher level of vibration isolation, but the effect when the isolators are placed at the nodal points has not been investigated. The new design in Figure 7.15 is similar to the alternate design in Figure 7.16b in that the symmetric and anti-symmetric bending modes are not excited.

In this chapter, however, the coherence data represent that the impact signal with steel hammer is not enough in the low frequency range, whereas, the technique of free fall steel ball with resilient material as the chapter 4 and 6 can not be employed to the experimental test resulting from the limited excitation space on the cement panel. Appendix B reports a further investigation (with low frequency range) on the effective of nodal-point support to eliminate the bending resonance effects of floating panel with smaller honeycomb panel of 170mm (L) X 170mm (W) X 15mm (H) on shaker test. It can be seen that the small honeycomb panel has very high isolation performance in the frequency range of 50-600Hz.

7.9 SUMMARY

Extensive experiments have been conducted to examine the effects of structure-borne and air-borne vibration transmission paths and confirm that an improved vibration isolation performance is achieved by the proposed new floating floor design. The results also confirm that the vibration isolation performance of a typical lightweight cement floor panel can be improved by pairing it with a honeycomb floor panel with proper isolator placement positions.

In general, to achieve the optimum vibration isolation performance, the following design features should be selected. First, a small floor panel with a high stiffness to mass ratio is recommended to increase the bending resonance frequencies of the system. Second, the isolators should be placed at the common nodal point of the lowest two symmetric bending modes of the floor panel. Third, lightweight and highly damped acoustic insulation material should be installed, together with acoustic absorption material, in the air cavity. Fourth, the receiver point should be located at the center point of the honeycomb panel so that the anti-symmetric bending modes and overturning problem can be eliminated.

The new floating floor design achieved a vibration reduction of 20-30dB in the frequency range of 120-600 Hz. In addition, the proposed floor was found to have a 20dB lower vibration level at the first bending resonance frequency than the conventional design in which the isolators are placed at the edges.

REFERENCES

- Baron, N. (2004). Some Acoustical Properties of Floating Floors Used in Trains, KTH Aeronautical and Vehicle Engineering, Thesis.
- Beranek, L. L. (1988). Noise and vibration control (rev. ed.). Washington D.C: Institute of Noise Control Engineering.
- Blevins, R. D. (1979). Formulas for natural frequency and mode shape. New York: Yan Nostrand Reinhold Company.
- Clark, M. D. and Harry, H. L. (1996). A systematic approach used to design floor panel isolation for a commercial aircraft, *Internoise*, 455-460.
- Cunningham, P. R., White, R. G. and Aglietti, G. S. (2000). The effects of various design parameters on the free vibration of doubly curved composite sandwich panels, *Journal of Sound and Vibration*, 230 (3), 617-648.
- Du, K., Wu, X. J., Cheng, G. L. and Zhu, S. J. (2005). Research of best isolation-fixing scheme of floating raft system, *Chinese Academic Journal of Naval University of Engineering*, 17(2) (92-94, 99).
- Harris, C. M. (1994). Noise control in buildings: a guide for architects and engineers. New York: McGraw-Hill.

Hui, C. K. and Ng, C. F. (2006). The control of vibration from rail viaduct at source and receiver, 9th Western Pacific Acoustics Conference.

Huang, C. W. and Ng, C. F. (1998). Sound insulation improvement using honeycomb sandwich panels, *Applied Acoustics*, 53(1-3) 163-177.

Jutulstad, H. (1985). Flytende gulv på fjaerer – lydreduserende konstruksjon for fartoy. Universitet I Trondheim. Norges Tekniske Hogskole, Institutet for Husbyggnadteknik, Norway.

Kawaharazuka, T., Hiramatsu, T. Ohkawa H. and Koyasu. M. (1996). Experimental study on vibration reduction by isolated railway, *Internoise*, 1549-1552.

Lee, Y. Y. (2002). Structural-acoustic coupling effect on the nonlinear natural frequency of a rectangular box with one flexible plate, *Applied Acoustics*, 63(11) 1157-117.

Mead, D. J. (1998). *Passive vibration control*. Chichester; New York: Wiley.

Nilsson, A. (1977). Some acoustical properties of floating-floor constructions, *JASA. Journal of the acoustical society of America*, 61(6) 1533-1539.

Yan, X. L. and Xie, Y. (1999). The effect of arrangement of isolators in coupled vibration. *Chinese Journal of Electronics Machinery Engineering*, 82(6).

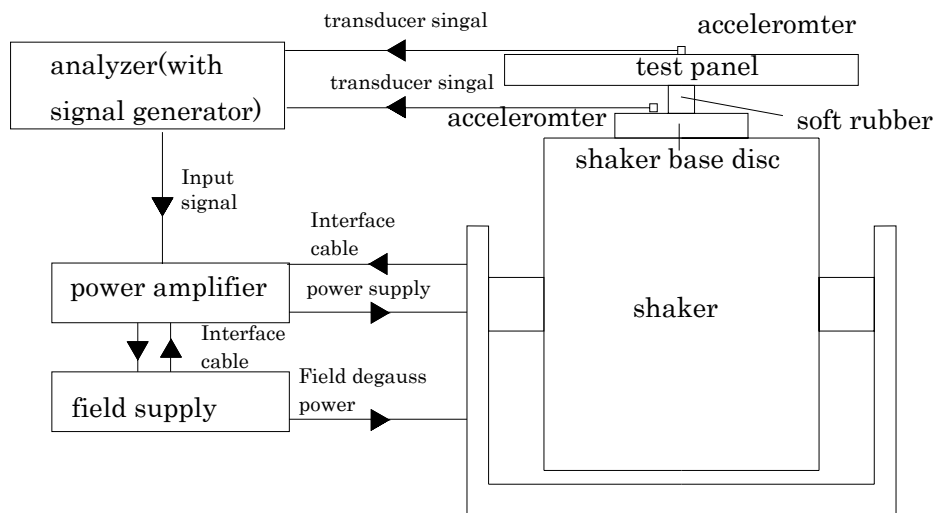
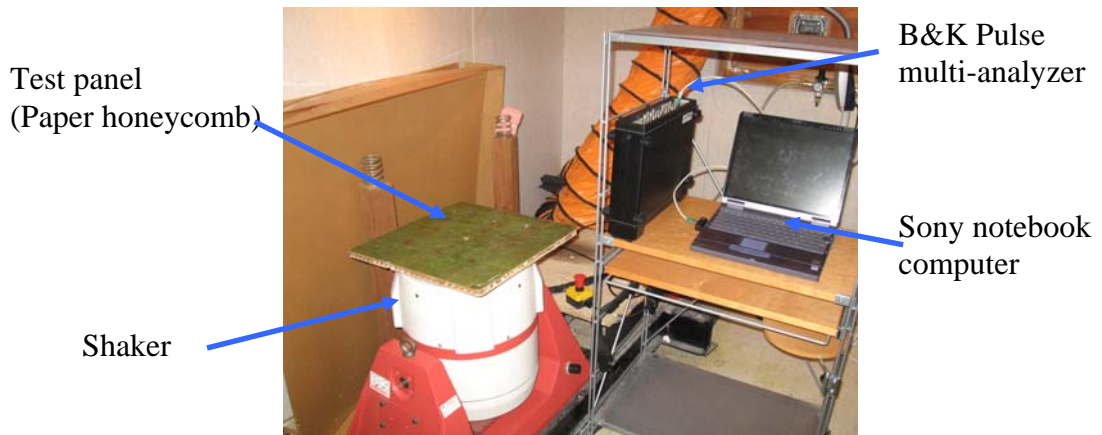


Figure 7.1 Experimental setup of the mode shapes and resonance frequencies measurement

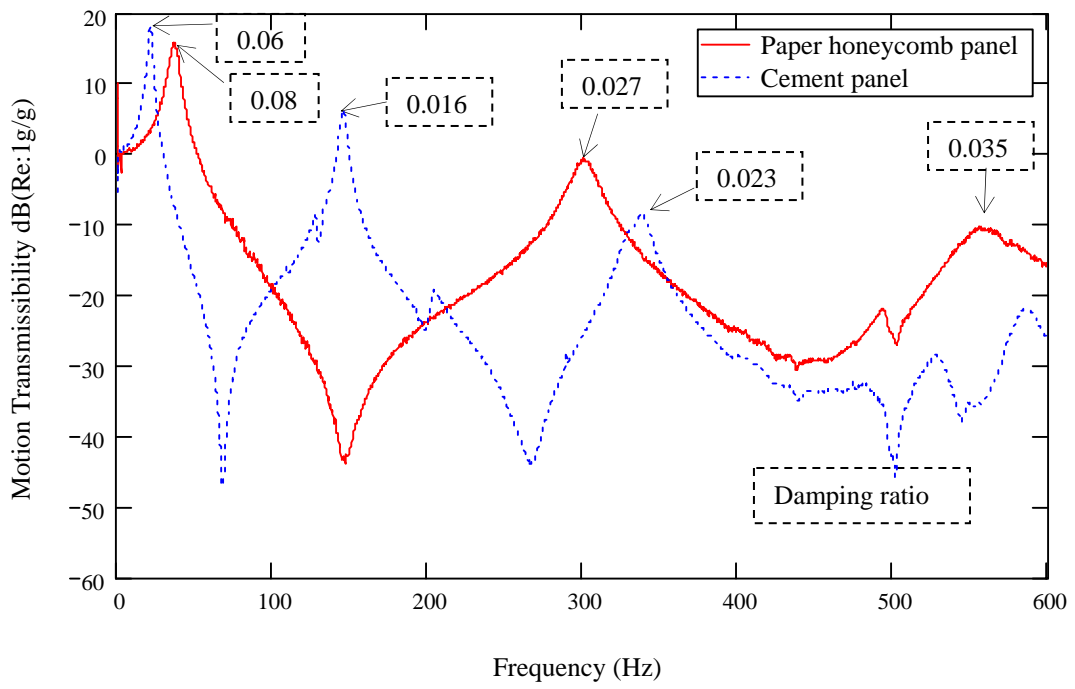


Figure 7.2 Motion transmissibility (magnitude) and damping ratio of paper honeycomb panel and cement panel

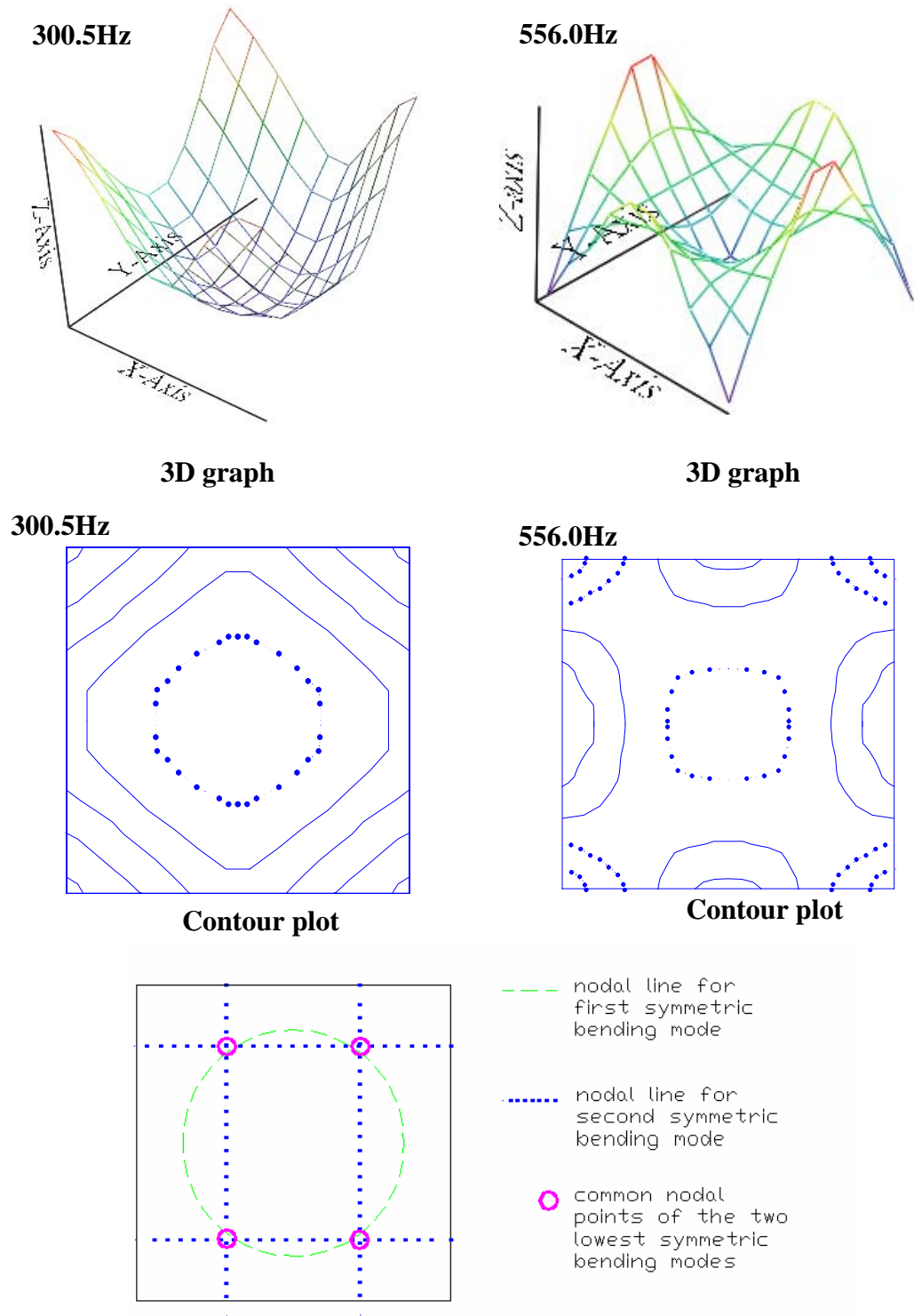


Figure 7.3 The mode shapes and identified common nodal points for the lowest two symmetric bending modes of paper honeycomb panel

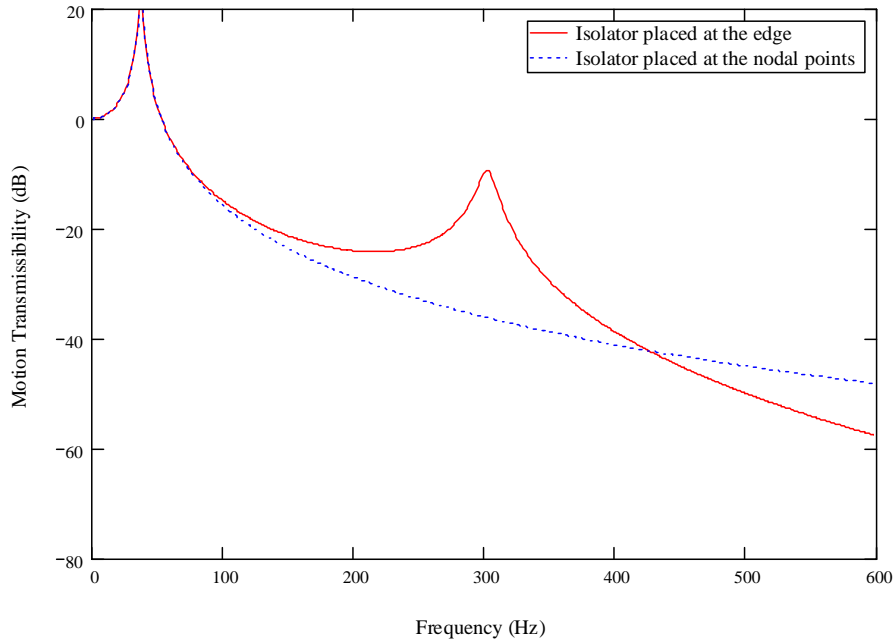


Figure 7.4 Theoretical results of motion transmissibility of honeycomb panel when isolators placed at the edge and nodal points

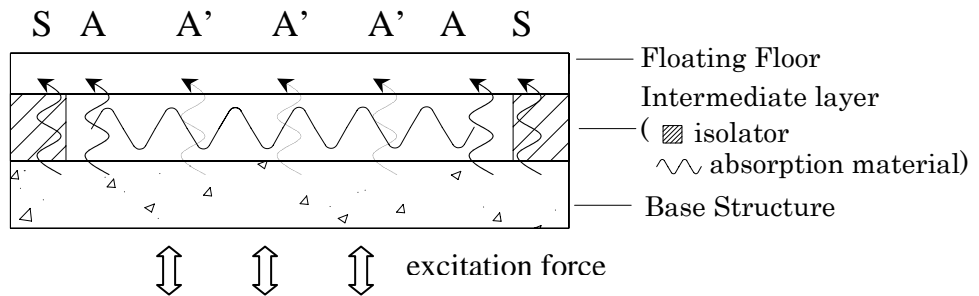


Figure 7.5 Energy transmission paths of typical floating floor structure from the base structure to the floating floor via the intermediate layer. The paths marked with S are structure-borne energy transmission path via isolator; the paths marked A are air-borne energy transmission path via air gaps; the paths marked A' are air-borne energy transmission path with energy attenuation device of absorption material.

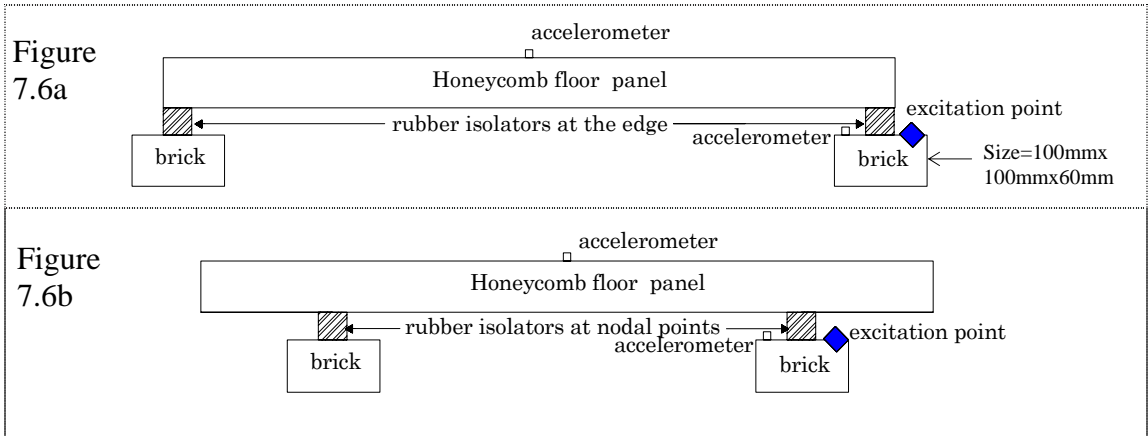
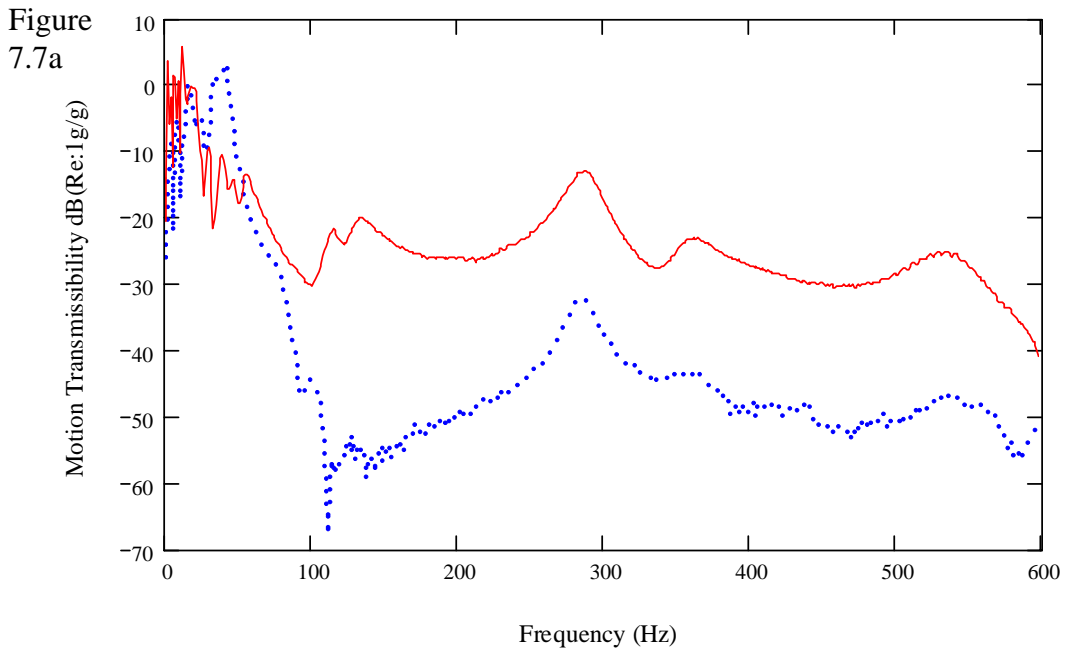


Figure 7.6 Experimental setup for the motion transmissibility measurement with structure-borne energy transmission path only. (a) isolators placed at the edge (b) isolators placed at the identified common nodal points of the lowest two symmetric bending modes



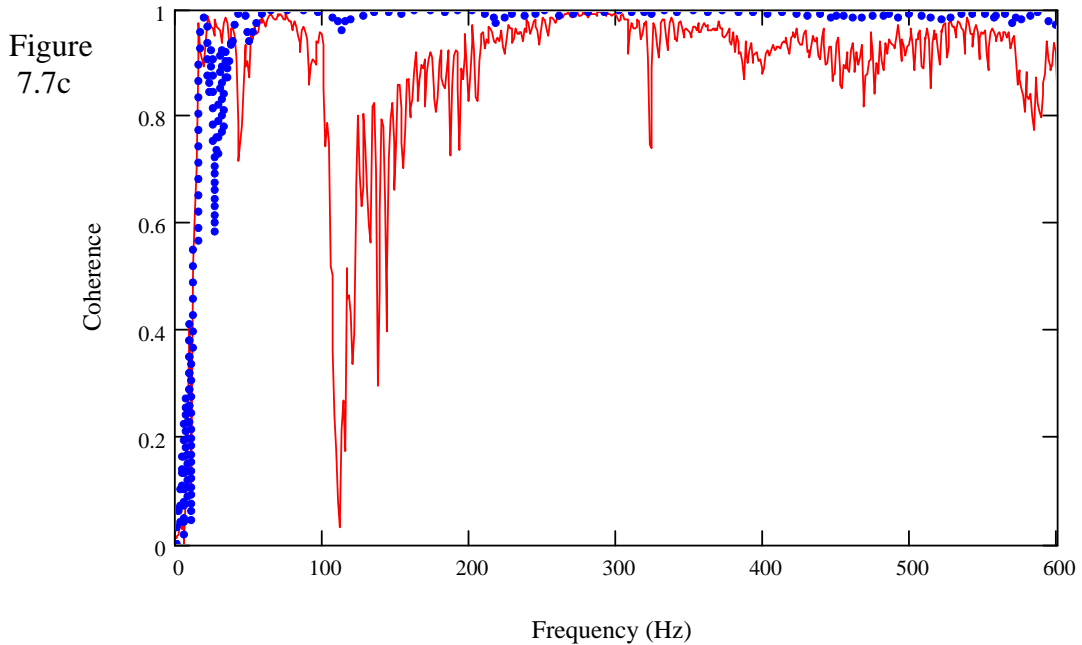
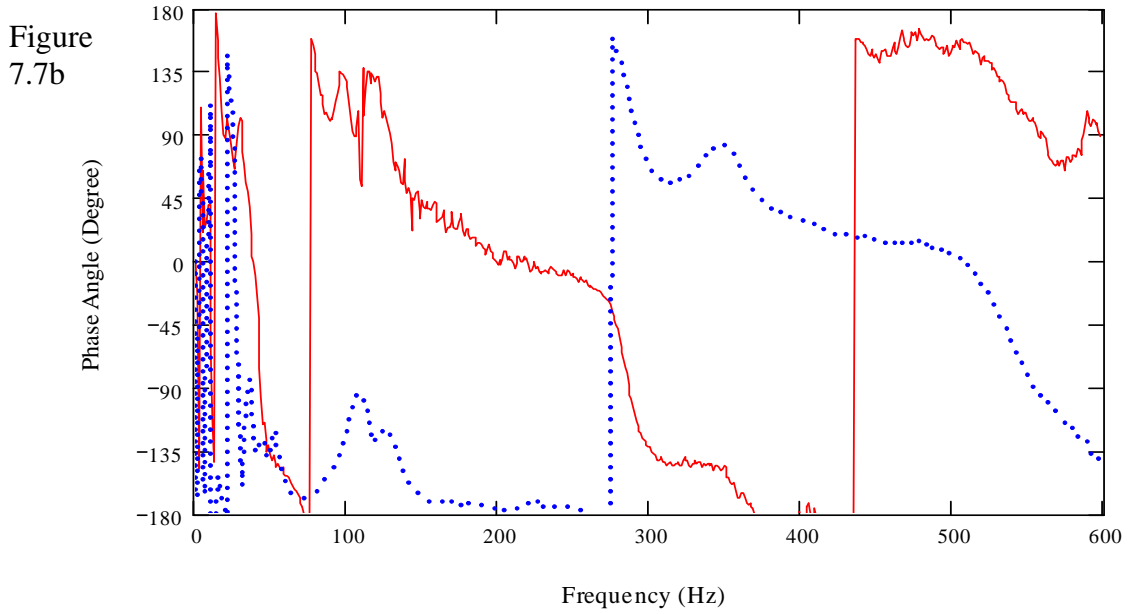


Figure 7.7 Motion transmissibility results with structure-borne energy transmission path only. 7a) Magnitude 7b) Phase 7c) Coherence — Sw+Awo+Ie+Amn (see Figure 7.6a) ---- Sw+Awo+In+Amn (see Figure 7.6b)

Sw	=	Energy transmission with structure-borne path
Awo	=	Energy transmission without air-borne path
Ie	=	Four isolators place at the edge points
In	=	Four isolators placed at the nodal points
Amn	=	No acoustic insulation material used

Figure 7.8a

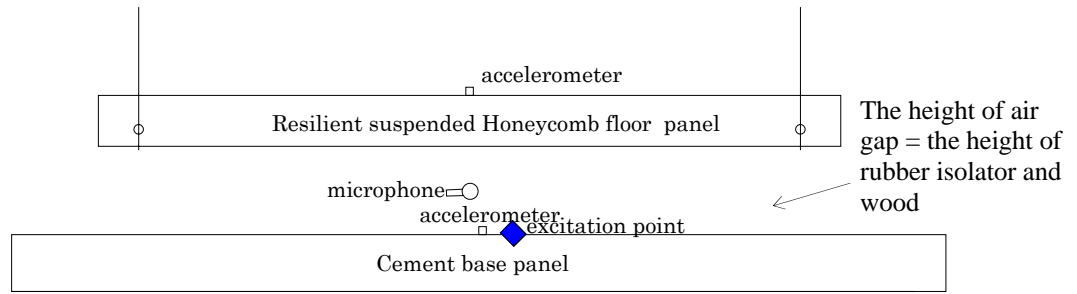


Figure 7.8b

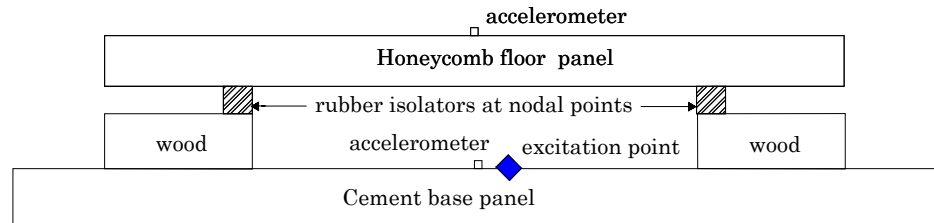
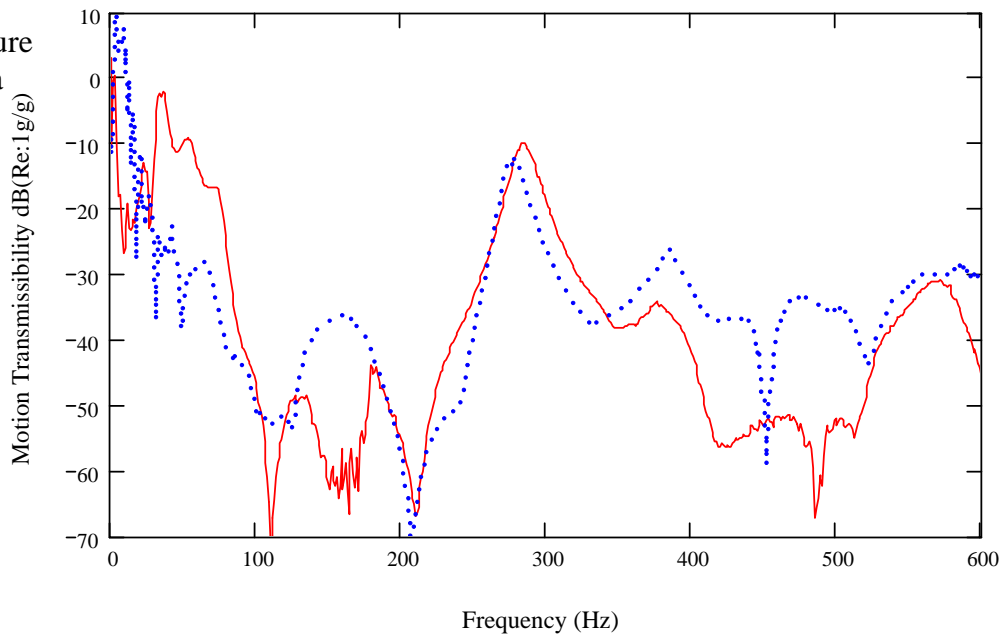


Figure 7.8 Experimental setup for the motion transmissibility measurement for air-borne energy transmission path investigation.(a) air-borne energy transmission path only (b) isolators placed at the identified common nodal points of the lowest two symmetric bending modes with both air-borne and structure-borne energy transmission paths

Figure 7.9a



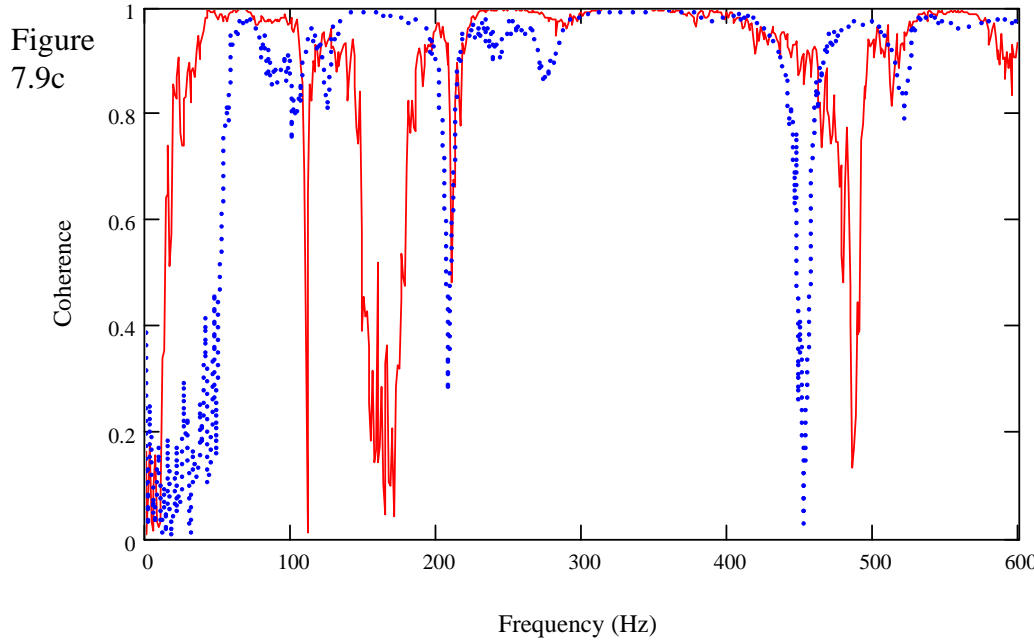
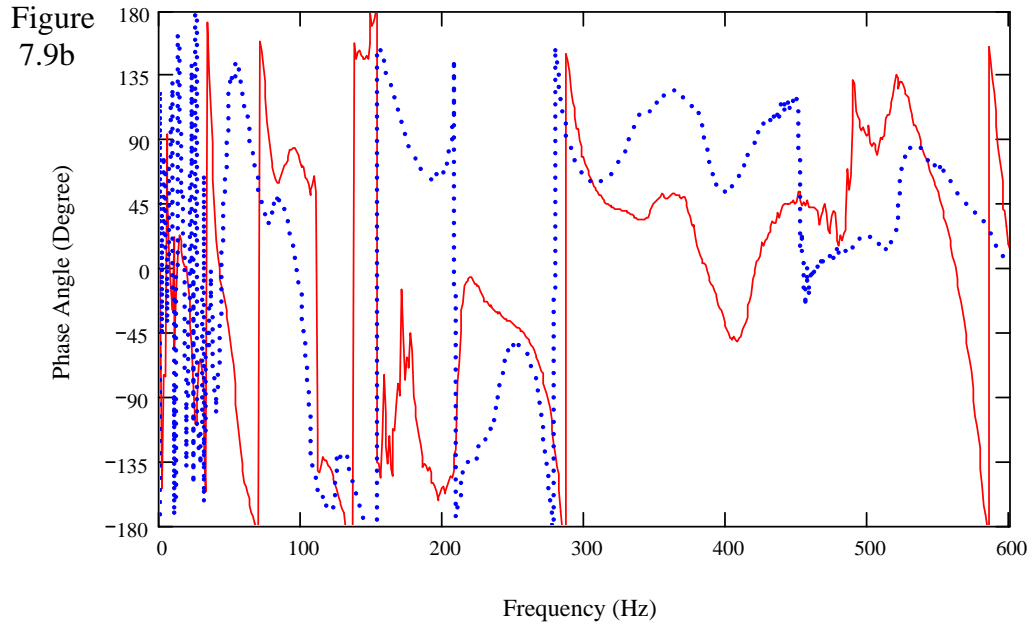


Figure 7.9 Motion transmissibility results for the air-borne energy transmission path investigation. a) Magnitude b) Phase c) Coherence ----- Swo+ Aw+Ino+Amn (see Figure 7.8a) ——— Sw+Aw+In+Amn(see Figure 7.8b)

Sw	=	Energy transmission with structure-borne path
Swo	=	Energy transmission without structure-borne path
Aw	=	Energy transmission with air-borne path
Ino	=	No isolator used
In	=	Four isolators placed at the nodal points
Amn	=	No acoustic insulation material used

Figure 7.10a

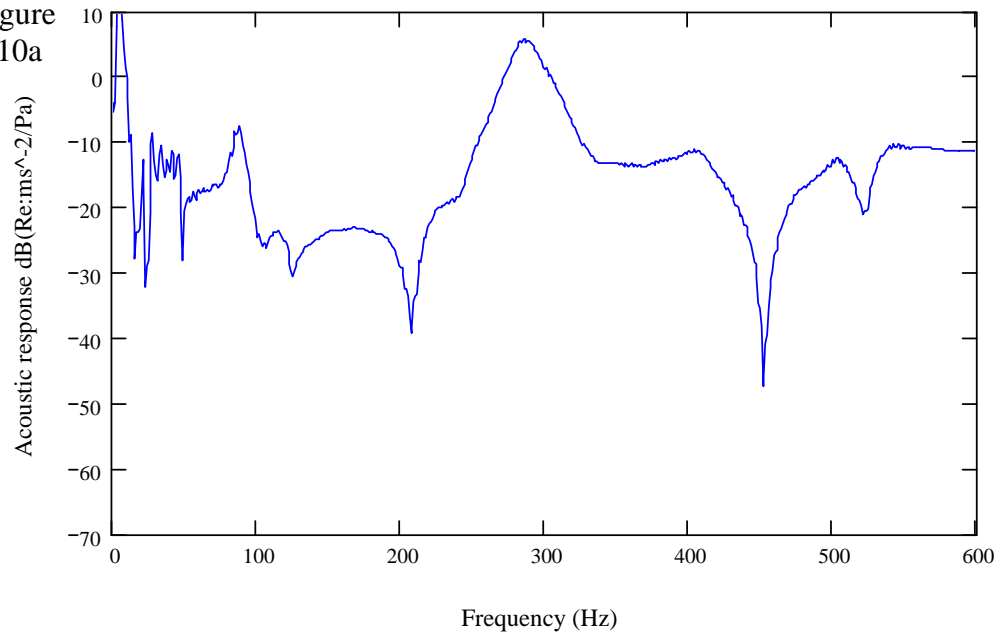
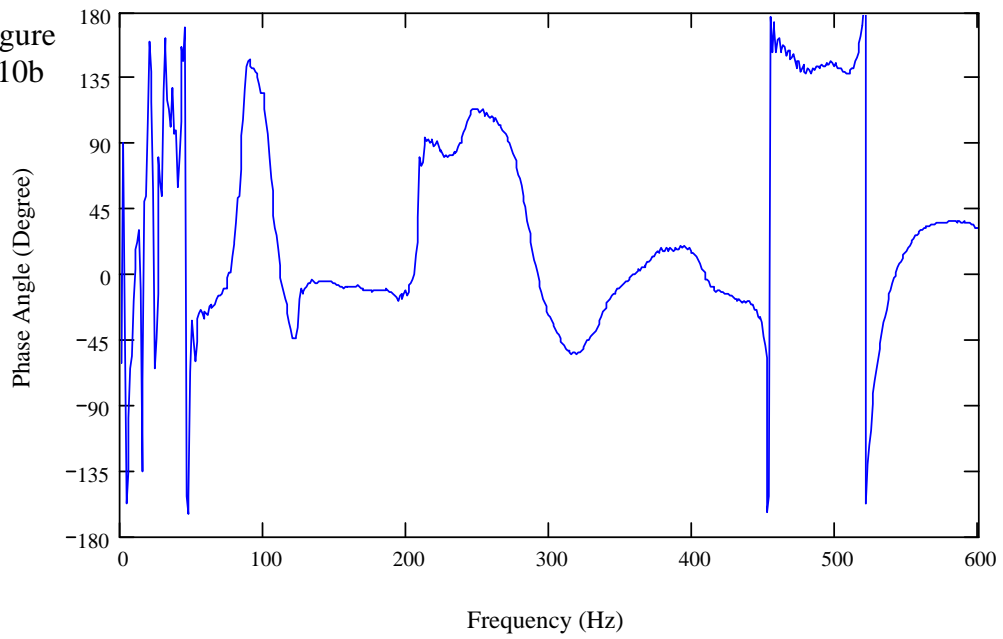


Figure 7.10b



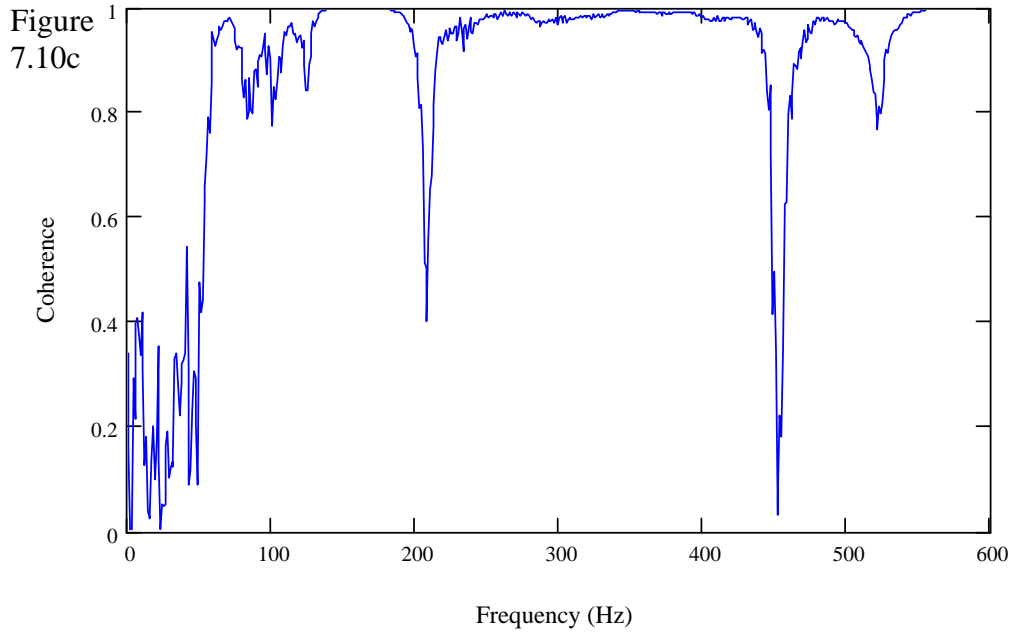
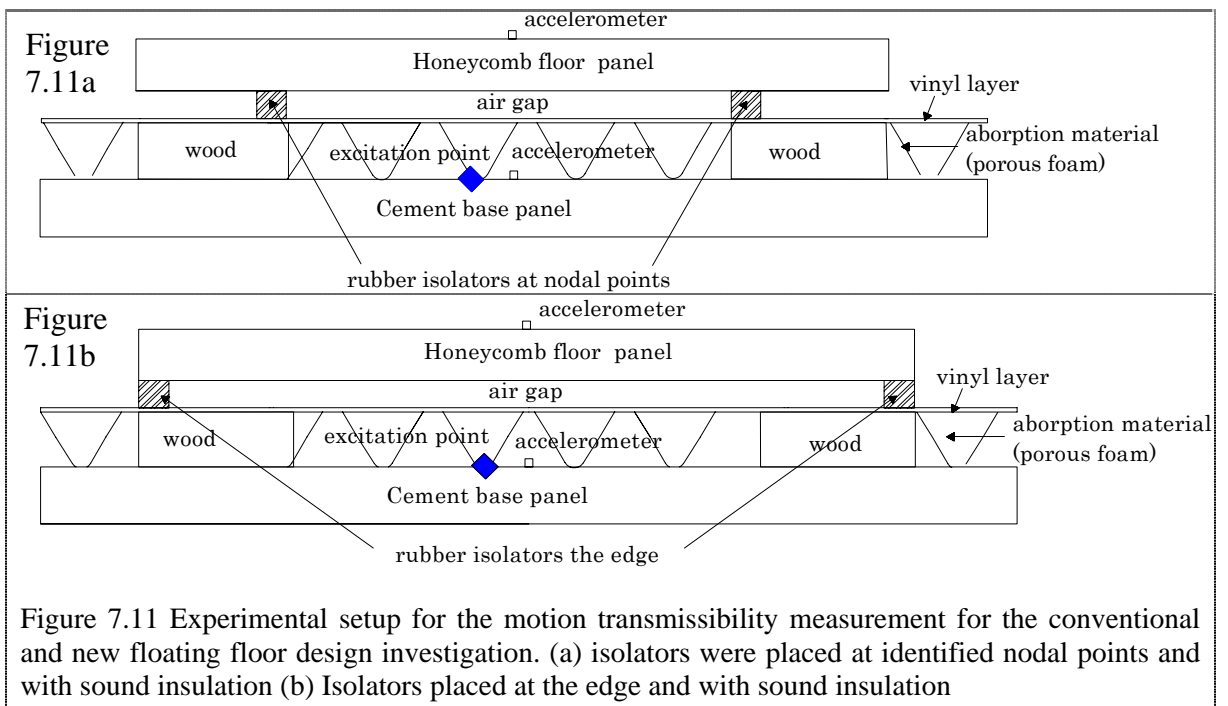


Figure 7.10 Acoustic induced response results for the air-borne energy transmission path.

a) Magnitude b) Phase c) Coherence — Swo+ Aw+Ino+Amn (see Figure 7.8a)

Swo	=	Energy transmission without structure-borne path
Aw	=	Energy transmission with air-borne path
Ino	=	No isolator used
Amn	=	No acoustic insulation material used



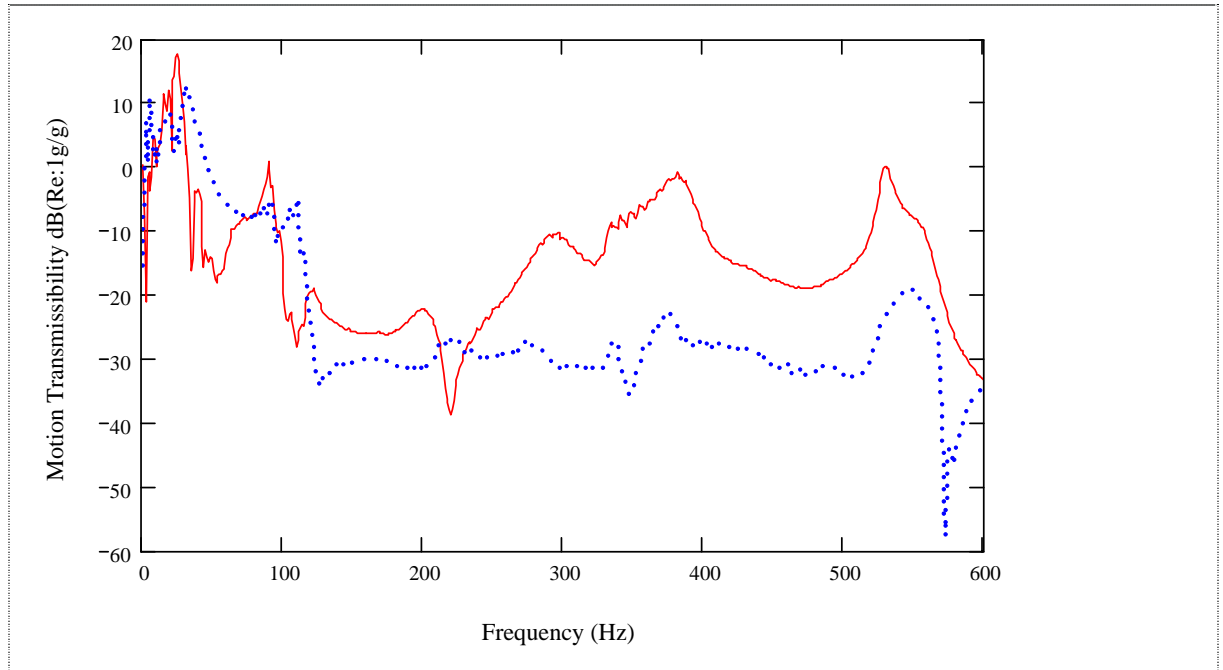


Figure 7.12a Comparison of vibration isolation performance with the conventional and new floating floor design.

----- Sw+Aw+In+Am (see Figure 7.11a) — Sw+Aw+Ie+Am (see Figure 7.11b)

Sw	=	Energy transmission with structure-borne path
Aw	=	Energy transmission with air-borne path
In	=	Four isolators placed at the nodal points
Ie	=	Four isolators placed at the edge points
Am	=	Acoustic insulation material used

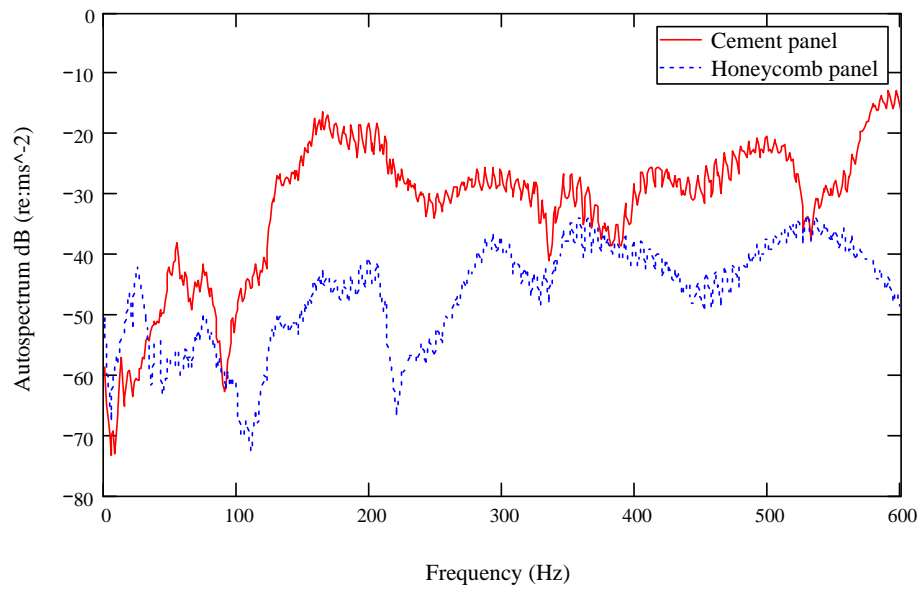


Figure 7.12b Autospectrum of vibration on cement base and honeycomb floor panel when the isolator placed at the edge of the honeycomb panel (see Figure 7.11b)

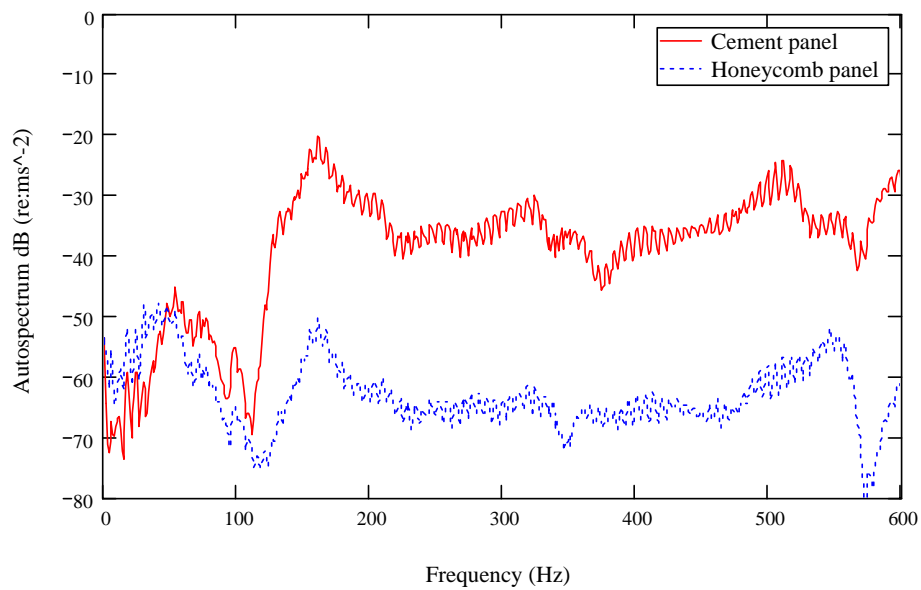


Figure 7.12c Autospectrum of vibration on cement base and honeycomb floor panel when the isolator placed at the nodal points of the honeycomb floor panel (see Figure 7.11a)

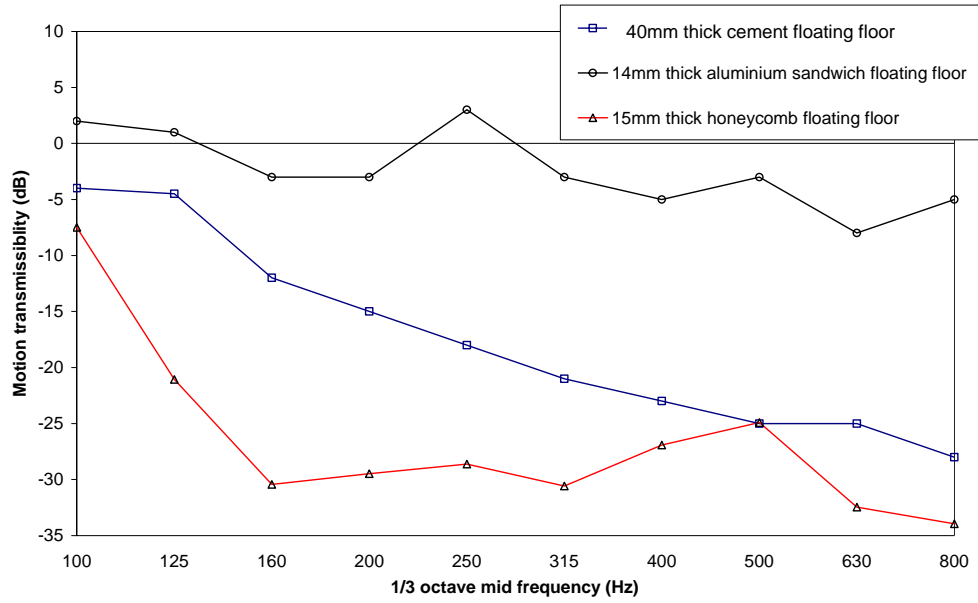


Figure 7.13 Comparison of the vibration isolation performance with typical floating floor design

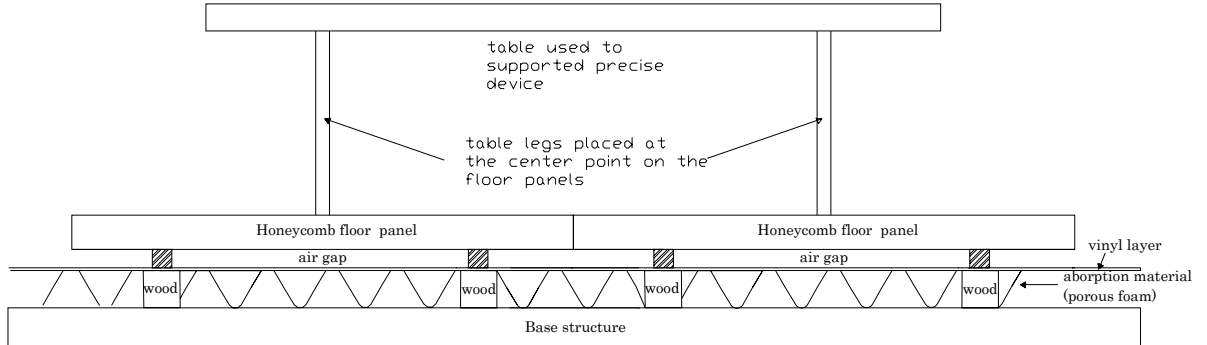


Figure 7.14 A special method to reduce the anti-symmetric bending resonances and overturn problem with the new proposed floating floor design

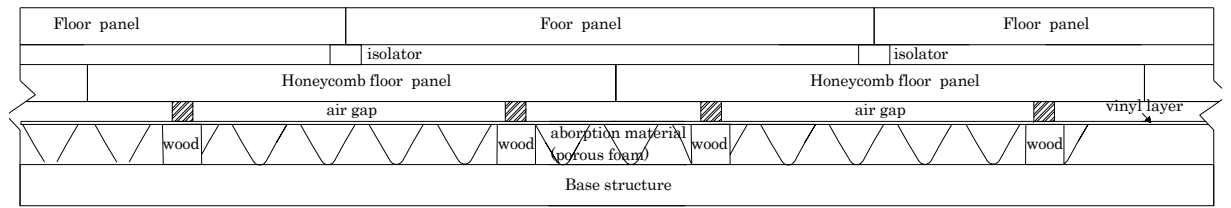


Figure 7.15 A general method to reduce the anti-symmetric bending resonances and overturn problem with new proposed floating floor design

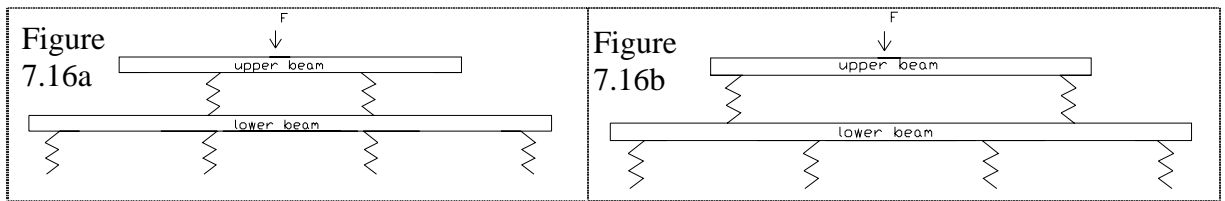


Figure 7.16. Vibration reduction devices a) isolators placed with in-line arrangement b) isolator placed with alternate arrangement. (From Du et. al ,2005)

Table 7.1 Dimensions and material properties of the testing material

Material	Description	Panel Size(mm) (Length x width x height)	Young's Modulus (E) ($\times 10^9$ N/m ²)	Density(ρ)
Paper honeycomb	Sandwich structure with Nomex paper core and covered with two glass reinforced plastics surface sheets (0.5mm thickness for each surface sheet)	415x415x15	overall=3.0 surface sheet=4.0 core shear=0.9	overall=5.8kg/m ² surface sheet=2550kg/m ³ core=244kg/m ³
Cement	Ref. to Table 2.2			

Table 7.2a The lowest two theoretical and experimental resonance frequencies of symmetric bending mode shapes for square honeycomb panel and cement panel

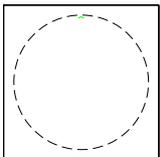
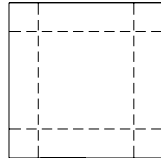
Sequence of symmetric mode	Mode shape	Corresponding theoretical resonance frequencies		Corresponding experimental resonance frequencies	
		Paper honeycomb panel	Cement panel	Paper honeycomb panel	Cement panel
1		273.5Hz	141.9 Hz	300.5 Hz	145.5 Hz
2		688.9 Hz	357.5 Hz	556.0 Hz	337.5 Hz

Table 7.2b Prediction of the lowest four resonance frequencies of anti-symmetric bending mode shapes for square honeycomb panel and cement panel

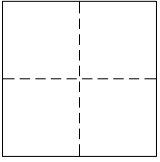
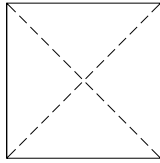
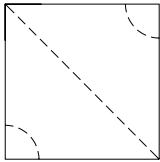
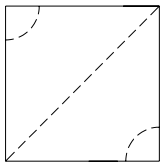
Sequence of anti-symmetric mode sequence	Mode shape --- nodal line	Corresponding theoretical resonance frequencies	
		Paper honeycomb panel	Cement panel
1		151.0 Hz	78.4 Hz
2		221.6 Hz	114.9 Hz
3		392.1 Hz	203.5 Hz
4		392.1 Hz	203.5 Hz

Table 7.3 Summary of experiments

	Target	Excitation Method	Findings	Reasons
Expt.1 (section 7.2)	Identify the dynamic properties of the cement and honeycomb panel	Shaker at the center point of the panel supported with soft rubber(see Figure 7.1)	The light weight honeycomb panel is a good selection for improving the vibration isolation performance of the typical light weight cement floor panel.	-Resonance at 145.5Hz of cement panel may be reduced by anti-resonance at around 140Hz of the honeycomb panel. -The bending mode at round 300Hz of honeycomb panel should be controlled by isolators placed at the nodal points of symmetric mode. (see Figure 7.2)
Expt.2 (section 7.4)	Verify the effects of isolator positions to transmissibility in idealized situation	Repeated impact on a small brick with steel hammer(see Figure 7.6)	Isolator placed at the nodal point of the symmetric bending mode of floor panel is an effective vibration isolation procedure in the idealized situation with structure-borne path	- The transmissibility of isolators placed at the nodal points of symmetric mode is much lower than that of the isolators placed at the edge. (see Figure 7.7a)
Expt.3 (section 7.5)	Verify the importance of air-borne energy transmission path	Repeated impact on the cement base panel with steel hammer(see Figure 7.8)	The air-borne energy transmission path for floating floor is very important.	- The magnitudes of transmissibility are similar for cases with and without structure-borne path. (see Figure 7.9a)
Expt.4 (section 7.6)	Verify the importance of isolator position in realistic situation	Repeated impact on the cement base panel with steel hammer(see Figure 7.11)	Isolator placed at the nodal points of honeycomb panel is an effective method to enhance the vibration isolation performance for the typical light weight cement panel in a practical situation.	- The magnitudes of transmissibility can be reduced significantly when the isolators placed at the nodal when air-borne path is blocked. (see Figure 7.12a)

CHAPTER 8

DISCUSSION

In this chapter two important findings are discussed. The first one is the significance of vibration modes analysis on isolated slab and the supporting box structure in the initial design of isolation systems. The other one is the use of optimum isolator position and the use of honeycomb panel to control the effects of bending resonances on isolation systems. The limitations in this project and the experimental techniques during the measurements are also discussed.

8.1 THE SIGNIFICANCE OF BENDING VIBRATION MODE ON THE ISOLATION SYSTEM DESIGN

This dissertation established a model for studying the resonance modes interaction between floating slabs and supporting hollow box structures, which can be applied to support a variety of heavy objects, such as, machinery on a concrete table, a rail support in the form of a concrete box girder viaduct, as well as humans and machinery in apartment buildings. The coupling mode may appear when the frequencies and vibration mode shapes are similar between the isolated slab and supporting box structure.

Two types of interaction modes were found in the experimental model. The first interaction mode is between the local distortion mode of box structure and the rotation mode of isolated slab. The second one is between the local combined mode of box structure and the

first bending mode of isolated slab. Both types of the coupling modes can cause high resonance response of supporting box structure. This corresponds to the suggestion from Wilson (2004) that bending resonance design of the floating floor of the theatre should not match with the resonances on the supporting frame.

The first coupling mode is not a significant sound radiator because of the mode shape and the low frequency (around 40Hz); whereas these are important for the vibration control since the displacement amplitudes are large at the low frequency. The second coupling mode is significant for noise radiation since the frequencies (around 160Hz) are higher than coincidence frequency of typical concrete structure (around 100Hz). The findings in the structure radiated sound from the box in accord with the prediction by Southward and Cooper (2002) that the noise radiation from viaduct box mainly contributes to local modes of the box.

It is noted that, however, there is little interaction effect between the viaduct and the floating slab can be identified in the site measurements at the bases of rail viaducts with floating systems. The problem of interaction in rail viaduct may be reduced by the high impedance in heavy structure of the long viaduct (around 30m). The problem of interactions between the supporting box and floating slab, however, should be still important in the situation of floating floor on the apartment building or the floating slab on the supporting table for vibrating machine. Thus, the estimation of resonance modes should be conducted in the initial design of isolation system to avoid the interaction mode between the floating slab and supporting structure.

The results of experimental test on floating slabs/floor, isolated box structures, rail viaduct structure with floating slab, and floating floor at the receiver confirmed that the bending vibration modes can degrade the vibration isolation performance and they have been verified with the modal analysis. This corresponds to the finding from Kawaharazuka et al. (1996) that the bending resonance of floating slab can degrade the vibration isolation performance. The

extensive data in this dissertation can further prove that the bending resonance on floating slab or supporting structure can also have adverse effect on the vibration reduction.

During the site test near the rail viaduct, it is found that the effects on vibration reduction becomes more significant when the bending resonance frequencies of floating slab is close to the passage support frequency or vertical isolator natural frequency. These situations should be avoided in the future design of floating slab using on rail.

8.2 THE SIGNIFICANCE OF ISOLATOR POSITION

Mead (1988) suggests the method of nodalization to reduce the vibration input from a source by placing the source at the nodal points of a beam. No published literature has been found to date about the concept of arranging the isolators at the nodal points of a plate to attenuate the bending mode vibration.

In Chapter 7, it was found that the vibration reduction of typical lightweight cement floor can be enhanced by floating honeycomb panel with optimum isolator arrangement. Four design features are required: 1) small floor panel with a high stiffness to mass ratio should be used 2) isolators should be placed at the common nodal point of the lowest two symmetric bending modes of the floor panel 3) lightweight and highly damped acoustic insulation material should be installed, together with acoustic absorption material, in the air cavity to reduce acoustic force transmission.

The concept of nodalization can also be applied to floating slab for supporting rail (Figure 8.1). The medium size floating slab instead of short size floating slab may be adopted to reduce vibration transmission from high speed train. The use of nodalization concept may alleviate the problem of the symmetric bending vibration of the slab. The anti-symmetric modes on medium size floating slab may difficult to be eliminated, except the uniform

excitation so that anti-symmetric mode can not be excited. However, a great deal of effort must be taken to achieve this, since numerous factors (e.g. safety, speed, riding quality etc) must be considered in design of floating slab on track.

8.3 THE LIMITATIONS

The deviation in the site measurement data under the rail viaducts can not be eliminated because of a great deal of variation factors, such as the train speed, and the defects on wheel or rail etc. Thus, numerous measurement data were obtained in each location to select at least three repeatable data and the highest within the three choices is presented.

The vibration data presented in Chapter 5 in different locations may not be compared to one another directly since they were obtained in different speed of train, type of train, measurement distance etc. The propagation of vibration in ground is not analysed since a large amount of parameters are required for reliable predictions. The impact force during the train running on crossover is an important source of vibration, which is still a current issue that is not covered in this project. In fact, there are still some patterns in vibration spectrum that can not be interpreted.

In the assessment of resonant modes of floating systems and box structures, it is hard to measure all the points on the structures, thus the mode shapes are established with curve fitting method.

8.4 THE EXPERIMENTAL TECHNIQUES

Modal analysis can be accomplished through mathematical method and experimental method. The experimental modal analysis can determine the relevant modal parameters as in

Chapters 4-7. Modal analysis were conducted with the broadband excitation force generation techniques using shaker or impact excitation, supported with signal detecting sensors and multi-channel FFT analyzer.

The selection of testing method should be based on the available sensors, analyzers, testing environment and the precise requirement etc. Free fall steel ball excitation was employed in Chapters 4 and 6 to identify the resonant modes of box and floating slab structures; impact hammer excitation was applied in Chapter 7 to examine the nodalization method to improve the vibration isolation of typical cement base panel. Whereas, the shaker test was used in dynamic behavior analysis on two test panel in Chapter 7 and a small panel in Appendix B.

Comparing with impact excitation, the use of shaker test can generate a more constant and repeatable excitation force signal. However, testing a large structure like the structure box (see Figure 4.12) with shaker should be difficult because of the requirement of large excitation force. To support the box, a rigid base must be installed on the shaker head, which would have made the static weight of the large rigid panel too heavy for the shaker. Thus, the impact excitation was applied to test large models.

The special force transducer with the size of 100mm diameter is required to measure the large force and wide area of impact with steel ball. The steel ball weight, height of free fall steel ball and layer of resilient material placed under the impact point can determine the duration of impact in order to generate flat force of spectrum in the interest frequency range.

For data acquisition, Schwarz and Richardson (1999) suggest that the use of the exponential window can reduce leakage in the spectrum of the response. Avitabile (2001) found that increasing the number of spectral lines or halving the bandwidth can avoid the hiding or distorting the modes in the measurement. However, the use of exponential window leads to the error in the mobility magnitudes and in the calculation of damping ratio, thus

correction must be employed. This step is not necessary in this dissertation, since the use of increasing the total time window as mentioned by Avitabile (2001) was employed.

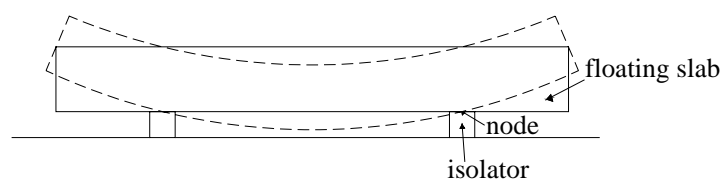


Figure 8.1 Recommendation design of medium size floating slab for high speed rail

REFERENCES

Avitabile P. (2001). When impact testing, can the use of an exponential window cause any problems? SEM Experimental Techniques, 1-2.

Kawaharazuka, T., Hiramatsu, T., Ohkawa, H. and Koyasu, M. (1996). Experimental study on vibration reduction by isolated railway. Internoise, 1549–1552.

Mead, D. J. (1998). Passive vibration control. Chichester; New York: Wiley.

Schwarz, B.J. & Richardson, M.H. (1999). Experimental Modal analysis. CSI Reliability Week, Orlando, 1-12.

Southward, N.J. and Cooper, J.H. (January 2002). The alternative design of the West Rail Viaducts . Hong Kong Engineer On Line, Cover Story.

Wilson, G.P. (2004). Isolation of the Jazz @ Lincoln Center Performance and Education Concert Theater, Rose Theate. Proceedings of Inter-noise.

CHAPTER 9

CONCLUSIONS AND RECOMMENDATIONS

In this chapter, conclusions of the dissertation and recommendations for further work are presented.

9.1 CONCLUSIONS

Most of the previous investigations of vibration isolation efficiency on the floating systems considered the resonant modes of floating slab/floor only, but not the interaction between floating systems and supporting structure, and few studies have examined the effects of bending mode on the vibration reduction. This study was an attempt to establish the responses of the global/local modes for any rectangular box structures like viaduct, buildings and identify their interaction with dynamic response of floating slab/floor and, in addition, to evaluate and control the effects of bending mode of floating slab/ floor on the isolation efficiency.

Two types of interaction mechanisms of rectangular concrete box and floating slab have been established in the experimental analysis. The first one is the interaction between local distortion mode of box structure and the rotation mode of isolated slab at around 40Hz, which are significant for the vibration control. The second one is the interaction between the local combined mode of box structure and the first bending mode of isolated slab at around 160Hz,

which are significant sound radiator when the resonance frequencies above the coincidence frequency of typical concrete structure (around 100Hz).

The bending vibration modes of isolation system can produce detrimental effects on vibration isolation and have been confirmed with extensive experimental and theoretical results on floating floor/slab with supporting box structure. Furthermore, The effects on vibration reduction becomes more significant when the bending resonance frequencies of floating slab is close to the passage support frequency or vertical isolator natural frequency.

The findings indicate that decreasing the length of floating slab/floor can increase the bending resonance frequency, which can improve the vibration isolation performance. To reduce the effect of bending resonance of floating floor, a small floor panel can also be used and isolators should be placed at the nodal points of the lowest two symmetric bending modes of the floor panel. The receiver point should be at the centre point of the panel to avoid the effect of anti-symmetric bending modes.

The research establishes the additional rules for the design of floating system; (1) the overlap of floating slab resonant mode with those of supporting structure and passage support frequency of the track should be avoided; 2) the installation of smaller floating slab/floor and nodal point support can reduce the bending modes effects on vibration isolation.

9.2 RECOMMENDATIONS

In the study of large and heavy structural models, the use of impact excitation is a fast, convenient way to find the resonant modes of structures, whereas, the shaker test is employed with light weight structures to have a more stable excitation signal. In the impact test, the excitation frequency range is controlled with weight and height of impact and the layer of resilient material on impact point.

To increase the accuracy of the impact excitation data, it is significant to analyse both input and output time history spectrum first in order to confirm the total decay of the response signal in the selected time window. The increasing the number of spectral lines or reducing the bandwidth can be employed to increase the total time window to allow the response signal have the natural decay.

The new concept of placing the isolators on the nodal point of symmetric bending modes of floor panel (In Chapter 7 and Appendix B) is suggested for further study. In this dissertation, the vibration isolation performance is assessed by centre point at the panel of the receiver to eliminate the anti-symmetric resonant modes. In practice, however, there may be residual anti-symmetric mode to deteriorate the vibration isolation performance, and the static stability problem should be overcome. The two stage floating isolation method can be tested with additional isolators placed at the center point of the lower panel. Furthermore, the use of nodalization concept in floating slab for rail vibration isolation can also be a new topic in further study.

APPENDIX A

THEORETICAL ANALYSIS ON THE STRUCTURE RADIATED NOISE

A.1. STRUCTURE ACOUSTICS IN PLATE ELEMENT

The structure-radiated noise from plate can be estimated according to the coincidence frequency and radiation efficiency. The estimation of sound pressure levels near the vibrating plate or in the room are described in this section to understand the main factors controlling the structure-radiated noise from plate.

The sound power radiating from one side of a plate during vibration is shown in Equation A.1. The radiated power W is related to density of the acoustic medium ρ_0 , sound velocity c , area of vibrating surface S , quadratic velocity of the vibrating structure average over space $\langle \bar{V}^2 \rangle$, and the radiation efficiency σ .

$$W = \rho_0 c S \langle \bar{V}^2 \rangle \sigma \quad (\text{A.1})$$

In Sound Power Level (SWL):

$$SWL = 10 \log \rho c + 10 \log S + 10 \log \langle \bar{V}^2 \rangle + 10 \log \sigma + 120 \quad (\text{A.2})$$

To predict the sound pressure level (SPL) closed to the vibrating surface, for the sound source in free-field condition Equation A.3 can be used:

$$SPL = SWL - 10 \log S \quad (\text{A.3})$$

For the SPL inside a room Equation A.4 should be applied:

$$SPL = SWL + 10 \log \left(\frac{1}{S} + \frac{4}{R} \right) \quad (A.4)$$

After substituting Equation A.3 to A.2, Equation A.5 can be used to identify the SPL radiated from a plate in free-field. Similarly, Equation A.6 can be used to identify the SPL radiated from a plate inside a room with R as the room constant.

$$SPL = 10 \log \rho c + 10 \log \langle \bar{V}^2 \rangle + 10 \log \sigma + 120 \quad (A.5)$$

$$SPL = 10 \log \rho c + 10 \log S + 10 \log \langle \bar{V}^2 \rangle + 10 \log \sigma + 120 + 10 \log \left(\frac{1}{S} + \frac{4}{R} \right) \quad (A.6)$$

In general, the radiation efficiency on finite plate structure can be approximated with the curve in Figure A.1. It is shown that the radiation efficiency become maximum when the frequency is at or above coincidence frequency of the structure. In this situation the panel bending wavelength coincides with the wavelength of the acoustic wave propagation. The coincidence frequency f_c can be estimated with Equation A.7

$$f_c = \frac{0.55c^2}{c_L h} \quad (A.7)$$

Where,

c =speed of sound in air (m/s),

c_L =compressional wave speed (m/s), and

h =panel thickness (m).

In summary, the SPL radiated from a panel structure depends on the vibration and frequency. There is, however, a variety of factors to affect the accuracy estimation of radiation efficiency, thus there may be deviation in the theoretical calculation. Detail studies on the radiation efficiency of bending wave on finite plates are given by Richards (1982); Fahy (1985) and Beranek (1988); those will not be further investigated in this dissertation.

REFERENCES

- Beranek, L.L. (1988). Noise and vibration control. Washington, D. C.: Institute of Noise Control Engineering.
- Fahy, Frank. (1985). Sound and structural vibration : radiation, transmission, and response . Publisher London ; Orlando : Academic Press.
- Richards, E.J. (1982). Noise from industrial machines. In R.G. White and J.G. Walker (Eds.) Noise and Vibration (pp.497-606). New York : Halsted Press.

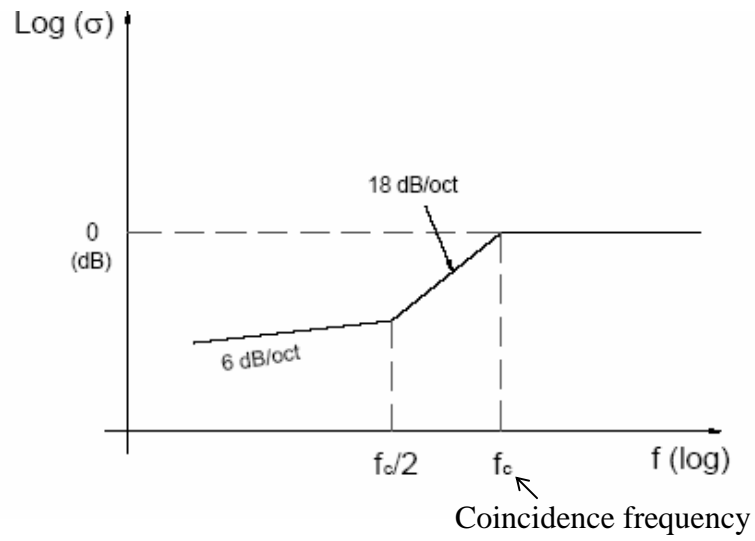


Figure A.1 Design curve for the approximation of radiation efficiency σ in general condition

APPENDIX B

NODALIZATION TEST ON SHAKER

The results in Chapter 7 confirms that the small honeycomb panel with optimum isolator support and acoustic insulation device can improve the vibration isolation performance of typical thin cement base panel. However, there is not enough excitation for low frequency range below 120Hz.

In this appendix, the vibration isolation performance of a single smaller honeycomb panel excited by the rigid base of shaker head in the frequency range of 0-800Hz was examined.

B.1 EXPERIMENTAL SETUP

The experimental setup is shown in Figure B.1, the dimensions of the honeycomb panel 170mm x 170mm x15mm with the same material properties of the original panel as shown in Table 7.1. Four rigid rubbers (each of which was 70 mm x 70 mm x 70 mm) were employed to support the rubber isolators to maintain a typical cavity depth of 100 mm between the floor and rigid shaker disc. The rigid rubbers were designed to support the rubber isolators at both the edge and nodal positions of the honeycomb panel. This ensured that the vibration energy transmission from the shaker disc via the rigid rubbers to the honeycomb floor panel was constant for different isolator positions. A vinyl sheet to cover the porous foam material installed inside the cavity to reduce the acoustic path energy transmission path between the shaker head base and the floating panel.

A white noise signal was used to drive the shaker to generate a wide band frequency (0-1kHz) force, and an accelerometer was mounted on the shaker head to register the input acceleration to the panels. A lightweight accelerometer was mounted at various points on the panels to measure their acceleration response. The frequency response functions (FRFs; the acceleration on the panel/shaker head) were obtained.

B.2 EXPERIMENTAL RESULTS

The boundary conditions were free along the circumference of the plate. The first symmetric bending resonance of the isolated plane was found at 735Hz, the mode shape is the same as the bending mode of original honeycomb panel at 300.5 Hz (Figure 7.3). Figures B.2a and B.2c show the effect of the position of the isolators on the motion transmissibility at the receiver. The high coherence from 0-800 Hz shows that the measurement result was accurate. The sudden dips at around 220Hz were probably due to a low vibration response. The phase angle of 90 degrees at the lowest symmetric bending mode resonance frequency confirms the effect of the resonance on the motion transmissibility. For both cases, the vibration from 60Hz to 600Hz is reduced by 20dB to 40dB. This should be due to the very small panel was adopted in this measurement, and the small panel is better for low frequency vibration reduction.

When the isolators were placed at the nodal points, the vibration reduction was 10dB higher in the frequency range of 200 Hz to 700 Hz. These experimental results also confirm the effect of isolator position in Figure B.1. Although, the peak at around 730 Hz was not totally eliminated, the vibration excitation problem is generally low at this frequency.

B.3 SUMMARY

A smaller honeycomb panel of 170mm x 170mm x15mm was employed to conduct shaker test to identify the effectiveness of nodal point support on the control of the vibration isolation degradation due to bending mode in the frequency range of 0-800Hz.

It is shown that the smaller honeycomb panel reduce vibration by 20-40dB for frequency 60-600Hz with isolator at the edge. There are 10dB more vibration reduction for frequency 200-700Hz when the panel with nodal point support.

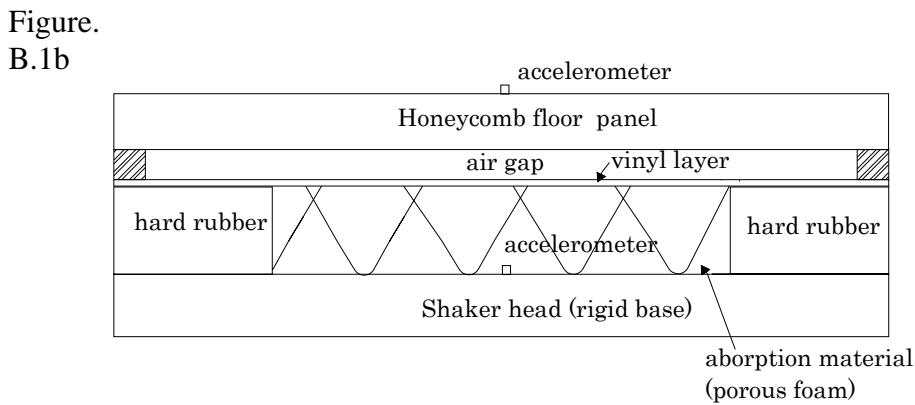
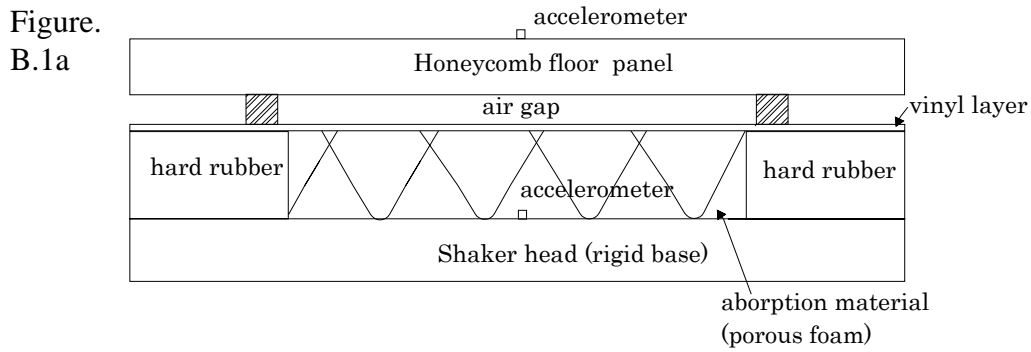


Figure B.1 Experimental setup for the motion transmissibility measurement for the conventional and new floating floor design investigation. (a) isolators were placed at identified nodal points and with sound insulation (b) Isolators placed at the edge and with sound insulation

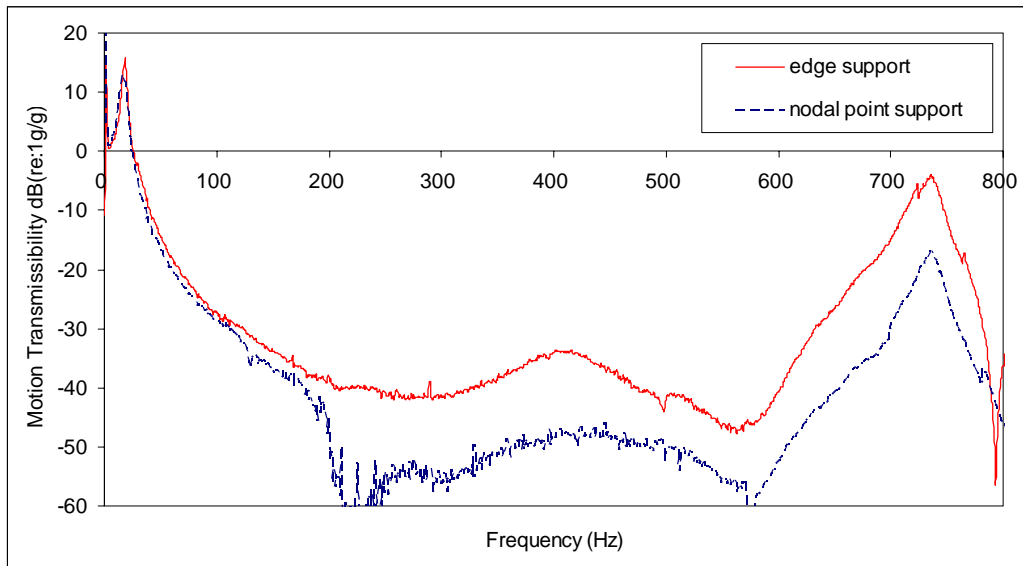


Figure B.2a Motion transmissibility of honeycomb panel with nodal point and edge support on shaker test

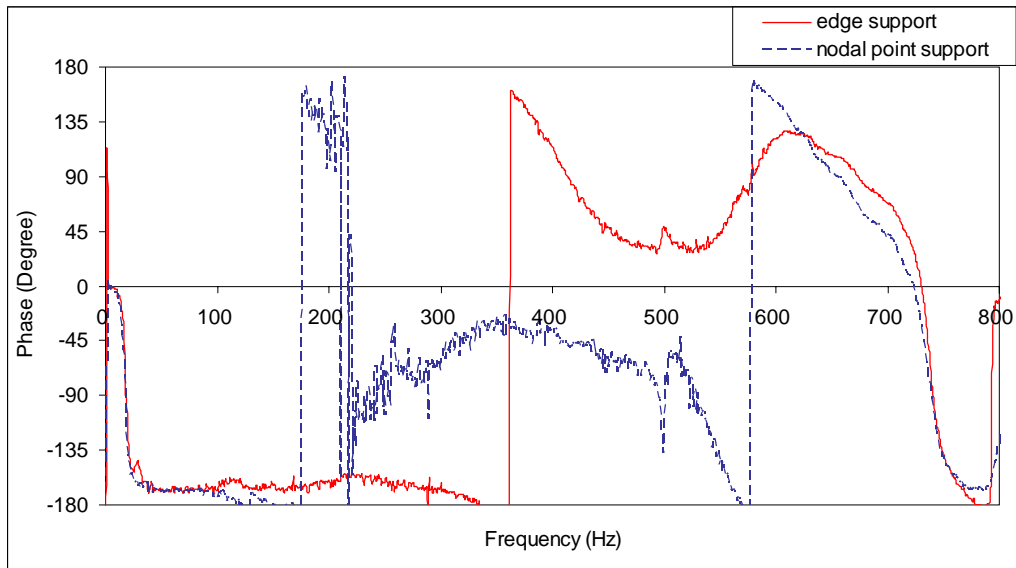


Figure B.2b Phase of the corresponding transmissibility measurement on honeycomb panel with nodal point and edge support on shaker test

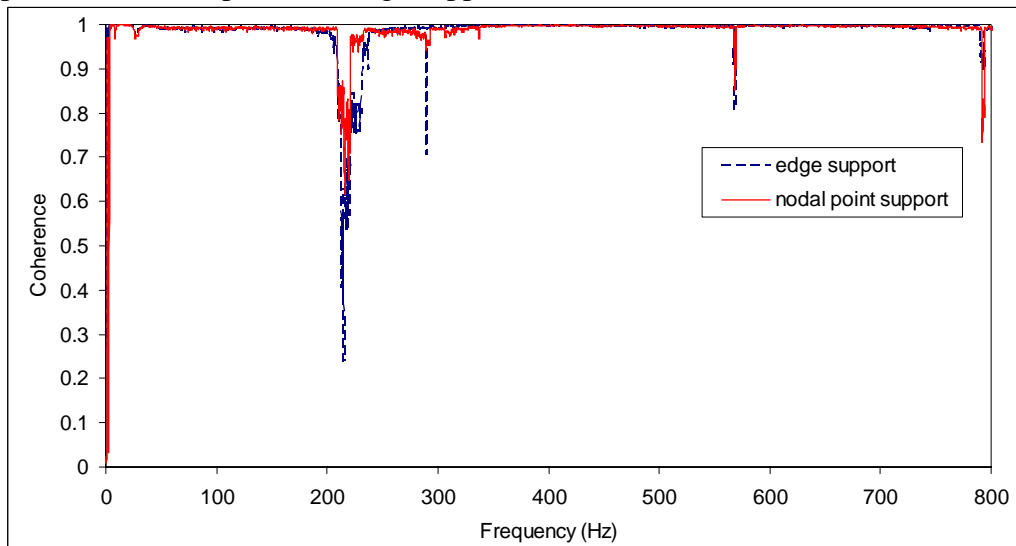


Figure B.2c Coherence of the corresponding transmissibility measurement on honeycomb panel with nodal point and edge support on shaker test

APPENDIX C

LIST OF INSTRUMENTS

Vibration and Acoustic Sensors

<u>Instruments</u>	<u>Serial number</u>
B&K 4518-003 Accelerometer	50530
ENDEVCO 752A12 Accelerometer	15008
PCB ICP Accelerometer	40300
PCB ICP Accelerometer	40607
B&K 4188 ½" Microphone	2180187
B&K 4189 ½" Microphone	1903779
HMS S9 Force Transducer	162963 A

Amplifiers

<u>Instruments</u>	<u>Serial number</u>
Delta-tron Microphone preamplifier 2671	2152740
Delta-tron Microphone preamplifier 2671	2400681
HBM Bridge Amplifier	015206024

Analyzers

<u>Instruments</u>	<u>Serial number</u>
B&K Pulse multi-analyzer 3560c	2380837
B&K Pulse Lite analyzer	2533713

Others**Instruments****Serial number**

B&K 4291 Calibrator Exciter	994839
B&K 4230 Sound Level Calibrator	1712272
LDS PA1000L Power Amplifier	75314/3
LDS V650 Series Vibrators	S6751-001/1
Sony Notebook Computer	2831650 710020